

Causality measures between neural signals from invasively and non-invasively obtained local field potentials in humans

Esther Florin

Causality measures between neural signals from invasively and non-invasively obtained local field potentials in humans

von

ESTHER FLORIN

27. Januar 2010

Dissertation zur Erlangung des

Doktorgrades (Dr. rer. nat.)

im

Fachbereich Mathematik und Naturwissenschaften
- Fachgruppe Physik -

an der

Bergischen Universität Wuppertal

Die Dissertation kann wie folgt zitiert werden:

urn:nbn:de:hbz:468-20100816-153747-5

[<http://nbn-resolving.de/urn/resolver.pl?urn=urn%3Anbn%3Ade%3Ahbz%3A468-20100816-153747-5>]

Forschungszentrum Jülich GmbH
Institute of Neuroscience and Medicine (INM)
Cognitive Neurology (INM-3)

Causality measures between neural signals from invasively and non-invasively obtained local field potentials in humans

Esther Florin

Schriften des Forschungszentrums Jülich
Reihe Gesundheit / Health

Band / Volume 29

ISSN 1866-1785

ISBN 978-3-89336-646-0

Bibliographic information published by the Deutsche Nationalbibliothek.
The Deutsche Nationalbibliothek lists this publication in the Deutsche
Nationalbibliografie; detailed bibliographic data are available in the
Internet at <http://dnb.d-nb.de>.

Publisher and
Distributor: Forschungszentrum Jülich GmbH
Zentralbibliothek
52425 Jülich
Phone +49 (0) 24 61 61-53 68 · Fax +49 (0) 24 61 61-61 03
e-mail: zb-publikation@fz-juelich.de
Internet: <http://www.fz-juelich.de/zb>

Cover Design: Grafische Medien, Forschungszentrum Jülich GmbH

Printer: Grafische Medien, Forschungszentrum Jülich GmbH

Copyright: Forschungszentrum Jülich 2010

Schriften des Forschungszentrums Jülich
Reihe Gesundheit / Helath Band / Volume 29

D 468 (Diss., Wuppertal, Univ., 2010)

ISSN 1866-1785
ISBN 978-3-89336-646-0

The complete volume ist freely available on the Internet on the Jülicher Open Access Server (JUWEL) at
<http://www.fz-juelich.de/zb/juwel>

Neither this book nor any part of it may be reproduced or transmitted in any form or by any
means, electronic or mechanical, including photocopying, microfilming, and recording, or by any
information storage and retrieval system, without permission in writing from the publisher.

Copyright by

Esther Florin

2010

Acknowledgments

First of all, I want to thank all coauthors who contributed to the different projects that led to the present work. Without their collaboration, most of this thesis would have been unthinkable.

I would like to express my gratitude to my Ph.D. supervisor Professor Dr. Uwe Pietrzyk for his constant interest in my work and many fruitful discussions. Furthermore, I want to thank him for supervising this interdisciplinary work with all its attached difficulties.

My special thanks go to Professor Dr. Gereon R. Fink for supporting this Ph.D. thesis in all possible ways and in particular for his detailed and critical reading of this work and the corresponding scientific articles. His valuable suggestions and precise comments helped to vastly improve my research and its presentation. Furthermore, I

thank him for providing me with the opportunity to work at his Institute of Neuroscience and Medicine (INM-3) at the Research Center Jülich.

I wish to thank Professor Dr. Hartwin Bomsdorf and Professor Dr. Andreas Klümper for accepting the responsibility of being my committee members.

I also want to thank Professor Dr. Lars Timmermann for raising the research questions that led to the topic of my Ph.D. thesis. Furthermore, I would like to acknowledge his vision of creating an interdisciplinary research group of young scientists with different scientific backgrounds. Although being the only physicist, I always enjoyed working in this group. It provided the intellectual atmosphere that stimulated my work. Here my thanks also go to my colleagues in Professor Timmermann's group. They all helped to expand my horizon and scientific interest in so many ways.

I am grateful to Professor Dr. Joachim Gross who introduced me to Matlab programming and neuroscientific data analysis and gave important input for the first design of the simulation study. Moreover, during intense research visits at the University of Glasgow he provided valuable suggestions on how to improve and advance the present work.

I thank Dr. Jürgen Dammers for our insightful "Friday" discussions and for providing valuable feedback in the final stages of my thesis. His constant challenging of my results was instrumental in further scrutinizing important issues and invaluable for improving the present work.

I wish to thank my mother and my family for their constant support throughout this work. Last, but not least I want to thank Johannes for the never-ending suggestions and discussions. Without these discussions and suggestions, but also the encouragement, this work would have been unthinkable. I hope I did not discourage him from voicing his critique during the last months.

Contents

List of Figures	xv
List of Tables	xix
Abbreviations	xxiii
Abstract	xxvii
1 Introduction	1
2 Neurophysiological Methods to Invasively and Non-Invasively Record Neural Activity	11
2.1 Origin of Neural Signals	12
2.2 Description of Recording Methods	15
2.2.1 Macroelectrode Recordings	15
2.2.2 Electroencephalography (EEG)	18
2.2.3 Magnetoencephalography (MEG)	22
2.2.4 Comparison of the Recording Methods	24

2.3	Muscle Activity Recording: Electromyography (EMG)	26
3	Causality and Directionality Measures – Theoretical Background	29
3.1	Phase Delay	31
3.2	Autoregressive Modeling	33
3.2.1	Stationarity	34
3.2.2	Model Order Selection	39
3.3	Statistical Causality Measures	41
3.3.1	Granger Causality	41
3.3.2	Directed Transfer Function (DTF) and Transfer Function (H)	43
3.3.3	Direct Directed Transfer Function (dDTF)	45
3.3.4	Partial Directed Coherence (PDC) and Squared Partial Directed Coherence (sPDC)	47
3.4	Methods for Significance Threshold Computation	48
3.4.1	Leave One Out Method	49
3.4.2	Random Permutation	51
3.4.3	Power and Size of the Significance Thresholds	54
4	Simulation Models and Theoretical Derivations	57
4.1	Simulation Models	57
4.1.1	Modified Kus (2004) - Model	58
4.1.2	Modified Schelter (2006) - Model	60

4.2	Stationarity	61
4.3	The Influence of Preprocessing: Theoretical Considerations	63
4.3.1	Filtering	63
4.3.2	Decimating and Interpolation	68
5	Simulations I: Influence of Preprocessing on Multivariate Causality Measures	71
5.1	Design of the Simulation Study	72
5.2	Results: Filtering	81
5.2.1	Filter Function	81
5.2.2	Filter Order	86
5.2.3	Phase Neutral vs. Non-Phase Neutral Filtering	87
5.2.4	Low-Pass Filtering	88
5.2.5	Notch Filter	89
5.2.6	Wavelet Filtering	90
5.3	Results: Decimating and Interpolation	92
5.3.1	Decimating	92
5.3.2	Interpolation	92
5.4	Discussion	94
5.5	Conclusion	102

6 Simulations II: Parameter Dependence and Data Types	105
6.1 Motivation of the Simulation Study	106
6.2 Design of the Simulation Study	107
6.3 Zero-and-One Inflated Beta Regression-Model	111
6.4 Results: Comparison of the Multivariate Autoregressive Causality Measures	117
6.5 Results: Data Types	119
6.6 Results: Parameter Dependence	119
6.6.1 Data Length	119
6.6.2 Model Order	120
6.6.3 Noise Level	123
6.6.4 Coupling Strength	124
6.6.5 Parameter Interaction	124
6.7 Results: Schelter-Model	125
6.8 Discussion	126
6.9 Conclusion	135
7 Application of the Causality Measures to Macroelectrode Recordings and Electromyograms	137
7.1 Experimental Design	141
7.1.1 Included Patients	141

7.1.2	Implantation of Electrodes for Deep Brain Stimulation and Intra-Operative Recordings	143
7.1.3	Data Analysis	144
7.2	Results	147
7.2.1	Placement of the Implanted Electrode for Deep Brain Stimula- tion	147
7.2.2	Causality between Electromyograms of Forearm Muscles and Local Field Potentials of the Subthalamic Nucleus	149
7.3	Discussion	152
8	Conclusion	159
	Bibliography	167
	Appendix A Results for all Causality Measures	193

List of Figures

1.1	A direct and an indirect causation	3
2.1	Neuron and synapse	12
2.2	Action potential	14
2.3	Local field potential	17
2.4	Tip of the combined micro- and macroelectrode	17
2.5	Pyramidal neurons in the cortex	19
2.6	Electroencephalographic recording	20
2.7	An electroencephalography cap with 128 electrodes	21
2.8	Magnetoencephalographic recording	23
2.9	Motor unit	26
2.10	Surface electromyogram recorded during tremor	27
3.1	Review of the currently applied analysis methods for local field potentials	30
3.2	Different types of instationarity	36

3.3	The sPDC in combination with LOOM for one connection	50
3.4	Histogram of the sPDC's maximum from 1000 repetitions	53
3.5	The sPDC in combination with random permutation for one connection	53
4.1	Kus-model	59
4.2	Connections implied by the Schelter-model	60
5.1	Design of the simulation study on the influence of data preprocessing	72
5.2	Filter functions of different filter types	73
5.3	Spectrum with 50 Hz artefact	76
5.4	Filter results for sPDC with LOOM	82
5.5	Filter results for sPDC with random permutation	84
5.6	Different filter algorithms for the sPDC with the Schelter-model . . .	85
5.7	Influence of the filter order on the sPDC	86
5.8	Comparison of phase neutral vs. non-phase neutral filter	87
5.9	Comparison of different low pass filters	88
5.10	Influence of notch filter for sPDC with LOOM	89
5.11	Different wavelet decompositions with Daubechies wavelets	91
5.12	Influence of decimating and interpolation for sPDC with LOOM . . .	93
5.13	Linear and FFT interpolation	99
5.14	Suggested steps for preprocessing data before a causality analysis . .	103

6.1	Design of the simulation study to determine the parameter dependencies	108
6.2	Probability density functions for two parameterizations of the beta distribution	112
6.3	Parameter dependence with LOOM	121
6.4	Parameter dependence with random permutation	122
7.1	Albin/DeLong basal ganglia model	139
7.2	LFP and EMG activity of PD patients during tremor and respective coherence spectra	145
7.3	Average active stimulation contact	149
7.4	Causalities for one patient during rest condition	151
7.5	Occurrence of input and output causalities for PD patients with tremor	152

List of Tables

2.1	Comparison of the different measurement methods	16
3.1	99% percentiles of the five causality measures for different numbers of random permutation repetitions	52
3.2	Size of random permutation (RP) and LOOM for the different causality measures	54
3.3	Power of random permutation (RP) and LOOM for the different causality measures	55
5.1	Cut-off frequencies corresponding to different levels of Daubechies wavelets	78
5.2	Recommendations based on the simulation results concerning the usage of filtering in combination with causality measures	81
6.1	Results of the five causality measures for real data	107

6.2	Parameter variation for the Kus-model in the simulations	109
6.3	Parameter variation for the Schelter-model in the simulations	110
6.4	Overall performance of the MVAR methods	118
6.5	Signs of the significant interaction terms	124
7.1	Patient characteristics	142
7.2	Localization of the active stimulation contact	148
7.3	Descriptive statistics of the application results	150
A.1	Results of the different filter types for LOOM with Kus-model	194
A.2	Results of the different filter types for random permutation with Kus- model	195
A.3	Results of the different filter types for LOOM with Schelter-model	196
A.4	Results of the different filter types for random permutation with Schelter-model	197
A.5	Variation of filter order with LOOM	198
A.6	Increase in low-pass filters with LOOM	199
A.7	Results for notch filter, decimating and interpolating the data with LOOM	200
A.8	Regression coefficients for the sPDC, PDC and DTF with MEG data in combination with LOOM	201

A.9 Regression coefficients for the dDTF and H with MEG data in combination with LOOM	202
A.10 Regression coefficients for the sPDC, PDC and DTF with EEG data in combination with LOOM	203
A.11 Regression coefficients for the dDTF and H with EEG data in combination with LOOM	204
A.12 Regression coefficients for the sPDC, PDC and DTF with EMG data in combination with LOOM	205
A.13 Regression coefficients for the dDTF and H with EMG data in combination with LOOM	206
A.14 Regression coefficients for the sPDC, PDC and DTF with LFP data in combination with LOOM	207
A.15 Regression coefficients for the dDTF and H with LFP data in combination with LOOM	208
A.16 Regression coefficients for the sPDC, PDC and DTF with MEG data in combination with random permutation	209
A.17 Regression coefficients for the dDTF and H with MEG data in combination with random permutation	210
A.18 Regression coefficients for the sPDC, PDC and DTF with EEG data in combination with random permutation	211

A.19 Regression coefficients for the dDTF and H with EEG data in combination with random permutation	212
A.20 Regression coefficients for the sPDC, PDC and DTF with EMG data in combination with random permutation	213
A.21 Regression coefficients for the dDTF and H with EMG data in combination with random permutation	214
A.22 Regression coefficients for the sPDC, PDC and DTF with LFP data in combination with random permutation	215
A.23 Regression coefficients for the dDTF and H with LFP data in combination with random permutation	216
A.24 Parameter dependencies for the Schelter-model in combination with LOOM (sPDC, PDC, DTF)	217
A.25 Parameter dependencies for the Schelter-model in combination with LOOM (dDTF, H)	218
A.26 Regression coefficients for the sPDC, PDC and DTF with Schelter-model in combination with random permutation	219
A.27 Regression coefficients for the dDTF and H with Schelter-model in combination with random permutation	220

Abbreviations

ADF – augmented Dickey-Fuller

AIC – Akaike Information Criterion

AR – autoregression/autoregressive

AR – akinetic-rigid (chapter 7)

butter – Butterworth filter

BIC – Bayesian Information Criterion

cheby1 – Chebychev filter of type 1

cheby2 – Chebychev filter of type 2

cs – coupling strength

DBS – Deep Brain Stimulation

DTF – Directed Transfer Function

dDTF – direct Directed Transfer Function

dl – data length

ellip – elliptic filter

ECoG – Electrocorticography

EDC – M. extensor digitorum communis

EEG – Electroencephalography

EMG – Electromyography

EPSP – excitatory postsynaptic potential

ffDTF – full frequency directed transfer function

FFT – fast Fourier Transform

FDL – M. flexor digitorum communis longis

fo – filter order

fMRI – functional magnetic resonance imaging

FT – Fourier Transform

GPe – Globus pallidus pars externus

GPi – Globus pallidus pars internus

H – Transfer Function

ICA – independent component analysis

iEEG – invasive Electroencephalography

i.i.d. – independent and identically-distributed

interp – interpolate

IPSP – inhibitory postsynaptic potential

LFP – local field potential

le – left

LOOM – leave one out method

moa – model order above the true one

mob – model order below the true one

MEG – Magnetoencephalography

MRI – Magnetic Resonance Imaging

mV – mili Volt

MVAR – multivariate autoregressive

MRI – magnetic resonance imaging

nf – noise factor

n.s. – not significant

nfn – non-phase neutral filter

OFF – medication off state

ON – medication on state

PCA – principal component analysis

PD – Parkinson’s Disease

PDC – Partial Directed Coherence

pn – phase neutral filter

PSD – Power spectral density

ri – right

RP – random permutation

SNc – substantia nigra pars compacta

SNR – signal-to-noise ratio

SNr – substantia nigra pars reticulata

sPDC – squared Partial Directed Coherence

std – standard deviation

SWA – Schaltenbrand-Wahren atlas

SQUID – Superconducting quantum interference device

STN – Subthalamic nucleus

TD – tremor-dominant

UPDRS – Unified Parkinson's Disease Rating Scale

VAR – Vector autoregression

Abstract

Understanding the processes underlying neural communication is crucial to improve the treatment of neurological diseases, but has been a great challenge in the past. To tackle this issue, the question of causality between certain brain areas and between muscles and brain areas is of great interest. In the past decade several multivariate causality measures based on Granger causality have been suggested to assess causality in systems of neural signals. To date, however, a detailed evaluation of the reliability of these measures and their sensitivity to data preprocessing techniques is largely missing.

The present work systematically evaluates the performance of five different causality measures and its dependence upon data length, noise level, coupling strength and model order. Moreover, the effect of two common numerical methods (bootstrapping and jackknife) to determine the significance threshold for the causality measures was analyzed. Two simulation models were used to generate a controlled environment: one based on artificial data and one based on four different neural data recording procedures (magnetoencephalography, electroencephalography, electromyography,

intraoperative local field potentials). The analysis shows the squared Partial Directed Coherence with the leave one out method to be the most reliable and robust choice for assessing directionality in neural data.

Moreover, the influence of data preprocessing on the working of the causality measures was investigated. In frequency domain analyses (power or coherence) of neural data it is common to preprocess the time series by filtering or decimating. However, in other fields it has been shown theoretically that filtering in combination with Granger causality may lead to spurious or missed causalities. A controlled simulation environment was used to investigate whether this result translates to the multivariate causality methods derived from Granger causality.

The simulation results suggest that preprocessing without a strong prior about the artifact to be removed disturbs the information content and time ordering of the data and leads to spurious and missed causalities. Only if apparent artifacts like a current or movement artifact are present, filtering out the respective disturbance seems advisable. While oversampling the data poses no problem, decimation by a factor greater than the minimum time shift between the time series may lead to wrong inference. Finally, with the simulation results in mind an application of the causality measures to real data demonstrates the usefulness of the simulation results

for practical applications.

Chapter 1

Introduction

Since ancient Greek times, the issue of causality has been of great interest to mankind. Understanding the cause of something helps to understand the nature of this phenomenon, thereby creating deeper knowledge of these processes. Important philosophers pondered about questions like: What is the cause of something and what is its effect? What happened first? The great Greek philosopher Aristotle was one of the first persons to give a formal definition. In the fourth century B.C. he defined four different types of causality: material cause, formal cause, efficient cause and final cause.¹ *Material cause* denotes the physical material of something. The *formal cause* provides an answer to the question why something is named the way it is. The *efficient cause* explains something from its starting or changing point.

¹The definition of the four causes given by Aristotle: "“Cause” means: (a) in one sense, that as the result of whose presence something comes into being – e.g. the bronze of a statue and the silver of a cup, and the classes which contain these; (b) in another sense, the form or pattern; that is, the essential formula and the classes which contain it – e.g. the ratio 2:1 and number in general is the cause of the octave – and the parts of the formula. (c) The source of the first beginning of change or rest; e.g. the man who plans is a cause, and the father is the cause of the child, and in general that which produces is the cause of that which is produced, and that which changes of that which is changed. (d) The same as “end”; i.e. the final cause; e.g., as the “end” of walking is health. For why does a man walk? “To be healthy,” we say, and by saying this we consider that we have supplied the cause.” (Aristotle 350 BC).

The *final cause* is the end, why a thing has been done. The third definition efficient cause comes closest to today's colloquial notion of cause. In contrast to these diverse interpretations of cause, classical physics typically employed a notion of causality based on the linearity of time: Events can only be caused by events preceding them. In the context of time series analysis, the area of interest in this study, Wiener (1956) was the first one to give the notion of causality as a time ordering a rigorous definition: If a signal can be better predicted by incorporating past information from another signal than by only using past information of the first one alone, then the second signal is called *causal* for the first one. As only earlier signals can influence later ones, the direction of causality is determined by this temporal order. Economics nobel laureate Clive W.J. Granger later incorporated this definition into a fully developed statistical framework, a concept that is today known as Granger causality (Granger 1969).

The original concept of Granger causality was a bivariate one, relating two time series to each other. By considering two time series the causal ordering can only be determined correctly, if no other signal is influencing these two signals (Granger 1980), which greatly limits its applicability. Identifying causal orderings has been of long interest in statistics, economics (Hiemstra and Jones 1994, Geweke 1984), political science (Freeman 1983, Reuveny and Kang 1996) or geophysics (Kaufmann et al. 2004, Elsner 2006), but was mostly restricted to bi- or trivariate cases.² Further interest has been on the development of concepts in the frequency domain (Geweke 1982, Hosoya 1991, Breitung and Candelon 2006, Chen et al. 2006), because many phenomena naturally lend themselves to interpretations in the frequency domain. In subsequent years, several researchers have tried to extend this idea of

²In the trivariate case, multiple triplet testings could be used, with the third signal, the reference signal being a composite of the other signal to control for (Zhou et al. 2008). While possible, this approach becomes very cumbersome with a large number of signals.

frequency based causality analysis to the analysis of multi-channel data by employing multivariate autoregressive models (MVAR) (Kaminski and Blinowska 1991, Baccala and Sameshima 2001, Astolfi et al. 2006, Korzeniewska et al. 2003). Only recently major advances have been achieved in neuroscience where truly multivariate methods have been developed (Astolfi et al. 2006, Baccala and Sameshima 2001). These methods have two advantages compared to the bi- or trivariate Granger causality analysis: First, they allow to analyze larger networks. Second they often allow to distinguish between direct and indirect causation. A direct causation exists, if information directly flows from A to B without an interim station C. In contrast, if information flow from A to B is mitigated via signal C, there still exists a causation from A to B, but it is only indirect, with the direct causation from A to C and from C to B. These two cases are depicted in figure 1.1.

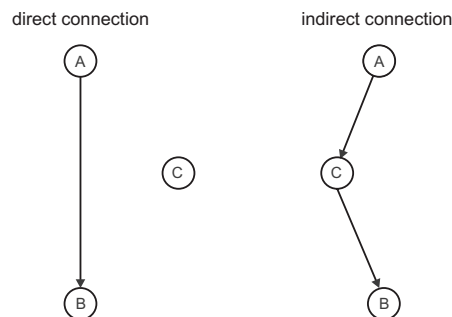


Figure 1.1: A direct and an indirect connection: In the case of a direct connection the information flow is from A to B without an interim station, whereas in the case of an indirect connection the information flow is from A to B via C.

All these new multivariate measures, which will be described in detail later on, are based on Granger causality. This statistical concept of causality must not be

confused with actual causality, as they need not necessarily imply each other.³ Of course, the appeal of Granger causality is that, when correctly applied with the correct information set, it should be able to capture actual causality. In the following we will use the terms “causal” and “causality” in the sense of the Wiener/Granger definition and usually omit the word “Granger”.

Developing accurate multivariate causality measures is particularly important for neuroscience, because they can help to understand the processes underlying neural communication enabling, for example, our motor control system, processes which to date still remain poorly understood. Accordingly, neuroscientific research has identified neural oscillations as a key mechanism for large-scale communication in the human brain and in the human motor system (Singer 1999, Buzsaki and Draguhn 2004). Oscillatory communication has also been reported between brain areas and the spinal motoneuron pool in a variety of tasks. For example, during a simple lifting of an arm, coherence⁴ can be observed between primary sensorimotor cortex, the brain area presumably responsible for that movement, and muscle activity (Conway et al. 1995, Gross et al. 2000). Likewise, a number of studies support the hypothesis that changes in oscillatory interactions (in terms of frequency or strength of interactions) may lead to movement disorders (Brown and Marsden 1998, Timmermann et al. 2007). Indeed, pathological oscillatory interactions have been identified in movement disorders such as essential tremor (Schnitzler et al. 2009) or Parkinson’s disease (Volkman et al. 1996, Timmermann et al. 2003). These pathological

³This is particularly relevant in the social sciences where research often deals with agents forming expectations. People may correctly anticipate the future of some variable X and adapt choice variable Y in response. However, a researcher looking at the relation between X and Y will, when not taking expectations into account, erroneously conclude that Y Granger causes X. While researchers in neuroscience usually do not deal with such kind of problems, this example warns about wrong inference when considering relationships between the wrong data series.

⁴Coherence determines the strength of a linear relationship between two signals by using the cross-spectral density of these two signals (Halliday et al. 1995).

changes are evident in neural activity recorded with electroencephalography (EEG) or magnetoencephalography (MEG), techniques described in Chapter 2. Traditional analysis usually quantified frequency-specific interactions using coherence (Volkmann et al. 1996, Timmermann et al. 2003). Unfortunately, coherence does not provide any information about the directionality or causality of the interaction, i.e. it cannot determine, if brain area A drives area B, B drives A or if there is a bidirectional interaction. But the causality of an interaction is a crucial aspect for the interpretation of these connectivity studies. Consider the case of Parkinson’s disease where a large fraction of patients develops tremor. Older studies found coherence at the tremor frequency between a brain area and an affected muscle. However, these studies were not able to distinguish, whether the brain area drives the tremor or if the coherence was driven by sensory feedback (e.g. the patient feels or sees his extremities trembling).

Multivariate causality measures could solve this problem due to their ability to analyze causality in brain networks (Ploner et al. 2009, Astolfi et al. 2006). They can help to distinguish the direction of information flow and to identify which pathologically changed brain area drives the symptoms. However, current research is only at the beginning of understanding the causality measures and how they work. Accordingly, much of the current research is still largely influenced by experience with classical methods of frequency analysis like coherence or Fourier transformation (Brovelli et al. 2004, Sharott et al. 2008, Wang et al. 2007, Bollimunta et al. 2008). The present work aims at a first comprehensive evaluation of the performance and applicability of these multivariate causality measures under different circumstances. This encompasses two related aspects: First, the preprocessing of recorded data, because for example filtering techniques that may be harmless for traditional frequency analysis may interfere with the working of causality measures. Second, the computation of a significance threshold, because usually numerical methods have to be used and

their behavior could influence the results. The goal of this work is to develop recommendations for applied research about how to process the data and which causality measure with which significance computation method to use for a certain type of data.

Before being able to apply causality measures to the data, these data have to be recorded. There are several methods currently available. In order to understand the particular characteristics of these methods first the electrophysiological origin of neural signals will be described in chapter 2 before describing how these signals can be recorded invasively with macroelectrodes and non-invasively with EEG and MEG. A particular focus will be on a detailed comparison of these methods. To be able to analyze motor control and deal with the question which brain area causes movement and which brain area receives sensory feedback, this chapter also explains how muscle activity is recorded with electromyograms.

In the third chapter possible analysis techniques to determine causality are presented. First, as the point of departure the concept of traditional Granger causality is introduced and formally defined. Second, the statistical framework of autoregressive modeling that is required for estimating both Granger causality and the multivariate causality measures based on this concept is presented. Third, it is described how the new multivariate causality measures under consideration - the Directed Transfer Function (DTF), the direct Directed Transfer Function (dDTF), the Partial Directed Coherence (PDC), the squared Partial Directed Coherence (sPDC) and the transfer function (H) - are defined and computed from the estimated autoregressive coefficient matrices. The present work will subsequently analyze the performance of these techniques. In contrast to Granger causality where a simple analytical significance measure for testing the null hypothesis of no causality is readily available, this is currently not the case for most multivariate causality measures. Fourth, two numerical

procedures for deriving significance thresholds from surrogate data, the leave one out method (LOOM) and random permutation (RP), are introduced.

In chapter 4 a framework to statistically evaluate the performance of the different causality measures is developed. In order to test and compare the performance of the causality measures, two different simulation models are introduced that generate a data set with a predefined causality structure. These models allow to evaluate the performance of the respective measures by analyzing the number of false positive (spurious) and missed causality detections while varying certain important parameters of the data and the autoregressive estimation. In a second step, theoretical considerations are presented about the effects of data preprocessing like the one that is commonly used in neuroscience to reduce the frequency spectrum of the data. It will be shown that filtering the data in general leads to spurious and missed connections when applying Granger causality and that this behavior should transfer to the multivariate causality measures.

Based on these theoretical considerations, a first simulation study is carried out in chapter 5 that traces out the effects of different commonly used data preprocessing techniques on multivariate causality analysis. In particular, different common filter types for the case of low- and high-pass filtering and notch filters of different filter orders are considered. In addition, the influence of a reduction and an increase in the sampling rate of the data relative to the true data generating process is tested. Consistent with the hypotheses derived from the theoretical considerations in chapter 4, preprocessing without removing an artifact present in the data generally leads to wrong inference about causality. Based on these results, guidelines for data processing prior to the application of causality measures are developed.

In addition to correct preprocessing, knowledge about which method to apply under certain parameter configurations of the data is essential for a reliable causality analysis. In particular, it is important to know the limiting parameters of such an analysis. Chapter 6 performs a second simulation study to systematically evaluate and compare the performance of the existing multivariate causality measures when varying parameters such as the data length, the model order of the autoregressive model or the signal-to-noise ratio (SNR). Moreover, the influence of using different data types and different significance measures is analyzed. This second simulation shows that some causality measures in combination with particular data types and significance measures perform better than other combinations. Overall, the sPDC with the LOOM turns out to be the most reliable and robust causality measure for most data types and parameter ranges.

In chapter 7 the usefulness and importance of the simulation results as derived before is demonstrated by a causality analysis of a neural data set from Parkinson's disease patients. Based on the results of the previous chapters, the causality measure that showed the best performance in chapter 6, the sPDC with LOOM, is applied to the data set that has been preprocessed according to the guidelines of chapter 5. The well known Albin-DeLong model (Albin et al. 1989, DeLong 1990), which describes causal connections between dysfunctional movements and specific brain areas in Parkinson's disease patients, is used to generate predictions about causality patterns between certain neural areas and arm muscles. Testing of these hypotheses suggests that actual causality patterns do only partially follow the predictions of the model and that a modification of the Albin-DeLong model may be necessary.

Finally, the results of the two simulation studies are summarized in chapter 8 and specific advice on the usage of the causality measures is provided. Furthermore,

the implication of the present work for future applications is discussed and possible directions for future research are pointed out.

Chapter 2

Neurophysiological Methods to Invasively and Non-Invasively Record Neural Activity

In the present work causality measures for the application to neural data are tested and applied. Specifically, we test for causality between a system of neural signals and signals from arm muscles. Thus, it is important to understand the origin and recording of these signals. Neuronal activity is either recorded from the outside of the head using electroencephalography (EEG) or magnetoencephalography (MEG) or invasively close to their origin with micro- or macroelectrodes. EEG and macroelectrodes both measure the electric potentials outside or inside the brain, respectively, while MEG measures the magnetic induction of the neuronal currents from the same origin. But where are the electric potentials and the magnetic induction generated and how can they be recorded?

Section 2.1 describes the origins of neural signals, before section 2.2 explains the currently available methods to record neural activity. Section 2.3 finally describes the electromyography, the method of choice to record muscular activity.

2.1 Origin of Neural Signals

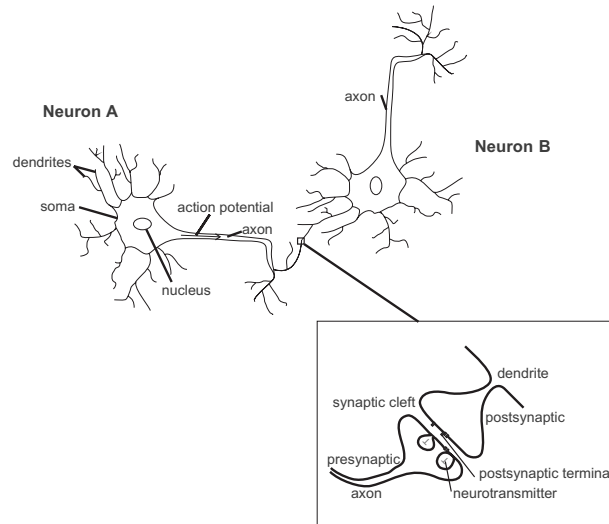


Figure 2.1: Scheme of two neurons: Neuron A transfers information to neuron B through the axon. In the magnified part of the figure a synapse between these two neurons is shown.

The human brain consists of about 10^{10} neurons (Hallez et al. 2007), which are excitable cells with characteristic intrinsic electrical properties. Communication between these neurons is mediated by electrochemical processes, whereby these cells produce electrical and magnetic fields that can be measured even at a distance from the sources (Lopes da Silva 2004). Each neuron has one axon that transfers information via synapses to other neurons. Moreover, it has up to thousands of dendrites for receiving signals from other neurons. The dendrites obtain their information through synapses. Figure 2.1 schematically shows signal transmission between 2 neurons. To transfer a signal through the synaptic cleft from one neuron to another, a neurotransmitter like glutamate, γ -aminobutyric acid (GABA) or dopamine is emitted from the first neuron A and received from the dendritic part of the synapse of the second neuron B

2.1. ORIGIN OF NEURAL SIGNALS

(Kumar and Gilula 1996).

If a neuron receives such a stimulus, its resting membrane potential, the potential difference between the inside and the outside of a cell membrane (about -70 mV), is increased. If this increase is above the threshold of -45 mV, an *action potential* is produced. This increase in membrane potential leads to an activation of the voltage-controlled sodium channels (channels through which Na^+ can flow), so that Na^+ ions flow into the cell body from the extracellular fluids. These sodium channels close, when the potential becomes positive. If this is the case, K^+ ions flow out of the cell through the now open potassium channels until the initial resting membrane potential is reached again. This whole fast sequence of depolarization and repolarization is called *action potential*. The typical time line of an action potential is shown in figure 2.2. These action potentials, which last for about 1–2 ms, induce the emission of a neurotransmitter through a chemical synapse of the emitting neuron's axon, as shown in figure 2.1 (Millhorn et al. 1989).

When neurotransmitters are released to the synaptic cleft, i.e. the gap between the axon of neuron A and the dendrite of neuron B, and reach the postsynaptic terminal, i.e. the synapse at the dendrite of the next neuron, the membrane potential of neuron B in figure 2.1 is changed. This induces a so called *postsynaptic potential* due to ionic currents. A postsynaptic potential is called *inhibitory postsynaptic potential*, if the membrane potential is further reduced by the ions, so that an action potential becomes less probable. In contrast, in case of an *excitatory postsynaptic potential* the membrane potential is further increased, thereby making the initiation of an action potential more probable. One postsynaptic potential lasts for about 10 to 100 ms. Signals measured with MEG, EEG and macroelectrodes are due to these ionic currents induced by postsynaptic potentials.

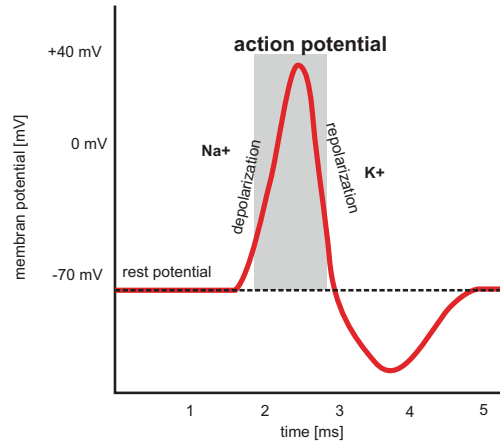


Figure 2.2: Action potential: The time course of depolarization and repolarization during one action potential (modified from (Kandel et al. 2000)).

To evoke the transmission of a signal to another neuron, the arriving postsynaptic potentials have to generate an action potential in this neuron. However, usually one arriving postsynaptic potential is not sufficient to lower the membrane potential of a cell to a threshold that is low enough to generate an action potential. Only the synchronous activation through action potentials from many neurons that induce postsynaptic potentials leads to the generation of a new action potential in another neuron and hence to a signal transfer. This threshold filters the information transfer. Thus, synchronization and desynchronization of neural activity are important for the integration and processing of information and neural communication (Varela et al. 2001, Schnitzler and Gross 2005).¹

¹Rhythmic activity is the result of the complex interaction between intrinsic oscillatory properties of specific neurons embedded into neural networks, synaptic interactions and signal inputs to these systems (Lopes da Silva 1991). This study cannot go into detail about how exactly oscillatory activity develops. Good starting points are (Lopes da Silva 1991, Buzsaki and Draguhn 2004).

2.2 Description of Recording Methods

In order to understand the brain's function synchronization and desynchronization must be studied. This can be achieved by means of analyzing oscillatory activity of cell groups, which reflects the synchronization and desynchronization of numerous neurons. But before being able to analyze the data, they have to be recorded. To better understand this step, different recording procedures will be presented in the following. In order to provide an overview of the four different recording methods used in this work a summary of these methods is given in table 2.1.

2.2.1 Macroelectrode Recordings

The first possibility to measure neural activity is to invasively place macroelectrodes into the brain region of interest. Such electrodes are called macroelectrodes, because they have a greater diameter than so called microelectrodes. Macroelectrodes not only measure the activity of one neuron, but the sum of membrane potentials of neurons within a region of tissue (Freeman 1975). The signals recorded with a macroelectrode are called *local field potentials* (LFP). A sample local field potential is shown in figure 2.3. A LFP represents the summation of excitatory postsynaptic potentials (EPSP) and inhibitory postsynaptic potentials (IPSP) of various neurons. Macroelectrode recordings usually have a time resolution of about 2500 Hz.

In the setup used for the present study, the local field potentials are measured with a macroring of 0.8 mm diameter of a combined micro- macroelectrode (see figure 2.4). The microelectrode is a high impedance electrode (at about 1-2 M Ω) made of tungsten, which records extracellular single cell activity. The macroelectrode is a low impedance electrode (at about 1 k Ω) that records LFPs and consists of stainless steel. For LFPs from low impedance microelectrodes the actual size of the tissue,

Table 2.1: Comparison of the different measurement methods

	invasive LFPs	EEG	MEG	EMG
Equipment	about 5 macro-electrodes	up to 256 electrode sensors	about 300 detectors	2 electrodes per lead
Coverage	restricted to invasive target point	whole head	whole head	local - muscle of interest
Measured Activity	electric potential of EPSPs and IPSPs	electric potential of EPSPs	magnetic induction of EPSPs	electric potentials of motor activity
Sources	very flexible, not restricted to cortex	mainly restricted to cortex	mainly restricted to cortex	“synchronized” muscle cells of interest
Source Orientation	radial and tangential	radial and tangential	tangential	radial and tangential
Spatial Resolution	very accurate (about 1 mm)	not homogeneous over the brain; good on the cortical surface	not homogeneous over the brain; good on the cortical surface; ability to localize deeper structures	accurate; depends on electrode placement
Sampling Frequency	≤ 0.4 ms	≤ 1 ms	≤ 1 ms	≤ 0.4 ms
Applicability	patients with indication for deep brain stimulation	healthy humans and patients	healthy humans and patients	healthy humans and patients

2.2. DESCRIPTION OF RECORDING METHODS

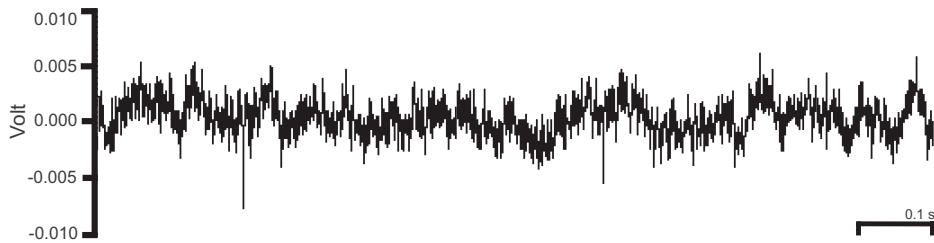


Figure 2.3: Sample recording of a local field potential obtained with an invasive macroelectrode

from which the postsynaptic potentials are recorded, has been determined recently to be in the range of $250 \mu\text{m}$ around the recording electrode (Katzner et al. 2009). As the diameter of the macroelectrode is substantially larger than the diameter of a microelectrode, it is very likely that the macroelectrode used in the present work records membrane potentials from a larger area of tissue than has been described by Katzner et al. (2009). This is important for interpreting the real data results obtained from LFPs in chapter 7.

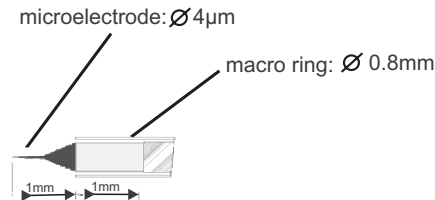


Figure 2.4: Tip of the combined micro- and macroelectrode

The distinct advantage of macroelectrode recordings is that the local field potentials are recorded closely at their origin, which makes the localization of the recorded signal very accurate. However, the main disadvantage of this recording procedure is the invasive nature, which limits its applicability: LFPs can only be recorded during the implantation of an electrode for deep brain stimulation (DBS) to treat movement

disorders (Kühn et al. 2005) or in animal studies (Brovelli et al. 2004).² This makes, at least in humans, a comparison to healthy brain activity impossible. For such comparisons, non-invasive recording procedures are needed, which are described next.

2.2.2 Electroencephalography (EEG)

Electroencephalography (EEG) (Berger 1929) was the first method to non-invasively measure neural activity.³ EEG measures the electrical activity of apical dendrites of large pyramidal neurons in the cerebral cortex (see figure 2.5).⁴ This activity originates when excitatory synaptic input activates the apical dendrites. Due to the resulting potential difference, an extracellular current flows from other sites of the dendrite, the current source, into the active and hence depolarized site, the current sink. If the active site of the dendrite is in a deep layer in the cortex, the current flows from the tip of the dendrite to this area, giving rise to a surface-positive and depth-negative electrical field distribution relative to the cortical surface. The EEG system measures this neural activity at the surface of the head by recording the electric potential difference between two EEG sensors (Niedermeyer and da Silva 2005). To be able to pick up neural activity at the scalp, thousands of apical dendrites or neurons that are aligned in the same orientation have to be activated simultaneously as the signals would otherwise cancel out each other (Shibasaki 2008). Hence, EEG signals reflect the summation of the synchronous activity of macrocolumns

²DBS is a surgical procedure, in which stimulation electrodes are placed in a certain target area.

³Related to this procedure is the intracranial EEG (iEEG), which is also called electrocorticography (ECoG) or subdural EEG (SD-EEG). In this case, EEG electrodes are placed subdurally near the surface of the brain, but in contrast to macroelectrode recordings not inside of the brain. This procedure is sometimes used for patients suffering from drug-resistant epilepsy, where the location of the seizure focus is unclear. Patients undergo invasive monitoring to localize the focus (Caplan et al. 2001, Cascino et al. 1993, Sederberg et al. 2003, Schindler et al. 2007). Apart from the better localization, these recorded signals are not different from traditional EEG and are thus not considered separately.

⁴The subsequent description follows Shibasaki (2008).

2.2. DESCRIPTION OF RECORDING METHODS

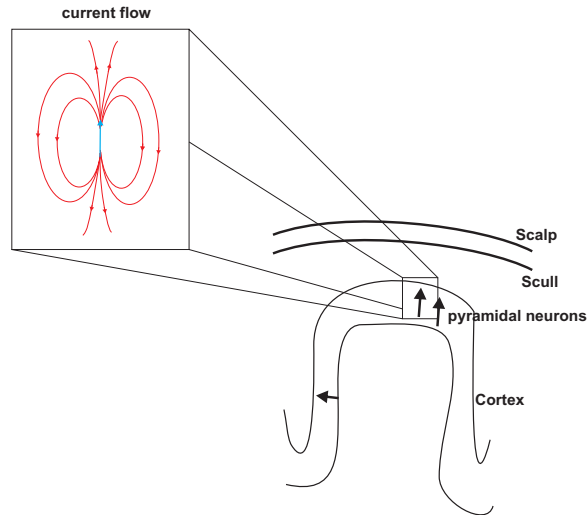


Figure 2.5: Pyramidal neurons in the cortex and their current (modified from Baillet et al. (2001))

of thousands of spatially organized large pyramidal cortical neurons and represent the spatial and temporal average of the activity of these macrocolumns (Lopes da Silva 2004). The current density of neural sources has the order of 100 nA/mm^2 (Hamalainen et al. 1993). This current density is high enough to be detectable with standard electric sensors. The recorded signals are mostly due to excitatory synaptic activity as IPSPs are usually not recorded with EEG due to their small extracellular currents (Shibasaki 2008). Figure 2.6 shows an example of an EEG signal.

Regarding the recording setup, the EEG sensors are usually either placed with a cap on the subject's head (see figure 2.7) or are directly glued onto it. Nowadays the brain activity is measured with up to 256 electrodes placed on the subject's head. However, placing all electrodes on the subjects head and achieving a low impedance with conductive gel or paste at each electrode can take up to 2 hours. The time

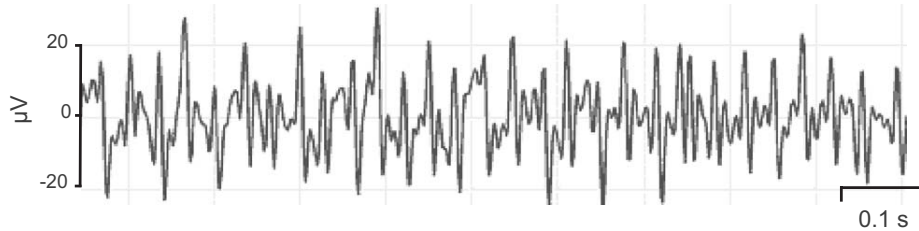


Figure 2.6: Electroencephalographic recording from one sensor

resolution of an EEG system is about 1 ms, making it possible to record the neural activity with its actual timing.

A main challenge of EEG recordings is to relate the signal measured by the sensors on the skull to the respective brain area. The usual approach to this problem combines the forward model (Hallez et al. 2007) and solving the inverse problem (Grech et al. 2008, Mosher et al. 1999). On the one hand, the *inverse model* works backward from the scalp potential recordings to estimate the sources within the brain potentially giving rise to these signals. Unfortunately, this solution is usually non-unique as there are usually fewer signals recorded than there are electrical sources generating these signals (Plonsey 1963) and the solution can be unstable⁵ (Grech et al. 2008, Pascual-Marqui 1999). On the other hand, the *forward model* works from the opposite site. Starting with the assumption of a particular source configuration that may be responsible for the recorded signals - usually based on the researcher's priors - the predicted electrical distribution on the scalp is calculated.⁶ This prediction is compared to the possible solutions of the inverse model. The inverse problem can then be solved through an iterative process by modifying the assumptions of the

⁵Unstable means that the solution is highly sensitive to small changes in noisy data.

⁶Therefore Maxwell's equations in the quasi-static approximation are used, as most EEG measurements commonly deal with frequencies below 100 Hz (Baillet et al. 2001). The current densities at a point \mathbf{r}' are related to the measurable potential $V(\mathbf{r})$ by solutions of the Poisson equation (Hallez et al. 2007).

2.2. DESCRIPTION OF RECORDING METHODS

forward solution and comparing its results with the possible solutions from the inverse model. This process is repeated as long as the solutions of the inverse problem are improving. In the end the source, which best describes the measured EEG activity, is determined.⁷ After the source configuration has been determined, a single time series for this particular source is constructed from the measured channels. Furthermore the source can be projected on a magnetic resonance image (MRI) of the brain to determine its actual anatomic location.



Figure 2.7: An electroencephalography cap with 128 electrodes

Following other studies, which applied causality measures to EEG measurements (Kus et al. 2004, Kaminski et al. 2001), the present work only considers recordings from single channels without making projections onto the source space. Introducing

⁷To determine solutions of the inverse problem numerous methods have been developed, which all have their advantages and disadvantages. For a current overview and comparison of the methods compare (Grech et al. 2008). For a good introduction into the matter compare (Koles 1998).

the issue of space projections, while adding to the reality of the simulations, would complicate the simulations additionally without materially affecting the results. The single channel recordings can be attributed to brain activity in the vicinity of the respective electrode.

2.2.3 Magnetoencephalography (MEG)

Magnetoencephalography (MEG) (Cohen 1968) is closely related to the EEG as it measures the magnetic field of the changes in the local field potentials. Like in the case of the EEG, MEG measures EPSPs and not IPSPs (Shibasaki 2008). However, in contrast to EEG also the intracellular current flows from the activated site to other sites of the apical dendrite are important. With a resolution of about 1 ms its temporal resolution is as good as the one of EEG. However, the amplitude of the magnetic field from neural sources can be as low as $50 - 500 * 10^{-15}$ Tesla (Hamalainen et al. 1993) and the strongest magnetic signals have also only an amplitude of a few pico Tesla.

To measure such low magnetic fields, superconducting quantum interference devices (SQUIDs) have to be used (Zimmerman and Thiene 1970). The working temperature of SQUIDs is about 4-5 K. Therefore they have to be cooled with liquid helium in the helmet in order to keep them superconducting (Hamalainen et al. 1993). Moreover, the recording has to be shielded from external magnetic fields, as for example the earth magnetic field is about 8-9 magnitudes larger. Thus, MEG measurements always have to be made in shielded rooms. An example of a MEG signal is shown in figure 2.8.

Today MEG systems consist of up to 300 detectors, all placed in a single helmet. They are placed in such a way that they cover the subject's head uniformly with a distance of about 2 cm. In contrast to the EEG, the helmet has simply to be placed

2.2. DESCRIPTION OF RECORDING METHODS

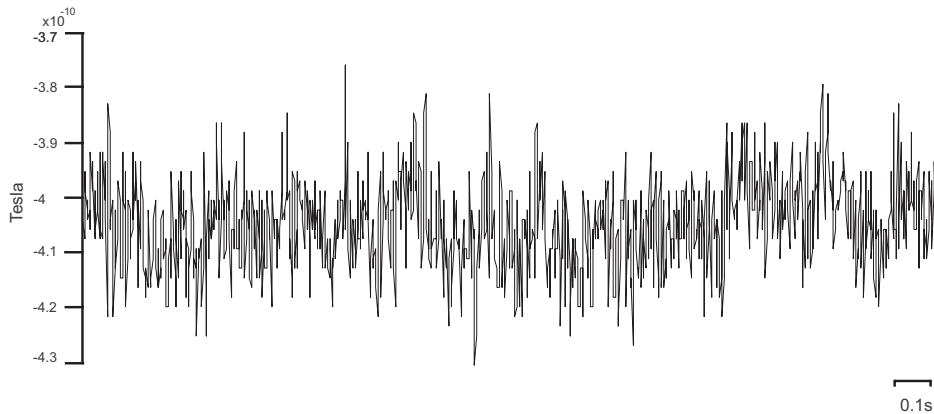


Figure 2.8: Magnetoencephalographic recording of one sensor from a 122-channel MEG system

above the subjects head and no further fixation is necessary. Hence, the preparation time of a MEG measurement is much shorter.

Similar to EEG, MEG measures brain activity from outside of the head. In order to localize the origin of the magnetic field, again the inverse problem has to be solved.⁸ However, as the magnetic field is hardly influenced by the inhomogeneous conductivity structure of the human skull and scalp (Haueisen et al. 1995), there is no “shunting effect”. Thus, the situation for solving the forward and inverse problem in order to find the underlying sources is theoretically better than compared to EEG (Shibasaki et al. 2007) besides the problem that MEG is blind to radial components. Since radial components of an electric dipole produce no magnetic field outside a spherically symmetric volume conductor (Sarvas 1987), MEG signals mainly originate from the sulci (a fissure between two convolutions of the brain) of the human cortex (Cohen and Cuffin 1983).

⁸Instead of solving the Poisson equation Biot-Savart’s law is solved to determine the magnetic induction outside the head resulting from the current density in the brain (Baillet et al. 2001).

2.2.4 Comparison of the Recording Methods

Three different recording methods have been introduced in the previous parts of this section. While they all measure neural activity, each method has its distinct advantages and disadvantages. Hence, a particular measure might be best suited for a particular application. All three measures have a very good temporal resolution, which allows to record neuronal processes on their actual time scale. Differences between the methods mainly arise in their ability to record signals from deeper brain areas and their accuracy to localize the source of the signal.

While EEG and MEG both record the signals from outside of the head, macroelectrodes record the LFPs invasively inside the brain. This allows for a very accurate localization with the macroelectrodes and the possibility to record activity from any region in the brain. However, in humans these recordings are only practical in patients undergoing an implantation of a deep brain stimulation electrode or neurosurgery to remove a tumor. Thus, the recording sites are essentially limited to the target points of deep brain stimulation.

The distinct advantage of using EEG or MEG measurements is that they require no operation and are thus not limited to patients, but can also be safely performed with healthy humans. Unfortunately, there are two important drawbacks. One drawback of EEG and MEG is that they usually have low signal-to-noise ratios (SNR), because the activity is non invasively measured at some distance from the source. Thus, the LFPs recorded by EEG and MEG usually originate in the cortex, as the SNR for deeper structures is even lower (Shibasaki 2008, Nunez and Srinivasan 2006).⁹

⁹However, some authors have reported recordings of deeper cortical structures like the hippocampus

2.2. DESCRIPTION OF RECORDING METHODS

As both EEG and MEG measure the signals outside the head, the recorded signals are commonly projected back to the human brain. In order to localize the sources first the forward model and then the inverse problem have to be solved. Due to the inhomogeneous conductivity structure of the human head the problem of source localization, in particular for deeper sources, can be better solved for the MEG.¹⁰ However, MEG is only able to measure the tangential components of the neural activity and thus the sources are mostly restricted to the sulci of the human brain. Therefore combining simultaneous recordings of EEG and MEG data can complement each other effectively (Shibasaki 2008).¹¹

A particular problem of MEG is the generally low signal-to-noise ratio due to the low strength of the measured magnetic fields relative to external noise sources. To improve this signal-to-noise-ratio, time-domain averaging of dozens of trial repetitions is usually advocated (Hillebrand et al. 2005). EEG on the other hand is not as sensitive to noise, as the signals are not as small as those of MEG and thus requires less shielding efforts. Furthermore the usage of EEG is more flexible, as it can be obtained on a moving subject and not only in the shielded room with the fixed MEG system. Lastly, due to higher purchase prices and higher maintenance costs MEG systems are not as widely available as EEG systems.

(Tesche and Karhu 2000), the thalamus (Tenke et al. 1993, Llinás et al. 1999, Rosanova et al. 2009) and the cerebellum (Tesche and Karhu 1997).

¹⁰Lopes da Silva indicates that a simple homogenous sphere model of the volume conductor may be sufficient for MEG recordings to achieve a satisfactory solution (Lopes da Silva 2004). When the shape of the head is not known, current localization methods achieve maximum errors of 10 mm for EEG and 15-20 mm for MEG. The lower localization error of the EEG is claimed to be due to the flexible cap that at least partially adjusts to individual head shapes. Recent efforts to create more realistic models of the human head may improve the performance of both methods. If the head shape was considered the MEG performed better (von Ellenrieder et al. 2009).

¹¹The combination of invasive procedures like iEEG and macroelectrode implantation and non-invasive procedures like EEG and MEG may also deliver an important cross-validation that could help to improve the localization algorithms to mitigate the inverse problem (Dalal et al. 2009, Benar et al. 2006).

2.3 Muscle Activity Recording: Electromyography (EMG)

Electromyography (EMG) allows to measure electric potential variations induced by muscle activity. This can either be done with a needle, i.e. intramuscular, or surface electromyogram. It records the summation of muscle action potentials. An action potential which arrives at the neuromuscular junction from the brain via the spinal cord, activates the voltage-controlled calcium and sodium channels of the muscle fibers. Thereby a muscle action potential is induced, which depolarizes the muscle membrane. Through an electro-mechanical coupling this leads to a contraction of the muscle fibers. Usually one motor neuron does not activate only one muscle fiber, but several. The entity of a motor neuron and its innervated muscle fibers is called motor unit (see figure 2.9) (Guyton and Hall 2006).

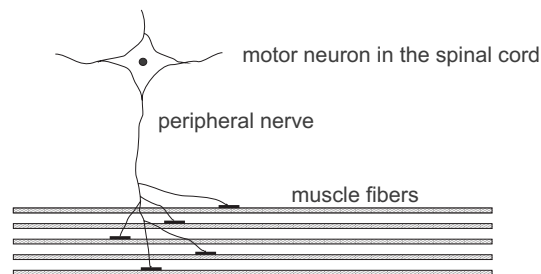


Figure 2.9: Motor unit: One motor unit consists of the shown motor neuron and its innervated muscle fibers

The surface EMG records a summation of motor action potentials of these motor units. The more motor units are activated, the higher the amplitude of the EMG. In the present work muscle activity is recorded during rest and tremor. A sample electromyogram of a tremor period is shown in figure 2.10.

2.3. MUSCLE ACTIVITY RECORDING: ELECTROMYOGRAPHY (EMG)

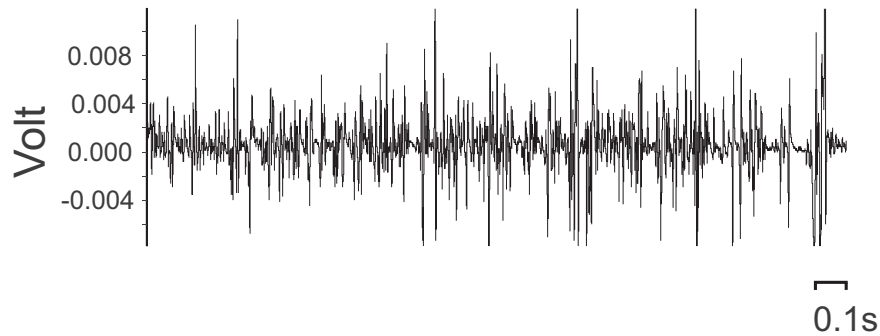


Figure 2.10: Surface electromyogram recorded during tremor

EMG achieves a time resolution below 1 ms. The recorded signals have an amplitude of up to 0.5 mV (Reaz et al. 2006). The muscle activity is recorded with two surface electrodes, i.e. one surface electromyograph records potential differences with reference to another electromyograph. This reference electromyograph should be placed over a silent area, so that the potential of this electrode is zero (Bischoff et al. 1999). The "active" electromyograph is then placed on the muscle of interest. Hence, localization can be performed as accurate as the placement of the electromyograph on the muscle. In order to actually record muscle activity it is very important to place the surface electrodes correctly on the muscle. Otherwise EMG picks up noise or muscle activity from neighboring muscles. In addition, one has to consider that "shunting effects" like for the EEG are present on the skin surface (De Luca 1997). Like all other methods considered in the present work, EMG is sensitive to artifacts, which can arise from cable movements and the power line artifact. A better signal-to-noise ratio can be achieved by needle electromyographs, but these are typically only used for clinical applications.¹² Furthermore they record only the activity of some muscle fibers and not the activity of a whole muscle. Accordingly, in the present work only surface

¹²For a comprehensive overview on EMG recordings and possible problems see De Luca (1997).

EMG was used.

Causality and Directionality Measures – Theoretical Background

For the analysis of neural data different techniques have been used in the past (see figure 3.1).¹ Usually the analysis of the data is performed in the frequency domain in order to characterize the oscillatory activity of the signals (Schnitzler and Gross 2005, Timmermann et al. 2007, Singer 1999). Two groups of analysis techniques are widely used: parametric and non-parametric methods. An example of a non-parametric approach is the Fourier Transform (FT) (Brillinger 1983) where the signal is transformed into the frequency domain. In contrast, a (semi)parametric approach is to estimate an autoregressive model. While the FT is another mathematically equivalent representation of the actual data, with an autoregressive model, a model is fitted to the data in order to extract their main characteristics.

¹The boundaries between the different analysis techniques are increasingly becoming blurred. For example, Fourier based approaches have been suggested to non-parametrically estimate Granger causality (Dhamala et al. 2008a, Dhamala et al. 2008b). However, as these approaches are still in their infancy, the present work concentrates on the classical autoregressive modeling.

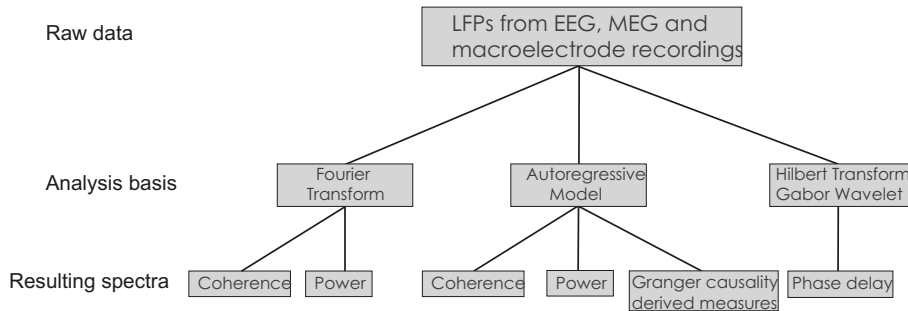


Figure 3.1: Review of the currently applied analysis methods for local field potentials

The aim of the present work is to identify the directionality between two signals. To date, most studies in neuroscience concentrate on identifying dominant frequencies with Power spectra (Brillinger 1983) or identifying coupling between two brain sources or between a brain source and muscle activity. In these studies coherence was commonly applied. Coherence is calculated from the cross-spectra of two time series, so that a correlation in the frequency domain between two time series can be determined (Halliday et al. 1995). However, with coherence an identification of the direction of coupling between two sources is not possible.

Hence, several methods to identify directionality have been developed in the last decade. One approach to detect the direction of an oscillatory coupling between different brain areas or between a peripheral muscle and a brain area is to compute the phase difference between these signals (Gross et al. 2000). Unfortunately, one disadvantage of phase delay calculations is that the direction cannot be determined with certainty, since the phase shifts are all projected to the unit circle.² Thus, recently methods based on the notion of Granger causality (Granger 1969, Wiener 1956), originally used in economics, were introduced to neuroscience (Baccala and Sameshima 2001, Korze-

²The maximal phase delay between two time series which can be distinguished is 2π . A real phase difference of e.g. 2.1π is represented as 0.1π .

3.1. PHASE DELAY

niewska et al. 2003).

In section 3.1 the concept of phase delays will be explained. Afterwards the basics of autoregressive modeling and the assumptions needed for a proper model estimation are presented in section 3.2. In section 3.3 the calculation of Granger causality is developed and its multivariate extensions in the frequency domain are explained. Finally, in section 3.4 two numerical significance thresholds for the multivariate causality measures will be introduced.

3.1 Phase Delay

Computing the phase delay between two time series was one of the first approaches to infer directionality in neural data. The intuition of this approach is simple: The leading signal is interpreted as being responsible for the shifted one. The phase difference between two signals x and y can either be determined by convolution with a complex Gabor wavelet or by using the Hilbert transform, which will both be explained shortly in the following.³

The phase difference is determined with Gabor wavelets from the coefficients W_x at time τ and frequency f of the wavelet transform of the signal $x(t)$ (Le Van Quyen et al. 2001):

$$W_x(\tau, f) = \int_{-\infty}^{+\infty} x(t) \Psi_{\tau, f}^*(t) dt \quad (3.1)$$

With $*$ the complex conjugate is denoted, so that $\Psi_{\tau, f}^*$ is the complex conjugate of

³Both methods are fundamentally equal (Le Van Quyen et al. 2001).

the following Morlet wavelet:

$$\Psi_{\tau,f}(t) = \sqrt{f} \exp(i2\pi f(t - \tau)) \exp\left(-\frac{(t - \tau)^2}{2\sigma^2}\right) \quad (3.2)$$

This is the product of a sinusoidal wave at frequency f with a Gaussian function centered at time τ and standard deviation σ . The phase difference $\varphi_y - \varphi_x$ between the two signals x and y is then determined from the angles of the wavelet coefficients:

$$\exp(i(\varphi_y(f, \tau) - \varphi_x(f, \tau))) = \frac{W_x(\tau, f)W_y^*(\tau, f)}{|W_x(\tau, f)||W_y(\tau, f)|} \quad (3.3)$$

The second method, the Hilbert transform, separates a signal $x(t)$ into its instantaneous phase $\varphi(t)$ and amplitude $A(t)$. The analytic signal $\zeta(t)$, which is a complex function of $x(t)$, is defined by (Rosenblum et al. 1997, Gabor 1946):

$$\zeta(t) = x(t) + i\tilde{x}(t) = A(t)e^{i\varphi(t)} \quad (3.4)$$

with $\tilde{x}(t)$ being the Hilbert transform of $x(t)$, given by:

$$\tilde{x}(t) = \frac{1}{\pi} P.V. \int_{-\infty}^{+\infty} \frac{x(u)}{u - \tau} d\tau \quad (3.5)$$

P.V. indicates that the integral is taken as a Cauchy principal value. By subtracting the phases of both signals and projecting it to the unit circle a distribution of the phase differences (modulo 2π) is obtained.

Regardless of the method used the phase difference can then be transformed into a time difference, yielding a time delay between two signals. Due to the projection onto the unit circle an ambiguity of 2π arises in the phase delay (Gross et al. 2000). One further has to note, that this procedure only works for a narrow frequency band, as it is determined for one frequency. Thus, the signals have to be band-pass filtered

3.2. AUTOREGRESSIVE MODELING

before determining the phase delay. Usually a band pass filter of ± 2 Hz around the frequency of interest is used (Le Van Quyen et al. 2001). This frequency of interest has to be determined before actually calculating the phase delay through an analysis of either the coupling between the two signals or the determination of phase synchrony.

Such methods have been successfully applied in MEG studies, where the phase delay between brain areas or between muscles and brain activity have been determined (Timmermann et al. 2003, Gross et al. 2000). The 2π ambiguity and the limitation to a narrow frequency band make the calculation of a phase delay often times impractical to determine the directionality between two signals. Thus, other methods were developed for this purpose. In the following the dominant approach based on Granger causality will be presented.

3.2 Autoregressive Modeling

To calculate Granger causality, first an autoregressive model has to be estimated.⁴ With an autoregressive model AR(p) the values of a time series y are described by the sum of the linearly weighted lagged values of the time series:

$$y_t = a_0 + a_1y_{t-1} + a_2y_{t-2} + \dots + a_p y_{t-p} + \eta_t, t = 1, \dots, N \quad (3.6)$$

y_t - time series at time point t

a_i - coefficient or weight of the y_{t-i} term

η_t - error term, which represents a white noise process

N - number of time points

p - model order

⁴There are of course other methods to proceed (Dhamala et al. 2008a, Dhamala et al. 2008b), but this is the most common approach.

In case of a multivariate setting like the present one that considers several simultaneously recorded signals, a multivariate version, a so called vector autoregression (VAR) is used:

$$\mathbf{X}(t) = \sum_{k=1}^p \mathbf{A}(k)X(t-k) + \mathbf{E}(t) \quad (3.7)$$

where $\mathbf{X}(t) = [X_1(t), X_2(t), \dots, X_n(t)]^T$ is the data vector of all signals at time t . $\mathbf{A}(k)$ is the matrix of autoregressive coefficients for the k^{th} time lag, while p is the model order that indicates the maximum number of time lags. $\mathbf{E}(t)$ represents a vector of white noise, which is the true error, if \mathbf{A} is known. However, usually \mathbf{A} is not known and thus estimated by its sample equivalent $\hat{\mathbf{A}}$. In this case the true error $\mathbf{E}(t)$ is estimated by the residual vector ϵ_t . In the following \mathbf{A} and $\mathbf{E}(t)$ are treated as known for presentational convenience, although they are often estimated from the sample.

Nevertheless, for the estimation of equation 3.7 to be possible two things have to be considered: stationarity of the time series and the choice of the model order. These issues will be explained in the following section.

3.2.1 Stationarity

For a consistent estimation of the coefficients,⁵ a time series $y(t)$ has to be at least weakly stationary. Thus, stationarity is the first point to be addressed. However, if the time series is not stationary, preprocessing methods can often be used to obtain a stationary time series.

⁵Consistency means, that if certain other conditions are met, $\text{plim}\hat{\mathbf{A}}(k) = \mathbf{A}(k)$. This definition says that for $n \rightarrow \infty$, the autoregressive coefficient estimates converge to the true coefficient values in probability (Greene 2007).

3.2. AUTOREGRESSIVE MODELING

Weak stationarity implies that the major characteristics of the stochastic process governing the time series do not change over time. In particular the following two conditions have to be fulfilled (Greene 2007):

1. mean stationarity: $E(y_t) = \mu$ for all $t \in Z$
2. covariance stationarity: The covariance function $Cov(y_s, y_t) = E[(y_t - \mu)(y_s - \mu)]$ depends only on the time displacement $t - s$ for all $s, t \in Z$.⁶

Condition 2 for $t = s$ also implies that the variance of the time series has to be constant over time. From the definition of stationarity it is clear that different types of instationarity may occur.

In particular, there are 3 important types of instationarity: i) a structural break, ii) a deterministic trend and iii) a stochastic trend,⁷ examples of which are depicted in figure 3.2. A *structural break* results in a change of (co)variance or mean at a certain point in the data, while a *deterministic trend* is the result of a deterministic function of time that enters the time series. Simple examples are a linear trend or an exponential trend. A *stochastic trend* occurs, if an infinite number of past time points influence the present one. This is equivalent to the time series having a permanent memory and an infinite unconditional variance. Usually these types of instationarity can be identified visually. But often the cases are not as clear-cut as in figure 3.2. Particularly the case of a structural break is highly relevant for neural data, whose signals reflect spatio-temporal patterns of the electric and magnetic fields of the brain.

⁶Even stronger would be *strong stationarity*: The process $(y_t), t \in Z$ is called strongly stationary, if and only if the joint distribution function of $(y_{t_1}, y_{t_2}, \dots, y_{t_n})$, i.e. $(x_1, x_2, \dots, x_n) \rightarrow P(y_{t_1} \leq x_1, y_{t_2} \leq x_2, \dots, y_{t_n} \leq x_n)$, corresponds to the joint distribution function of $(y_{t_1+s}, y_{t_2+s}, \dots, y_{t_n+s})$ for all $s, t_1, t_2, \dots, t_n \in Z$ and $n = 1, 2, \dots$ (Greene 2007).

⁷A simple case of stochastic trend is a random walk. $x_t = x_{t-1} + \varepsilon_t$, $\varepsilon_t \stackrel{iid}{\sim} N(0, 1)$. Substituting iteratively gives $x_t = \varepsilon_t + \varepsilon_{t-1} + \varepsilon_{t-2} + \dots$. Hence, even infinitely distant points have an influence on x_t ($var(x_t) = \sum_{i=0}^{\infty} (\varepsilon_{t-i}) = \infty$.)

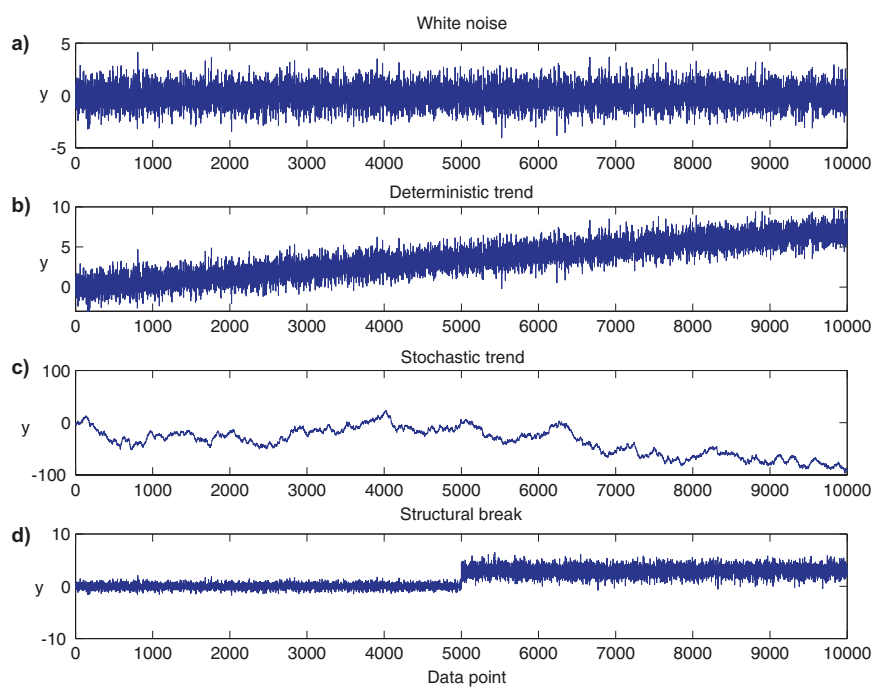


Figure 3.2: Different types of instationarity: In a) a simple stationary white noise process is shown. By adding a linear constant to the data, they show a deterministic trend as evident in b). A stochastic trend and a structural break is shown in c) and d), respectively.

3.2. AUTOREGRESSIVE MODELING

Neural signals may be interpreted as a function of the underlying brain functional states (Lehmann et al. 1987). It is well known that neural networks can exhibit complex behavior with nonlinear dynamics that may for example include bifurcations, i.e. changes of the signal system from one state to another (Lopes da Silva 1991), which is usually a clear case of a structural break. A case in point is epilepsy where the same brain area may suddenly switch from regular information processing into pathological abnormal excessive or synchronous neural activity in the brain (Fisher et al. 2005). In this case, where such a transition between states occurs, it may be inappropriate to treat the signals as stationary. Fortunately, such breaks can often be found by visual inspection.⁸ Moreover, there are also formal tests like the Chow- or Quandt-test available to test for a structural break (Chow 1960, Andrews and Ploberger 1994, Ploberger and Krämer 1992, Nyblom 1989, Hansen 2000, Quandt 1960). A related but different problem can arise with EMG data, where the signal may be influenced by the stability of the electrode position with respect to the active muscle fibers and the stability of the motor unit activation pattern. While it is not always clear how to deal with these problems, considering only isometric tasks as is done in the present work, alleviates much of these concerns (De Luca 1997).

For the case of stochastic trends, one usually has to test for so-called unit roots (see below) with one of several methods available in econometrics. To understand these tests, first define the Lag-operator L with:

$$L^i y_t = y_{t-i} \tag{3.8}$$

⁸While this may not be an issue in the present study, where only periods of clearly defined neural activity are considered, this may be an issue in event-related studies, where the event may trigger a transition between states. In this case, repeated trials with a windowing technique may be used to mitigate the problem (Ding et al. 2000).

Then apply it to the autoregressive model (3.6):

$$y_t = a_0 + a_1 y_{t-1} + a_2 y_{t-2} + \dots + a_p y_{t-p} + \eta_t$$

so that one obtains:

$$y_t(1 - a_1 L + a_2 L^2 + \dots + a_p L^p) = a_0 + \eta_t \quad (3.9)$$

The left hand side of equation 3.9 is called the characteristic polynomial. If it is set to 0 and solved for L , the solutions are called roots of the characteristic polynomial. The autoregressive process is stationary, if all roots of the characteristic polynomial lie outside the unit circle ($|L| > 1$) (Hamilton 1994). If the process has one or more roots on or inside the unit circle the process is not stationary.⁹

One commonly used test for unit roots is the augmented Dickey-Fuller test (Dickey and Fuller 1979, Dickey and Fuller 1981).¹⁰ Elliot (1996) found this test to be the best performing test in terms of small sample performance and power. Certainly one can argue for one or another test, but as Müller and Elliot pointed out, all presently available tests are nearly optimal (Müller and Elliott 2003) and there exists no uniformly most powerful test (Elliott et al. 1996). For the augmented Dickey-Fuller Test with constant term, the following difference regression is estimated:

$$\Delta y_t = \alpha + \beta t + \gamma y_{t-1} + \delta_1 \Delta y_{t-1} + \dots + \delta_p \Delta y_{t-p} + u_t \quad (3.10)$$

α is a constant term and βt represents a possible time trend in the data. In many

⁹Consider the easiest case of the random walk in footnote 7: $x_t = (1 - L)\varepsilon_t$. Hence $(1 - L) = 0 \Rightarrow L = 1$.

¹⁰It is called augmented as it considers a constant and a possible time trend in the time series, which the usual Dickey-Fuller test does not do.

3.2. AUTOREGRESSIVE MODELING

cases the test is performed without the constant term α . In the differenced form of equation 3.10 the null hypothesis of a unit root corresponds to $\gamma = 0$. The test statistic is then defined as:

$$t = \frac{\hat{\gamma}}{\hat{\sigma}_{\hat{\gamma}}} \quad (3.11)$$

$\hat{\gamma}$ is the empirical estimate of γ and $\hat{\sigma}_{\hat{\gamma}}$ is the empirically determined standard deviation of $\hat{\gamma}$. Unfortunately, under the null of a unit root this test statistic does not follow the usual t-distribution. The correct distribution and its critical values have been derived with Monte Carlo experiments by Dickey and Fuller (Fuller 1976, Dickey and Fuller 1979, Dickey and Fuller 1981).

If the time series is integrated, i.e. has a unit root, the stochastic trend can be removed by differentiating:

$$\Delta y_t = y_t - y_{t-1} \quad (3.12)$$

To obtain a stationary process the time series has to be differentiated as many times as unit roots are found in the time series (Box and Jenkins 1970). The further analysis then proceeds with this time series.

In the case of a deterministic trend (Figure 3.2b), the time series can also be transformed into a stationary series by either subtracting the trend or by explicitly considering the time trend in the autoregressive equation.

3.2.2 Model Order Selection

Another important issue of AR modeling is the proper choice of the model order p . If one has an infinite data length N to estimate the coefficient matrices \mathbf{A} , the estimation of the model order would not be necessary. Due to the law of large numbers all redundant lags would consistently be 0. However, in real measurements

time series are finite and thus the correct choice of the model order is of importance for an efficient estimation.

Usually the correct model order p of an autoregressive model is not known a priori. Thus, p has to be estimated. This is often done by evaluating the noise covariance matrix Σ , because its absolute value Σ decreases, if an additional lag helps to explain X . However, as is always the case with additional regressors, a larger model order will weakly decrease the residual variance estimates. Hence, a degree of freedom correction has to be applied in order to avoid using too many lags.

Therefore, several criteria have been suggested to determine the correct model order. The two most common ones are the Akaike information criterion (*AIC*) (Akaike 1973, Akaike 1974) and the Bayesian information criterion (*BIC*) (Schwarz 1978). They are expressed as (Lütkepohl 2005):

$$AIC(p) = 2\log[\det(\Sigma)] + \frac{2m^2p}{N_{total}} \quad (3.13)$$

$$BIC(p) = 2\log[\det(\Sigma)] + \frac{2m^2p \log N_{total}}{N_{total}} \quad (3.14)$$

m is the number of data channels analyzed and N_{total} is the number of time points contained in each time series. To obtain the optimal model order the respective criterion has to be minimized. The *BIC* penalizes a higher model order p more than the *AIC*, which can be seen by the additional multiplicative factor $\log N_{total}$ in the second term. This additional term makes the *BIC* consistent, whereas the *AIC* is not. A model selection criterion is called consistent, if the probability of asymptotically choosing the correct model order is 1, i.e. $\lim_{T \rightarrow \infty} Pr\{\hat{p} = p\} = 1$ (Lütkepohl 2005). For the *AIC*, the degrees of freedom correction would asymptoti-

3.3. STATISTICAL CAUSALITY MEASURES

cally vanish. Thus, one would with zero probability underestimate the model order and with positive probability overestimate the model order. Although this bias may be small for large VAR-dimensions m (Paulsen 1985), it renders the *AIC* inconsistent. The *BIC* prevents this behavior by correcting for the sample size. Thus, in the following application the *BIC* will be considered.

3.3 Statistical Causality Measures

3.3.1 Granger Causality

For the so-called “Granger causality”, Granger (1969) formalized Wiener’s idea of causality (Wiener 1956). Wiener defined causality for two simultaneously measured signals in a statistical framework as follows: If one can predict the first signal better by incorporating the past information from the second signal than only using information from the first one, then the second signal can be called causal for the first one. Granger adopted this idea to autoregressive models of time series. By comparing the fit of the autoregressive model from only the first time series with the one, where a second time series is taken into account, he established a measure of causality between two time series.

Granger causality in its original notation is a bivariate concept. It is based on the temporal ordering of two time series. The idea is that a cause must always precede the effect. The temporal causation is tested statistically, so that it does not necessarily imply true causality.

To calculate Granger causality, first an autoregressive model of the time series X_t

has to be estimated.

$$X_t = \sum_{j=1}^p a_j X_{t-j} + \varepsilon_t \quad (3.15)$$

The second time series Y_t is said to Granger cause X_t , if the addition of time lags from the second time series Y_t to 3.15 improves the prediction of X_t . That implies, that after correction for degrees of freedom, the variance of η_t must be smaller than the one of ε_t .

$$X_t = \sum_{j=1}^p c_j X_{t-j} + \sum_{j=1}^p d_j Y_{t-j} + \eta_t \quad (3.16)$$

Statistically this dependence is tested with a F-test. For the specific case of Granger causality the null hypothesis H_0 formulates that “Y is not Granger causal for X”, i.e. that the d_j are jointly 0. The value of the F-test is obtained from the squared sum of the residuals from the restricted (equation 3.15) and unrestricted regression (equation 3.16), with the latter being the AR-model with past values of X and Y (Hamilton 1994):¹¹

$$F_{p,T-2p-1} = \frac{(SSR_R - SSR_u)/p}{SSR_u/(T - 2p - 1)} \quad (3.17)$$

SSR_u – sum of squared residuals of the unrestricted autoregressive model

SSR_r – sum of squared residuals of the restricted autoregressive model

T – number of observations or number of recorded data points

p – number of time lags, which are included in the model estimation (model order)

To estimate Granger causality in the frequency domain, Geweke developed a frequency representation for bivariate Granger causality (Geweke 1982). As there is usually a complex system of interactions between several signals underlying the

¹¹Critical values for $F_{p,T-2p-1}$ are tabulated in Greene (2007).

3.3. STATISTICAL CAUSALITY MEASURES

dynamics in neural time series, the bivariate concept of Granger causality and its frequency decomposition by Geweke is only of limited use in neuroscience. Granger (1980) pointed out that causality between two time series can only be estimated correctly, if no other signal influences the first two. Neglecting such a third signal would lead to an omitted variable bias. Even multiple, pair-wise analysis of the channels does not provide proper results (Franaszczuk et al. 1985) and may therefore lead to erroneous conclusions (Kus et al. 2004). One possible way to overcome this problem is the so called *conditional linear feedback* (Geweke 1984). With this method an indirect influence in a three-dimensional system can be determined. For a system with more than three channels the method can be applied multiple times (Chen et al. 2006, Ding et al. 2006). However, with more channels this approach becomes cumbersome and either many triplets have to be tested or the reference signal has to be constructed as a composite vector of the remaining data channels (see e.g. Zhou et al. (2008)). Thus, conditional Granger causality is not considered any further in the following work, because this work is restricted to the truly multivariate methods.

3.3.2 Directed Transfer Function (DTF) and Transfer Function (H)

The first truly multivariate approach to the analysis of neural signals based on Granger causality in the frequency domain was the Directed Transfer Function (DTF) suggested by Kaminski and Blinowska (1991). To obtain the DTF of a set of signals first a MVAR model as given in equation 3.7 has to be estimated (Kus et al. 2004).

For the frequency representation the matrix $\mathbf{A}(\mathbf{k})$ is transferred to the frequency

domain using (Astolfi et al. 2005, Kaminski and Blinowska 1991):

$$\mathbf{A}(f) = \sum_{k=1}^p \mathbf{A}(k) e^{-2\pi f \Delta t k}. \quad (3.18)$$

$\mathbf{A}(f)$ is the coefficient matrix at a certain frequency f . Δt is the temporal interval between two time points of observation.

The matrix inverse of $\mathbf{A}(f)$ is denoted by $\mathbf{H}(f)$ and is called transfer matrix:

$$\mathbf{H}(f) = \mathbf{A}^{-1}(f). \quad (3.19)$$

Its elements H_{ij} represent the connection between the j^{th} input and the i^{th} output of the system. The simulations were also performed with the absolute value of H , which is in the following simply denoted by H .

After obtaining H , the DTF from channel j to i can be calculated (Kaminski and Blinowska 1991):

$$\gamma_{ij}^2(f) = \frac{|H_{ij}(f)|^2}{\sum_{m=1}^N |H_{im}(f)|^2} \quad (3.20)$$

Regarding its interpretation, γ_{ij}^2 describes the causal influence of the j^{th} signal on the i^{th} signal at a frequency f by computing the ratio between the inflow of signal j to i and all inflows to signal i . The values of γ_{ij}^2 range from 0 to 1, where 1 indicates that all of signal i is caused by signal j (Kus et al. 2004). In contrast to the bivariate Granger causality the DTF is designed to be capable of finding the right connections in a multivariate system of interactions by considering all signals simultaneously. In addition, not only information regarding the existence of a connection is obtained, but couplings in a particular frequency range can also be identified. However, one

3.3. STATISTICAL CAUSALITY MEASURES

disadvantage of the DTF is its inability to distinguish direct and indirect relations between signals. An indirect relation is one which goes from source A to source B via a third source C. The DTF would identify a connection between A and B, even though the true actual connection is from A to C and then to B and no direct connection exists between A and B (see figure 1.1). To mitigate this drawback two other concepts have been suggested to differentiate between direct and indirect connections and will be presented in the following.

3.3.3 Direct Directed Transfer Function (dDTF)

The direct Directed Transfer Function (dDTF) constitutes a conceptual advancement over and above the DTF in order to distinguish between direct and indirect causal relations of signals (Korzeniewska et al. 2003). It combines the concepts of the partial coherence and the DTF in order to gain from their individual advantages. To obtain the dDTF, first the so-called full frequency Directed Transfer Function (ffDTF), η_{ij}^2 , has to be computed. Its equation is given by:

$$\eta_{ij}^2(f_k) = \frac{|H_{ij}(f_k)|^2}{\sum_f \sum_{m=1}^N |H_{im}(f)|^2} \quad (3.21)$$

For the ffDTF the squared absolute value of the respective element ij of the transfer function H is divided by a double summation over all inflows to signal i and all frequencies f . The frequency peaks of the ffDTF correspond mainly to the peaks found by coherence analysis (Korzeniewska et al. 2003). This is important because in a second step the ffDTF is multiplied with the partial coherence in order to estimate the dDTF. The partial coherence χ_{ij}^2 is supposed to determine whether a connection between two sources is mediated by a third signal. However, the direction of information flow cannot be determined using partial coherence alone. The partial

coherence is estimated with the coefficients of the multivariate model through

$$\chi_{ij}^2(f) = \frac{M_{ij}^2(f)}{M_{jj}(f)M_{ii}(f)} \quad (3.22)$$

M_{ij} is the minor from the power spectral matrix \mathbf{S} . It is the determinant of the matrix obtained by removing the i^{th} row and j^{th} column from \mathbf{S} , where \mathbf{S} is given through:

$$\mathbf{S}(f) = \mathbf{H}(f)\mathbf{V}\mathbf{H}^H(f) \quad (3.23)$$

$\mathbf{H}^H(f)$ denotes the conjugate transpose matrix of \mathbf{H} . \mathbf{V} is the covariance matrix of the noise $\mathbf{E}(f)$ in system 3.7 (Baccala and Sameshima 2001). Finally, in a last step, the dDTF is obtained by multiplying the partial coherence (3.22) with the fDTF (3.21):

$$\delta_{ij}(f) = \chi_{ij}(f)\eta_{ij}(f) \quad (3.24)$$

The dDTF combines the properties of the partial coherence, which can distinguish between direct and indirect connections, but cannot determine the direction of the information flow, and the DTF, which is able to infer directionality. Hence, it is supposed to only detect direct causalities, which will be tested in the following work.

As the dDTF uses the partial coherence to distinguish between direct and indirect connections it is known to have problems with “marrying parents of a joint child”¹² (Dahlhaus et al. 1997, Winterhalder et al. 2005). The reason is that the partial coherence is unable to distinguish these spurious connections from real ones (Winterhalder et al. 2005). We include the dDTF nevertheless in our study as it might be a good measure in cases where such a scheme is not present. Moreover, the use of a model

¹²“Marrying parents of a joint child” are two time series (“the parents”) which have a causal influence on a third time-series, “their child”. The dDTF detects in this case a false causality between the two first time series.

3.3. STATISTICAL CAUSALITY MEASURES

with and one without such a scheme allows us to distinguish, if this problem drives the results for the dDTF.

3.3.4 Partial Directed Coherence (PDC) and Squared Partial Directed Coherence (sPDC)

The partial directed coherence (PDC) was introduced for the analysis of multi channel systems. It is based on the notion of Granger causality and is supposed to disentangle direct and indirect connections (Baccala and Sameshima 2001, Sameshima and Baccala 1999).

The PDC is also based on a MVAR model as described in equation (3.7) and is defined as:

$$\pi_{ij}(f) = \frac{A_{ij}(f)}{\sqrt{\sum_{k=1}^N A_{ki}(f)A_{kj}^*(f)}} \quad (3.25)$$

The PDC is normalized in such a way, that $0 \leq |\pi_{ij}(f)|^2 \leq 1$ and $\sum_{i=1}^N |\pi_{ij}(f)|^2 = 1$ for all $1 \leq j \leq N$. This normalization is an important difference of the PDC compared to the DTF. The PDC describes the information flow from j to i with respect to all interactions of j to other structures, i.e. the PDC represents a ratio between the outflow from channel j to i in respect to all outflows from j , while the DTF is a ratio in respect to all inflows to i (Kus et al. 2004). A second important difference of the PDC to the DTF is that it does not involve an inversion of the matrix \mathbf{A} . This has computational advantages and is also the reason for the PDCs ability to distinguish between direct and indirect connections (Astolfi et al. 2007).

Recently a modification of the PDC has been suggested to increase its sensitivity (Astolfi et al. 2006). The so called squared partial directed coherence (sPDC) is given

by the following equation:

$$\overline{sPDC}_{ij}(f) = \frac{|\bar{A}_{ij}(f)|^2}{\sum_{m=1}^N |A_{mj}(f)|^2} \quad (3.26)$$

Squaring the autoregressive coefficients is supposed to increase the sensitivity of this causality measure compared to the PDC by giving larger values a greater weight. This is achieved by making use of Jensen's inequality in the denominator. Hence, the sPDC is not simply the square of the PDC. The sPDC was included in the simulations to test whether it really increases the sensitivity.

3.4 Methods for Significance Threshold Computation

All multivariate methods require the determination of a significance level in order to differentiate between real connections and noise as causality measures with values greater than 0 might simply occur by chance. With a correct significance measure the null hypotheses H_0 of the causality measure being 0 should only be rejected, if a causality exists, except for $\alpha\%$ of all cases, where α is the pre-specified type-1 error.

For sake of comparability of the results from the different causality measures only non-analytical methods will be considered in this work, as there are currently only analytical measures available for the PDC and the DTF (Eichler 2006, Schelter et al. 2005). Furthermore, numerical methods often perform better in finite samples than analytical measures based on asymptotic considerations (Davidson and MacKinnon 2004). Thus, in the present work two different methods, which have been suggested in the literature to overcome this problem, are used: the random permutation of the data (Kaminski et al. 2001) and the leave one out method (LOOM) (Schlögl and Supp 2006). While with the LOOM still a distribution is assumed, the random

3.4. METHODS FOR SIGNIFICANCE THRESHOLD COMPUTATION

permutation approach is solely numerical.

3.4.1 Leave One Out Method

The first significance measure, the leave one out method (LOOM), is a semi-parametric method based on the jackknife (Quenouille 1947, Tukey 1958).

From a sample X a set of observations x_i of length N is deleted and left out. Schlögl and Supp have tested this approach and derived two restrictions for the optimal choice of the segment length (Schlögl and Supp 2006):

$$N\sqrt{n} > p \tag{3.27}$$

$$\frac{Nn}{Mp} > 1 \tag{3.28}$$

N is the number of data points of the segment, p is the model order, n is the number of segments, which fit into the data set and M is the number of channels considered. In the present work N was chosen to be 200 data points in accordance with these suggestions.

For the resulting shorter sample $X_{(-i)}$ the causality measures were calculated. This procedure was repeated n times with

$$n = \text{round}\left(\frac{L}{N}\right) \tag{3.29}$$

L is the data length. Let $C_{(-i)}$ denote the value of the respective multivariate causality measures applied to the shorter sample. The standard error of the test

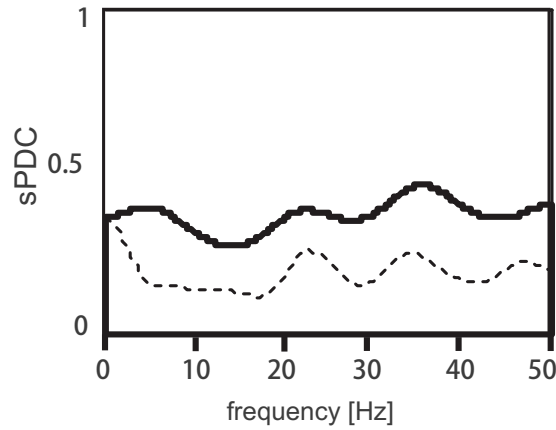


Figure 3.3: The sPDC in combination with LOOM for one connection: The constant line shows the result of the sPDC and the dashed line presents the significance threshold of the LOOM. x-axis: frequency from 0 to 50 Hz; y-axis: value of the sPDC ranging between 0 and 1.

statistic can then be estimated as (Efron 1992):

$$SE(C) = \left[\frac{n-1}{n} \sum_{i=1}^n (C_{(-i)} - \bar{C})^2 \right]^{1/2} \quad (3.30)$$

where \bar{C} is the sample mean

$$\bar{C} = \sum_{i=1}^n C_i / n. \quad (3.31)$$

For the analyzed causality measures a 99% confidence interval was computed from the estimated standard error by using the t-distribution with n degrees of freedom:

$$k = SE * tinv((1 - k)/2, n) \quad (3.32)$$

k denotes here the chosen significance level, for example for a 5 % confidence limit $k = 0.05$. $tinv$ is the inverse cumulative density t-distribution. As the causality measures have only positive values, a one sided test is used and the p-value of the

3.4. METHODS FOR SIGNIFICANCE THRESHOLD COMPUTATION

inverse cumulative density function has to be divided by 2.

Figure 3.3 shows an example of the sPDC in combination with LOOM. The graph represents one causality, which was implied in the data and should accordingly be detected. The x-axis displays the frequency and the y-axis the value of the sPDC. The dashed line corresponds to a 99% significance threshold obtained with LOOM. It is not a straight line, as the LOOM can detect parts in the signal with more noise and accordingly adapts the threshold. Thus, the significance threshold with the LOOM is frequency-specific and increases, if the standard error increases.

3.4.2 Random Permutation

Random permutation of the data is a surrogate numerical method to obtain a significance estimate. The random permutation derives its name from randomly interchanging observations of a time series (Scheinkman and LeBaron 1989). With this method surrogate data based on the original observations are produced, but where any causality should be removed by randomly changing the time ordering. As any causality should be removed from the data, the null hypothesis of no causation is true. Thus, the distribution of the causality measures for no causation can be determined. In contrast to the LOOM it does not assume an asymptotical normal distribution. While Brovelli et al. (2004) used a trial based random permutation approach, this approach is modified, as only non trial based time series data are tested in the present work. The LOOM approach used here is similar to Brovelli's approach except for dividing the data into time segments instead of trials.

First the time-order of each time series was randomized. Then an autoregressive model was fitted to the surrogate data and the respective causality measure was calculated. For each repetition the maximum over all connections and frequencies is

Table 3.1: 99% percentiles of the five causality measures for different numbers of random permutation repetitions

repetitions	sPDC	PDC	DTF	dDTF	H
50	0.0297	0.1723	0.1688	0.000695	0.1829
100	0.0258	0.1607	0.1629	0.000869	0.1694
200	0.0290	0.1703	0.1715	0.000761	0.1696
500	0.0283	0.1682	0.1713	0.000733	0.1719
1000	0.0290	0.1703	0.1677	0.000794	0.1715

taken. Kaminski et al. (2001) repeated this procedure 100 times in their study. In our simulations this value was tested with the Kus-model with its baseline parameters given below (see section 4.1.1). Table 3.1 shows the effect of increasing the number of repetitions on the 99% percentile of the maxima from all repetitions for the random permutation. With 100 repetitions the percentile still showed a large variability compared to 1000 repetitions. As a compromise between computational speed and accuracy, 200 repetitions were chosen for further simulations. The histogram of the maximum values of the sPDC for 1000 repetitions is shown in figure 3.4. It is obvious that the distribution is not normal, so that it is more appropriate to chose a percentile instead of a parametric p-value derived from assumed normality.¹³ The 99%-percentile of the 200 repetitions used in this work takes the third largest value as confidence threshold.

Figure 3.5 shows the same application as in figure 3.3, but with random permutation instead of LOOM. The graph reads as the one in figure 3.3. The null hypotheses is correctly rejected for the implied connection. In contrast to LOOM the significance threshold here is a straight line – it takes the same value over the complete frequency range and is also the same for each connection.

¹³As the PDC, sPDC and DTF are bounded by 0 and 1, they can by definition not be normally distributed.

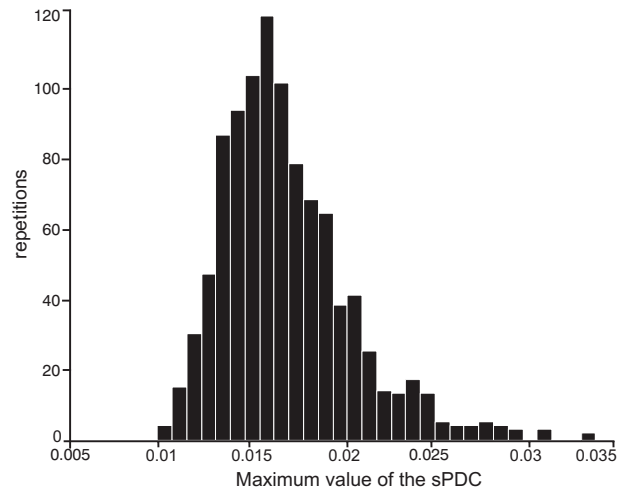


Figure 3.4: Histogram of the sPDC's maximum from 1000 random permutation repetitions: This histogram is obtained from the randomly interchanged data of the Kus-model, where no causality should be present.

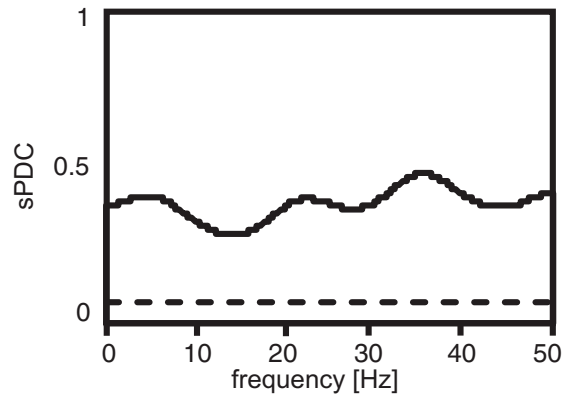


Figure 3.5: The sPDC in combination with random permutation for one connection: The dashed line represents the significance threshold obtained with random permutation (further explanations see figure 3.3).

3.4.3 Power and Size of the Significance Thresholds

In order to assure that the size¹⁴ of the two numerical significance computation methods is correct and that they have a high power, two simulation studies were performed. Assuring that the size is correct is important as a wrong size would bias all subsequent results. First, two time series with 50000 data points each consisting of i.i.d. white noise were simulated. These two time series have no causal influence on each other and the significance measures should reflect this. To test the size of the two significance approaches, random permutation and LOOM, we calculated all 5 tested causality measures with a model order of 2 and determined the significance with each significance threshold. This procedure was repeated 1000 times. If the size of the 99% significance threshold is correct, about 1% false positive detections should be made.

As can be seen from the results in table 3.2, both significance thresholds have approximately the correct size. In particular, both significance thresholds perform well with the sPDC. Only the PDC and DTF in combination with the LOOM show slightly more than 1% false positives.

Table 3.2: Size of random permutation (RP) and LOOM for the different causality measures

	sPDC	PDC	DTF	dDTF	H
RP false positives (%)	0.7	0.7	0.7	1.0	0.6
LOOM false positive (%)	0.0	1.1	1.1	0.0	1.0

In the second simulation, we tested the power of the significance computation

¹⁴The size of a test refers to the probability of rejecting the null hypothesis when it is actually true. Hence, the size should coincide with the pre-specified alpha level.

3.4. METHODS FOR SIGNIFICANCE THRESHOLD COMPUTATION

methods. We again used one time series with 50000 data points consisting of i.i.d. white noise. The second time series was created by shifting the first time series by one lag and adding additional white noise. Thus, one causal relation from time series 2 to time series 1 should be detected. We again applied the 5 causality measures with a model order of 2 and determined the significance with the two approaches random permutation and LOOM. This procedure was repeated 1000 times.

Table 3.3: Power of random permutation (RP) and LOOM for the different causality measures

	sPDC	PDC	DTF	dDTF	H
RP missed (%)	0.0	0.0	0.0	0.0	0.0
LOOM missed (%)	0.0	0.0	0.0	0.0	0.0

As can be seen from the results in table 3.3 both significance thresholds have good power as they do not miss any existing causalities. Thus, in conclusion both random permutation and LOOM show an appropriate power and size for all causality measures tested in the present work.

Chapter 4

Simulation Models and Theoretical Derivations

After having explained the basics of neural signals and the principles of the causality measures tested in this work, this chapter focuses on the environment needed for testing these measures. The analysis proceeds with two simulation studies, in which a controlled environment is created, where the true causalities are known. To create such a controlled environment two different models are used, one based on a real data set and one that only uses artificial data. Furthermore the question of stationarity and preprocessing is discussed and theoretical derivations are presented, why preprocessing like filtering induces problems, if traditional Granger causality is determined. Finally, it is argued that this result transfers to the multivariate causality measures presented in chapter 3.

4.1 Simulation Models

In order to compare the different causality measures, two different models from the literature are adapted and modified to suit our purpose. These models impose a

predefined causality structure on the data so that one knows, which causalities ought to be detected. After creating such a structure the respective causality measure is applied to explore, if the predefined causality structure is detected correctly.

The first model was suggested by Kus et al. (2004). It uses a neural signal as the first input signal. Based on this signal, subsequent channels are created using a predefined causality structure. The use of this model with a real data segment makes it more realistic, but also more dependent on the data type. In contrast, the second model, the Schelter-model (Schelter et al. 2006), uses completely artificial data, avoiding the influence of specific data types. Both model structures are adapted suitable for analyzing the effects of decimation and misestimation of model-order.

4.1.1 Modified Kus (2004) - Model

For the Kus-model originally real data from EEG recordings were taken as basis. The implied connections for this model are shown in figure 4.1.

Mathematically, the model is described as follows:

$$\begin{aligned}
 x_1(t) &= rd(t) + a_1\eta_1(t) \\
 x_2(t) &= c_2x_1(t-8) + a_2\eta_2(t) \\
 x_3(t) &= c_3x_2(t-4) + a_3\eta_3(t) \\
 x_4(t) &= c_4x_1(t-4) + a_4\eta_4(t) \\
 x_5(t) &= c_5x_4(t-4) + a_5\eta_5(t) \\
 x_6(t) &= c_6x_4(t-8) + a_6\eta_6(t) \\
 x_7(t) &= a_7\eta_7(t)
 \end{aligned} \tag{4.1}$$

where $c_i, i = 1, \dots, 7$ denotes the coupling strength, a_i is a pre-factor to scale the variance of the Gaussian white noise η_i to a_i^2 . rd is any real data signal. The term

4.1. SIMULATION MODELS

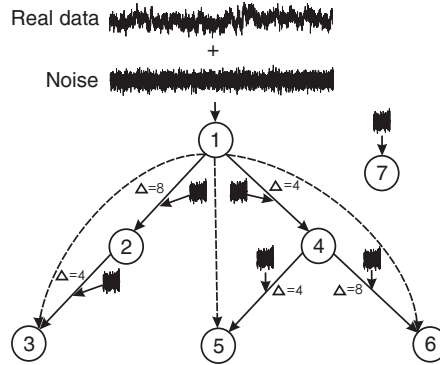


Figure 4.1: Kus-model modified from Kus and colleagues (2004): The first data channel is created of a real data signal and white noise. The second time series is obtained by shifting the first time series by Δ time points and adding further noise. The solid arrows between the data channels indicate direct causal relations, while the dashed arrows indicate indirect causal relationships. The seventh time series only consists of white noise.

$x_1(t - 8)$ refers to the value of the time series x_1 at time point $t - 8$. Note, that the noise η_i generates the subsequent channel and thus becomes part of the real signal in the next channel. Thus, this noise is called *internal noise* in the following discussion. This internal noise was scaled in such a way that it had a quarter of the variance of the original data. After the generation of the simulated channels, additional Gaussian white noise was added to all channels to produce a noise term similar to the measurement noise in real data, called *external noise* in the following. The sampling rate for this model was 1000 Hz.

In the original Kus et al. (2004) model, the time series were lagged by 1 time point in each subsequent step. For the present work this lag structure has been changed to the one given in equation 4.1. The reasoning behind this modification is that i) with this greater time shift the influence of an underestimation of the model order (i.e. a model order below 12) can be tested; ii) the variation in the time shifts in the

various steps of the model make it possible to test the influence of different down sampling factors; iii) a time shift of only one time step is not very realistic in real data. The Kus-model contains no “marrying parents of a joint child scheme” (Dahlhaus et al. 1997), so that no spurious causalities due to this phenomenon can arise.

4.1.2 Modified Schelter (2006) - Model

Scheltes and colleagues (2006) suggested the following five dimensional model :

$$\begin{aligned}
 x_1(t) &= 0.4x_1(t-4) - 0.5x_1(t-8) + 0.4x_5(t-4) + \eta_1(t) \\
 x_2(t) &= 0.4x_2(t-4) - 0.3x_1(t-16) + 0.4x_5(t-8) + \eta_2(t) \\
 x_3(t) &= 0.5x_3(t-4) - 0.7x_3(t-8) - 0.3x_5(t-12) + \eta_3(t) \\
 x_4(t) &= 0.8x_4(t-12) + 0.4x_1(t-8) + 0.3x_2(t-8) + \eta_4(t) \\
 x_5(t) &= 0.7x_5(t-4) - 0.5x_5(t-8) - 0.4x_4(t-4) + \eta_5(t)
 \end{aligned} \tag{4.2}$$

This model has been modified from the original one by increasing all time lags by a factor of 4. The reasoning behind this modification is the same as the one given for the Kus-model.

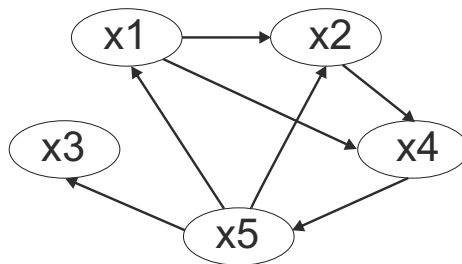


Figure 4.2: Connections implied by the Scheltes-model: The arrows indicate the implied causalities between the 5 sources of the Scheltes-model.

4.2. STATIONARITY

The connections implied by this model are shown in figure 4.2. As initial values for the time series a vector of Gaussian white noise is taken. The η_i are also Gaussian white noise:

$$\eta_i \stackrel{iid}{\sim} N(0, 1) \quad (4.3)$$

After obtaining the model according to 4.2, further noise was added, the so-called external noise. This external noise was scaled by a noise factor. A noise factor of 0.5 scales the variance of the noise to a quarter of the variance of the original model. The Schelker-model poses an interesting testing case for the dDTF and the other causality measures as a false connection from channel 2 to 1 might occur due to the existence of a “marrying parents of a joint child scheme”.

4.2 Stationarity

A priori, theoretical reasoning suggests that the continuously recorded neural data considered in this work should be stationary,¹ as all three types of instationarities introduced in 3.2.1 seem highly unlikely. First of all, the presence of a deterministic trend can be commonly excluded in neural data as it would imply a continuously increasing or decreasing time series, which would be easily visually identifiable after some time. Second, a structural break should also not be an issue, as the data analyzed in the present work were recorded continuously and are not event related. Third, a stochastic trend seems very improbable as this would imply an infinite variance of the signal under consideration and seem incompatible with orderly signal processing in the human brain.

The impression that the signals are stationary is also obtained when looking at the

¹For a formal definition of stationarity see chapter 3.2.1.

graphs of the raw data (see for example figures 2.3, 2.6, 2.8 and 2.10). However, to exclude a stochastic trend in the data, which is not easily identified, the data were also tested with the augmented Dickey-Fuller (ADF) test for a unit root. The test against the presence of a unit root is motivated by the fact that the neural signals often show a large persistence with autoregressive coefficient estimates close to 1. Test routines for the ADF in neuroscience commonly apply this test without a constant term. If this specification is used, for some of the EMG recordings and some of the MEG recordings the null hypothesis of a unit root cannot be rejected. Hence, based on these tests, it cannot be excluded that these time series may not be stationary. However, if a constant term is assumed in the ADF test, H_0 is rejected.

Unit root tests are notorious for their low statistical power, which can fortunately be overcome by using very long data sets. Indeed, for such longer data sets, H_0 can routinely be rejected, indicating that the neural data considered in the present work are stationary. This result obtained from longer data sets should also transfer to shorter time segments, as long as no structural change is present. Accordingly, the results of the ADF with a constant term seem to be correct, while the variant without a constant term suffers from misspecification and low power.

These results indicate that stationarity, a central requirement for a consistent estimation of autoregressive coefficients, is fulfilled. Thus, a calculation of the causality measures based on these estimates is valid.

4.3 The Influence of Preprocessing: Theoretical Considerations

First applications of the MVAR causality measures in neuroscience typically made extensive use of preprocessing techniques such as filtering and decimating, which were adapted from earlier analysis methods (Brovelli et al. 2004, Sharott et al. 2008, Wang et al. 2007, Bollimunta et al. 2008).² Such procedures had become common practice in the preprocessing of neuroscientific data before executing, for example, a frequency domain analysis. In contrast to classical methods like coherence or power, the concrete behavior of the MVAR methods in response to these preprocessing techniques has not been studied yet, although this issue is of great importance, as data processing might corrupt their working and lead to spurious or missed causalities.

In particular, it has been shown in economics - although this is not well recognized in neuroscience - that filtering and temporal aggregation like decimating in general lead to spurious causalities when applying Granger causality to this modified data (Sargent 1987, Sims 1971). In the following the theoretical basis for this behavior is presented.

4.3.1 Filtering

To compute Granger causality autoregressive model estimates are required. The resulting test statistic is a function of the estimates of these autoregressive coefficients. Hence, it is important that these estimates are not altered by preprocessing, as otherwise wrong inference may be drawn. Unfortunately, this is generally not the case. To see this, consider two covariance stationary time series y_t and x_t , related

²As a notable exception, Roebroek et al. (2005) pointed at potential errors induced by filtering.

by:³

$$y_t = \sum_{j=0}^{\infty} a_j x_{t-j} + \varepsilon_t \quad (4.4)$$

where ε_t is a white noise process with variance σ_ε . The least squares regression coefficients a_j from a projection of y_t on x_t are given by (Sargent 1987):

$$a_j(L) = \frac{g_{xy}(L)}{g_x(L)} \quad (4.5)$$

g_{xy} is the covariance generating function and g_x is the autocovariance generating function. In the following, we use operator notation as this greatly simplifies the equations. Formally, the covariance generating function is defined as $g_{xy}(z) = \sum_{k=-\infty}^{\infty} c_{xy}(k) z^k$, where the coefficient on z^k is the k^{th} lagged covariance, i.e.

$$E(y_t - Ey_t)(x_{t-k} - Ex_{t-k}).$$

Note that (4.5) is just the usual calculation of the regression coefficient as the covariance between x and y divided by the variance of x . L denotes the lag operator, which simply shifts a time series by one point in time. If it is applied L^i times the time series is shifted by i time points:

$$L^i y_t = y_{t-i} \quad (4.6)$$

³The following exposition draws on Sargent (1987).

4.3. THE INFLUENCE OF PREPROCESSING: THEORETICAL CONSIDERATIONS

The covariance generating function can be written as:

$$\begin{aligned}
 g_x(L) &= \sum_{k=-\infty}^{\infty} c_x(k)L^k \\
 &= \sigma_\varepsilon^2 \sum_{j=-\infty}^{\infty} b_j L^{-j} \sum_{j=-\infty}^{\infty} b_j L^j \\
 &= \sigma_\varepsilon^2 B(L^{-1})B(L),
 \end{aligned} \tag{4.7}$$

where $B(L) = \sum_{j=-\infty}^{\infty} b_j L^j$ and b_j are the coefficients of the Wold infinite moving average representation $x_t = \sum_{j=0}^{\infty} b_j u_{t-j}$, which exists for every covariance-stationary process (Hamilton 1994). The second equality in (4.7) follows from the fact that u_t is a serially uncorrelated random process with $E u_{t-j} u_{t-h} = 0 \forall j \neq h$.⁴ If, as it is the case with Granger causality, only positive time lags are considered for the projection, the least square coefficients are given as follows (Sargent 1987, p. 313):

$$a_j(L) = \left[\frac{g_{yx}(z)}{B(L^{-1})} \right]_+ \frac{1}{B(L)}, \tag{4.8}$$

where the $[\]_+$ sign denotes, that only positive lags are allowed. Now consider the application of a filter function $f(L)$ to both time series x_t and y_t :

$$x_t^f = \sum_{j=-\infty}^{\infty} f_j L^j x_t = f(L)x_t \text{ and } y_t^f = \sum_{j=-\infty}^{\infty} f_j L^j y_t = f(L)y_t \tag{4.9}$$

with $f(L) = \sum_{j=-\infty}^{\infty} f_j L^j$ and $\sum_{j=-\infty}^{\infty} f_j^2 < \infty$.

The filter function $f(L)$ represents linear time-invariant filters that can always be expressed in this form. A filter is called *linear*, if the amplitude of the original time series is proportional to the amplitude of the filtered time series. The term

⁴For an extensive derivation, see (Sargent 1987, p. 233).

time-invariant refers to the fact, that these filter functions do not change over time (Smith III 2007). The classical filters tested in the present work belong to the class of linear time-invariant filters. The filter function usually operates on a finite number of lags, which are considered in the filter function. This maximum number of lags with non-zero coefficients f_j is referred to as filter order. A very simple example of such a filter is a moving average filter, as shown in the following example:

$$\begin{aligned} y_t &= \frac{1}{3}x_{t+1} + \frac{1}{3}x_t + \frac{1}{3}x_{t-1} \\ &= x_t\left(\frac{1}{3}L^{-1} + \frac{1}{3}L^0 + \frac{1}{3}L\right) \\ y_t &= D(L)x_t \end{aligned} \tag{4.10}$$

In this example $D(L)$ represents the filter function.

After applying the filter function f the autoregressive series from equation 4.4 can be written as:

$$y_t^f = \sum_{j=0}^{\infty} a_j^f x_{t-j}^f + \tilde{\varepsilon}_t \tag{4.11}$$

Say x^f has the Wold representation $x^f = c(L)\eta_t$. Again using covariance generating functions, the coefficients of the projection for the filtered time series can be computed analogously to equation (4.8) as:

$$a_j^f(L) = \frac{g_{y^f x^f}}{g_{x^f}} = \left[\frac{f(L)f(L^{-1})g_{yx}(L)}{c(L^{-1})} \right]_+ \frac{1}{c(L)} \tag{4.12}$$

The first equality makes use of the fact that $g_{y^f x^f} = f(z)f(z^{-1})g_{yx}(z)$, which can be derived from the Wold representation analogously to the derivation in equation

4.3. THE INFLUENCE OF PREPROCESSING: THEORETICAL CONSIDERATIONS

(4.7). Comparing expressions (4.8) and (4.12) shows that the coefficients of the filtered and unfiltered series are in general not equal.⁵ Thus, the projection of y_t on x_t is changed by filtering. This also means that the results of Granger causality may change after filtering, thereby opening up the possibility of detecting spurious causalities or failing to detect existing causalities. The only exception arises, if Y does not *Granger cause* X . In this case filtering does not make a difference (Sims 1972). This case of non-existing causalities is of no interest in this work, as we aim to unveil existing Granger causalities.

A further important dimension of filtering is applying a filter in a “phase neutral” manner. In this case the phase of the signal is not changed by the filter function. However, there is theoretical reason to believe that phase-neutral filtering destroys the causality structure of the data. In order to achieve a zero phase-shift, the data is filtered forward and backward during offline analysis.⁶ While this eliminates the phase-shift, the time ordering of the signal becomes blurred. Note also the terminology in the signal-processing literature: by filtering forward and backward the resulting filter is no more “causal” (Smith III 2007).

The previous theoretical results all have been developed for the framework of traditional Granger causality. For more recent MVAR methods considered in the current work the issue is not as clear-cut. The computation of the respective measure and of a corresponding significance threshold is much more complicated, as besides their multivariate character also the transformation into the frequency domain has to be considered. Consider, for example, the DTF. As with the other measures it is based on the autoregressive coefficient estimates. But these are then transferred

⁵This would only be the case, if we were considering a two sided projection, i.e. a regression on past and future values. In this case (4.12) would simplify to (4.8) due to a different denominator.

⁶This is equivalent to using future time points to build current time points in the lag polynomial.

into the frequency (f) domain, according to (Kaminski and Blinowska 1991, Astolfi et al. 2005)):

$$\mathbf{a}(f) = \sum_{L=0}^{\infty} \mathbf{a}(L) e^{-2\pi i f \Delta t L} \quad (4.13)$$

where Δt is the temporal interval between two samples. As shown in section 3, this or a similar transformation of the autoregressive coefficients is made for all 5 multivariate causality measures used in the present work.

In the previous section it was shown that filtering in general changes the estimates of the autoregressive coefficients. This result carries over after transferring the coefficients to the frequency domain. Further difficulties arise when considering the effect of a particular significance measure. If filtering only generates small deviations in the estimated coefficients, these changes might not be picked up as significant, leaving the original causality estimate unaltered. Unfortunately, for most of the MVARs no analytical significance measure is available. Only for the PDC and DTF the asymptotical distribution has been derived recently (Schelter et al. 2005, Eichler 2006).

Due to these difficulties, tracing out the effect analytically must be left for future research. In the following another approach is pursued by considering the effect of several most commonly applied filters directly through a simulation study.⁷

4.3.2 Decimating and Interpolation

Besides filtering the effects of decimating a time series are also important. Theoretical considerations are found in (Quenouille 1957, Sims 1971, Wei 1982, Breitung and

⁷This analysis follows the spirit of studies like Harvey and Jäger (1993), Canova (1998) and Chan et al. (1977), who analyzed the issue of spuriousness introduced by filters commonly applied in their respective field.

4.3. THE INFLUENCE OF PREPROCESSING: THEORETICAL CONSIDERATIONS

Swanson 2002, Chan 1999).⁸ Using asymptotic arguments, Breitung and Swanson (2002) show that temporal aggregation, of which decimation is one important example, may result in loss of information contained in the variance-covariance matrix. Due to aggregation, cause and effect may then become muddled, so that Granger causality in the original sample results in instantaneous causality or contemporaneous causality in the aggregated sample. Using Monte Carlo simulations with at most a time shift between the series of 1 lag, i.e. 1 sampling point, they show that the asymptotic results may also provide a good approximation for finite samples. This prior work will be extended in chapter 5.3 by decimating data from a more realistic model, i.e. the Kus-model, presented in section 4.1.1, which uses real data and does not only consider one lag.

Moreover, the reverse case is considered, where the natural sampling frequency of the data generating process is lower than the recorded sampling frequency, i.e. the effect of interpolating the data is analyzed. This consideration is of importance, as neural data could be recorded by the equipment with a higher sampling rate than the actual neural process. In this case it would be important to still detect the correct causality pattern.

⁸For a good introduction into the wide range of consequences of time aggregation see Marcellino (1999).

Chapter 5

Simulations I: Influence of Preprocessing on Multivariate Causality Measures

After having provided the theoretical considerations concerning filtering, decimating and interpolation for Granger causality in chapter 4.3, in this chapter the results from simulations are described in order to test the influence of data preprocessing.¹ The simulations should extend our understanding of the influence of preprocessing techniques on MVAR causality measures. To this end the Kus- and Schelter-model are used and the two numerical procedures, LOOM and random permutation, are applied to obtain a significance threshold.

¹Most of the simulations presented in this chapter have been published as: E. Florin, J. Gross, J. Pfeifer, G.R. Fink, L. Timmermann (2010): The effect of filtering on Granger causality based multivariate causality measures, *NeuroImage*, 50(2): 577-588. Furthermore a poster with these results has been presented at the 15th Annual meeting of the Organization for Human Brain Mapping: E. Florin, J. Gross, J. Pfeifer, G. R. Fink, L. Timmermann (2009): The effect of filtering on Granger causality derived multivariate measures, *NeuroImage*, 47(1), S101.

5.1 Design of the Simulation Study

This section gives a detailed description of the simulation study. An overview over the different analysis steps is presented in figure 5.1. In the first step, the model

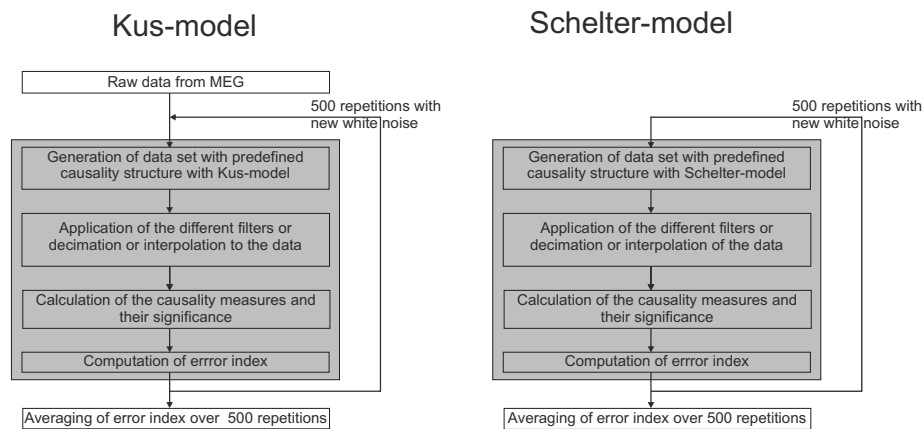


Figure 5.1: Design of the simulation study on the influence of data preprocessing

suggested by Kus et al. (2004) and the model suggested by Scheluter et al. (2006) were used to impose a predefined causality structure on the data. For the Kus-model a MEG channel (here channel 96) was used as the basis of the first signal channel in order to generate subsequently the other channels. The MEG recording was obtained with a whole-head Neuromag 122 MEG-system during rest (passband filter, 0.03 to 330 Hz).

After generation of the data channels different filters were applied. The four most common linear time invariant filter types were analyzed: a Butterworth filter (the most common one in neuroscience), a Chebyshev filter of type 1 and type 2 and an elliptic filter, all as implemented in Matlab (version 7.5.0 R2007b, The MathWorks, Inc., Natick, MA). The difference in the filter functions for a 80 Hz low-pass filter are illustrated in figure 5.2. All of these principal filter types are optimal in some

5.1. DESIGN OF THE SIMULATION STUDY

sense.

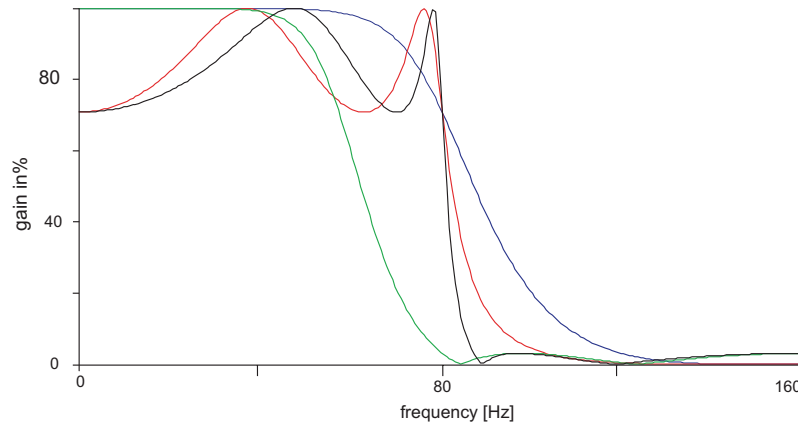


Figure 5.2: The different filter functions for a 80 Hz low-pass filter with a filter order of 4: Butterworth (blue), Chebyshev type 1 (red), Chebyshev type 2 (green), Elliptic (black). x- axis: frequency; y-axis: The gain in percent is the percentage of how much of the particular frequency passes through the filter.

The optimal filter gain function for a given filter order should have an i) as steep as possible drop-off at the desired cut-off frequency, and ii) no so-called “ripples” in the pass- and/or stopband. The term passband refers to those frequencies, which are left in the signal after filtering and which should be unaffected by the applied filter. Stopband refers to the frequency components, which are filtered out. “Ripples” are any deviations of the filter function in the stop- or passband from a completely flat function.² The Butterworth filter function is optimal in the sense that it has no “ripples”, i.e. it is maximally flat in the passband, but is therefore not as steep. The two Chebyshev filter functions have only “ripples” in either the stop- or passband,

²As in the present work only the application of filters is tested, only finite filter orders can be considered due to a finite amount of data.

but are therefore steeper than the Butterworth filter. They are optimal in that they minimize the error between the idealized filter characteristics and the actual one over the range of the filter. The elliptic filter is optimally steep, but this comes at the cost of “ripples” in both stop- and passband.

The magnitude squared of the frequency response function (G) of these filters are as follows (Parks and Burrus 1987, Shenoit 2006):

n^{th} -order Butterworth low-pass filter:

$$|G(jf)|^2 = \frac{1}{1 + D_{2n}g^{2n}} \quad (5.1)$$

n is the order of filter

f is the frequency

D_{2n} is a constant. It determines at which value of f the transition from pass- to stopband occurs.

n^{th} order Chebychev type I low-pass filter:

$$|G(jf)|^2 = \frac{H_0^2}{1 + \varepsilon^2 C_n^2 f} \quad (5.2)$$

ε controls the ripple size.

$C_n(f)$ is a Chebyshev polynomial of n^{th} order. It is defined by:

$$C_n(f) = \cos(ncos^{-1}f) \quad (5.3)$$

n^{th} order Chebychev type II low-pass filter:

$$|G(\frac{1}{jf})|^2 = \frac{1}{1 + \varepsilon^2 C_n^2(\frac{1}{f})}. \quad (5.4)$$

5.1. DESIGN OF THE SIMULATION STUDY

n^{th} order elliptic low-pass filter:³

$$|G(jf)|^2 = \frac{1}{1 + \varepsilon^2 E^2(f)} \quad (5.5)$$

$E(f)$ is the elliptic rational function. It can be expressed in zero-pole form (Lutovac et al. 2001):

$$\begin{aligned} E(n, \xi, x) &= r_0 \frac{\prod_{i=1}^{n/2} (x - x_i^2)}{\prod_{i=1}^{n/2} (x - x_{p,i}^2)} \\ r_0 &= \frac{\prod_{i=1}^{n/2} (1 - x_{p,i}^2)}{\prod_{i=1}^{n/2} (1 - x_i^2)}, \text{ n even} \\ E(n, \xi, x) &= r_0 x \frac{\prod_{i=1}^{(n-1)/2} (x - x_i^2)}{\prod_{i=1}^{(n-1)/2} (x - x_{p,i}^2)} \\ r_0 &= \frac{\prod_{i=1}^{(n-1)/2} (1 - x_{p,i}^2)}{\prod_{i=1}^{(n-1)/2} (1 - x_i^2)}, \text{ n odd} \end{aligned} \quad (5.6)$$

r_0 normalizes $E(n, \xi, 1)$ to 1. ξ is the so-called selectivity factor, which can be interpreted as the slope of E at $x = 1$. If $\xi \rightarrow \infty$, the rational function $E(n, \xi, x)$ degrades to the Chebyshev polynomial $C_n(x)$ (Lutovac et al. 2001).

For each of these different filter functions two different kinds of filters are tested. The first type are those filters, which reduce the frequency spectrum, i.e. high- and low-pass filters. A high-pass filter is commonly used to remove e.g. low-frequency

³The elliptic filter is the most complicated one. For a thorough review of its characteristics and details about its specific design, compare (Lutovac et al. 2001).

movement artifacts, while a low-pass filter is applied to reduce the high frequency spectrum to the frequencies of interest. As high-pass filter a 1 Hz high-pass filter was tested. As low-pass filters a 80, 100, 120, 160, 320 and 480 Hz filter were applied to the data. The second type of filters are those which remove an artifact in the frequency range of interest. A very common artifact of this kind is the 50 Hz power-line artifact. To remove this artifact commonly a notch filter is applied. To evaluate the performance of the notch filter a sine wave of 50 Hz was added to the data to simulate power-line noise. The power spectrum of the constructed signal is shown in figure 5.3. Afterwards a notch filter that is provided by the EEGLAB routines (<http://www.sccn.ucsd.edu/eeglab>) was applied.

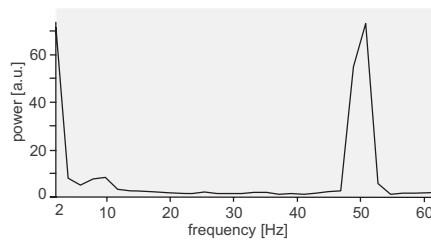


Figure 5.3: Power spectrum of the simulated data with 50 Hz artifact

It is quite common to use these filters in a so-called phase neutral manner, i.e. that the phase of a time series is not shifted by the filter process. However, there is theoretical reason to believe that phase neutral filtering destroys the causality structure of the data. Thus, for each of the above discussed filter settings both the phase neutral filtering option and the non-phase neutral one were analyzed. Note that applying a phase neutral filter automatically doubles the filter order by filtering forward and backward. Hence, to compensate for the effect of phase neutral filtering, one has to compare the respective phase neutral filter to the non-phase neutral filter

5.1. DESIGN OF THE SIMULATION STUDY

of twice the filter order.

As the filter order influences the steepness of the frequency cut-off, it is also likely that it influences the results of causality measures. Furthermore with a greater filter order more past lags are used to calculate the present time point, so that a change in the causality structure becomes more likely with a higher filter order. Thus, to test this conjecture the filter order was systematically varied for the 80 Hz low-pass filter. This variation was only performed with this filter in order to reduce the computational burden. The effect of increasing the filter order should be similar for the other filters.

Besides these classical linear time-invariant filter functions, the reduction of the frequency spectrum with a wavelet decomposition was tested. Using wavelets has been proposed recently for the application of Granger causality in a time-scale approach (Dhamala et al. 2008a, Dhamala et al. 2008b). For this purpose the signal was described with Daubechies wavelets (Daubechies 1990, Daubechies 1992) of order 4, because this has been determined to be a good approximation for EEG data (Adeli et al. 2003). Unfortunately there exists no closed form that could be presented here. Thus, only the square modulus of the transfer function of Daubechies wavelets is given (Misiti et al. 2006):

$$|G_0(f)|^2 = (\cos^2(\frac{f}{2}))^N P(\sin^2(\frac{f}{2})) \quad (5.7)$$

N – wavelet order

$P(y) = \sum_{k=0}^{N-1} C_k^{N-1+k} y_k$, where C_k^{N-1+k} denotes the binomial coefficients.

Daubechies wavelets are a family of orthogonal wavelets that define a discrete wavelet transform characterized by a maximal number of vanishing moments for a given support (Walnut 2004). To mimic the different low-pass settings the 1st, 2nd and 3rd

level of the wavelet decomposition were removed from the signal.⁴ By applying a wavelet decomposition to a signal the signal is decomposed into two parts at each level. One part contains the high frequency components and the other the low frequency components. By further decomposing the low frequency components, the frequencies contained in the resulting low frequency signal can be further reduced. Table 5.1 shows the resulting cut-off frequencies for a Daubechies wavelet of order 4 and a sampling rate of 1000 Hz. In a first step, "the first level" cut-off is 357.1 Hz. Iteratively applying this procedure each time halves the frequencies. Thus, each removed wavelet level acts as a low-pass filter. To construct something similar to a 1 Hz high-pass filter the 9th level and all higher levels were removed from the signal.

Table 5.1: Cut-off frequencies corresponding to different levels of Daubechies wavelets of order 4 for a sampling rate of 1000 Hz

Level	1	2	3	4	5	6	7	8	9	10
Frequency [Hz]	357.1	178.6	89.3	44.6	22.3	11.2	5.6	2.8	1.4	0.7

Besides the different filter settings described above, the channels were down-sampled by a factor of 10, 6, 4 and 3 with the "decimate" function implemented in Matlab. These decimating factors were chosen, as 10 is greater than the largest displacement of the underlying lag structure, while a factor of 4 is a common divisor and should preserve the lag structure. The factor 6 is in between the original lag structure and allows to test whether the causality structure can still be identified in this case. The factor of 3 is shorter than the actual lag structure.

For the model estimation the true lag length of 12 was used as the AR-model order such that all direct and indirect connections should be detected and distinguished.

⁴For more information about these wavelet filter banks, compare (Mallat 1999).

5.1. DESIGN OF THE SIMULATION STUDY

3000 data points were used as data length, as this led to reliable causality measure estimates in the baseline case of unfiltered data and is reasonable from a computational point of view. Moreover, this is by more than a factor of 30 larger than the 84 estimated coefficients, thus yielding reliable MVAR parameter estimates.

In order to have a rationale for using high- and low-pass filters, only frequencies from 2.5 to 48 Hz were regarded for the analysis of the causality measures as this is the most common frequency range for neural data. In particular, with this frequency range the alpha (8-12 Hz) and beta band (12-30 Hz) are covered, as well as parts of the low gamma band (30-80 Hz) (Schnitzler and Gross 2005). Importantly, for the baseline case without preprocessing all simulated connections are found when restricting the analysis to this frequency range. There may be information about connections implied by the model contained outside of this frequency band, but the information inside the window of 2.5 to 48 Hz is sufficient to identify all connections correctly. Filters were then applied subsequently to exclude regions of no interest or to remove artifacts while theoretically leaving the data in the range of interest from 2.5 Hz to 48 Hz unaltered. To leave an error margin due to the non-infinite slope of a non-optimal filters' gain function, the lowest applied low-pass filter was 80 Hz and the high-pass filter was at 1 Hz. The 50 Hz notch filter is a critical case. While it is near to the frequency range of interest, it is still applied as one hopes to offset the negative effect of the current artifact on the data. Thus, our approach imitates practical applications where filtering may exclude potentially relevant information but one nevertheless aims at deriving correct conclusions as the area of interest in the data should not be affected.

In contrast to ideal theoretical settings one has to deal with finite filter orders and finite samples giving rise to imperfect approximations to optimal filters and artifacts at the beginning and end of the sample as an infinite number of lags and leads is

not available. To avoid introducing artifacts at the beginning and end of the data, additional 100 data points at the beginning and end of the data set were generated. The filters were applied to this larger data set and afterwards these extra data points were discarded for the estimation of the model.⁵

To validate the results each different filter setting was sampled 500 times. For each of these 500 repetitions each channel was created with new Gaussian white noise, the significance computation was repeated and both the falsely detected connections and the missed connections were counted. A false positive connection was counted, if the particular MVAR was significant at any frequency in the range from 2.5 Hz to 48 Hz for a not implied connection. For the missed connections the undetected implied connections were counted. For the Kus-model the implied connections are those, which are shown in figure 4.1. For example a connection from channel 1 to 2 should be detected. If it is not detected, it is treated as a missed connection for this particular direction. The falsely detected connections or false positive ones (all those which are not shown in figure 4.1) are also summed up. Besides those implied and not implied connections the Kus-model contains some indirect connections, which are those from channel 1 to channels 3, 5 and 6. If these connections are detected they are counted in the same way as the false positive detections, in order to determine, which of the measures is able to discriminate between direct and indirect connections. After the 500 repetitions the average over the missed and false detections was counted. For the missed connections an average of 5 indicated, that 100 % were missed, and for the false positives an average of 37 indicated 100 % false detections. For the Schelter model in total 7 connections were implied and thus a maximum of 13 false positive

⁵Alternatively, to avoid discarding part of the data set, which may be particularly important for trial based studies, where the time dimension is often short, one could use the estimated autoregressive model to forecast additional data points and then apply the filter to this extended data set (Kaiser and Maravall 2005).

5.2. RESULTS: FILTERING

detections could be made during each repetition.

To compare the results of the different filters and causality measures, a non-parametric test statistic was used, because the distribution of the causality measures was not normal. Furthermore, the comparisons were made between independent samples. Thus, to statistically evaluate the different filter settings they were compared to the case with no filtering using the Mann-Whitney-U-test (Mann and Whitney 1947). The comparisons between the phase neutral and non-phase neutral filtering and the influence of the low-pass filter were also made with the Mann-Whitney-U-test. Results were corrected for the inflated type I error with a Bonferroni correction in case of multiple comparisons (Bonferroni 1936).

5.2 Results: Filtering

To give the reader a quick summary of the results presented in the following of this section, they are summarized in table 5.2.

Table 5.2: Recommendations based on the simulation results concerning the usage of filtering in combination with causality measures

Filter function	Low-pass filter	High-pass filter	Notch filter	Filter order	Phase shift
Butterworth	no	as low as possible	yes	as low as possible	non-phase neutral

5.2.1 Filter Function

First, the results of the different filter types, i.e. 1 Hz high-pass, 80 and 160 Hz low-pass filter with the 4 different filter functions, in combination with the LOOM will

be presented. Figure 5.4 displays the results of the squared partial directed coherence (sPDC) with the LOOM and the Kus-model.⁶ The sPDC results are presented as it led to the best results compared to the other causality measures. The results of the other causality measures are given in table A.1.

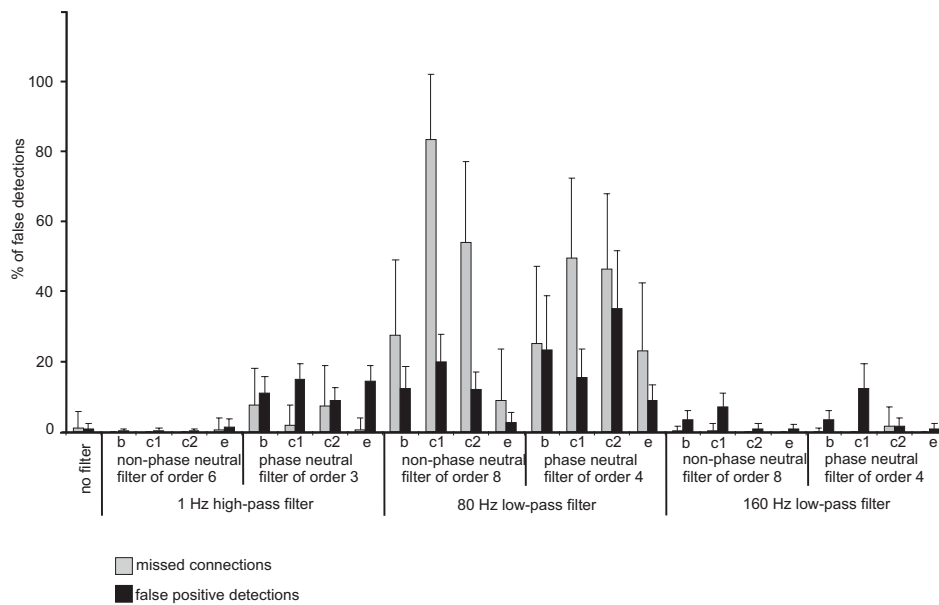


Figure 5.4: Different filter types for the sPDC with LOOM:

Butterworth (b), Chebyshev type 1 (c1), Chebyshev type 2 (c2) and elliptic (e) for a 1 Hz high-pass filter, a 80 Hz and 160 Hz low-pass filter with once a phase neutral and once with a non-phase neutral filter option. The error bars indicate the standard deviation. y-axes: percentage of false/missed connections.

In contrast to the baseline case, for all 80 Hz low-pass filter settings, most of the

⁶Note that the filter order for the phase neutral filter has only half the size of the non-phase neutral one in order to make the two comparable.

5.2. RESULTS: FILTERING

160 Hz low-pass filter settings, and the phase neutral 1 Hz high-pass filter significantly more false positive and missed detections were observed. In particular with the 80 Hz low-pass filter up to 83% false positive detections were made and 35% connections were missed. Only for the non-phase neutral 1 Hz high-pass filter and the 160 Hz low-pass elliptic filter a positive significant influence of filtering was found compared to the baseline case. A higher low-pass filter led to fewer false detections of the causality measure compared to a lower low-pass. Furthermore, the non-phase neutral filtering gave better results with the high-pass filter. In the baseline case, the PDC behaved very similar to the sPDC. It made, however, slightly more false detections for some of the filters. The DTF can by construction not distinguish between direct and indirect connections and thus produces 18% false positive detections in the baseline case. The dDTF and H also performed not appropriate with 75% missed connections in the baseline case. Some filters led to a clear reduction of the missed connections. The dDTF showed a good behavior with only 1% missed connections after applying the 160 Hz low-pass filter to the data. H, however, did not show such a positive influence of the filter.

Second, when computing the significance threshold with random permutation all filter settings considered led to significantly worse results than without filtering (results figure 5.5 and table A.2). For many filter settings, however, no connections were missed, but many false detection were made. This indicates that with filtering the random permutation underestimates the significance threshold. i.e. the size of the test statistic is too large. Interestingly, the only exception from this behavior was obtained with the phase neutral 1 Hz high-pass filter. With this filter as many as 50% of the true connections were missed, while the same non-phase neutral filter missed no connections. This indicates that the phase neutral filtering disrupted the causality structure. Furthermore, increasing the low-pass cut-off led to fewer false positive

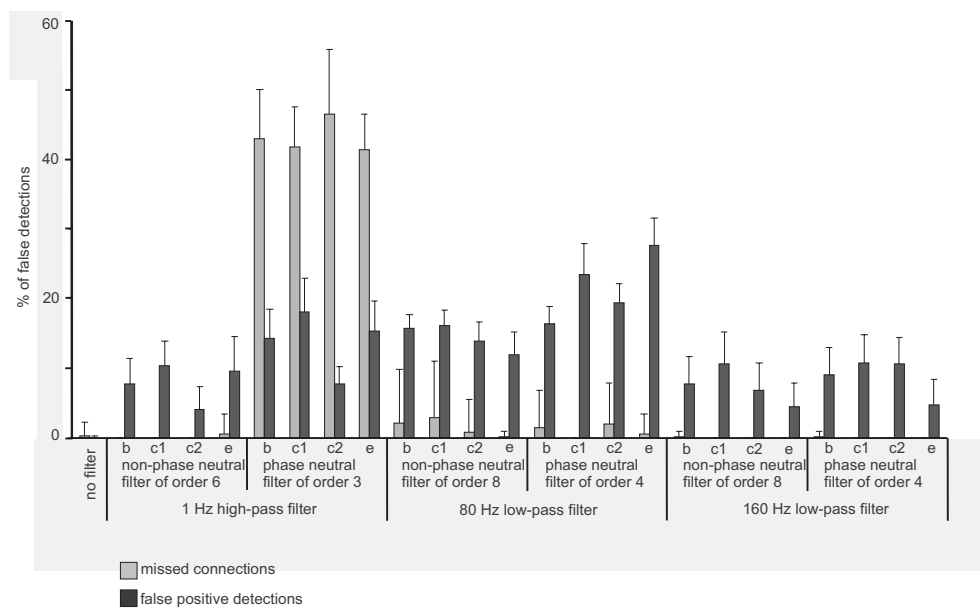


Figure 5.5: Different filter algorithms for the sPDC with random permutation: Butterworth (b), Chebyshev type 1 (c1), Chebyshev type 2 (c2) and elliptic (e) for a 1 Hz high-pass filter, a 80 Hz and 160 Hz low-pass filter with once a phase neutral and once with a non-phase neutral filter option. The error bars indicate the standard deviation. y-axes: percentage of false/missed connections.

5.2. RESULTS: FILTERING

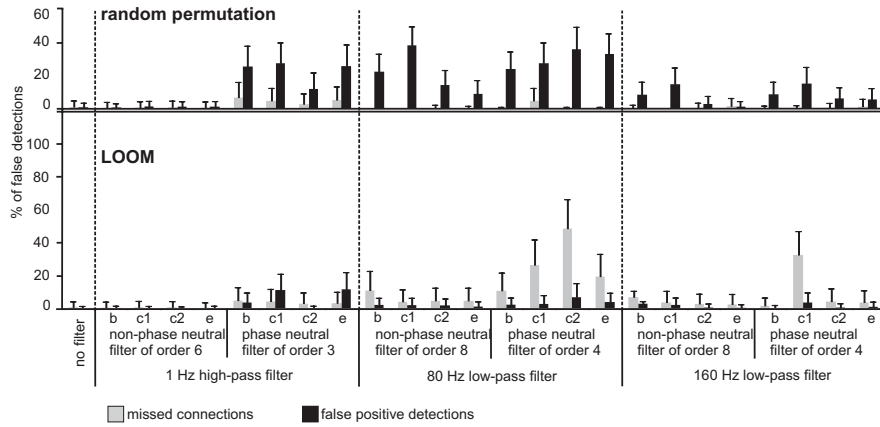


Figure 5.6: Different filter algorithms for the sPDC with the Schelter-model: Butterworth (b), Chebyshev type 1 (c1), Chebyshev type 2 (c2) and elliptic (e) for a 1 Hz high-pass filter, a 80 Hz and 160 Hz low-pass filter using both a phase neutral and a non-phase neutral filter option. y-axes: percentage of false/missed connections. Upper Panel: sPDC with random permutation; lower panel: sPDC with LOOM.

detections. Note that the results of PDC and sPDC with random permutation are identical. Already in the baseline case DTF, dDTF and H performed worse than the PDC/sPDC and detected some false positive connections while missing many of the implied connections. With filtering the number of false positive detections increased even more for these measures. But interestingly the number of missed connections decreased for most filters, indicating that the random permutation indeed underestimated the significance threshold, when filtering was applied.

If the Schelter-model was used instead of the Kus-model and the different filter settings were applied, the results were essentially the same. The results for the sPDC are shown in figure 5.6 and the results for the other measures can be found in table A.3 and A.4. With the 80 Hz and 160 Hz low-pass filter a significant increase in false detections is seen. The only exception from this behavior is again the 1 Hz

high-pass filter. Here again the non-phase neutral filter performed better than the phase neutral filter. However, the 1 Hz non-phase neutral filter did not lead to an improvement compared to the baseline case and did not worsen the result either. Applying a low-pass filter led to false positive detections with the Scheluter-model and the LOOM, while with the random permutation this led to more missed connections.

5.2.2 Filter Order

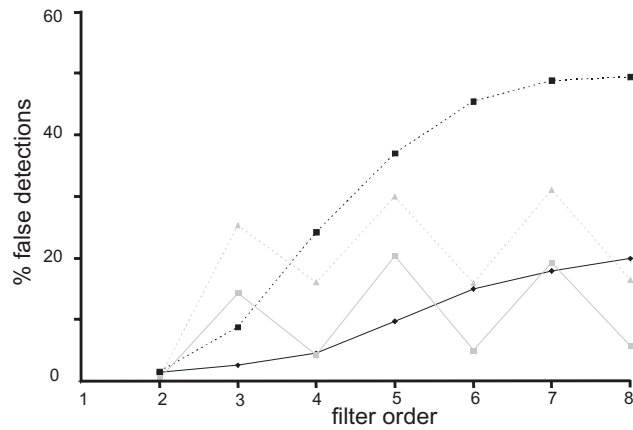


Figure 5.7: Dependence on the filter order: x-axis: filter order; y-axis: error index for the sPDC with LOOM; black solid line - non-phase neutral Butterworth filter; black dotted line - phase neutral Butterworth filter; grey solid line - non-phase neutral elliptic filter; grey dotted line - phase neutral elliptic filter.

In a next step the influence of the filter order was investigated. As the elliptic and Butterworth filter were the best performing filter types with the LOOM in these first simulations, the two Chebyshev filters and the random permutation are not further considered in the following. Figure 5.7 displays the results of the sPDC with LOOM for both, elliptic and Butterworth 80 Hz low-pass filters, with different filter orders,

5.2. RESULTS: FILTERING

with and without the phase neutral filter option (results for other MVAR see table A.5). For better comparison an overall error index was computed as the mean of the percentage of false positives and missed connections. Averaging false positives and missed connections is justified, as one is usually interested in the overall performance of a causality measure. As an extreme example, if connections are detected between all signals, one would not look at the correctly found true connections and think of this as a good behavior in the sense that all implied connections were found. As is evident from figure 5.7 for the Butterworth filter, the number of false detections increased with the filter order. While the Butterworth filter led to a monotonous increase in the error index, such a simple relationship was not observed for the elliptic filter. Rather the error index oscillated with increasing filter order.

5.2.3 Phase Neutral vs. Non-Phase Neutral Filtering

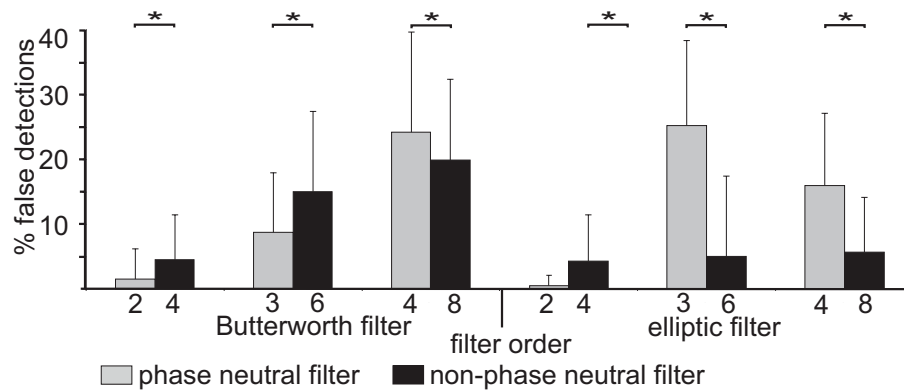


Figure 5.8: Phase neutral vs. non-phase neutral filter. Note that the filter order for the non-phase neutral filter was chosen twice as large as the one for the phase neutral filter.

When comparing the phase neutral with the non-phase neutral filtering of equal

filter order, phase neutral filtering led to significantly worse results for both, elliptic and Butterworth filter, for all measures. However, when the filter order for the non-phase neutral filter was chosen twice as large as the one of the phase neutral filter in order to correct for the phase neutral filtering (see figure 5.8 and table A.5), the phase neutral Butterworth filter was significantly better than the non-phase neutral Butterworth filter up to a filter order of 6. For the elliptic filter only the 80 Hz phase neutral low-pass filter of order 2 was significantly better than the corresponding non-phase neutral filter of order 4 (for all reported results: $p < 0.05$).

5.2.4 Low-Pass Filtering

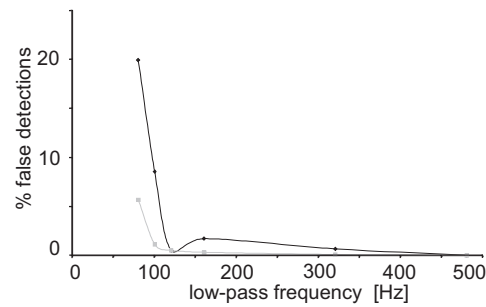


Figure 5.9: Decrease in error index with increase in low-pass filter frequency threshold: grey line - non-phase neutral elliptic filter; black line - non-phase neutral Butterworth filter; both with a filter order of 8.

The simulations shown in figure 5.4 revealed that both a Butterworth and an elliptic low-pass filter of 80 Hz led to many false detections, despite only considering the frequency range of 2.5-48 Hz. This naturally raises the question, whether there is an upper bound from which on a low-pass filter has no further influence on the causality measures. Figure 5.9 displays the behavior of the sPDC with LOOM depending on increasing low-pass filters (results for other MVARs see table A.6). Only results for

5.2. RESULTS: FILTERING

the non-phase neutral case are presented, as it was previously shown that phase neutral filtering leads to worse results. Both filter types showed a dramatic decline of false detections when moving upwards from the 80 Hz low-pass. However, the speed of this decline differed. The elliptic non-phase neutral filter reached the threshold of less than 5% false detections for the sPDC already for a 100 Hz low-pass filter, while the non-phase neutral Butterworth filter reached this threshold with a low-pass of 120 Hz.

5.2.5 Notch Filter

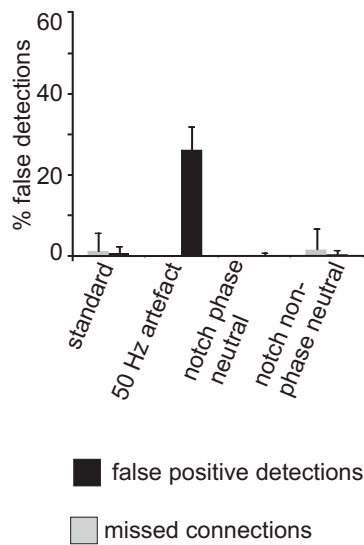


Figure 5.10: Influence of notch filter for sPDC with LOOM

Up to this point the data generated from the model were regarded as reflecting the true data generating process and it was considered what filtering did to this signal. In order to gauge the effect of external noise of the type that could be introduced by

e.g. 50 Hz current the setup was modified by adding a 50 Hz sine wave to the signals, which had $1/5^{th}$ of the variance of the original signal, leading to a pronounced current artifact (see figure 5.3). A notch filter has been applied to these data in order to remove the 50 Hz artifact now contained in the data.

As expected, the simulated power-line noise resulted in several false positive detections for all causality measures with LOOM (see figure 5.10 and table A.7). Applying the notch filter was successful and led to a decrease in false detections to less than 1 % for the sPDC. This is consistent with the 1% alpha-level of the LOOM. For the other MVARs the effect was similar, but as the error index was already higher in the baseline case, the improvement in performance was not as pronounced as for the sPDC (see table A.7).

5.2.6 Wavelet Filtering

Besides the classical linear time invariant filter functions the application of Daubechies wavelets was tested. As can be seen in figure 5.11 removing more wavelet components from the signal, which is equivalent to lowering the low-pass filter increases the number of false detections. This is similar to the behavior of the different low-pass filter settings, where an increase in false detections was seen with decreasing cut-off frequency. Furthermore the wavelet reconstruction, which comes closest to the 1 Hz high-pass filter poses only few problems, even though about 5% false positive detections are still more than what should be made with a 99% significance threshold. In combination with random permutation the behavior for the different levels of the wavelet decompositions was even worse.

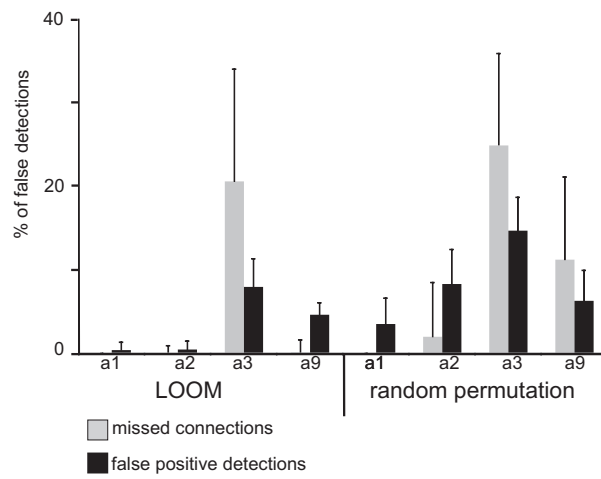


Figure 5.11: Influence of wavelet decomposition with Daubechies wavelets of order 4 for sPDC with LOOM and random permutation. The “a” indicates the highest wavelet component removed from the signal. In the case of a9 all higher wavelet components were removed to construct a high-pass filter.

5.3 Results: Decimating and Interpolation

After considering the different filter settings, in the following the influence of decimating the data and interpolation will be evaluated. The simulation setup is the same as before.

5.3.1 Decimating

Besides the different filter settings the influence of reducing the sampling rate of the channels was evaluated. For this purpose the “decimate” function implemented in Matlab was used to reduce the sampling rate by a factor of 10, 6, 4 and 3.

As can be seen in figure 5.12 for the sPDC, applying decimation greater than the minimum time lag between two signals led to wrong conclusions: 9% false positive connections were detected and 18% were missed with the LOOM. This is in accordance with theoretical considerations. The other causality measures performed even worse (see table A.7). If decimation proceeded with a factor equal to the common divisor of the time lag of 4, the lag structure was not disrupted and no misbehavior for the sPDC, DTF, H and dDTF became apparent. In contrast, decimating by a factor which was not a common divisor of the lag structure led again to false positive detections, but not to as many as with a decimating factor greater than the lag structure.

5.3.2 Interpolation

To gauge the effect of recording the data with a higher sampling frequency than the natural frequency of the data generating process, the case of oversampling was mimicked by interpolating the data. The interpolation exercise mirrors the decimation approach with interpolation factors of 4. A linear, a cubic, a cubic spline and a fast

5.3. RESULTS: DECIMATING AND INTERPOLATION

fourier (FFT) interpolation algorithm were used. For the latter one, the data are transformed into the frequency domain with a FFT and then transformed back into the time domain with more data points.

The results are presented in figure 5.12. Generating the model with a shorter time lag and then interpolating it with a linear or cubic approach by a factor of 4, likewise did not lead to misbehavior for sPDC and dDTF, when the model order was adjusted accordingly from 12 to 48 due to the interpolation of a factor of 4. With this increase the new lag structure is correctly detected. Interestingly, the frequency domain based FFT interpolation led to many false detections (5% false positive and 33% missed connections).

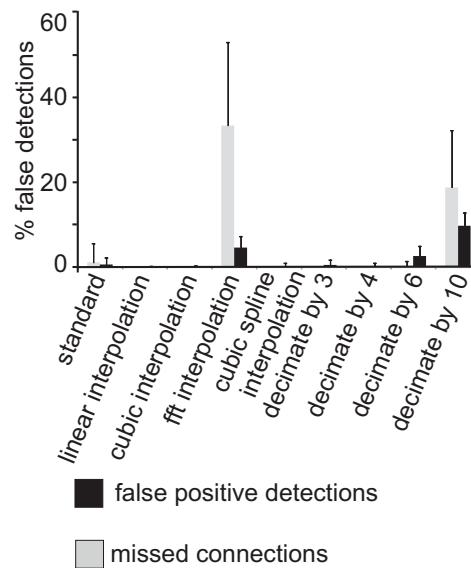


Figure 5.12: Influence of decimating and interpolation for sPDC with LOOM

5.4 Discussion

Knowledge about the behavior of the MVAR measures with different preprocessing techniques is crucial for correctly applying causality measures to the wide range of open neuroscientific problems. In section 4.3 it was argued on theoretical grounds, that filtering and decimating in general leads to both spurious and missed causalities in the application of traditional Granger causality. This resulted in the conjecture that this behavior would carry over to the MVARs derived from Granger causality. Thus, simulations were performed to analyze whether commonly applied preprocessing techniques do affect the MVAR causality measures.

As expected from both theoretical considerations and the literature (Sargent 1987, Roebroek et al. 2005), a significant increase in misdetections arose with almost all filters applied with both significance thresholds. In particular, the 80 Hz low-pass led to many false detections independently of the filter function used. The only filters that did not lead to a significant increase in false detections were the 1 Hz high-pass filter and the 160 Hz low-pass, when the causality measure was applied in combination with LOOM. In addition, non-phase neutral filtering gave better results than phase neutral filtering. Interestingly, with random permutation none of the filters gave results as good as without filtering. A wavelet decomposition with subsequent reduction of the frequency spectrum led to very similar results with many false detections. In the following the results will be discussed in detail with respect to the different influencing factors.

Wavelets

Using a wavelet decomposition with Daubechies wavelets to low-pass filter the

5.4. DISCUSSION

data did also lead to an increase in false detections. This increase was, however, not as pronounced as with classical filters. Still about 15% false detections are not acceptable in a real application. Furthermore, creating a high-pass filter did also worsen the results, so that removing a movement artifact seems not possible with a wavelet decomposition. Wavelets are apparently not well suited to substitute or improve the results of classical linear time invariant filters in combination with a causality analysis. Based in the time-scale domain they may be better suited for applications with non-stationary data where they can help to identify the changing causality pattern (Dhamala et al. 2008a, Dhamala et al. 2008b).

Filter Order

The filter order represents the number of time points considered in the filter algorithm to obtain the current filtered time point. A higher filter order leads to a steeper filter function, thus making the cut-off at the desired frequency sharper. However, with an increase of filter order one would expect to disrupt the time order more severely, as more past time points are used to create the present time point and thus the time dimension is aggregated more severely. Thus, more misdetections are made with the causality measures. In accordance with these expectations the Butterworth filter, whose filter function has no “ripples”, shows an increase in false detections with increasing filter order (see figure 5.7 and table A.5) for all causality measures. For the elliptic filter, which has the steepest filter function but therefore “ripples” in the stop- and passband, this relationship is also seen, but with an additional oscillating pattern. With an odd filter order more false detections were made than with an even filter order. An explanation could be the different functional form of the elliptic rational function for even and odd filter orders, as shown in equation 5.6. The additional multiplication with x for the elliptic rational function with the products going to the

same integer as for the lower even filter order could explain the oscillatory behavior. For both even and odd orders, x_i are the zeroes and x_{pi} are the poles. However, the odd orders differ from the even ones insofar as there will always be a zero at $x = 0$ and a pole at $x = \infty$. In any case the filter order should be chosen as low as possible.

Phase Neutral vs. Non-Phase Neutral Filtering

If a phase neutral and a non-phase neutral 80 Hz low pass filter of adjusted filter order, for example a phase neutral filter of order 4 and a non-phase neutral filter of order 2, were applied to the data, non-phase neutral filtering led to significantly more false detections than phase neutral filtering in the case of a low filter order for the sPDC, PDC and DTF (see figure 5.8 and table A.5). For both the Butterworth and the elliptic filter, however, with increased filter order the phase neutral filter performed significantly worse than the non-phase neutral filter. Even after correcting for the steepness of the filter function by choosing the filter order twice as large for the non-phase neutral filter as for the phase neutral filter this effect was present. This result is in line with the theoretical consideration that applying a phase neutral filter, which is a “non-causal filter” (Smith III 2007), destroys the time structure of a time series, thereby mixing cause and effect. Since non-causal filters are often used in neuroscientific analysis, as one hopes to conserve the phase relationship, results derived after using these filters have to be interpreted with caution. Even though the results of the Butterworth filter are better with the phase neutral filter of order 2 and 3 than those with the non-phase neutral filter of order 4 and 6, it is important to keep in mind that the non-phase neutral filter still performs better with a low filter order than a phase neutral filter of the same filter order. Thus, if it is necessary to filter, one should use a non-phase neutral filter with a filter order as low as possible.

5.4. DISCUSSION

Low-Pass Filter

As the application of a 80 Hz low-pass filter led to many false detections, also higher low-pass filters were applied to the data. The simulations suggest that the use of very high low-pass filters has no effect on the results (see figure 5.9 and A.6). Theoretically, this allows for low-pass filtering of the data, but only if the low-pass is far beyond the frequency range of interest. However, a low-pass filter of 100 Hz, which should not have an influence on the considered frequency range from 2 to 48 Hz, still led to a significant increase in false detections. Thus, as the critical threshold for the low-pass frequency cannot be easily derived, low-pass filtering cannot be recommended. The low-pass of 320 Hz and 480 Hz did not remove much, if any, information from the simulated data, as the MEG signal used for the simulations was bandpass filtered from 0.03 to 330 Hz at recording. Thus, the only information in the signals beyond 330 Hz was the internal noise that became part of the simulated signals.

Filtering to Remove Concrete Artifacts

One further important finding is that the 1 Hz Butterworth high-pass filter and the notch filter did not significantly worsen the performance of the sPDC. With the Kus-model, the 1 Hz high-pass actually led to an improvement of the results. The results of the baseline case with 1% false detections for the sPDC were in line with the 99% significance threshold. The slight improvement upon this level after 1 Hz high-pass filtering in the Kus-model is most probably a result of the removed low-frequency noise, which is almost always present in raw MEG data. This conjecture is supported by the results of the Schelter-model which demonstrate that the 1 Hz high-pass filter does not lead to false detections, if no artifact is present in the data. Having available a well behaved 1 Hz high-pass filter is important to remove movement artifacts, which

could potentially lead to spurious causalities. The best performing 1 Hz high-pass filter in our simulations was the non-phase neutral 1 Hz high-pass filter with a low filter order.

A further artifact which is quite common in real data is a current artifact. To mimic this artifact a 50 Hz sine wave was added to the data which, if not removed with a notch filter, led to many false detections. Applying the notch filter allowed for the elimination of 50 Hz noise in the signal and thus a correct determination of the causality structure. Therefore, reducing power-line noise using a notch filter should not be problematic. On the contrary it is important to remove this artifact, as otherwise false positive detections might be made.

Decimating and Interpolation

In section 5.3 it has been demonstrated that in accordance with theoretical considerations (Quenouille 1957, Breitung and Swanson 2002, Granger 1980, Chan 1999, Wei 1982) decimating the data potentially destroys its causality structure. This led to many false detections, if the decimating factor was chosen greater than the original lag structure in the data. If the decimating factor was chosen as a common divisor of the lag structure, no significant increase in false detections occurred. Importantly, however, even if the decimating factor was smaller than the lag length, but not an exact multiple of the lag structure, false positive detections were made. In real settings, where the true causality and lag structure is usually not known, decimating the data thus seems not advisable. With sufficient data and hence enough degrees of freedom it may be better to simply increase the model order to capture the whole dynamics instead of decimating the data.

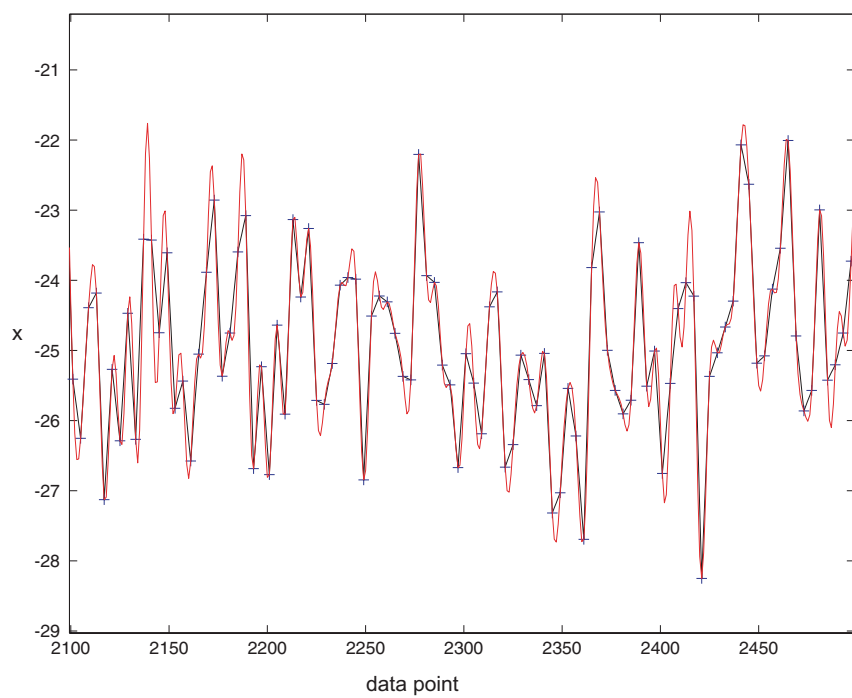


Figure 5.13: In black a time series is shown with linear interpolation. In red the same time series has been interpolated with the FFT approach. The blue crosses indicate the original time points.

In contrast to the negative effect of decimating, oversampling due to interpolation of the data by e.g. the recording equipment appears to be not much of an issue, as long as the model order is adjusted accordingly. Linear, cubic, and cubic spline interpolation had no negative effect on the detection of the causality structure. Only with FFT interpolation a significant increase in false detections occurs. A possible explanation of this effect is, that contrary to the other interpolation techniques, the data are transformed into the frequency domain and then transformed back into the time domain with more data points. While with this approach the power in the frequency spectrum of the data is unchanged, the time structure can be changed. This effect can be seen from figure 5.13, where the resulting peaks of the different time series are sometimes at different time points. Furthermore, the frequency spectrum of the interpolated series with the higher sampling rate shows an abrupt cut-off at the former Nyquist frequency that may introduce an artifact. Although the data is interpolated to have a sampling frequency of 4000 Hz the FFT-interpolated series only contains frequency components up to 500 Hz. In contrast, the linear interpolation results in a signal with frequency components up to the Nyquist frequency of 2000 Hz. In the context of linear models like the ones used in the present work, these additional frequency components introduced by interpolation seem to be important for correctly disentangling the signal transmission in the different data series.

Significance Threshold

Regarding the combination of filtering with the different significance computation measures, the effect for random permutation is in general very similar to that of the LOOM: filtering led for both methods to false detections. However, none of the filter settings showed a satisfying result with random permutation. This effect is due to the fact that smoothing of the data by filtering led to an overall underestimation

5.4. DISCUSSION

of the 99% percentile with random permutation. Accordingly many false positive detections were made. The LOOM did not underestimate the threshold and at least some filters did not exhibit a significant negative influence.

Methodological considerations

Recently, Dhamala et al. (2008a) have proposed a non-parametric approach that does not rely on autoregressive modeling. While we did not test such a non-parametric method and can only conjecture about the influence of filtering on these non-parametric methods, we are led to believe that they should be similar to the results presented here. The non-parametric approach aims at robustly estimating the spectral density matrix, i.e. the frequency domain equivalent of the covariance (Priestley 1981). As was seen in the theoretical considerations, filtering alters the latter, which was reflected in the estimates. When using a correct autoregressive model, both approaches, parametric and non-parametric, should asymptotically consistently estimate the spectral density and thus deliver same results. However, it is well known that estimation bias may arise when misspecifying the autoregressive model (Mitra and Pesaran 1999) and this bias may amplify the problems induced by filtering. In these cases, non-parametric methods may prove to be more robust.

Some words of caution are required concerning the two models used in the present work. They are both linear autoregressive models so that they cannot answer the question, how the causality measures would have performed after filtering, if nonlinear models had been used. It is well known that the underlying data generating model may play an important role (Wendling et al. 2009, Ansari-Asl et al. 2006). However, Schelter et al. (2004) and Gourevitch et al. (2006) demonstrated that at least in some cases the PDC is capable of detecting the causalities correctly in nonlinear

models. Own simulations with a nonlinear model of Gourevitch et al. indicated that the influence of filtering on the causality measures is very similar: Still many false detections were made due to filtering. Tracing out the interaction between nonlinear models, traditional filters that are usually of the linear time invariant class and the causality measures must be left for future research.

5.5 Conclusion

In summary, it is obvious from the simulations and theoretical considerations that preprocessing, which changes the time structure of a time series, such as filtering and decimating, should, if at all, only be applied with caution for causality analysis. In order to summarize the results of the simulations concerning the different preprocessing techniques and to give the researcher a guideline, when to filter, a decision algorithm is shown in figure 5.14. In this graphic the possible preprocessing techniques for certain artifacts are considered. Only in the presence of noise/artifacts that clearly interfere with the working of the causality measures filtering improved the results and hence seems advisable. Often, artifacts can be easily identified from the power spectrum of the data as it is the case with a 50 Hz power-line artifact. In less obvious cases, it might be helpful to estimate the artifacts present in the data, which could help to choose the appropriate preprocessing for real data. An interesting option is the use of state-space representations like the ones developed by Nalatore (2007, 2009). Unfortunately, for these more advanced preprocessing techniques, their effect on causality measures remains largely unknown, e.g. what happens, if data are incorrectly denoised. Analyzing the performance of methods to remove artifacts like the Kalman smoother with the expectation and maximization algorithm will be an important task for future research. The simulations also showed that filtering is inadvisable in situations where no artifact is present and the sole purpose of filtering

5.5. CONCLUSION

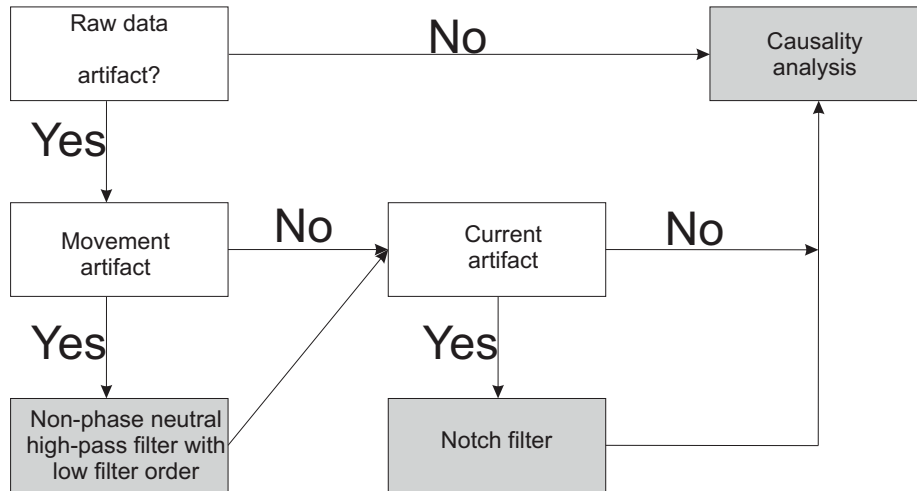


Figure 5.14: Suggested steps for preprocessing data before a causality analysis

is to reduce the frequency spectrum to the region of prior interest. Here two cases were presented where filtering was advisable. In both of these cases the artifact was clearly visible in the power spectrum of the data.

The first case, where filtering was advisable, was the presence of a simulated 50 Hz power-line artifact that led to a huge increase of misdetections. The application of a notch filter had the desired effect of removing these adverse effects while at the same time not introducing new artifacts. The second case was the 1 Hz high-pass filter. This filter did not lead to an increase in false detections, if no artifact was present (Schelter-model) and led to an improvement, if low frequency components were in the signal, as it was the case for the Kus-model. Thus, filtering can only be recommended, if strong artifacts are present. In contrast, the application of filters without the presence of strong artifacts just to reduce the frequency spectrum as is common in frequency domain analysis of time series data, does not lead to any

obvious advantage, but may rather lead to spurious or missed causalities. In any case, before applying a filter it seems advisable to analyze the effects of this data processing step in order to exclude the possibility that the obtained results are only an artifact of the filtering. Cross-checking the results derived from unprocessed data to that derived from preprocessed data is important to gauge the role of such data treatment.

Chapter 6

Simulations II: Parameter Dependence and Data Types

In this chapter¹ simulations to evaluate the performance of the five different causality measures (sPDC, PDC, DTF, dDTF and transfer function (H)) are presented. These measures are tested in combination with the two numerical significance computation approaches - random permutation (Kaminski et al. 2001) and the leave-one-out method (LOOM) (Schlögl and Supp 2006). The dependence of these measures on the parameters noise level, data length, model order and coupling strength are evaluated. In practice, model order and data length are under the researcher's control: The model order is critical for a correct evaluation of the causality measure, so that it is important to know, which influence an over- or underestimation of the model order might have. The other two parameters, coupling strength and noise level, are not as

¹Parts of this chapter have been presented at the 14th Annual meeting of the Organization for Human Brain Mapping: E. Florin, J. Gross, G.R. Fink, L. Timmermann (2008): Reliability of multivariate causality measures for neural data, *NeuroImage*, 41(1), S128. An article is currently submitted: E. Florin, J. Gross, J. Pfeifer G.R. Fink, L. Timmermann: Reliability of multivariate causality measures for neural data.

easy to influence, but knowing the boundaries in which the causality measures work well, is still important in order to correctly apply them.

The Kus-model as described in section 4.1.1 and the Schelter-model (section 4.1.2) were used. To gauge the effect of data length, noise level, model order, coupling strength and underlying real data type, these parameters were systematically varied when generating the model and afterwards a regression analysis was performed to obtain a statistically valid estimate of the parameters' influence on the causality measures.

6.1 Motivation of the Simulation Study

In order to demonstrate the need for a complete evaluation and comparison of the causality measure, here an application of all five causality measures to real data is presented. Electromyographic data and subthalamic nucleus' local field potentials of a patient with Parkinson's disease have been analyzed to determine the direction of interaction between central and muscle activity.

Table 6.1 shows the overall pattern of detected cases, where the LFP is causal for the EMG and vice versa. These results are for a representative patient suffering from Parkinson's disease with the different causality measures in combination with random permutation and LOOM. The patient was instructed to perform two conditions: a hold and a rest condition. During the hold condition the patient was instructed to lift his arm for 30 seconds, while during the rest condition he was instructed to relax and not to move. These conditions were repeated at two locations of the electrodes. A more detailed explanation of the setup can be found in chapter 7. The numbers

6.2. DESIGN OF THE SIMULATION STUDY

shown in table 6.1 represent the sum over these two conditions, rest and hold, and two locations of the electrodes, on which the patient performed both conditions.

Table 6.1: Results of the five causality measures for real data: The “→” represents the causality direction.

	LOOM		RP		total connections	
	LFP	EMG	LFP	EMG	RP	LOOM
	→ EMG	→ LFP	→ EMG	→ LFP		
PDC	17	22	2	32	34	39
sPDC	4	11	2	32	34	15
DTF	21	21	2	37	39	42
dDTF	1	2	10	22	32	3
H	4	8	13	32	45	12

The number of output and input causalities² highly depends upon both the causality measure and the numerical method for computing significance thresholds. The only common pattern, as shown in table 6.1, is that always more input than output causalities were detected, but still the ratio varied from 1:2 (dDTF + LOOM) to more than 1:16 (DTF + RP). Unfortunately, a priori one does not know which results are more likely to be correct. Currently little is known about the performance and appropriateness of a particular causality measure under different circumstances. Thus, this chapter provides a systematic evaluation of the causality measures.

6.2 Design of the Simulation Study

The Kus-model (Kus et al. 2004) was used to compare the performance of the causality measures. The complete design of this simulation study is summarized in

²Consistent with the notion of Granger causality (Granger 1969) as a temporal ordering, the term output causality is used, when the STN signal is statistically causal for the EMG activity in an autoregressive system and input causality for the opposite case.

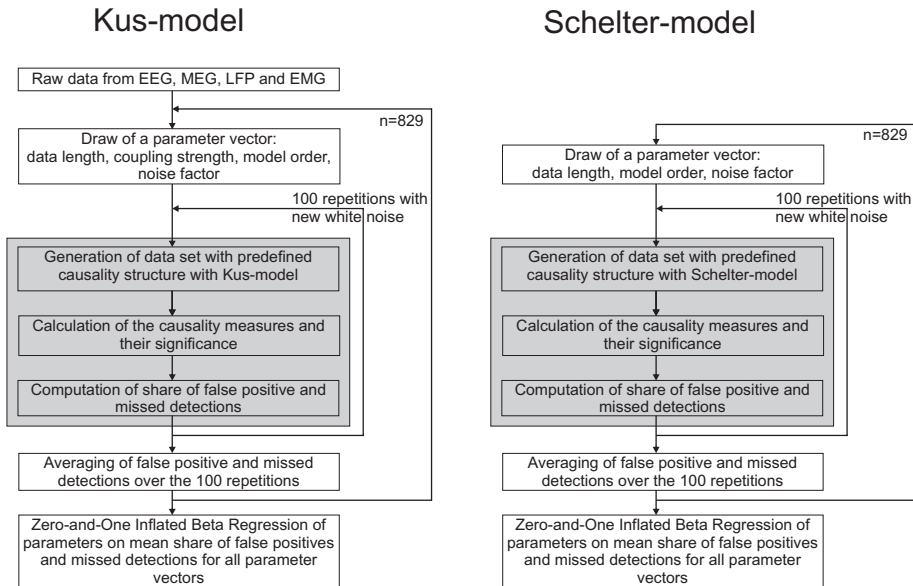


Figure 6.1: Design of the simulation study to determine the parameter dependencies

figure 6.1. Real data from EEG, EMG, MEG and macroelectrode (LFP) recordings were taken as the basis of the first signal channel and to generate subsequently the other channels according to the equation system 4.1.

As standard parameters for the simulation, 3000 data points, a model order of 12, a coupling strength of 0.8 and an internal noise level ($a_i\eta_i$) with a variance of 25% compared to the variance of the real data (rd) in channel 1 were used. In the baseline case no external noise was added. For the simulations only frequencies from 0 to 50 Hz were regarded, because this is the most common frequency range for neural data (Schnitzler and Gross 2005, Timmermann et al. 2007). This greater frequency range compared to the one chosen in chapter 5 can be used, as here no filter settings were applied to the data and thus no negative influence by the filter is expected.

6.2. DESIGN OF THE SIMULATION STUDY

In subsequent simulations the parameters were varied as summarized in table 6.2. The data length was varied in steps of 100 data points ranging from 100 to 1000 and in steps of 250 data points from 1000 to 5000 data points. The model order was varied in steps of 2 from 2 to 50 and the coupling strength was varied in steps of 0.2 up to 2. As only realistic parameter settings should be considered in the present study, the coupling strength was only varied up to a value of 2. A greater coupling strength leads to coherence values of 1, which are rarely found in biological signals. The external noise level was determined as a fraction of the variance in the real data. This fraction was varied in steps of 0.2 up to 3. In a first step, during variation of one parameter, all other parameters were kept constant at the baseline values defined above. In a second step, to get reliable estimates of the effects over the whole parameter space, the multivariate methods were calculated for 750 vectors randomly drawn from the 4 dimensional parameter grid. Overall, 829 parameter vectors were created.

Table 6.2: Parameter variation for the Kus-model in the simulations

	Starting values	Min. value	Max. value	Step size
Data length	3000	100	5000	100 from 100 to 1000 250 from 1000 to 5000
Model order	12	2	50	2
External noise level	0	0	3	0.2
Coupling strength	0.8	0.2	2	0.2

To obtain data type independent results the Schelter-model was also used (Schelter et al. 2006). Almost all parameter variations have been chosen in the same way as for

the Kus-model (see table 6.3). Only the coupling strength was not varied, as it has a complex structure in the original model and changing it might change the stability of the model. The further simulation design and analysis proceeded as for the Kus-model.

Table 6.3: Parameter variation for the Schelter-model in the simulations

	Starting values	Min. value	Max. value	Step size
Data length	3000	100	5000	100 from 100 to 1000 500 from 1000 to 5000
Model order	17	2	50	2
External noise level	0	0	3	0.2

In order to create an error index for the false positive and missed connections of each causality measure in dependence on the chosen parameter combination, each parameter vector was sampled 100 times and the false detections were counted. By a standard law of large numbers the number of false and missed detections should converge to their expectation value. 100 repetitions were chosen as it provided a good compromise between computational speed and accuracy as it delivered a sufficiently small standard error of the estimate. During these 100 repetitions each channel was created with new white Gaussian noise, the significance computation was repeated and both the falsely detected connections and the missed connections were counted. A false positive connection was counted, if the particular MVAR was significant at any frequency in the range from 0 Hz to 50 Hz. To further summarize the results, we calculated the average percentage of missed and false positive connections. Note, that this procedure does not entail multiple comparisons, but rather aggregates individually significant results.

6.3 Zero-and-One Inflated Beta Regression-Model

In order to control for the marginal effects of the varied parameters a regression analysis was performed.³ As dependent variable the average percentage of missed/false positive connections for the respective parameter vector was used. As this dependent variable has bounded support $[0,1]$ with mass points at the respective endpoints of this interval a mixed continuous-discrete distribution, the zero-and-one inflated beta distribution (Ospina and Ferrari 2008) was used for the regression. A standard linear regression would be inappropriate as it would allow predicted values below 0 and above 1, which is at odds with the causality measures ranging between 0 and 1. Two examples of possible beta distributions are shown in figure 6.2. With only 2 parameters the beta distribution is very flexible in the distribution shape it can approximate. The zero-and-one inflated beta distribution is aimed at dealing with the necessarily nonlinear effects of the explanatory variables and the fact that the conditional variance must be a function of the conditional mean (Kieschnick and McCullough 2003).⁴ A normal beta regression would also be inappropriate, as it assumes a continuous distribution of the variance. Hence each value has mass 0. However, a lot of parameter vectors have values of 0 and 1. Tests for linear parameter restrictions were performed using likelihood ratio tests (Engle 1984).

To avoid confusion with the parameterizations of the beta distribution, the parameters of the Kus-model that were varied and serve as explanatory variables in the regression are denoted as regressors in the following. Let X denote the matrix of regressors, x_i the vector corresponding to row/observation i and x_j a particular regressor j . As dependent variable the average percentage of missed or false positive

³For statistical analysis the statistical package R (<http://www.r-project.org/>) with the GAMLSS package (<http://www.gamlss.com/>) was used (Stasinopoulos and Rigby 2007).

⁴Due to the restriction to 0 and 1 the variance at the border of this range is smaller than in the middle of this range, i.e. for a value of 0 the variance is also 0.

detections for one parameter vector is taken.

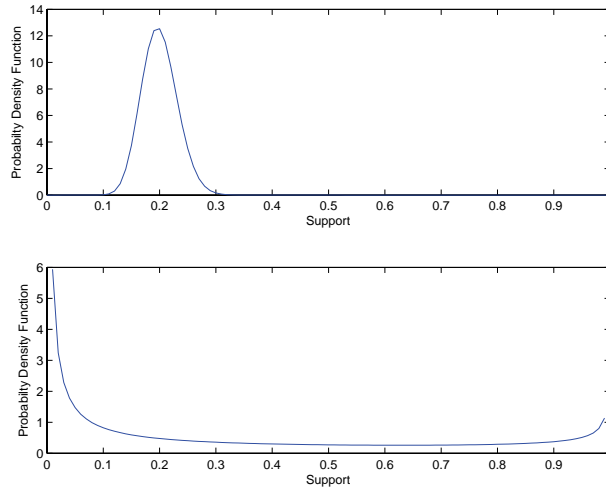


Figure 6.2: Probability density functions for two parameterizations of the beta distribution. Both have the same mean, but in the upper panel the variance is set to 0.001 and in the lower panel to 0.1.

The most important building block of the zero-and-one inflated beta distribution is the beta distribution. Let

$$f(y; \mu, \varphi) = \frac{\Gamma(\varphi)}{\Gamma(\mu\varphi)\Gamma((1-\mu)\varphi)} y^{\mu\varphi-1} (1-y)^{(1-\mu)\varphi-1} \quad (6.1)$$

denote the density function of a beta distributed variable y with location parameter μ ($0 < \mu < 1$) and dispersion parameter φ ($\varphi > 0$). In this more intuitive way of parameterizing a beta distribution (Ferrari and Cribari-Neto 2004), the parameter μ has a natural interpretation as it corresponds to the expected value of the beta-distributed variable $E(y)=\mu$. For a given μ , the dispersion parameter φ determines the variance σ^2 of y as $\sigma^2 = \frac{\mu(1-\mu)}{\varphi+1}$ (Smithson and Verkuilen 2006). The zero-and-

6.3. ZERO-AND-ONE INFLATED BETA REGRESSION-MODEL

one inflated beta distribution (beinf) now is a mixture of a Bernoulli and a beta distribution (see (Ospina and Ferrari 2008)). Its density can be represented as:

$$\text{beinf}(y; p_0, p_1, \mu, \varphi) = \begin{cases} p_0 & \text{if } y = 0 \\ (1 - p_0 - p_1) f(y; \mu, \varphi) & \text{if } y \in (0, 1) \\ p_1 & \text{if } y = 1 \end{cases} \quad (6.2)$$

For a variable $y \sim \text{beinf}(p_0, p_1, \mu, \varphi)$, its expected value is then given as

$$E(y) = p_1 + (1 - p_0 - p_1) \mu \quad (6.3)$$

Let x_i and w_i denote column vectors corresponding to row i of the regressor matrices X and W . Following (Smithson and Verkuilen 2006) a regression model in the generalized linear model (GLM) framework can be formed by specifying a logit link function

$$f(\mu_i) = \ln[\mu_i / (1 - \mu_i)] = x_i' \beta \quad (6.4)$$

for the location parameter μ and a log link

$$g(\varphi_i) = \ln(\varphi_i) = -w_i \delta \quad (6.5)$$

for the dispersion parameter φ_i in order to map the unbounded space of linear predictors into the proper sample space of the observations. Use of the logit is motivated by Cox (1996) who showed that this link function usually performs well in quasi-likelihood models of our type. The same set of independent variables for both μ_i and φ_i is used such that $w_i = x_i$. In the remainder, focus is on the location parameter μ_i as the main interest. The probabilities p_0 and p_1 are estimated as

constants. Inverting the link function for μ_i gives predicted values

$$\hat{\mu}_i = 1 / (1 + e^{-x_i' \hat{\beta}}) \quad (6.6)$$

Hence, the conditional expectation follows

$$E(y_i | x_i) = p_1 + (1 - p_0 - p_1) \mu_i \quad (6.7)$$

while the marginal effect of a regressor x_j follows from 6.6 and 6.7 as

$$\frac{\partial E(y_i | x_i)}{\partial x_j} = (1 - p_0 - p_1) \frac{\frac{\partial x_i' \hat{\beta}}{\partial x_j} e^{-x_i' \hat{\beta}}}{(1 + e^{-x_i' \hat{\beta}})^2} \quad (6.8)$$

In order to account for the unknown functional form of the regressor influence and possible interactions between the regressors x_j while still preserving the linear predictor form $x_i' \beta$ in the link functions, an approximation by second order polynomials is used. To discern the effect of the different causality measures, the regression uses dummy variables for the different causality measures with the sPDC being the baseline case (Wooldridge 2009). This choice of a baseline case, which has to be made to avoid the dummy variable trap (Greene 2007), does not influence the regression results, but only their way of presentation. Any other causality measure could have been taken as the baseline with all other regressions coefficients relative to this baseline. Hence, the marginal effect of a parameter variation on, for example, the DTF consists of the marginal effect found for the baseline case plus the marginal effect of the respective DTF dummy term. A significant coefficient of the DTF dummy term indicates that the respective parameter has a different effect on the DTF than on the sPDC. Thus, if a slope coefficient for the DTF-dummy is not statistically significant different from 0, the varied parameter may still have a significant effect on the performance of the

6.3. ZERO-AND-ONE INFLATED BETA REGRESSION-MODEL

DTF, if the coefficient of the baseline sPDC case is significant. Due to the use of a second order polynomial the partial effects can depend upon both the estimated regression coefficients and the value of the independent variable. The partial effects at a certain point in the regressor space X_0 are found by taking the derivative with respect to the parameter of interest x_j at \mathbf{x}_i .

$$\begin{aligned} \left. \frac{\partial E(y_i | \mathbf{x}_i)}{\partial x_j} \right|_{x_i=x_0} &= (1 - p_0 - p_1) \left. \frac{\frac{\partial x'_i \hat{\beta}}{\partial x_j} e^{-x'_i \hat{\beta}}}{(1 + e^{-x'_i \hat{\beta}})^2} \right|_{x_i=x_0} \\ &= \frac{\partial x'_i \hat{\beta}}{\partial x_j} (1 - p_0 - p_1) \left. \frac{e^{-x'_i \hat{\beta}}}{(1 + e^{-x'_i \hat{\beta}})^2} \right|_{x_i=x_0} \end{aligned} \quad (6.9)$$

That is, the marginal effect is given by the partial derivative of the polynomials in $x'_i \hat{\beta}$ with respect to the parameter x_j (which would be the effect in a usual normal regression) weighted with an expression depending on the point in the parameter space.

Example: Assume just two causality measures, sPDC and DTF and two parameters data length (dl) and coupling strength (cs) and let b_j denote the estimated coefficients. Then the linear predictor $x'_i \hat{\beta}$ would look like:

$$x'_i \hat{\beta} = \text{const}_{sPDC} + b_1 \cdot DTF_i + b_2 \cdot dl_i + b_3 \cdot dl_i^2 + b_4 \cdot dl_i \cdot DTF + \quad (6.10)$$

$$b_5 \cdot dl_i^2 \cdot DTF + b_6 \cdot cs_i + b_7 \cdot cs_i^2 + b_8 \cdot cs_i \cdot DTF + b_9 \cdot cs_i^2 \cdot DTF + \quad (6.11)$$

$$b_{10} \cdot cs_i \cdot dl_i + b_{11} \cdot cs_i \cdot dl_i \cdot DTF \quad (6.12)$$

$$(6.13)$$

For the sPDC at the parameter vector $X_0 = (dl_0, cs_0, DTF = 0)$ the unweighted

marginal effect of dl is then given as:

$$\left. \frac{\partial x'_i \hat{\beta}}{\partial dl} \right|_{x_i=X_0} = b_2 + 2 \cdot b_3 \cdot dl_0 + b_{10} \cdot cs_0 \quad (6.14)$$

The full marginal effect follows from equation 6.9 as

$$\frac{\partial E(y_i | x_i)}{\partial dl} \Big|_{x_i=X_0} = \frac{[b_2 + 2 \cdot b_3 \cdot dl_0 + b_{10} \cdot cm_0] (1 - p_0 - p_1) e^{-\text{(const}_{sPDC} + b_2 \cdot dl_0 + b_3 \cdot dl_0^2 + b_6 \cdot cs_0 + b_7 \cdot cs_0^2 + b_{10} \cdot cs_0 \cdot dl_0)}}{\left(1 + e^{-\text{(const}_{sPDC} + b_2 \cdot dl_0 + b_3 \cdot dl_0^2 + b_6 \cdot cs_0 + b_7 \cdot cs_0^2 + b_{10} \cdot cs_0 \cdot dl_0)}\right)^2} \quad (6.15)$$

It can be easily seen that the partial effect is dependent on both the estimated coefficients as well as the point in the parameter space. Analogously, for the DTF the unweighted marginal effect of dl at the parameter vector $X_1 = (dl_0, cs_0, DTF = 1)$ is then given as:

$$\left. \frac{\partial x'_i \hat{\beta}}{\partial dl} \right|_{x_i=X_1} = (b_2 + b_4) + 2(b_3 + b_5) \cdot dl_0 + (b_{10} + b_{11}) \cdot cs_0 \quad (6.16)$$

with the corresponding total marginal effect

$$\frac{\partial E(y_i | x_i)}{\partial dl} \Big|_{x_i=X_1} = \frac{[(b_2 + b_4) + 2(b_3 + b_5) \cdot dl_0 + (b_{10} + b_{11}) \cdot cm_0] (1 - p_0 - p_1) e^{-\text{(const}_{sPDC} + b_1 + (b_2 + b_4) \cdot dl_0 + (b_3 + b_5) \cdot dl_0^2 + (b_6 + b_8) \cdot cs_0 + (b_7 + b_9) \cdot cs_0^2 + (b_{10} + b_{11}) \cdot cs_0 \cdot dl_0)}}{\left(1 + e^{-\text{(const}_{sPDC} + b_1 + (b_2 + b_4) \cdot dl_0 + (b_3 + b_5) \cdot dl_0^2 + (b_6 + b_8) \cdot cs_0 + (b_7 + b_9) \cdot cs_0^2 + (b_{10} + b_{11}) \cdot cs_0 \cdot dl_0)}\right)^2} \quad (6.17)$$

As the estimation of the zero-and-one inflated beta regressions is performed in a quasi-likelihood framework, parameter restrictions can be easily tested by comparing

6.4. RESULTS: COMPARISON OF THE MULTIVARIATE AUTOREGRESSIVE CAUSALITY MEASURES

the log-likelihoods from the restricted and unrestricted models (Greene 2007):

$$-2(\loglikelihood_{restricted} - \loglikelihood_{unrestricted}) \quad (6.18)$$

This is χ_1^2 distributed with a critical value of 3.84 for a 5% significance.

6.4 Results: Comparison of the Multivariate Autoregressive Causality Measures

To obtain a simple measure for the performance of the MVAR methods independent of the parameter variation, the percentage of missed/false positively detected connections over all simulated parameter vectors was calculated. The results are given in table 6.4.

Using the RP approach, the dDTF had the least false positive detections while H missed the fewest connections. However, both results were due to misbehavior of the respective measure. The dDTF missed many of the true connections, while H detected many false positive connections, indicating that the significance threshold for H was underestimated, while it was overestimated for dDTF. Thus, both false positive and missed connections must be viewed in conjunction. With the RP the DTF performed best, except for the EEG data, where H performed best. When combined with the LOOM, the sPDC was the best performing MVAR, except for the EMG data, where H was the best performing measure in respect to the totally missed and false positive detections followed by the sPDC. However, this unconditional univariate analysis is dependent on the particular parameter combinations chosen for the regressions and may be driven by the particular behavior of the measures in one area of the parameter space.

Table 6.4: Performance of the MVAR methods: Percentage of missed and false positive (FP) connections averaged over the parameter range. The individual best performance is emboldened.

		LOOM			
		MEG	EEG	LFP	EMG
FP	PDC	55.14	64.25	48.75	44.1
	sPDC	7.45	23.74	8.45	11.69
	DTF	65.06	72.07	65.6	54.41
	dDTF	6.61	25.66	6.52	5.52
	H	10.74	16.33	14.75	12.04
missed	PDC	6.76	7.38	9.11	21.36
	sPDC	24.23	26.22	36.3	47.28
	DTF	4.39	4.98	5.95	12.47
	dDTF	54.05	50.36	70.1	85.81
	H	24.51	39.9	41.46	41.91
total	PDC	30.95	35.82	28.93	32.73
	sPDC	15.84	24.98	22.38	29.49
	DTF	34.73	38.53	35.78	33.44
	dDTF	30.53	38.01	38.31	45.67
	H	17.68	28.18	28.11	26.98
random permutation					
FP	PDC	7.16	10.91	6.24	5.88
	sPDC	7.79	10.9	6.24	5.88
	DTF	16.86	18.9	17.83	13.17
	dDTF	4.91	8.96	6.00	2.54
	H	42.24	30.89	51.29	26.81
missed	PDC	48.69	70.91	55.86	52.63
	sPDC	48.36	70.95	55.86	52.63
	DTF	34.87	60.85	41.73	41.77
	dDTF	68.56	89.33	67.36	75.98
	H	23.04	42.62	20.96	31.77
total	PDC	27.93	40.91	31.05	29.26
	sPDC	28.08	40.93	31.05	29.26
	DTF	25.87	39.88	29.78	27.47
	dDTF	37.24	49.15	36.68	39.26
	H	32.64	36.76	36.13	29.29

6.5 Results: Data Types

All results were obtained for EEG, MEG, LFP and EMG recordings. The results for all data recording types were largely similar. In the following, the results are presented for the MEG data. Differences in regression coefficient for the other data types are also reported in case they differ in their overall behavior compared to the MEG data.

The complete regression results for all data types are given in the Appendix and are summarized for the MEG data in figures 6.3 and 6.4. The graphs in these figures show the variation of one parameter while keeping all other parameters at their starting values (see tables 6.2 and 6.3). As the partial effects are also dependent on the other parameter values, the shown partial effects are strictly speaking not representative of the partial effects at other points of the parameter space under consideration. Following the usual presentation in the literature, the behavior at an important point in the regressor space is presented. But rather than using the mean, which would be biased towards a high model order due to the natural bound of 0 for the model order, the results are described at the baseline parameter values given in table 6.2, where coupling strength and noise have been chosen in accordance with Kus et al. (2004).

6.6 Results: Parameter Dependence

6.6.1 Data Length

Increasing the data length led to fewer false positives and missed ones when LOOM was used. For the methods other than the sPDC the decrease in false positives with increasing data length was not as pronounced, with H being completely insensitive. Only for the EMG data the influence of increasing the data length was different for

the detection of false positives ones, leading to an increase rather than a decrease of false positives for sPDC, PDC and H.

When using random permutation instead of LOOM, increasing the data length led to a slight increase in false positives, reaching a plateau with no more changes for data length greater than 3500. This increase in false positives is due to the fact that with random permutation for data length below 1000 data points no connections were detected which is opposite to the behavior of the LOOM. As this steep increase is not easily modeled with the regression coefficients, this leads to a predicted increase up to 3500 data points. For the missed connections, a decrease in missed connections with increasing data length was found, with the decrease being even faster for DTF and H.

6.6.2 Model Order

A priori, one may expect an asymmetric behavior of an under- and overestimation of the model order: the autoregressive coefficients on redundant lags in case of an overestimation of the model order should at least asymptotically simply be 0, while an underestimation should make it impossible to capture effects that are mediated with a longer time lag. Thus, to allow for such an asymmetric behavior, a dummy variable for overestimation with corresponding interaction terms was used to control for a change in both the regression constant and the slopes.

For the detection of false positive ones when using LOOM, an over- and underestimation of the model order had only a weak influence for the sPDC. An increase in model order from 12 to 50 led to 0.4% more false detections. For DTF and PDC overestimation of the model order resulted in an increase in false positives, while it led to a decrease in false positives for H and dDTF. For the missed connections

LOOM

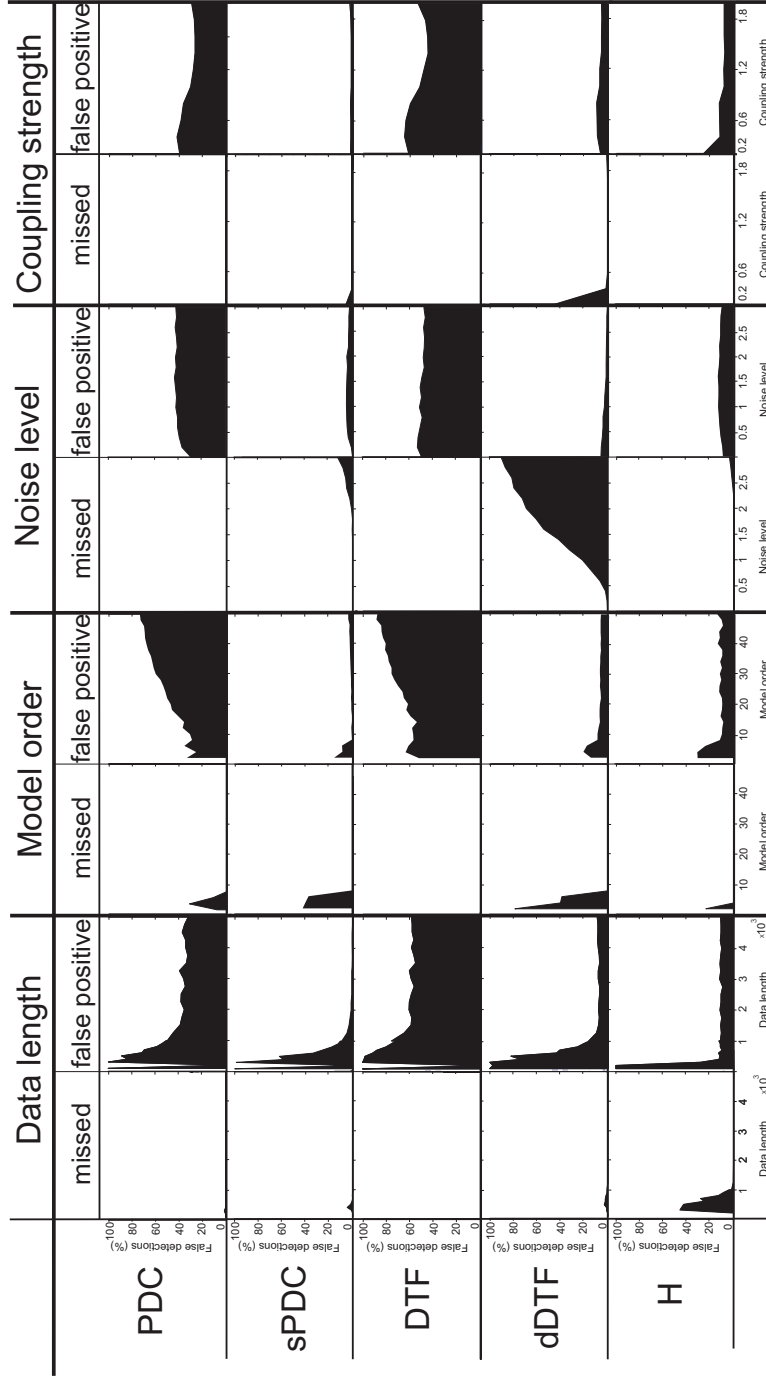


Figure 6.3: Parameter dependence with LOOM:

One row represents one causality measure and one column the varied parameter. Each column is divided in two parts: the left side shows the average of the missed connections, the right side shows the average of the false positive detections. x- axis: varied parameter; y- axis: number of missed or falsely detected connections.

Random Permutation

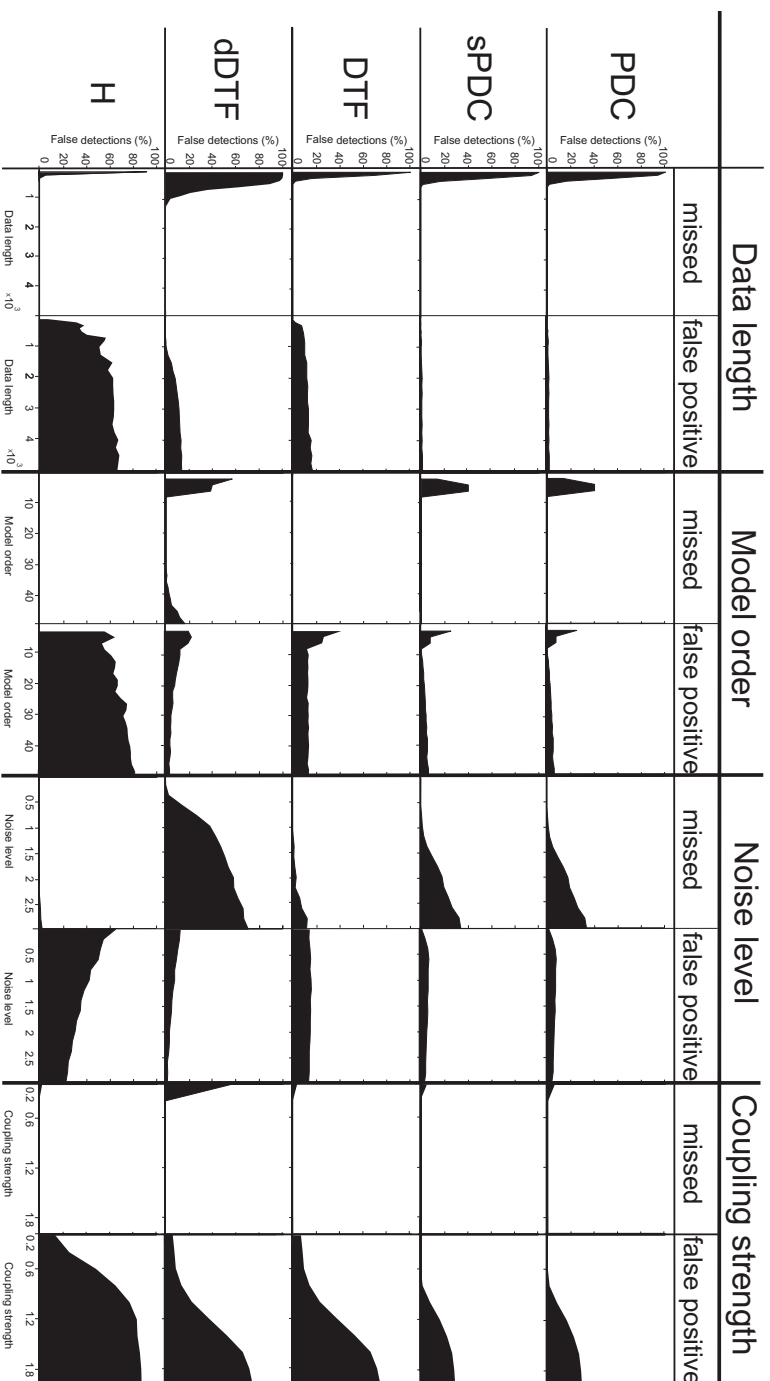


Figure 6.4: Parameter dependence with random permutation:

One row represents one causality measure and one column the varied parameter. Each column is divided in two parts: the left side shows the average of the missed connections, the right side shows the average of the false positive detections; x- axis: varied parameter; y- axis: number of missed or falsely detected connections.

6.6. RESULTS: PARAMETER DEPENDENCE

an overestimation had also almost no influence, while an underestimation led to an immediate increase in missed connections compared to the correct model order.

If random permutation was used, an increase in model order led to a weak decrease in false positive ones for all measures. Only for H this effect was opposite. An underestimation of the true model order has the same effect as for the LOOM with an immediate jump in the number of false positive detections as soon as the model order is underestimated. A further increase has almost no effect of the underestimation. In case of missed connections, there is a stronger increase for an underestimation compared to an overestimation. However, while for an underestimation the increase in missed connections peaks at a model order of 6 compared to the true one of 12, an overestimation leads to a consistent albeit slow increase in missed detections over the whole range of model orders considered here.

6.6.3 Noise Level

With LOOM an increase in the noise level resulted in a slight increase in false positive connections (i.e. about 1% for the sPDC over the noise range considered). This negative effect of noise was smallest for the sPDC and stronger for all other MVAR methods. In addition, a strong increase with about 30% more missed connections for a noise level of 3 compared to one of 0 was found. However, with LFP and EMG data for sPDC and dDTF counterintuitively a very slight, although statistically significant decrease in false positives was seen.

In combination with random permutation, an increase in the noise level remarkably had no negative influence on the detection of false positive ones, but rather led to an increase in missed connections. This increase in missed connections was strongest for the sPDC and somewhat weaker for the other measures.

6.6.4 Coupling Strength

For both the LOOM and random permutation an increasing coupling strength resulted in an increase in false positive detections for all measures. With LOOM a decrease was found for the missed connections when the coupling strength increased. In contrast, when random permutation was used, the behavior for the missed connections was different: a minimum of missed connections was reached around a coupling strength of 1 with an increase in misdetections for both higher and lower coupling strengths.

6.6.5 Parameter Interaction

Table 6.5: Signs of the significant interaction terms. Above the diagonal results for the random permutation and below the diagonal results for the LOOM. Abbreviations: n.s. – not significant; cs – coupling strength; dl – data length; nf – noise factor; moa – model order above the true one; mob – model order below the true one; / – no interaction.

missed	cs	dl	nf	moa	mob
cs		+	-	-	n.s.
dl	-		+	-	+
nf	-	+		+	n.s.
moa	n.s.	n.s.	+		/
mob	+	+	-	/	
false positive	cs	dl	nf	moa	mob
cs		-	-	+	-
dl	+		+	+	n.s.
nf	+	+		-	-
moa	n.s.	-	-		/
mob	n.s.	+	n.s.	/	

Besides the individual effects, parameters also had some significant regression

6.7. RESULTS: SCHELTER-MODEL

interactions terms with each other.⁵ For the missed and false positive connections using random permutation, overestimation of the model order, the coupling strength, the noise and the data length had significant interaction terms with each other. The signs of the individual interaction terms for the MEG data are shown in table 6.5. Only for the LFP data the interaction term between model order above and coupling strength for the detection of missed connections was significant and had a positive sign instead of a negative sign like for all other data types (a complete list of all results is given in the Appendix).

Using LOOM, the coupling strength and the model order above the true one (moa) interacted with noise as well as data length, which also had a significant interaction term with each other. For an underestimation of the model order only a significant interaction with the data length was found. For the missed connections the model order below the true one (mob) and noise showed an interaction with all other parameters. Moreover, the coupling strength interacted with the data length. All interaction terms were smaller for the PDC and DTF. The interaction terms for the other data types showed some variation but still yielded largely the same picture.

6.7 Results: Schelter-Model

In addition to the Kus-model the causality measures were also tested with the Schelter-model. This model has the advantage of being data type independent.

While with LOOM and random permutation some individual parameters varied, the overall partial effects for the parameters were essentially the same as for the Kus-model (see tables A.24, A.25, A.26 and A.27). For example, the overestima-

⁵For an introduction to regression analysis with interaction terms, see (Greene 2007).

tion of the model order had a positive sign for the missed connections instead of a negative one. Since the sign for the quadratic term also changed, the overall effect was still the same with more missed connections with a higher overestimation. The only different behavior observed was the dependence on the noise factor for random permutation. With the Schelter-model more false positive detections occurred and less connections were missed with increasing noise factor in contrast to the Kus-model.

A further difference of the Schelter-model is that a false connection from channel 2 to channel 1 might occur due to the fact of a “marrying parents of a joint child scheme”. However, in combination with both random permutation and LOOM this false connection was not more frequently detected than other connections.

6.8 Discussion

The second simulation study tested the influence of the parameters data length, coupling strength, model order and noise level on the five different causality measures sPDC, PDC, DTF, dDTF and H with the Kus- and Schelter-model. Moreover, two different significance measures, LOOM and random permutation, were evaluated. With these results a comparison of the causality measures, the two significance thresholds and an evaluation of the influence of different data types used for the Kus-model is possible.

Data Type

As input signal for the Kus-model MEG, EEG, EMG and LFPs from intraoperative macroelectrode recordings were used. Importantly, while some individual

6.8. DISCUSSION

regression estimates differed, the overall effect of the varied parameters was largely consistent. Further supporting the finding of data type independence, the results with Schelter-model were mainly the same. However, for some parameters there was a significantly different influence depending on the data type. If not single parameter dependencies are considered, but the average over all parameter combinations, the most striking difference was H being the best performing measure with EMG data and the LOOM. The sPDC was the best measure for all other data types. However, even for the EMG data the sPDC was the second best measure with the difference to H not being statistically significant. As H is by construction unable to discern direct and indirect connections, using the sPDC instead of H is recommended. The largely congruent results of the data types may be partially due to the model setup where the noise subsequently becomes internal noise, thereby smoothing out differences in the data types making the differences found even more striking. Nevertheless, the differences between data types should be sufficiently small to allow - at least in principle - for a combination of different data types like in the present application, where LFP and EMG recordings were combined. Further support for the finding of data type independence comes from the results of the Schelter-model, which is completely independent of the input data type. They were the same as the ones of the Kus-model. This allows for a careful generalization of the results.

Data Length

With an increase in data length better results were obtained with both random permutation and LOOM. With a sufficient data length, i.e. more than 1000 data points, the overall results did not change much and from 3500 data points on no change was seen. This behavior was expected, as with more data points the estimation of the autoregressive coefficients becomes better, but as soon as a sufficient data

length is reached the coefficients are estimated consistently.

As seen in figures 6.3 and 6.4 the causality measures showed a completely opposite behavior for small data lengths when using the LOOM and random permutation. While the LOOM detected connections between each pair of channels, random permutation detected no connections at all. This differential behavior could be used for a simple test whether the data length is appropriate. If random permutation shows no connections, while the LOOM detects connections between almost every channel, the data length may be too short for a proper estimation. Moreover, this effect explains the increase in false positive detections for the DTF and H with an increase in data length, as both measures start detecting indirect connections they cannot distinguish by construction.

These results are in accordance with studies by Astolfi et al. (Astolfi et al. 2006, Astolfi et al. 2007). They also found that an increase in data length led to better results. However, their smallest data set consisted of 2500 data points. The present work shows that 1000 data points already may lead to good results. For a more parsimonious model even a smaller data set may be appropriate.

Model Order

An increase of the model order beyond the true model order had almost no influence on the detection of false positive ones for the sPDC with LOOM and random permutation, while it had a positive influence on DTF and PDC with LOOM and H with random permutation. The underestimation of the model order led to an immediate increase in missed connections for both significance computation measures. When using random permutation it additionally resulted in an increase in false positives.

6.8. DISCUSSION

These results are in accordance with the literature, where it has been shown that the correct choice of model order is important (Schelter et al. 2006). However, in case of a model order larger than the true one, its importance seems to be overestimated (Schlögl and Supp 2006). Indeed, the results show that overestimation of the model order does not have an effect as severe as its underestimation. With the LOOM an increase from a model order of 12 to 50 led to 0.4% more false detections and with the random permutation even to an decrease in false positives of 0.4 % for the sPDC. Still, a too large overestimation may lead to false positives as well as missed connections. It is more important to use a model order that is equal or larger than the true time shift between the series as otherwise the implied connections cannot be detected. Apparently, underestimating the model order is worse than overestimating it. This is particularly true as an underestimation leads to both more misdetections and a lower frequency resolution.

In many neuroscientific applications one is not only interested in the direction of the coupling, but also in the frequency, with which two regions couple. In principle, all presented causality measures are determined in the frequency domain. However, regarding the frequency specific interpretation of the causality measures, a few words of caution are required as the number of frequency components, which can be resolved, is half of the model order (Schlögl and Supp 2006). Of course, if the true model order is known, no better resolution is needed than the one given by the true model. But in real applications, where the true model is usually unknown, the researcher always faces a trade-off between a good frequency resolution and an increase in possible false detections due to an overestimation of the correct model order. The simulation results show that the sPDC's and PDC's performance with random permutation and sPDC with LOOM only slightly decreases when the model order is overestimated. Thus, sPDC and PDC are the most appropriate and robust choices when a higher

frequency resolution is needed.

Noise

Newbold (1978) and more recently Nalatore et al. (2007) have shown that the addition of uncorrelated noise to time series may lead to spurious as well as missed causalities when employing Granger causality. This is sensible as one would assume that with more noise, the detection of the true causality structure becomes harder. In accordance with these findings, when using LOOM, the MVAR measures derived from time domain Granger causality used in the present work showed an increase in spurious causalities and missed connections. This increase was weakest for the sPDC, indicating that it seems to be the most robust measure, if a high external noise component was added to the data. This noise component added to the data varies the signal-to-noise-ratio: The more external noise is added the lower is the signal-to-noise-ratio. However, with random permutation and the Kus-model the behavior of the MVARs was the opposite: increasing the noise resulted only in an increase of missed detections but did not result in spurious causalities. This might be due to an overestimation of the significance threshold with an increasing noise level in the data. As with the Schelter-model the same behavior for the random permutation was found as with LOOM and the Kus-model, the underestimation of the significance threshold with random permutation for the Kus-model seems to result from the real data used.

Astolfi et al. tested the influence of the signal-to-noise ratio for EEG data on the causality measures dDTF, DTF, PDC, sPDC and found the sPDC to be more robust than the PDC (Astolfi et al. 2006, Astolfi et al. 2007). As in their work, a better signal-to-noise-ratio gave slightly better results in our study, but did not lead to a

6.8. DISCUSSION

major improvement.

Coupling Strength

With random permutation increasing the coupling strength increased the number of false detections. A closer inspection of the results showed that these false detections were from all other channels to channel 1 and channel 7, the ones which structurally differed compared to the other channels (see section 4.1.1). Channel 7 only consisted of noise. Channel 1 was the source for all subsequent channels, so that its signal content did not change with increasing coupling strength, leading to large differences in the signal-to-noise-ratio (SNR). Thus, the calculation of the causality measures against an “open channel” should be avoided for the MVARs.⁶ In any case, if one realizes that a connection is found from every channel to a certain channel, it should be checked whether these connections may be due to large differences in their SNRs.

In combination with LOOM an increase in false positives was also detected with increasing coupling strength, but this increase was weaker than with random permutation. Moreover, the number of missed connections decreased with increasing coupling strength, indicating that the MVARs in combination with LOOM are not as sensitive to the coupling strength as with random permutation.

Parameter Interactions

Interestingly, significant negative interaction terms were found between an over-estimation of the model order and coupling strength as well as data length with random permutation for the missed connections. This indicates that a higher coupling

⁶A channel is called open, if it only records background noise and no real signal.

strength or a great data length mediate the negative impact of misestimating the model order. This behavior is in accordance with the asymptotic consistency of the underlying autoregressive parameter estimates. While the effect for the false positive detections was the same with LOOM, it was the opposite with random permutation, counteracting the effect to the missed connections. Thus, as LOOM shows the same positive behavior for false positives and missed connections, its use is recommended.

The positive interaction between noise and model order for the missed connections with both random permutation and LOOM shows that a lower SNR in combination with a greater overestimation of the model order leads to more missed connections. However, at the same time it leads to a reduction in false positive detections. This indicates the presence of a tradeoff: the causality measures become less sensitive to detecting connections at all. Overall, an overestimation of model order can be partly compensated by a greater sample length as well as a higher coupling strength. However, as the researcher usually has neither an influence on coupling strength nor on the SNR, choosing the correct model order is still important.

In addition, for the LOOM a significant interaction was detected between coupling strength and noise as well as data length for the false positive detections. This indicates that a too large coupling strength in combination with a low SNR and a large data length leads to more spurious causalities (Nalatore et al. 2007). In combination with random permutation the interaction between noise and coupling strength was opposite, indicating that in this case a high coupling strength mediates the negative effect of a bad SNR. The same effect of a negative interaction between coupling strength and noise is also seen for the missed connections with the LOOM.

Random Permutation vs. LOOM

6.8. DISCUSSION

Even though a precise statistical comparison of the two methods random permutation and LOOM is not possible with the regression results and beyond the scope of this work, some comments on the usage of either of them are in order. A comparison of both methods suggests that the random permutation leads to more reliable results for the PDC and DTF in particular with respect to the detection of false positives. In contrast, the LOOM worked better for the sPDC, dDTF and H. But one has to keep in mind that these results were somewhat dependent on the data type: the dDTF with LOOM was only better than dDTF with random permutation in the simulations with MEG and EEG data.

Overall, it hence seems advisable to chose the computational approaches for the significance determination depending on the causality measure and data type employed: sPDC and H with LOOM for all data types and PDC and DTF with random permutation also for all data types. For the dDTF the best suited significance measures also depended on the data type: for the MEG and EEG data the LOOM was best and for EMG and LFP data the random permutation was best. This listing only names the best combination for each MVAR method. One can only conjecture why the LOOM performed best in most cases. One reason may be that it conserves the time structure of the data and is able to use this information for more reliable estimates of the confidence interval.

Recently, analytical measures based on asymptotic considerations have been suggested for both DTF and PDC for determining the significance (Eichler 2006, Schelter et al. 2005). In the present work the focus was on numerical approaches for 2 reasons: First, for comparability and due to their currently rare use in the literature, they were not tested, because for the other measures considered in the present work analytical

methods do not yet exist. Second, there are theoretical and empirical reasons that methods based on numerical test statistics, such as the LOOM, often perform better in finite samples than analytical methods based on approximate asymptotic distributions (Davidson and MacKinnon 2004). Nevertheless, it may be possible that the use of an analytical significance measure significantly improves the performance of one measure, making this the preferred one. This hypothesis should be tested in the future.

Comparison of the MVAR Causality Measures

Based on the simulation results concerning the parameter dependencies the sPDC in combination with the LOOM is the most appropriate multivariate method for inferring causality. It obtained only 7.5% false detections and missed 24.2% of the true connections for all parameter variations with the MEG data. When referring to these percentages one has to keep in mind, that this percentage value is an average over the whole parameter range, including parameter choices which can be avoided in a real application. In particular, for the sPDC they are a result of the bad performance for small data length and an underestimation of the model order. Thus, in a real application, where these conditions can often be avoided, the number of missed and false positive detections should be even smaller. The sPDC and PDC also performed well, if the significance was determined with random permutation (7.7% false positive detections and 48.4% missed connections for the sPDC with the MEG data), but not as good as the sPDC in combination with the LOOM. For both PDC and sPDC in combination with random permutation, one limitation was that false connections were detected for a high coupling strength. The DTF worked well with the random permutation, too, but did by design also detect indirect connections. The dDTF, which was introduced to resolve this weakness, was not always reliably able to distinguish direct and indirect connections in the simulations.

6.9. CONCLUSION

Moreover, it detected some additional false connections and should only be applied with caution. The related measure H suffered from the same problems, even though its performance in combination with the LOOM is almost as good as the sPDC with LOOM (sPDC: 7.5% false positive detections and 24.4% missed connections; H: 10.74% false positive detections and 24.5% missed connections with the MEG data).

The results suggest that the inferior performance of the dDTF was not due to problems with a “marrying parents of a joint child” scheme. Even in the Kus-model, where such a scheme does not exist, its performance was not as good as that of the sPDC. One explanation for the different results found with the different causality measures is that the different significance measures lead to differences in the results. This might be due to a non optimal power and size for certain parameter combinations and causality measures. In particular, estimation bias arises in finite samples and the causality measures do not perform uniformly over the complete parameter range.

6.9 Conclusion

As the introductory real data example of this chapter has shown, the choice of a causality measure already has a great influence on the results and one has to be aware of possible errors made by choosing inappropriate causality measures. Thus, in this second simulation study the influence of the parameters data length, coupling strength, model order and noise level on the five different causality measures sPDC, PDC, DTF, dDTF and H with the Kus and Schelter-model was tested. Furthermore two different significance measures, LOOM and random permutation, were evaluated. The simulation results have revealed in a regression analysis that the sPDC in combination with the LOOM is the most robust measure, independently of the type of data used.

Chapter 7

Application of the Causality Measures to Macroelectrode Recordings and Electromyograms

The usefulness of the simulation results for the causality measures will be demonstrated by an application to local field potentials of the subthalamic nucleus from Parkinson's disease patients. These were recorded, as explained in chapter 2, during the implantation of deep brain stimulation electrodes. Muscle activity was simultaneously recorded from affected arm muscles and the causality of this coupling was identified.

Parkinson's disease (PD) is characterized by three main symptoms: akinesia, rigidity¹ and tremor (Bergman and Deuschl 2002, Lang and Lozano 1998a). According to the dominating symptom patients are divided into the tremor-dominant or akinetic-rigid type. During disease progression usually the non-dominant symptom also develops.

¹akinesia: inability to initiate movement; rigidity: resistance to passive movements

PD is a neurodegenerative disease including the degeneration of dopaminergic neurons in the substantia nigra. While in the earlier stages of the disease medical therapy with levodopa, a dopamine precursor, is very successful, in the later stages it often results in ON/OFF fluctuations of the mobility, i.e. changes from involuntary movements (hyperkinesia) to inability to move (hypokinesia). In these later stages the motor symptoms of Parkinson's disease are often successfully treated by deep brain stimulation (DBS) of the subthalamic nucleus (STN) (Deuschl et al. 2006, Weaver et al. 2009). Deep brain stimulation is a surgical procedure, in which electrodes are placed in a certain target area of the brain. In Parkinson's disease usually the STN is targeted by the electrode. By applying high frequency electric stimulation to the target area, usually around 130 Hz, the motor symptoms like tremor and akinesia can be improved remarkably in PD.

To describe the pathophysiology of PD, Albin and DeLong (Albin et al. 1989, DeLong 1990) put forward a now well-established model (Alberts et al. 2008, Mallet et al. 2008) of basal ganglia pathophysiology (see 7.1). According to this model, the system of basal ganglia is structured in two pathways with a direct and indirect influence from striatal γ -amino-butter-acid (GABA) releasing neurons to the output nuclei, i.e. the globus pallidus pars internus (GPi) and substantia nigra pars reticulata (SNr). The activity of the output nuclei modulates thalamic nuclei and therefore cortical areas (compare figure 7.1). If dopaminergic neurons in the substantia nigra pars compacta (SNc) are depleted due to PD, an imbalance between direct and indirect pathway occurs: The basal ganglia output nuclei are less inhibited by striatal neurons (direct pathway), while subthalamic neurons enhance the activation of the basal ganglia output nuclei through the indirect pathway. This results in an increased inhibition of the thalamic nuclei, which leads to a modification of the motor

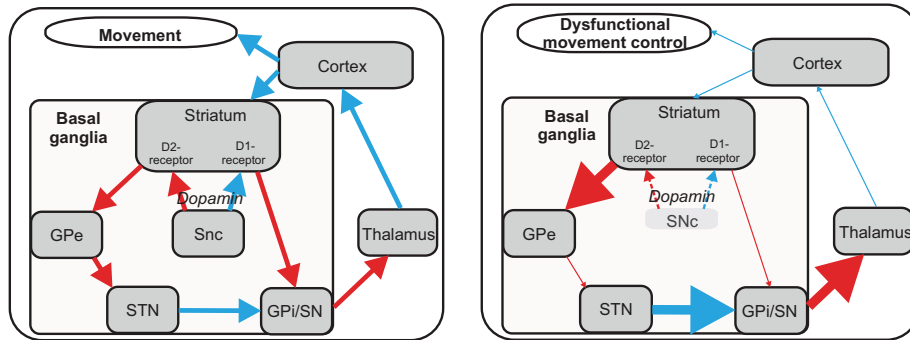


Figure 7.1: Basal ganglia model in healthy humans on the left and in Parkinson patients according to Albin and DeLong (Albin et al. 1989, DeLong 1990, Lang and Lozano 1998b). The arrows in the left figure are thicker, if the inhibition/excitation is stronger than in healthy subjects and thinner, if it is reduced. Red arrow – excitation; blue arrow – inhibition; abbreviations: STN – subthalamic nucleus; GPe – globus pallidus pars externus; GPi – globus pallidus pars internus; SNc – substantia nigra pars compacta; SNr – substantia nigra pars reticulata.

cortical projections and to Parkinsonian symptoms like akinesia and rigidity. Thus, this model can successfully explain akinesia and rigidity in PD patients through inhibitory/excitatory mechanisms in the basal ganglia loops. In contrast, however, it has been unable to fully explain PD tremor, because it cannot explain the excess of movement during tremor. Thus, there seems to be a different mechanism and possibly pathophysiology for the tremor-dominant PD subtype. Evidence for a differential pathophysiology was generated by a histopathological study, where different regions of degenerated dopaminergic neurons were identified in the substantia nigra pars compacta (SNc) for the two Parkinson subtypes (Jellinger 1999). This finding of PD subtype-specific pathology in the SNc areas could indicate that different SNc-STN pathways are affected in the two subtypes.

Based upon these histopathological findings differential causality patterns between the two PD subtypes are hypothesized. Moreover, as the Albin and DeLong model, which primarily explains the akinetic-rigid disease progression, describes the STN as an output structure, it is hypothesized that for akinetic-rigid patients more STN output to the periphery, i.e. the muscle, than input from the latter to the STN should be present. To test these hypotheses the squared partial directed coherence (Astolfi et al. 2006) is used, as it gave the most reliable results in combination with LOOM. Consistent with the notion of Granger causality as a temporal ordering, the term *output causality* is used, when the STN signal is statistically causal for the EMG activity and *input causality* for the opposite case.

To test the hypothesis of differential causalities of tremor generation in the two PD subtypes, local field potential (LFP) activity between the wider STN area and affected arm muscles of 14 PD patients with tremor in the upper extremity were analyzed. Six of the patients were classified as akinetic-rigid and 8 as tremor-dominant. Furthermore 19 akinetic-rigid patients without tremor were analyzed in order to compare their results to those during tremor in order to find possible differences in their pathophysiology.²

²The application presented here contains parts of two articles: The results for the akinetic-rigid patients without tremor are published as: E. Florin, J. Gross, C. Reck, M. Maarouf, A. Schnitzler, V. Sturm, G.R. Fink, L. Timmermann (2010): Causality between subthalamic nucleus and forearm muscles in Parkinson's disease, *European Journal of Neuroscience*, 31: 491-498. The article related to the results of the tremor-dominant patients is currently under revision (E. Florin, M. Himmel, C. Reck, M. Maarouf, A. Schnitzler, V. Sturm, G.R. Fink, L. Timmermann: Differential statistical causality in Parkinsonian subtypes during tremor episodes.)

7.1. EXPERIMENTAL DESIGN

7.1 Experimental Design

7.1.1 Included Patients

A total of 19 akinetic-rigid PD patients during periods without tremor, 6 akinetic-rigid PD patients during tremor and 8 tremor-dominant Parkinsonian patients during tremor were analyzed. The PD classification akinetic-rigid and tremor-dominant was made according to part 3 of the patients' preoperative Unified Parkinson's Disease Rating Scale (UPDRS; table 7.1) (Fahn et al. 1987). The UPDRS part 3 is a standard test score, by which a neurologist determines the motor impairment due to PD.³ A patient was classified as akinetic-rigid, if the average of items related to akinesia and rigidity was larger than the one of items related to tremor and as tremor-dominant in the opposite case.

In all patients the usual dopaminergic medication resulted in ON/OFF fluctuations. Hence, DBS electrodes were implanted bilaterally in the STN. The decision for STN-DBS was made in accordance with the pre-operative selection criteria reviewed in Lang et al. and the German guidelines of DBS in PD (Lang et al. 2006, Hilker et al. 2009). The study was approved by the local ethics committees (study no. 2459 and 08-158) and conducted in accordance with the Declaration of Helsinki. All patients gave written informed consent.

³The UPDRS part 3 consists of 14 scoring items, for example for arm tremor, and each one is scored with a value between 0 and 4, where 0 stands for no impairment. The maximum score is 108, as several items are rated for the left and right side separately.

Table 7.1: PD patient characteristics: Upper panel: akinetic-rigid patients without tremor; lower panel: patients with tremor. Abbreviations: m – male; f – female; le – left STN; ri – right STN; UPDRS – motor score of the Unified Parkinson’s Disease Rating Scale; ON – with medication; OFF – without medication; AR – akinetic-rigid; TD – tremor-dominant.

patient no.	gender	age	disease duration	UPDRS (ON/OFF)	recording site	number of trajectories	PD subtypes
1	f	70	15	17/32	le	4	AR
2	m	58	9	43/52	le	5	AR
3	f	58	14	14/41.5	le	5	AR
4	f	64	20	21/61	le/ ri	5/3	AR
5	m	61	10	23/35	le/ri	5/4	AR
6	m	57	4	13/32.5	le	5	AR
7	m	62	12	24/60	le	5	AR
8	m	63	9	25/62	le	3	AR
9	f	67	15	27/37	le	4	AR
10	f	57	18	29/58	le	5	AR
11	f	44	6	9/31	le	4	AR
12	m	70	17	25/43	le/ri	5/5	AR
13	m	65	10	27/42	le	4	AR
14	m	74	17	18/38	le	5	AR
15	m	73	19	20/50	le	3	AR
16	m	69	18	20/32	ri	4	AR
17	m	41	4	35/59	ri	5	AR
18	f	46	5	7/27	le	5	AR
19	f	71	10	14/40	le/ri	5/5	AR
1	m	65	10	27/42	le/ri	3/4	AR
2	m	50	11	/	le/ri	5/5	AR
3	m	69	18	20/32	le/ri	4/4	AR
4	m	71	10	27/56	le/ri	5/5	AR
5	m	70	13	14/32	le/ri	4/5	AR
6	m	58	9	42/54	le/ri	5/5	AR
7	m	73	7	38/50	le/ri	5/5	TD
8	m	72	12	13/28	le/ri	3/2	TD
9	m	76	8	40/46	ri	5	TD
10	m	71	8	22/59	le	4	TD
11	f	65	10	35/44	le	4	TD
12	m	60	12	3/11	le	4	TD
13	m	70	11	15/42	ri	4	TD
14	m	54	4	25/32	ri	4	TD

7.1. EXPERIMENTAL DESIGN

7.1.2 Implantation of Electrodes for Deep Brain Stimulation and Intra-Operative Recordings

All patients were withdrawn from their anti-Parkinsonian medication for at least 12 hours so that any influence on the neural activity due to medication was minimized during the operation. The target points in the STN were assessed by stereotactic magnetic resonance imaging (MRI) and computer tomography (CT) by a neurosurgeon. The MRI and the CT were merged and the electrode trajectory and the target point were determined on this merged image. The complete procedure of determining the DBS target point has been described elsewhere (Voges et al. 2002).

During electrode implantation 5 combined micro-macroelectrodes recorded single cell activities and LFPs using the INOMED ISIS MER-system (INOMED corp., Teningen, Germany) (see figure 2.4). The single cell activity was recorded with the micro tip 1 mm below the macroelectrode. It was used to determine the border of the STN. When entering the STN, background activity increases and neurons spike with a high amplitude and mean frequency of about 37 Hz (Hutchison et al. 1998). Localization of the electrodes in the STN was confirmed from microelectrode recordings of typical cell activity for each structure.

The LFP recordings with the macroelectrode were used after the operation for the causality analysis. Four of the electrodes were distributed equally in a circle with 2 mm radius around the central electrode (Florin et al. 2008). Recording started at most 9 mm above the target point in the STN and proceeded in steps of 1 mm downwards until up to 1 mm below the target point. Simultaneously, surface electromyograms of the arm muscles *M. extensor digitorum communis* (EDC) and *M. flexor digitorum communis longis* (FDL) were recorded. To analyze rest tremor, patients were asked

to rest without moving their arm for at least 30 seconds at each recording depth. Furthermore patients resting tremor developed during that time. In the second patient group no tremor occurred during that period. A sample raw data set during rest tremor of one akinetic-rigid patient and one tremor-dominant patient is shown in figure 7.2. Note that tremor is reflected in periodic activity in EMG activity during rest.

7.1.3 Data Analysis

After the implantation, macroelectrode and EMG recordings from each patient were visually inspected off-line for movement artifacts. If artifacts were detected, the respective sequences were excluded from further analysis. Additionally, a 2 Hz high-pass filter was used for the electromyograms to remove drifts due to movements and a 50 Hz notch filter was employed to remove potential electric artifacts. These filter settings have been chosen in accordance to the simulation results in chapter 5. To analyze periods of tremor, only recordings which showed tremor in the electromyogram were included.

To determine causality of information flow the sPDC (Astolfi et al. 2006) was used in Matlab. The model order of the autoregressive model for the sPDC was determined with the Bayesian Information Criterion (BIC) and the significance threshold was computed with the leave one out method (LOOM, see chapter 3) (Schlögl and Supp 2006). The sPDC in combination with LOOM has been used, because it was the most robust measure in the previous simulation study (chapter 6).

To determine the statistical significance, in a first step the significance of the causality measures was analyzed on the level of the individual patient. After computing the

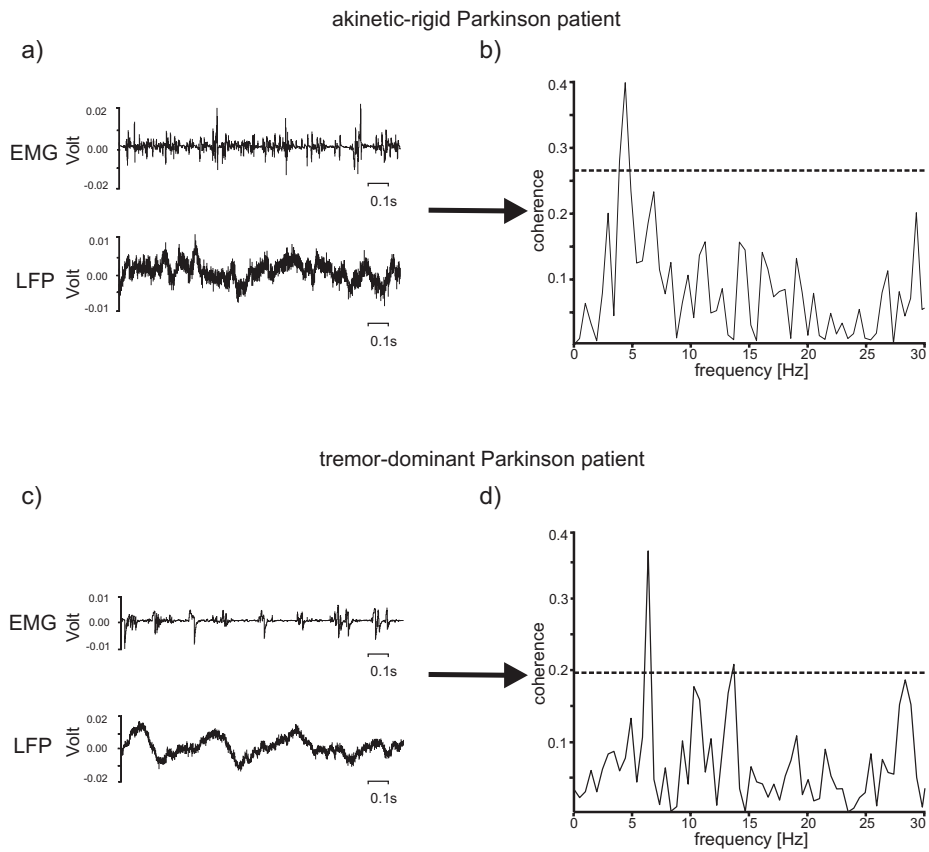


Figure 7.2: On the right, EMG and LFP recordings are shown. The EMG recording presents in figure a) a recording from the EDC during rest tremor from one akinetic-rigid patient. In part c) a recording of the FDL from a tremor-dominant patient is shown. Note the activity at tremor frequency. In the right part of this figure the resulting coherence spectra of the EMG and LFP are shown. The dashed line is the significance threshold.

sPDC and the confidence intervals, all cases were counted where the causality measure in the frequency range from 3 to 45 Hz exceeded the patient-specific significance threshold. This frequency range was chosen as it i) is the frequency range, in which probably most communication between neural areas is taking place and ii) should be unaltered by the preprocessing with a 2 Hz high-pass and a 50 Hz notch filter. Unfortunately, the sPDC practically does not allow for a detailed frequency resolution (Schlögl and Supp 2006). Although the sPDC as a frequency-dependent measure based on multivariate autoregressive modeling is in principle capable of distinguishing frequency ranges, the discrimination relies on the model order, which in this case was determined with the BIC. With this criterion the model orders ranged from 9 to 56 in our data. To get a better frequency resolution, a higher model order than the optimal one indicated by the BIC would be required, thereby decreasing the efficiency of the MVAR-estimation and increasing the likelihood of false and missed causalities, as seen in chapter 5. Thus, distinguishing between tremor (4-6 Hz) and double tremor frequency, as has been done in previous studies using coherence is impossible (Timmermann et al. 2003, Reck, Florin, Wojtecki, Krause, Groiss, Voges, Maarouf, Sturm, Schnitzler and Timmermann 2009). To exclude that differing connectivity patterns in both groups are originating from completely different frequency bands, thereby invalidating the comparison, the coherence spectra were calculated. The right panel of figure 7.2 presents sample coherence spectra of one akinetic-rigid patient and one tremor-dominant patient during tremor. The coherence spectra in both patient groups are dominated by coherence in the tremor frequency. Thus, it is unlikely that the results are driven by the tremor frequency band for tremor-dominant patients (Timmermann et al. 2003, Reck, Florin, Wojtecki, Krause, Groiss, Voges, Maarouf, Sturm, Schnitzler and Timmermann 2009, Volkmann et al. 1996) and the beta band (12-30 Hz) for akinetic-rigid patients (Kühn et al. 2006, Brown and Williams 2005, Reck, Florin, Wojtecki, Groiss, Voges, Sturm, Schnitzler and

7.2. RESULTS

Timmermann 2009).

Due to the individual anatomy and blood vessels in some patients only less than 5 macroelectrodes could be used for recording. In order to make the occurrence of input and output causalities comparable between patients, the number of input and output causalities were divided by the number of possible connections. Further statistical analysis for the second step, the inpatient and intergroup analysis, was conducted with this quotient. As the Shapiro-Wilk's test rejected normality of the data ($p < 0.05$), inpatient testing was performed with the non-parametric Wilcoxon test (Wilcoxon 1945). The occurrence of output causalities (i.e. the LFP of the subthalamic region is causal for electromyogram) and input causalities was compared (i.e. the EMG is causal for the LFP of the subthalamic region) for all patients and for the two subgroups: tremor-dominant and akinetic-rigid PD patients. Intergroup comparison was made with the Mann-Whitney-U test (Mann and Whitney 1947). To correct for the inflated type 1 error due to the multiple pairwise testing, a step-down-procedure suggested by Benjamini and Hochberg (Benjamini and Hochberg 1995) was used. This procedure has more statistical power than the classically used Bonferroni correction (Bonferroni 1936, Miller 1991).

7.2 Results

7.2.1 Placement of the Implanted Electrode for Deep Brain Stimulation

During the implantation of DBS electrodes in PD patients, single cell activity and LFPs were recorded in the STN and ZI. In total, neural activity was recorded in 55 hemispheres (see table 7.1). In 21 patients one hemisphere could not be included

due to intraoperative restrictions such as patients' fatigue, possible brain shift, blood vessels or no sufficient data for the particular condition.

The active stimulation contact was individually determined for each patient by a neurologist as the contact with the best clinical outcome. The average active stimulation contact was in the dorsolateral part of the STN (see figure 7.3 and table 7.2), which is known to be the most effective location for deep brain stimulation in PD (Benabid et al. 1994). No significant difference was found in the stimulation location between the akinetic-rigid and tremor-dominant patients during tremor (STN right: x: $p = 0.857$, y: $p = 0.857$, z: $p=0.629$; STN left: x: $p = 1.000$; y: $p = 0.286$, z: $p = 0.413$). In patient 14 of the tremor group, possibly in combination with a head accident, a postoperative displacement of the electrode occurred. To be on the safe side, the coordinates of this patient were excluded from the analysis of the average placement of the effective stimulation location. The electrode was replaced three months later and put back to the original target location. However, according to the microelectrode recordings, the intraoperative placement was correct, so that the LFP recordings were obtained from the subthalamic area and can hence be used for the analysis.

Table 7.2: Localization of the active stimulation contact in Schaltenbrand-Wahren coordinates with standard deviation.

	Hemisphere	x [mm]	y [mm]	z [mm]
AR without tremor	left	-12.2 ± 1.9	-1.3 ± 1.8	-2.6 ± 1.8
TD and AR with tremor	left	-12.8 ± 1.6	-2.2 ± 1.7	-2.6 ± 1.8
AR without tremor	right	12.5 ± 1.4	-1.1 ± 1.1	-2.6 ± 1.9
TD and AR with tremor	right	11.7 ± 1.1	-1.4 ± 1.2	-3.8 ± 2.1

7.2. RESULTS

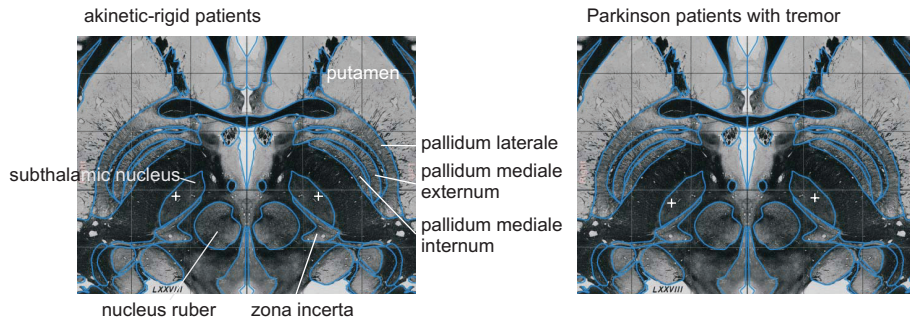


Figure 7.3: Average active stimulation contact (white cross) in the STN projected on the Schaltenbrand-Wahren atlas (axial slice -3.5 mm). The grid size is 10 mm.

7.2.2 Causality between Electromyograms of Forearm Muscles and Local Field Potentials of the Subthalamic Nucleus

For the causality analysis only signals with sufficiently long tremor periods during rest (i.e., at least 10 seconds) and without artifacts were included for the analysis of the tremor group. For the akinesic-rigid patients in the tremor group this led to more exclusions, as tremor is usually not as continuous for the akinesic-rigid patients. Overall, 107 recording depths could be included for the comparison of the tremor in the two Parkinson's disease subtypes akinesic-rigid and tremor-dominant (tremor-dominant patients: 67 depths; akinesic-rigid patients: 40 depths). In total 44 recording depths for the akinesic-rigid patients without tremor were included. Here periods with akinesia and rigidity were included.

Figure 7.4 visualizes the detected causalities over all recording heights for one tremor-dominant PD patient with causalities depicted by arrows. It shows that for this representative tremor-dominant patient more input causalities (black arrows)

Table 7.3: Descriptive statistics of the results: The mean percentage of input and output causalities with the standard error of the mean is reported for the different conditions rest and hold. For one patient the rest condition in the STN had to be excluded because of tremor in the recording.

	akinetic-rigid		tremor-dominant	
	output	input	output	input
with tremor	$3.5 \pm 1.3 \%$ n=40	$1.4 \pm 0.8 \%$ n=40	$17.5 \pm 2.4 \%$ n=67	$33.1 \pm 3.9 \%$ n=67
without tremor	$12.7 \pm 3.6 \%$ n=44	$21.4 \pm 4.7 \%$ n=44	–	–

than output causalities (red arrows) were found. The green arrows indicate a bidirectional causality, which is treated as one input and one output causality in the further statistical analysis.

To test the hypothesis that tremor pathology is different in both PD subtypes, the occurrence of output and input causalities in the complete subthalamic region was compared between the two subtypes during tremor. All recordings from the STN as well as those above are referred to as subthalamic region. For the tremor-dominant patients significantly more input than output causalities were found ($p=0.003$), while, in contrast, for the akinetic-rigid patients significantly more output causalities were detected ($p=0.040$). This finding is consistent with the Albin and DeLong model, which describes the STN as an output structure for the akinetic-rigid patients. When directly comparing both patient groups, significantly more output causalities ($p<0.001$) and input causalities ($p<0.001$) were found in the tremor-dominant than in the akinetic-rigid patients (figure 7.5). In contrast, for akinetic-rigid patient during periods without tremor significantly more input causalities were detected ($p=0.045$; see table 7.3).

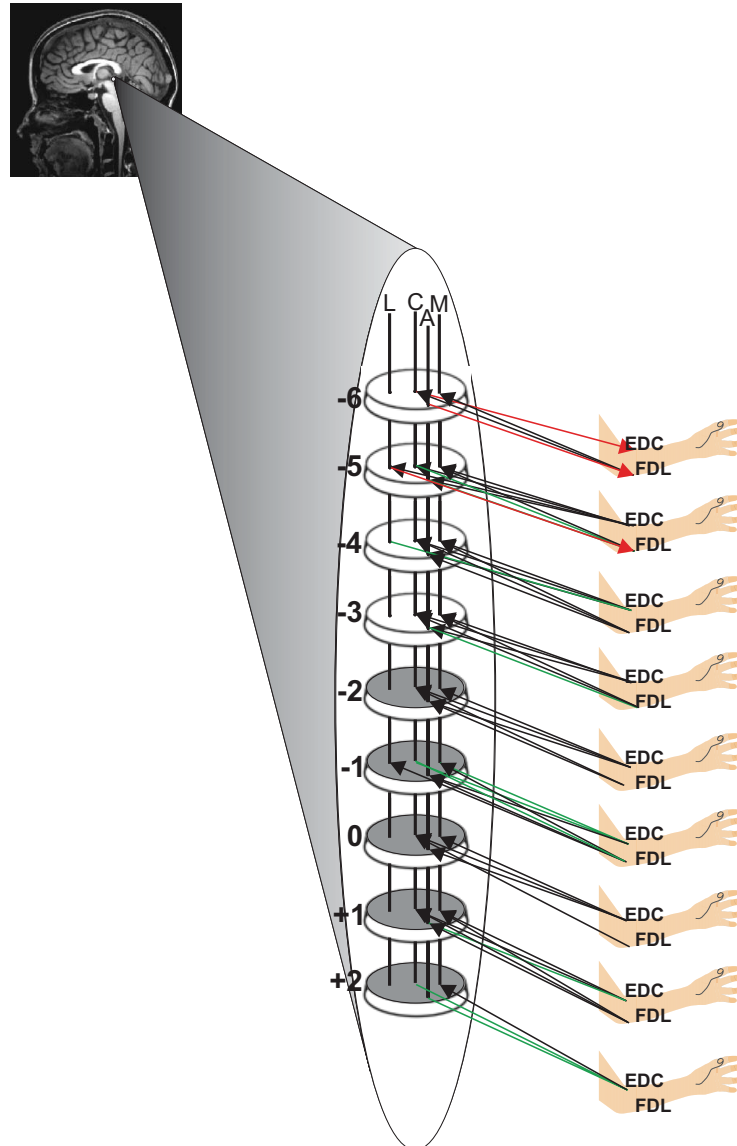


Figure 7.4: Causalities for one tremor-dominant Parkinson patient during rest condition: Note that more connections originate from the arm to the brain. In this patient only four electrodes were used. Black arrows indicate an input connection, red arrows indicate an output connection and green ones a bidirectional connection. Abbreviations: C – central electrode; A – anterior electrode; L – lateral electrode; M – medial electrode; EDC – M. extensor digitorum communis; FDL – M. flexor digitorum communis longis.

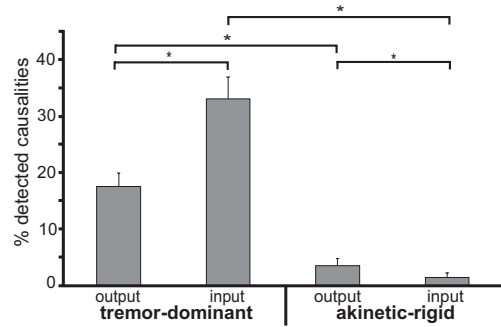


Figure 7.5: Occurrence of input and output causalities for PD patients with tremor during rest. For the tremor-dominant patients significantly more input causalities were detected, while for the akinetic-rigid patients significantly more output causalities were detected. * $p < 0.05$ after correcting for type I error; x-axis: patient type; y-axis: percentage of detected causalities; the error bars indicate the standard error.

7.3 Discussion

In this application the causality between oscillatory activity in the subthalamic region and muscle activity of the upper extremity of Parkinson's disease patients during tremor and non-tremor episodes were analyzed. The aim was to identify, whether a different pathophysiology underlies tremor in the two subtypes of PD.

Methodological Issues

Due to the intraoperative recordings it was possible to accurately localize the recording site. Correct localization of the electrode in the STN and subthalamic region was assessed by microelectrode recordings as well as by projecting the final DBS electrode placement from intraoperative stereotactic x-rays onto the preoperative

7.3. DISCUSSION

stereotactic MRI. At present, single cell activity is the best way for accurately localizing the STN in vivo (Hutchison et al. 1998), even though a definitive confirmation of the correct localization can only be obtained from post-mortem studies (Gross et al. 2004). However, as the STN firing patterns are very characteristic, localization and identification is reliably achieved (Hutchison et al. 1998). Nevertheless, it cannot be excluded that the macroelectrode recordings also included far-field potentials. However, these effects should be minor without having a great influence on the overall results.

At first sight, the band edge of the 2 Hz high-pass filter might seem too low to completely remove all movement artifacts. This conservative high-pass setting was chosen for two reasons. First, it has been shown in the first simulation study of this work that filtering potentially destroys the causality structure. Hence, it was aimed at leaving the frequency band of parkinsonian tremor (4-7 Hz) unaltered. Due to the finite slope of practical filter functions, a 2 Hz high-pass filter may still affect frequency ranges up to 3 Hz. Second, movement during the operation with a frequency of more than 2 Hz seems rather fast given the fixation to the operation-desk. In the context of a directional coupling analysis Smirnov et al. (2008) also use a 2 Hz high-pass filter and show their results to be insensitive to a higher band-edge, suggesting the sufficiency of this filter.

Comparison to Previous Studies

Previously, Wang et al. analyzed causality between LFPs of the STN and EMG activity of the contra lateral arm in four PD patients by means of bivariate Granger causality (Wang et al. 2007). They found bidirectional connectivity during discontinuous tremor and output causalities during continuous tremor. Smirnov et al. also found

a bidirectional coupling for a zero phase shift and an output causality for a phase shift of 1-2 tremor periods by means of a phase dynamical modeling for three PD patients (Smirnov et al. 2008). Their study only analyzed episodes of continuous tremor. In accordance with this literature significantly more output than input causalities were found for the akinetic-rigid patients with tremor during rest in the subthalamic region as a whole, which was not the case for the tremor-dominant subtype. However, Wang et al. did not give an exact classification of the four patients and Smirnov et al. used a different analysis approach, which limits a direct comparison of the results.

Tremor-Dominant Patients vs. Akinetic-Rigid Patients

Following Jellinger's finding of PD-type specific degeneration the first hypothesis tested whether a difference exists in the causality pattern between the two subtypes. Consistent with this hypothesis we found a significant difference for these two subtypes in the wider subthalamic region: our data suggest that neural activity in the wider STN area reflects more output than input causalities for the akinetic-rigid patients, and more input than output causalities for the tremor-dominant patients. This result in combination with the histological findings of Jellinger (1999) indicates that different SNc-STN pathways may be predominantly affected in both subtypes. Tremor in the two subtypes might originate from different pathways from the SNc to the subthalamic region, thereby creating specific pathological loops in each PD type. Future research should test the conjecture about this putative pathway as opposed to any other. The results for the wider subthalamic area during tremor also support the second hypothesis, derived from the Albin and DeLong model, that there should be more output than input causalities for the akinetic-rigid patients.

Further supporting the hypothesis of a different pathology pattern is the signifi-

7.3. DISCUSSION

cantly higher coupling between STN activity and electromyograms in tremor-dominant patients compared to akinetic-rigid patients during tremor. While only few connections were found in akinetic-rigid patients (2.5% of all possible connections in the subthalamic area), significantly more were detected for the tremor-dominant patients (25.3% of all possible connections in the subthalamic area). This result is due to both less output and input causalities in the akinetic-rigid patient group compared to the tremor-dominant patients. Note that this result does not necessarily imply differing signal-to-noise ratios (SNR) between both types, but only that the signal components of the STN activity and electromyograms are better able to predict each other. There may be a lot of other signal components, e.g. from other brain regions, entering our recorded signals, which clearly do not constitute noise. However, it cannot be excluded in general that the SNRs systematically differ between both types, but the simulation results in chapter 6 indicate that the sPDC with LOOM is relatively robust against such differences.

This striking pattern of less causalities may be the result of either a stronger pathological tremor network in the tremor-dominant patients or of a reduced signal processing in the wider subthalamic area due to akinesia and rigidity. The hypothesis of a pathological tremor network which has already further progressed in tremor-dominant patients than in akinetic-rigid ones is supported by previous data which showed the existence of clusters of "tremor cells" in tremor-dominant PD patients (Bergman et al. 1994, Reck, Florin, Wojtecki, Krause, Groiss, Voges, Maarouf, Sturm, Schnitzler and Timmermann 2009). Furthermore, a single cell study detected tremor cells almost solely in tremor-dominant patients, which also had a higher UPDRS tremor score. In contrast, in non tremor-dominant patients only 1 tremor cell was detected in a total of 84 analyzed STN cells. Even in tremor-dominant patients, only 10 % of the recorded STN cells were tremor cells (Levy et al. 2000). Thus, the

result of fewer causalities in the akinetic-rigid patients during tremor than in the tremor-dominant patients might be due to even more sparse tremor cells present in the akinetic-rigid patients, as tremor is only a “secondary” symptom for them. Hence, one can conjecture that fewer “tremor cells” develop in the STN as most cells have already been altered to “akinetic cells clusters”, whose LFP signal is, in contrast to tremor cells, unrelated to the electromyograms. Thus, a detection of a tremor-related causality is more difficult in the akinetic-rigid patient group. In support of the hypothesis that more cells in the STN of the akinetic-rigid patients are responsible for akinesia and rigidity than for tremor, almost as many causalities were detected for the akinetic-rigid patients during periods without tremor as was the case for the tremor-dominant patients.

To further analyze the conjecture of different pathological cell clusters in the two subtypes future research should analyze, if the LFPs from both types exhibit different characteristics. One might in particular want to compare the dominant oscillatory frequency of the causality to potentially identify frequency specific communication pathways. For tremor-dominant patients one would expect pronounced activity in the tremor range and less in the beta band (13-30 Hz), which is commonly associated with akinesia and rigidity with the converse for akinetic-rigid patients. However, the currently available causality measures are unable to provide a sufficient frequency resolution with the determined optimal model order (Schlögl and Supp 2006), which renders this differentiation impossible at present.

As for both patient groups during their main symptom, i.e. tremor for the tremor-dominant patients and akinesia and rigidity for the akinetic-rigid patients, more input causalities to the STN were detected, the results tentatively suggest that the STN is not a “purely” or predominantly driving nucleus. One possible explanation

7.3. DISCUSSION

for the observed characteristics of STN neuronal activity could be that it acts as an integrative convergence relay nucleus for information from the periphery, thus receiving more input causalities. This conjecture is supported by analysis of connections of the STN from and to the motor cortex and electromyograms (Marsden et al. 2001, Lalo et al. 2008). Lalo et al. found significantly more input to the STN from the primary motor cortex and supplementary motor area during periods of no medication in PD (Lalo et al. 2008). Hence, the STN could play an important role in motor control by integrating peripheral feedback and input information from these two cortical areas. Anatomical support for this conjecture comes from rats and cats, in which the STN has been described as a converging and integrating nucleus with far-reaching dendrites (Bevan et al. 1997). Moreover, axon terminals from the globus pallidus, sensorimotor cortex and nucleus tegmenti pedunculopontinus pars compacta synapse at the STN (Moriizumi et al. 1987). In this case, DBS in the STN is operational because it effectively modulates this input information transfer to the STN. This conjecture is supported by a recent study in mice, where high frequency stimulation (130 Hz) of afferent axons ameliorated PD symptoms (Gradinaru et al. 2009). Hence, DBS may not block STN output, but rather afferent information processing. If the feedback from the periphery and cortical motor areas is disrupted, the efferent part of the basal ganglia-cortical loops would receive less pathological input and might subsequently produce less or no pathological oscillatory output leading to PD symptoms. This explanation would in general be consistent with the Albin and DeLong model (Albin et al. 1989, DeLong 1990), but at the same time suggests that an important role in processing of input information must be added to it.

Summarizing the results, a different pattern of causality has been identified between tremor-dominant and akinetic-rigid patients during episodes of tremor. While in accordance with the current basal ganglia model, more output causalities to the STN

were found in akinetic-rigid patients during tremor, more input causalities were found in the same region for tremor-dominant patients and akinetic-rigid patients during periods without tremor. Moreover, both more output and input causalities for the tremor-dominant than for the akinetic-rigid patients during tremor were detected. This suggests different pathological mechanisms underlying tremor generation of these two types.

Overall this application of the sPDC to local field potentials and electromyograms of PD patients has demonstrated the importance of the causality measures. With the sPDC it was possible to gain insights into the pathophysiology of PD: With older methods, it was only possible to measure coupling between arm muscle and central neural signal. With the MVAR causality measures it is now possible to determine the direction of this coupling. In the present study this information added important new insights to the theoretical model of PD pathophysiology by Albin and DeLong (Albin et al. 1989, DeLong 1990) and suggests important modifications that are in line with recent animal studies (Gradinaru et al. 2009).

Conclusion

In the present work, causality measures based on the idea of Granger causality have been tested for their applicability to time series data obtained from neural recordings. For a better understanding of these recordings, in chapter 2 an overview of the electrophysiological origins of neural signals was given and three types of recording procedures were presented. While EEG and MEG both measure neural signals non-invasively at the scalp, macroelectrodes record local field potentials invasively at their actual origin, i.e. in the brain. Although the latter allow for the most exact spatial localization, they can only be used during the implantation of deep brain stimulation electrodes. Thus, EEG and MEG were presented, which have a lower spatial resolution, but can also be recorded in healthy humans. As the question of causality is of particular interest for the generation of movement, electromyography to record muscle activity was also introduced.

In chapter 3 five MVAR causality measures were presented that allow to statistically determine the direction of information flow in neural signals. These were the squared partial directed coherence, the partial directed coherence, the directed

transfer function, the direct directed transfer function and the transfer function. These measures are all multivariate extensions of Granger causality in the frequency domain. In order to distinguish true statistical causalities from spurious ones, two different numerical methods for determining the significance of the causality measures were introduced: the leave one out method and random permutation. While with the LOOM still a distribution is assumed, the random permutation approach is a completely non-parametric approach. The analysis was restricted to these two methods for two reasons. First, there only exist analytic methods for the PDC and DTF so that a comprehensive comparison would otherwise not be possible. Second, numerical methods often perform better in finite samples (Davidson and MacKinnon 2004).

As a systematical evaluation of the causality measures and significance threshold computation methods is still lacking, first a controlled environment was introduced in chapter 4 to test the performance of the causality measures. To create data with a predefined causality structure two models from the literature were introduced and extended to the particular needs of the present work. First, the Kus-model was used to analyze possible data-type specific dependencies of the causality measures, because it uses a real data set for the first signal channel and subsequently generates the other channels from this data. As basis for this first channel all 4 data types introduced in chapter 2 were evaluated: EEG, MEG, intraoperative LFPs and EMG. The second model, the so called Schelter-model, uses only simulated data to generate the system of signals and is thus data-type independent.

All tested causality measures are based on autoregressive modeling. Hence, two important prerequisites for a proper and consistent model estimation were considered in chapter 4, i.e. stationarity and preprocessing of the data. It was shown that carefully chosen neural data fulfill the requirements for a consistent estimation of the

autoregressive coefficients. A second and very important factor in data analysis is the preprocessing of raw data. Very commonly data in neuroscience are filtered in such a way that only frequencies of interest are left in the data. It was theoretically derived in chapter 4 that filtering and decimating of time series data changes autoregressive coefficient estimates and leads to wrong conclusions about causality when traditional Granger causality is used. Based on these results, it was hypothesized, that the multivariate causality measures presented in chapter 3 would also exhibit such a behavior. Due to the transfer of the coefficient-matrices into the frequency domain and the application of numerical significance measures, it was not possible to theoretical prove, that the change in the coefficient matrix due to filtering would lead to changes in the detection of significant causalities.

Within chapter 5 this hypothesis was tested by means of a simulation approach. In accordance with the hypothesis derived in chapter 4 the multivariate causality methods showed the expected behavior: Almost every filter and decimation method led to misleading results. Only in the presence of noise/artifacts that clearly disturb the working of the causality measures, filtering improved the results and seemed advisable. The first such case was the presence of a simulated 50 Hz power-line artifact that led to a huge increase of misdetections. The application of a notch filter had the desired effect of removing these adverse effects while at the same time not introducing new artifacts. The second case were movement artifacts, which could be removed with a 1 Hz high-pass filter. Thus, filtering can only be recommended, if obvious artifacts are present. In contrast, the application of filters without the presence of obvious artifacts just to reduce the frequency spectrum does not lead to any obvious advantage, but may rather lead to spurious or missed causalities.

Of equal importance for an application is knowledge about parameter dependen-

cies of the causality measures and a comparison of these measures with different significance thresholds. In chapter 6 a systematic evaluation of the performance of the multivariate causality measures based on the models presented in chapter 4 was performed. The simulations specifically used the Schelter- as well as the Kus-model, which allow to disentangle data-type specific and non data-type specific effects. The parameters tested in this chapter were data length, coupling strength, external noise and model order. The data length was considered to identify the minimal data length required for a correct model estimation. The influence of external noise was tested to determine the effect of a low signal-to-noise ratio while the coupling strength was varied to determine when it becomes impossible to correctly detect a coupling. The last parameter under consideration was the model order.

With the results of this second simulation study it was possible to compare the performance of the 5 different causality measures and the significance thresholds used. Overall, the choice of the best performing significance threshold depends on the causality measure and the data type used. The best performing and most robust causality measure for most data types and parameter ranges was the sPDC with LOOM. Hence its usage is recommended for most applications.

In accordance with prior expectations, an increasing data length, a low noise level in the data and an appropriate model order had a positive influence on the performance of the causality measures. As the number of frequency components which can be resolved is half of the model order, frequency specificity of the causality measures relies on the model order. Thus, in real applications, where the true model is usually unknown, the researcher always faces a trade-off between a good frequency resolution and an increase in possible false detections due to an overestimation of the correct model order. A change in coupling strength had almost no influence on the results.

Only in combination with random permutation false positive detections were made when the coupling strength increased. These false positive detections were observed in connections to channels which largely varied in the signal-to-noise ratio compared to the other channels. If a connection to one channel from every other channel is observed, it should be checked whether these connections may be due to large differences in the signal-to-noise ratios of these channels.

In chapter 7 an application was presented that demonstrated the potential for scientific progress inherent in these causality measures. As the sPDC with LOOM was previously identified as the best performing causality measure, it was used to determine causality between muscle and brain activity of Parkinson's disease patients. Muscle activity was measured using EMG and brain activity by invasively obtained local field potentials. Data preprocessing followed the guidelines developed in chapter 5. Only a high-pass filter and a notch filter were applied to the data in order to remove potential movement and power-line artifacts. Hence no negative effects due to filtering or decimating were introduced to the data. Knowledge about the direction in signal processing between subthalamic nucleus and affected arm muscles is important for understanding deep brain stimulation – an effective treatment in the later stages of Parkinson's disease. Previous studies were only able to determine connectivity, but not the direction of information flow between muscle and brain activity. Reliable information about causality allows to better understand the mechanisms underlying deep brain stimulation. The results of the application were in part consistent with the current basal ganglia model of Albin and DeLong (Albin et al. 1989, DeLong 1990), but also showed that this model may have to be modified in order to incorporate the new evidence. Thus, the causality measures have proven to be useful by extending our current knowledge and showing the potential for improving the treatment of Parkinson's disease with deep brain stimulation.

Scientific progress is not limited to the methods and measures considered in the present work. There are currently several interesting developments in the area of causality analysis of neural data. The current work focused on recording procedures with high temporal resolution. A highly active area of causality analysis research has developed in the field of fMRI connectivity studies (Roebroeck et al. 2005, Friston 2009, Goebel et al. 2003, Gao et al. 2008, Wilke et al. 2009, Upadhyay et al. 2008, Uddin et al. 2009), which offers a better spatial resolution. Here the problem is that the data is usually short but high-dimensional, meaning that the problem becomes ill-posed as the number of variables is larger than the number of observations. In this case, the dimensionality of the data has to be reduced prior to the application of a causality measure. One prominent approach to do so in the context of Granger causality is based on a principal component analysis (Zhou et al. 2008, Zhou et al. 2009, Zhong et al. 2009). Based on an eigenvalue decomposition of the covariance matrix, only the signal components contributing most to the variance, the principal components, are considered for the further analysis. However, while a principal component analysis (PCA) acts like a filter that reduces the dimensionality of the data, a thorough evaluation of this procedure is currently missing and should be an important task for future research. The same caveat applies to similar approaches that employ the independent component analysis (ICA) instead of a PCA (Londei et al. 2007).

Further interesting developments have occurred in the field of time-frequency causality analysis of EEG and MEG data (Schlögl and Supp 2006, Ploner et al. 2009). These approaches could be very helpful for the analysis of event-related signals, in which the time pattern of causality is also of interest. Traditional analysis may be limited by a structural break due to the transition between brain micro-states following the event. Time-frequency causality analysis aims at uncovering this structural change by

considering the change in the causality measures over time. Similar approaches based on locally stationary time series due to short-windowing have also been proposed in Ding et al. (2000) and Wang et al. (2008). However, in these latter approaches trial averages are considered and again the consequences of this aggregation remain poorly understood. A different approach to circumvent the problems introduced by these instationarities has been to augment the standard VARs by the use of wavelets that are able to capture the changing stochastic pattern (Fujita et al. 2007, Sato et al. 2006, Dhamala et al. 2008a). While these approaches seem to be successful in detecting the presence of a structural break in selected examples, not much guidance is available in how to specify the underlying model, i.e. for example which mother wavelet to use.

Regarding event-related data, one particular problem of Granger causality is that it tries to explain the neural signal processing exclusively by considering endogenous inputs. This may be an inappropriate assumption if the researcher applies an external stimulus to the patient. Hence, an important task will be to incorporate exogenous stimuli and their influence on brain areas. First results have been presented in (Guo et al. 2008, Li et al. 2010).

The application to event related data in addition increases the need for nonlinear causality analysis techniques, because due to potential event related actions, nonlinearities might arise in the data. There have been some very interesting developments in extending Granger causality to the nonlinear case, which could make the causality measures more widely applicable (Bezruchko et al. 2008, Gourevitch et al. 2006, Marinazzo et al. 2008a, Marinazzo et al. 2008b, Chavez et al. 2003, Marinazzo et al. 2006).¹

¹One commonly found approach is to construct the autoregressive model as a polynomial of order p and to then evaluate the nonlinear Granger causality.

However, as soon as the domain of linear estimators is left, not much is known about the exact properties of these measures like, for example, their distribution.

In conclusion, causality analysis has and continues to provide researchers with important tools to study the signal processing inside the brain and the neural communication between the structures constituting the motor control system. In doing so, considerable progress has already been achieved as a large number of prominently published applied studies confirm. Nevertheless, despite all progress there still remain many open methodological questions that may be the topic of interesting and innovative future research.

The present work contributed its share to solving some of the open methodological issues. The theoretical simulation results delivered guidelines to enable researchers to correctly apply the considered multivariate causality measures. These guidelines will help to minimize errors and wrong inference made due to an improper choice of parameters, causality measure and significance threshold computation method. The possible potential of the causality measures for applications in neuroscience was demonstrated in the last chapter by applying it to real data. Thus, the present work gives researchers concrete advice on the correct choice of a causality measure and parameters and should enable future studies to better answer questions of causality in neural data.

Bibliography

- Adeli, H., Zhou, Z. and Dadmehr, N.: 2003, Analysis of EEG records in an epileptic patient using wavelet transform, *Journal of Neuroscience Methods* **123**(1), 69–87.
- Akaike, H.: 1973, *Information theory and an extension of the likelihood ratio principle*, Academia Kiado, pp. 267–281.
- Akaike, H.: 1974, A new look at the statistical model identification, *IEEE transactions on automatic control* **19**(6), 716–723.
- Alberts, J. L., Voelcker-Rehage, C., Hallahan, K., Vitek, M., Bamzai, R. and Vitek, J. L.: 2008, Bilateral subthalamic stimulation impairs cognitive-motor performance in Parkinson’s disease patients, *Brain* **131**, 3348–3360.
- Albin, R., Young, A. and Penney, J. B.: 1989, The functional anatomy of basal ganglia disorders, *Trends in Neurosciences* **12**, 366–375.
- Andrews, D. and Ploberger, W.: 1994, Optimal tests when a nuisance parameter is present only under the alternative, *Econometrica* **62**, 1183–1414.
- Ansari-Asl, K., Senhadji, L., Bellanger, J. and Wendling, F.: 2006, Quantitative evaluation of linear and nonlinear methods characterizing interdependencies between brain signals, *Physical Review E* **74**(3), 31916.

Bibliography

- Aristotle: 350 BC, *Metaphysics, Book 5*, Translated by Hugh Tredennick, Harvard University Press.
- Astolfi, L., Cincotti, F., Mattia, D., Babiloni, C., Carducci, F., Basilisco, A., Rossini, P. M., Salinari, S., Ding, L., Ni, Y., He, B. and Babiloni, F.: 2005, Assessing cortical functional connectivity by linear inverse estimation and directed transfer function: simulations and application to real data, *Clinical Neurophysiology* **116**(4), 920–932.
- Astolfi, L., Cincotti, F., Mattia, D., Marciani, M. G., Baccala, L. A., Fallani, F. D., Salinari, S., Ursino, M., Zavaglia, M. and Babiloni, F.: 2006, Assessing cortical functional connectivity by partial directed coherence: Simulations and application to real data, *IEEE Transactions on Biomedical Engineering* **53**(9), 1802–1812.
- Astolfi, L., Cincotti, F., Mattia, D., Marciani, M. G., Baccala, L. A., Fallani, F. D., Salinari, S., Ursino, M., Zavaglia, M., Ding, L., Edgar, J. C., Miller, G. A., He, B. and Babiloni, F.: 2007, Comparison of different cortical connectivity estimators for high-resolution EEG recordings, *Human Brain Mapping* **28**(2), 143–157.
- Baccala, L. A. and Sameshima, K.: 2001, Partial directed coherence: a new concept in neural structure determination, *Biological Cybernetics* **84**(6), 463–474.
- Baillet, S., Mosher, J. C. and Leahy, R. M.: 2001, Electromagnetic brain mapping, *IEEE Signal Processing Magazine* **18**(6), 14–30.
- Benabid, A. L., Pollak, P., Gross, C., Hoffmann, D., Benazzouz, A., Gao, D. M., Laurent, A., Gentil, M. and Perret, J.: 1994, Acute and long-term effects of subthalamic nucleus stimulation in Parkinson's disease, *Stereotactic and Functional Neurosurgery* **62**(1-4), 76–84.

Bibliography

- Benar, C.-G., Grova, C., Kobayashi, E., Bagshaw, A. P., Aghakhani, Y., Dubeau, F. and Gotman, J.: 2006, EEG-fMRI of epileptic spikes: Concordance with EEG source localization and intracranial EEG, *NeuroImage* **30**(4), 1161 – 1170.
- Benjamini, Y. and Hochberg, Y.: 1995, Controlling the false discovery rate: a practical and powerful approach to multiple testing, *Journal of the Royal Statistical Society Series B* **57**, 289–300.
- Berger, H.: 1929, Über das Elektrenkephalogramm des Menschen, *European Archives of Psychiatry and Clinical Neuroscience* **87**(1), 527–570.
- Bergman, H. and Deuschl, G.: 2002, Pathophysiology of Parkinson’s disease: from clinical neurology to basic neuroscience and back, *Movement Disorders* **17**(3), 28–40.
- Bergman, H., Wichmann, T., Karmon, B. and DeLong, M. R.: 1994, The primate subthalamic nucleus. II. Neuronal activity in the MPTP model of parkinsonism, *Journal of Neurophysiology* **72**(2), 507–20.
- Bevan, M. D., Clarke, N. P. and Bolam, J. P.: 1997, Synaptic integration of functionally diverse pallidal information in the entopeduncular nucleus and subthalamic nucleus in the rat, *Journal of Neuroscience* **17**(1), 308–24.
- Bezruchko, B., Ponomarenko, V., Prokhorov, M., Smirnov, D. and Tass, P.: 2008, Modeling nonlinear oscillatory systems and diagnostics of coupling between them using chaotic time series analysis: applications in neurophysiology, *Physics-Uspekhi* **51**(3), 304–310.
- Bischoff, C., Fulgsang-Fredriksen, A., Vendelbo, L. and Sumner, A.: 1999, *Standards of instrumentation of EMG*, Elsevier, pp. 199–211.

Bibliography

- Bollimunta, A., Chen, Y., Schroeder, C. E. and Ding, M.: 2008, Neuronal mechanisms of cortical alpha oscillations in awake-behaving macaques, *Journal of Neuroscience* **28**(40), 9976–88.
- Bonferroni, C. E.: 1936, Teoria statistica delle classi e calcolo delle probabilità, *Pubblcazioni del R Istituto Superiore di Scienze Economiche e Commerciali di Firenze* **8**, 3–62.
- Box, G. E. P. and Jenkins, G. M.: 1970, *Time series analysis: forecasting and control*, Holden-Day, San Francisco, Calif.
- Breitung, J. and Candelon, B.: 2006, Testing for short- and long-run causality: A frequency-domain approach, *Journal of Econometrics* **132**, 363–378.
- Breitung, J. and Swanson, N.: 2002, Temporal aggregation and spurious instantaneous causality in multiple time series models, *Journal of Times Series Analysis* **23**(6), 651–665.
- Brillinger, D. R.: 1983, The finite fourier transform of a stationary process, in D. R. Brillinger and P. A. Krishnaiah (eds), *Handbook of Statistics*, Vol. 3, Elsevier Science Publishers, Amsterdam, pp. 21–37.
- Brovelli, A., Ding, M., Ledberg, A., Chen, Y., Nakamura, R. and Bressler, S. L.: 2004, Beta oscillations in a large-scale sensorimotor cortical network: directional influences revealed by Granger causality, *Proceedings of the National Academy of Sciences* **101**(26), 9849–54.
- Brown, P. and Marsden, C. D.: 1998, What do the basal ganglia do?, *Lancet* **351**(9118), 1801–4.
- Brown, P. and Williams, D.: 2005, Basal ganglia local field potential activity:

Bibliography

- character and functional significance in the human, *Clinical Neurophysiology* **116**(11), 2510–2519.
- Buzsaki, G. and Draguhn, A.: 2004, Neuronal oscillations in cortical networks, *Science* **304**(5679), 1926–1929.
- Canova, F.: 1998, Detrending and business cycle facts, *Journal of monetary economics* **41**(3), 475–512.
- Caplan, J. B., Madsen, J. R., Raghavachari, S. and Kahana, M. J.: 2001, Distinct patterns of brain oscillations underlie two basic parameters of human maze learning, *Journal of Neurophysiology* **86**(1), 368–380.
- Cascino, G. D., Andermann, F., Berkovic, S. F., Kuzniecky, R. I., Sharbrough, F. W., Keene, D. L., Bladin, P. F., Kelly, P. J., Olivier, A. and Feindel, W.: 1993, Gelastic seizures and hypothalamic hamartomas: Evaluation of patients undergoing chronic intracranial EEG monitoring and outcome of surgical treatment, *Neurology* **43**(4), 747–750.
- Chan, K. H., Hayya, J. C. and Ord, J. K.: 1977, A note on trend removal methods: the case of polynomial regression versus variate differencing, *Econometrica* **45**(3), 737–744.
- Chan, N. H.: 1999, The ET Interview: Professor George C. Tiao, *Econometric Theory* **15**(03), 389–424.
- Chavez, M., Martinerie, J. and Quyen, M. L. V.: 2003, Statistical assessment of nonlinear causality: application to epileptic EEG signals, *Journal of Neuroscience Methods* **124**(2), 113 – 128.
- Chen, Y., Bressler, S. L. and Ding, M.: 2006, Frequency decomposition of conditional

Bibliography

- Granger causality and application to multivariate neural field potential data, *Journal of Neuroscience Methods* **150**(2), 228–37.
- Chow, G. C.: 1960, Tests of equality between sets of coefficients in two linear regressions, *Econometrica* **28**(3), 591–605.
- Cohen, D.: 1968, Magnetoencephalography: evidence of magnetic fields produced by alpha-rhythm currents, *Science* **161**(3843), 784–786.
- Cohen, D. and Cuffin, B.: 1983, Demonstration of useful differences between magnetoencephalogram and electroencephalogram, *Electroencephalography and Clinical Neurophysiology* **56**, 38–51.
- Conway, B. A., Halliday, D. M., Farmer, S. F., Shahani, U., Maas, P., Weir, A. I. and Rosenberg, J. R.: 1995, Synchronization between motor cortex and spinal motoneuronal pool during the performance of a maintained motor task in man, *The Journal of Physiology* **489**(3), 917–24.
- Cox, C.: 1996, Nonlinear quasi-likelihood models: applications to continuous proportions, *Computational Statistics & Data Analysis* **21**(4), 449–461.
- Dahlhaus, R., Eichler, M. and Sandkühler, J.: 1997, Identification of synaptic connections in neural ensembles by graphical models, *Journal of Neuroscience Methods* **77**(1), 93–107.
- Dalal, S., Baillet, S., Adam, C., Ducorps, A., Schwartz, D., Jerbi, K., Bertrand, O., Garnero, L., Martinerie, J. and Lachaux, J.: 2009, Simultaneous MEG and intracranial EEG recordings during attentive reading, *NeuroImage* **45**(4), 1289–1304.
- Daubechies, I.: 1990, The wavelet transform time-frequency localization and signal analysis, *IEEE Transactions on Information Theory* **36**, 961–1004.

Bibliography

- Daubechies, I.: 1992, *Ten Lectures on Wavelets*, Society for Industrial Mathematics.
- Davidson, R. and MacKinnon, J.: 2004, *Econometric Theory and Methods*, Oxford University Press, New York.
- De Luca, C.: 1997, The use of surface electromyography in biomechanics, *Journal of Applied Biomechanics* **13**, 135–163.
- DeLong, M.: 1990, Primate models of movement disorders of basal ganglia origin, *Trends in Neurosciences* **13**(7), 281–5.
- Deuschl, G., Schade-Brittinger, C., Krack, P., Volkmann, J., Schafer, H., Botzel, K., Daniels, C., Deutschlander, A., Dillmann, U., Eisner, W., Gruber, D., Hamel, W., Herzog, J., Hilker, R., Klebe, S., Kloss, M., Koy, J., Krause, M., Kupsch, A., Lorenz, D., Lorenzl, S., Mehdorn, H. M., Moringlane, J. R., Oertel, W., Pinsker, M. O., Reichmann, H., Reuss, A., Schneider, G. H., Schnitzler, A., Steude, U., Sturm, V., Timmermann, L., Tronnier, V., Trottenberg, T., Wojtecki, L., Wolf, E., Poewe, W. and Voges, J.: 2006, A randomized trial of deep-brain stimulation for Parkinson's disease, *The New England Journal of Medicine* **355**(9), 896–908.
- Dhamala, M., Rangarajan, G. and Ding, M.: 2008a, Analyzing information flow in brain networks with nonparametric Granger causality, *NeuroImage* **41**, 354–362.
- Dhamala, M., Rangarajan, G. and Ding, M.: 2008b, Estimating Granger causality from fourier and wavelet transforms of time series data, *Physical Review Letters* **100**, 018701.
- Dickey, D. A. and Fuller, W. A.: 1979, Distribution of the estimators for autoregressive time series with a unit root, *Journal of the American Statistical Association* **74**(366), 427–431.

Bibliography

- Dickey, D. A. and Fuller, W. A.: 1981, Likelihood ratio statistics for autoregressive time-series with a unit-root, *Econometrica* **49**(4), 1057–1072.
- Ding, M., Bressler, S. L., Yang, W. and Liang, H.: 2000, Short-window spectral analysis of cortical event-related potentials by adaptive multivariate autoregressive modeling: data preprocessing, model validation, and variability assessment, *Biological Cybernetics* **83**(1), 35–45.
- Ding, M., Chen, Y. and Bressler, S. L.: 2006, Granger causality: Basic theory and application to neuroscience, in B. Schelter, M. Winterhalder and J. Timmer (eds), *Handbook of Time Series Analysis*, Wiley-VCH Verlag, Weinheim, pp. 437–460.
- Efron, B.: 1992, Jackknife-after-bootstrap standard errors and influence functions, *Journal of the Royal Statistical Society Series B-Methodological* **54**(1), 83–127.
- Eichler, M.: 2006, On the evaluation of information flow in multivariate systems by the directed transfer function, *Biological Cybernetics* **94**(6), 469–482.
- Elliott, G., Rothenberg, T. J. and Stock, J. H.: 1996, Efficient tests for an autoregressive unit root, *Econometrica* **64**(4), 813–836.
- Elsner, J.: 2006, Evidence in support of the climate change – Atlantic hurricane hypothesis, *Geophysical Research Letters* **33**, L16705.
- Engle, R.: 1984, *Wald, likelihood ratio, and Lagrange multiplier tests in econometrics*, Vol. 2, Elsevier Science, chapter 13, pp. 775–826.
- Fahn, S., Elton, R. and the members of the UPDRS Development Committee: 1987, The Unified Parkinson’s Disease Rating Scale, in S. Fahn, C. Marsden, D. Calne and M. Goldstein (eds), *Recent developments in Parkinson’s disease*, Vol. 2, Macmillan Healthcare, Florham Park, pp. 153–163.

Bibliography

- Ferrari, S. and Cribari-Neto, F.: 2004, Beta regression for modelling rates and proportions, *Journal of Applied Statistics* **31**(7), 799 – 815.
- Fisher, R., Boas, W., Blume, W., Elger, C., Genton, P., Lee, P. and Engel, J.: 2005, Epileptic seizures and epilepsy: definitions proposed by the International League Against Epilepsy (ILAE) and the International Bureau for Epilepsy (IBE), *Epilepsia* **46**(4), 470–472.
- Florin, E., Reck, C., Burghaus, L., Lehrke, R., Gross, J., Sturm, V., Fink, G. R. and Timmermann, L.: 2008, Ten hertz thalamus stimulation increases tremor activity in the subthalamic nucleus in a patient with Parkinson’s disease, *Clinical Neurophysiology* **119**(9), 2098–103.
- Franaszczuk, P. J., Blinowska, K. J. and Kowalczyk, M.: 1985, The application of parametric multichannel spectral estimates in the study of electrical brain activity, *Biological Cybernetics* **51**(4), 239–247.
- Freeman, J.: 1983, Granger causality and the times series analysis of political relationships, *American Journal of Political Science* **27**, 327–358.
- Freeman, W.: 1975, *Mass Action in the Nervous System*, Academic Press, New York.
- Friston, K.: 2009, Causal modelling and brain connectivity in functional magnetic resonance imaging, *PLoS Biol* **7**(2), e1000033.
- Fujita, A., Sato, J., Garay-Malpartida, H., Morettin, P., Sogayar, M. and Ferreira, C.: 2007, Time-varying modeling of gene expression regulatory networks using the wavelet dynamic vector autoregressive method, *Bioinformatics* **23**(13), 1623–1630.
- Fuller, W.: 1976, *Introduction to statistical time series*, John Wiley & Sons, Inc., New York.

Bibliography

- Gabor, D.: 1946, Theory of communication, *Journal of Institutional Electrical Engineering London* **93**(3), 429–457.
- Gao, Q., Chen, H. and Gong, Q.: 2008, Evaluation of the effective connectivity of the dominant primary motor cortex during bimanual movement using Granger causality, *Neuroscience Letters* **443**, 1–6.
- Geweke, J. F.: 1982, Measurement of linear-dependence and feedback between multiple time-series, *Journal of the American Statistical Association* **77**(378), 304–313.
- Geweke, J. F.: 1984, Measures of conditional linear-dependence and feedback between time-series, *Journal of the American Statistical Association* **79**(388), 907–915.
- Goebel, R., Roebroeck, A., Kim, D.-S. and Formisano, E.: 2003, Investigating directed cortical interactions in time-resolved fMRI data using vector autoregressive modeling and Granger causality mapping, *Magnetic Resonance Imaging* **21**(10), 1251 – 1261.
- Gourevitch, B., Bouquin-Jeannes, R. and Faucon, G.: 2006, Linear and nonlinear causality between signals: methods, examples and neurophysiological application, *Biological Cybernetics* **95**, 249–369.
- Gradinaru, V., Mogri, M., Thompson, K. R., Henderson, J. M. and Deisseroth, K.: 2009, Optical deconstruction of parkinsonian neural circuitry, *Science* **324**(5925), 354–9.
- Granger, C. W. J.: 1969, Investigating causal relations by econometric models and cross-spectral methods, *Econometrica* **37**(3), 424–438.
- Granger, C. W. J.: 1980, Testing for causality - a personal viewpoint, *Journal of Economic Dynamics & Control* **2**(4), 329–352.

Bibliography

- Grech, R., Cassar, T., Muscat, J., Camilleri, K. P., Fabri, S. G., Zervakis, M., Xanthopoulos, P., Sakkalis, V. and Vanrumste, B.: 2008, Review on solving the inverse problem in EEG source analysis, *Journal of Neuroengineering and Rehabilitation* **5**, 25.
- Greene, W.: 2007, *Econometric analysis*, 6th edn, Prentice Hall, Upper Saddle River.
- Gross, J., Tass, P. A., Salenius, S., Hari, R., Freund, H. J. and Schnitzler, A.: 2000, Cortico-muscular synchronization during isometric muscle contraction in humans as revealed by magnetoencephalography, *Journal of Physiology* **527 Pt 3**, 623–31.
- Gross, R. E., Jones, E. G., Dostrovsky, J. O., Bergeron, C., Lang, A. E. and Lozano, A. M.: 2004, Histological analysis of the location of effective thalamic stimulation for tremor. Case report, *Journal of Neurosurgery* **100**(3), 547–52.
- Guo, S., Seth, A., Kendrick, K., Zhou, C. and Feng, J.: 2008, Partial granger causality – eliminating exogenous inputs and latent variables, *Journal of Neuroscience Methods* **172**, 79–93.
- Guyton, A. and Hall, J.: 2006, *Textbook of Medical Physiology*, 11th edn, Elsevier, Philadelphia.
- Hallez, H., Vanrumste, B., Grech, R., Muscat, J., De Clercq, W., Vergult, A., D’Asseler, Y., Camilleri, K. P., Fabri, S. G., Van Huffel, S. and Lemahieu, I.: 2007, Review on solving the forward problem in EEG source analysis, *Journal of Neuroengineering and Rehabilitation* **4**, 46.
- Halliday, D., Rosenberg, J., Amjad, A., Breeze, P., Conway, B. and Farmer, S.: 1995, A framework for the analysis of mixed time series/point process data – theory and application to the study of physiological tremor, single motor unit

Bibliography

- discharges and electromyograms, *Progress in Biophysics and molecular Biology* **64**(2-3), 237–278.
- Hamalainen, M., Hari, R., Ilmoniemi, R., Knuutila, J. and Lounasmaa, O.: 1993, Magnetoencephalography - theory, instrumentation, and applications to noninvasive studies of the working human brain., *Reviews of Modern Physics* **65**, 413–497.
- Hamilton, J.: 1994, *Time series analysis*, Princeton University Press, NJ.
- Hansen, B.: 2000, Testing for structural change in conditional models, *Journal of Econometrics* **97**(1), 93–115.
- Harvey, A. C. and Jäger, A.: 1993, Detrending, stylized facts and the business cycle, *Journal of applied econometrics* **8**(3), 231–247.
- Haueisen, J., Ramon, C., Czapski, P. and Eislet, M.: 1995, On the influence of volume currents and extended sources on neuromagnetic fields: a simulation study, *Annals of Biomedical Engineering* **23**, 728–739.
- Hiemstra, C. and Jones, J. D.: 1994, Testing for linear and nonlinear granger causality in the stock price-volume relation, *Journal of Finance* **49**(5), 1639–64.
- Hilker, R., Benecke, R., Deuschl, G., Fogel, W., Kupsch, A., Schrader, C., Sixel-Doring, F., Timmermann, L., Volkmann, J. and Lange, M.: 2009, Tiefe Hirnstimulation bei idiopathischem Parkinson-Syndrom : Empfehlungen der Deutschen Arbeitsgemeinschaft Tiefe Hirnstimulation, *Nervenarzt* **80**(6), 646–655.
- Hillebrand, A., Singh, K., Holliday, I., Furlong, P. and Barnes, G.: 2005, A new approach to neuroimaging with magnetoencephalography, *Human Brain Mapping* **25**(2), 199–211.

Bibliography

- Hosoya, Y.: 1991, The decomposition and measurement of the interdependency between second-order stationary processes, *Probability Theory* **88**, 429–444.
- Hutchison, W. D., Allan, R. J., Opitz, H., Levy, R., Dostrovsky, J. O., Lang, A. E. and Lozano, A. M.: 1998, Neurophysiological identification of the subthalamic nucleus in surgery for Parkinson’s disease, *Annals of Neurology* **44**(4), 622–8.
- Jellinger, K. A.: 1999, Post mortem studies in parkinson’s disease—is it possible to detect brain areas for specific symptoms?, *Journal of Neural Transmission Supplement* **56**, 1–29.
- Kaiser, R. and Maravall, A.: 2005, Combining filter design with model-based filtering (with an application to business-cycle estimation), *International Journal of Forecasting* **21**(4), 691–710.
- Kaminski, M., Ding, M. Z., Truccolo, W. A. and Bressler, S. L.: 2001, Evaluating causal relations in neural systems: Granger causality, directed transfer function and statistical assessment of significance, *Biological Cybernetics* **85**(2), 145–157.
- Kaminski, M. J. and Blinowska, K. J.: 1991, A new method of the description of the information-flow in the brain structures, *Biological Cybernetics* **65**(3), 203–210.
- Kandel, E., Schwartz, J. and Jessel, T.: 2000, *Principals of Neural Science*, 4th edn, McGraw-Hill.
- Katzner, S., Nauhaus, I., Benucci, A., Bonin, V., Ringach, D. L. and Carandini, M.: 2009, Local origin of field potentials in visual cortex, *Neuron* **61**, 35–41.
- Kaufmann, R. K., D’Arrigo, R. D., Laskowski, C., Myneni, R. B., Zhou, L. and Davi, N. K.: 2004, The effect of growing season and summer greenness on northern forests, *Geophysical Research Letters* **31**, L09205.

Bibliography

- Kieschnick, R. and McCullough, B. D.: 2003, Regression analysis of variates observed on $(0, 1)$: percentages, proportions and fractions, *Statistical Modeling* **3**(3), 193–213.
- Koles, Z.: 1998, Trends in EEG source localization, *Electroencephalography and clinical Neurophysiology* **106**(2), 127–137.
- Korzeniewska, A., Manczak, M., Kaminski, M., Blinowska, K. J. and Kasicki, S.: 2003, Determination of information flow direction among brain structures by a modified directed transfer function (dDTF) method, *Journal of Neuroscience Methods* **125**(1-2), 195–207.
- Kühn, A., Doyle, L., Pogosyan, A., Yarrow, K., Kupsch, A., Schneider, G., Hariz, M., Trottenberg, T. and Brown, P.: 2006, Modulation of beta oscillations in the subthalamic area during motor imagery in Parkinson's disease, *Brain* **129**(3), 695–706.
- Kühn, A., Trottenberg, T., Kivi, A., Kupsch, A., Schneider, G. and Brown, P.: 2005, The relationship between local field potential and neuronal discharge in the subthalamic nucleus of patients with Parkinson's disease, *Experimental Neurology* **194**(1), 212–20.
- Kumar, N. and Gilula, N.: 1996, The gap junction communication channel, *Cell* **84**(3), 381–388.
- Kus, R., Kaminski, M. and Blinowska, K. J.: 2004, Determination of EEG activity propagation: Pair-wise versus multichannel estimate, *IEEE Transactions on Biomedical Engineering* **51**(9), 1501–1510.
- Lalo, E., Thobois, S., Sharott, A., Polo, G., Mertens, P., Pogosyan, A. and Brown, P.: 2008, Patterns of bidirectional communication between cortex and basal ganglia

Bibliography

- during movement in patients with Parkinson disease, *Journal of Neuroscience* **28**(12), 3008–16.
- Lang, A. E., Houeto, J. L., Krack, P., Kubu, C., Lyons, K. E., Moro, E., Ondo, W., Pahwa, R., Poewe, W., Troster, A. I., Uitti, R. and Voon, V.: 2006, Deep brain stimulation: preoperative issues, *Movement Disorders* **21 Suppl 14**, S171–96.
- Lang, A. E. and Lozano, A. M.: 1998a, Parkinson’s disease. first of two parts, *The New England Journal of Medicine* **339**(15), 1044–53.
- Lang, A. E. and Lozano, A. M.: 1998b, Parkinson’s disease. second of two parts, *The New England Journal of Medicine* **339**(16), 1130–43.
- Le Van Quyen, M., Foucher, J., Lachaux, J., Rodriguez, E., Lutz, A., Martinerie, J. and Varela, F.: 2001, Comparison of hilbert transform and wavelet methods for the analysis of neuronal synchrony, *Journal of Neuroscience Methods* **111**(2), 83–98.
- Lehmann, D., Ozaki, H. and Pal, I.: 1987, EEG alpha map series: brain micro-states by space-oriented adaptive segmentation, *Electroencephalography and clinical neurophysiology* **67**(3), 271.
- Levy, R., Hutchison, W. D., Lozano, A. M. and Dostrovsky, J. O.: 2000, High-frequency synchronization of neuronal activity in the subthalamic nucleus of parkinsonian patients with limb tremor, *Journal of Neuroscience* **20**(20), 7766–75.
- Li, X., Marrelec, G., Hess, R. F. and Benali, H.: 2010, A nonlinear identification method to study effective connectivity in functional MRI, *Medical Image Analysis* **14**(1), 30 – 38.

Bibliography

- Llinás, R., Ribary, U., Jeanmonod, D., Kronberg, E. and Mitra, P.: 1999, Thalamocortical dysrhythmia: a neurological and neuropsychiatric syndrome characterized by magnetoencephalography, *Proceedings of the National Academy of Sciences* **96**(26), 15222–15227.
- Londei, A., D'Ausilio, A., Basso, D., Sestieri, C., Gratta, C. D., Romani, G. and Belardinelli, M. O.: 2007, Brain network for passive word listening as evaluated with ICA and Granger causality, *Brain Research Bulletin* **72**(4-6), 284 – 292.
- Lopes da Silva, F.: 2004, Functional localization of brain sources using EEG and/or MEG data: volume conductor and source models, *Magnetic resonance imaging* **22**(10), 1533–1538.
- Lopes da Silva, S.: 1991, Neural mechanisms underlying brain waves: from neural membranes to networks., *Electroencephalography and Clinical Neurophysiology* **79**(2), 81.
- Lütkepohl, H.: 2005, *New introduction to multiple time series analysis*, Springer, Berlin.
- Lutovac, M. D., Tomic, D. V. and Evans, B.: 2001, *Filter Design for Signal Processing using MATLAB© and Mathematica©.*, Prentice Hall, New Jersey, USA.
- Mallat, S.: 1999, *A wavelet tour of signal processing*, Academic Press.
- Mallet, N., Pogosyan, A., Marton, L. F., Bolam, J. P., Brown, P. and Magill, P. J.: 2008, Parkinsonian beta oscillations in the external globus pallidus and their relationship with subthalamic nucleus activity, *Journal of Neuroscience* **28**(52), 14245–14258.
- Mann, H. and Whitney, D.: 1947, On a test of whether one of two random variables

Bibliography

- is stochastically larger than the other, *The Annals of Mathematical Statistics* **18**(1), 50–60.
- Marcellino, M.: 1999, Some consequences of temporal aggregation in empirical analysis, *Journal of Business & Economic Statistics* **17**(1), 129–136.
- Marinazzo, D., Pellicoro, M. and Stramaglia, S.: 2006, Nonlinear parametric model for Granger causality of time series, *Physical Review E (Statistical, Nonlinear, and Soft Matter Physics)* **73**(6), 066216.
- Marinazzo, D., Pellicoro, M. and Stramaglia, S.: 2008a, Kernel-Granger causality and the analysis of dynamical networks, *Physical Review E (Statistical, Nonlinear, and Soft Matter Physics)* **77**(5), 056215.
- Marinazzo, D., Pellicoro, M. and Stramaglia, S.: 2008b, Kernel method for nonlinear Granger causality, *Physical Review Letters* **100**(14), 144103.
- Marsden, J. F., Limousin-Dowsey, P., Ashby, P., Pollak, P. and Brown, P.: 2001, Subthalamic nucleus, sensorimotor cortex and muscle interrelationships in Parkinson's disease, *Brain* **124**(Pt 2), 378–88.
- Miller, R. G. J.: 1991, *Simultaneous Statistical Inference*, Springer-Verlag, New York.
- Millhorn, D., Bayliss, D., Erickson, J., Gallman, E., Szymeczek, C., Czyzyk-Krzeska, M. and Dean, J. B.: 1989, Cellular and molecular mechanisms of chemical synaptic transmission, *American Journal of Physiology (AJP): Lung Cellular and Molecular Physiology* **257**, L289–310.
- Misiti, M., Misiti, Y., Oppenheim, G. and Poggi, J.-M.: 2006, *Wavelet Toolbox – For Use with MATLAB*, The MathWorks, Natick.

Bibliography

- Mitra, P. and Pesaran, B.: 1999, Analysis of dynamic brain data, *Biophysical Journal* **76**, 691–708.
- Moriizumi, T., Nakamura, Y., Kitao, Y. and Kudo, M.: 1987, Ultrastructural analyses of afferent terminals in the subthalamic nucleus of the cat with a combined degeneration and horseradish peroxidase tracing method, *The Journal of Comparative Neurology* **265**(2), 159–74.
- Mosher, J. C., Leahy, R. M. and Lewis, P. S.: 1999, EEG and MEG: forward solutions for inverse methods, *IEEE Transactions on Biomedical Engineering* **46**(3), 245–59.
- Müller, U. K. and Elliott, G.: 2003, Tests for unit roots and the initial condition, *Econometrica* **71**(4), 1269–1286.
- Nalatore, H., Ding, M. and Rangarajan, G.: 2007, Mitigating the effects of measurement noise on Granger causality, *Physical Review E* **75**(3), 031123.
- Nalatore, H., Ding, M. and Rangarajan, G.: 2009, Denoising neural data with state-space smoothing: Method and application, *Journal of Neuroscience Methods* **179**, 131–141.
- Newbold, P.: 1978, Feedback induced by measurement errors, *International Economic Review* **19**(3), 787–781.
- Niedermeyer, E. and da Silva, F.: 2005, *Electroencephalography - Basic Principles, Clinical Applications and Related Fields*, Lippincott Williams & Wilkens, Philadelphia.
- Nunez, P. and Srinivasan, R.: 2006, *Electric fields of the brain: The neurophysics of EEG*, Oxford University Press, USA.

Bibliography

- Nyblom, J.: 1989, Testing the constancy of parameters over time, *Journal of the American Statistical Association* **84**, 223–230.
- Ospina, R. and Ferrari, S.: 2008, Inflated beta distributions, *Statistical Papers* -, -.
- Parks, T. and Burrus, C.: 1987, *Digital filter design*, Wiley-Interscience.
- Pascual-Marqui, R.: 1999, Review of methods for solving the EEG inverse problem, *International Journal of Bioelectromagnetism* **1**(1), 75–86.
- Paulsen, J. Tjøstheim, D.: 1985, On the estimation of residual variance and order in autoregressive time series, *Journal of the Royal Statistical Society. Series B (Methodological)* **47**(2), 216–228.
- Ploberger, W. and Krämer, W.: 1992, The CUSUM test with OLS residuals, *Econometrica* **60**, 271–285.
- Ploner, M., Schoffelen, J., Schnitzler, A. and Gross, J.: 2009, Functional integration within the human pain system as revealed by Granger causality, *Human Brain Mapping* **30**, 4025 – 4032.
- Plonsey, R.: 1963, Reciprocity applied to volume conductors and the ECG, *IEEE transactions on bio-medical engineering* **10**, 9.
- Priestley, M.: 1981, *Spectral Analysis and Time Series - Volume 1*, Academic Press.
- Quandt, R.: 1960, Tests of the hypothesis that a linear regression system obeys two separate regimes, *Journal of the American Statistical Association* **55**(290), 324–330.
- Quenouille, M.: 1957, *The Analysis of Multiple Time Series*, Griffin, London.
- Quenouille, M. H.: 1947, Approximate tests of correlation in time-series, *Journal of the Royal Statistical Society. Series B (Methodological)* **11**(1), 68–84.

Bibliography

- Reaz, M., Hussain, M. and Mohd-Yasin, F.: 2006, Techniques of EMG signal analysis: detection, processing, classification and applications, *Biological procedures online* **8**(1), 11–35.
- Reck, C., Florin, E., Wojtecki, L., Groiss, S., Voges, J., Sturm, V., Schnitzler, A. and Timmermann, L.: 2009, Differential distribution of coherence between beta-band subthalamic oscillations and forearm muscles in Parkinson’s disease during isometric contraction, *Clinical Neurophysiology* **120**(8), 1601–1609.
- Reck, C., Florin, E., Wojtecki, L., Krause, H., Groiss, S., Voges, J., Maarouf, M., Sturm, V., Schnitzler, A. and Timmermann, L.: 2009, Characterisation of tremor-associated local field potentials in the subthalamic nucleus in Parkinson’s disease, *European Journal of Neuroscience* **29**(3), 599–612.
- Reuveny, R. and Kang, H.: 1996, International trade, political conflict/cooperation, and Granger causality, *American Journal of Political Science* **40**(3), 943–970.
- Roebroek, A., Formisano, E. and Goebel, R.: 2005, Mapping directed influence over the brain using Granger causality and fMRI, *NeuroImage* **25**(1), 230–42.
- Rosanova, M., Casali, A., Bellina, V., Resta, F., Mariotti, M. and Massimini, M.: 2009, Natural frequencies of human corticothalamic circuits, *Journal of Neuroscience* **29**(24), 7679–7685.
- Rosenblum, G., Pikovsky, A. and Kurths, J.: 1997, Phase synchronization in driven and coupled chaotic oscillators, *IEEE Transactions on Circuits and Systems – I: Fundamental Theory and Applications* **44**(10), 874–881.
- Sameshima, K. and Baccala, L. A.: 1999, Using partial directed coherence to describe neuronal ensemble interactions, *Journal of Neuroscience Methods* **94**(1), 93–103.
- Sargent, T.: 1987, *Macroeconomic Theory*, 2nd edn, Academic Press, San Diego.

Bibliography

- Sarvas, J.: 1987, Basic mathematical and electromagnetic concepts of the biomagnetic inverse problem, *Physics in Medicine and Biology* **32**(1), 11–22.
- Sato, J. R., Amaro, E. J., Takahashi, D. Y., de Maria Felix, M., Brammer, M. J. and Morettin, P. A.: 2006, A method to produce evolving functional connectivity maps during the course of an fMRI experiment using wavelet-based time-varying Granger causality, *NeuroImage* **31**(1), 187 – 196.
- Scheinkman, J. A. and LeBaron, B.: 1989, Nonlinear dynamics and stock returns, *Journal of Business* **62**(3), 311–337.
- Schelter, B., Winterhalder, M., Eichler, M., Peifer, M., Hellwig, B., Guschlbauer, B., Lucking, C. H., Dahlhaus, R. and Timmer, J.: 2005, Testing for directed influences among neural signals using partial directed coherence, *Journal of Neuroscience Methods* **152**(1-2), 210–219.
- Schelter, B., Winterhalder, M., Hellwig, B., Guschlbauer, B., Lucking, C. H. and Timmer, J.: 2006, Direct or indirect? graphical models for neural oscillators, *Journal of Physiology-Paris* **99**(1), 37–46.
- Schelter, B., Winterhalder, M. and Timmer, J.: 2004, Detection of coupling directions in multivariate oscillatory systems, *in* S. Boccaletti, B. J. Gluckman, J. Kurths, L. Pecora, R. Meucci and O. Yordanov (eds), *8th Experimental chaos conference*, AIP Conference Proceedings.
- Schindler, K., Leung, H., Elger, C. E. and Lehnertz, K.: 2007, Assessing seizure dynamics by analysing the correlation structure of multichannel intracranial EEG, *Brain* **130**(1), 65–77.
- Schlögl, A. and Supp, G.: 2006, Analyzing event-related EEG data with multivariate

Bibliography

- autoregressive parameters, *in* Neuper and Klimesch (eds), *Progress in Brain Research*, Vol. 159, Elsevier, Amsterdam, pp. 135–147.
- Schnitzler, A. and Gross, J.: 2005, Normal and pathological oscillatory communication in the brain, *Nature Reviews Neuroscience* **6**(4), 285–96.
- Schnitzler, A., Münks, C., Butz, M., Timmermann, L. and Gross, J.: 2009, Synchronized brain network associated with essential tremor as revealed by magnetoencephalography., *Movement disorders: official journal of the Movement Disorder Society* **24**, 1629 – 1635.
- Schwarz, G.: 1978, Estimating the dimension of a model, *The annals of statistics* **6**(2), 461–464.
- Sederberg, P. B., Kahana, M. J., Howard, M. W., Donner, E. J. and Madsen, J. R.: 2003, Theta and Gamma Oscillations during Encoding Predict Subsequent Recall, *Journal of Neuroscience* **23**(34), 10809–10814.
- Sharott, A., Grosse, P., Kühn, A. A., Salih, F., Engel, A. K., Kupsch, A., Schneider, G. H., Krauss, J. K. and Brown, P.: 2008, Is the synchronization between pallidal and muscle activity in primary dystonia due to peripheral afference or a motor drive?, *Brain* **131**(Pt 2), 473–84.
- Shenoi, B.: 2006, *Introduction to digital signal processing and filter design*, Wiley-Interscience.
- Shibasaki, H.: 2008, Human brain mapping: hemodynamic response and electrophysiology, *Clinical Neurophysiology* **119**(4), 731–743.
- Shibasaki, H., Ikeda, A. and Nagamine, T.: 2007, Use of magnetoencephalography in the presurgical evaluation of epilepsy patients, *Clinical Neurophysiology* **118**(7), 1438–1448.

Bibliography

- Sims, C.: 1971, Discrete approximations to continuous time distributed lags in econometrics, *Econometrica* **39**(3), 545–563.
- Sims, C. A.: 1972, Money, income, and causality, *The American economic review* **62**(4), 540–552.
- Singer, W.: 1999, Neuronal synchrony: a versatile code for the definition of relations?, *Neuron* **24**(1), 49–65, 111–25.
- Smirnov, D., Barnikol, U., Barnikol, T., Bezruchko, B., Hauptmann, C., Bührle, C., Maarouf, M., Sturm, V. and Tass, P.: 2008, The generation of parkinsonian tremor as revealed by directional coupling analysis, *A letters journal exploring the frontiers of physics* **83**, 20003–p1– 20003–p6.
- Smith III, J.: 2007, *Introduction to digital filters*, W3K Publishing.
- Smithson, M. and Verkuilen, J.: 2006, A better lemon squeezer? Maximum-likelihood regression with beta-distributed dependent variables, *Psychological Methods* **11**(1), 54–71.
- Stasinopoulos, D. and Rigby, R.: 2007, Generalized additive models for location scale and shape (gamlss), *R Reference* **23**(7), –.
- Tenke, C., Schroeder, C., Arezzo, J. and Vaughan, H.: 1993, Interpretation of high-resolution current source density profiles: a simulation of sublaminal contributions to the visual evoked potential, *Experimental Brain Research* **94**(2), 183–192.
- Tesche, C. D. and Karhu, J.: 1997, Somatosensory evoked magnetic fields arising from sources in the human cerebellum, *Brain Research* **744**(1), 23 – 31.
- Tesche, C. and Karhu, J.: 2000, Theta oscillations index human hippocampal activation during a working memory task, *Proceedings of the National Academy of Sciences* **97**(2), 919–924.

Bibliography

- Timmermann, L., Florin, E. and Reck, C.: 2007, Pathological cerebral oscillatory activity in Parkinson's disease: a critical review on methods, data and hypotheses, *Expert Review of Medical Devices* **4**(5), 651–61.
- Timmermann, L., Gross, J., Dirks, M., Volkmann, J., Freund, H. J. and Schnitzler, A.: 2003, The cerebral oscillatory network of parkinsonian resting tremor, *Brain* **126**(Pt 1), 199–212.
- Tukey, J.: 1958, Bias and confidence in not quite large samples, *Annals of Mathematical Statistics* **29**(2), 614.
- Uddin, L., Clare Kelly, A., Biswal, B., Xavier Castellanos, F. and Milham, M.: 2009, Functional connectivity of default mode network components: correlation, anticorrelation, and causality, *Human Brain Mapping* **30**, 625–637.
- Upadhyay, J., Silver, A., Knaus, T. A., Lindgren, K. A., Ducros, M., Kim, D.-S. and Tager-Flusberg, H.: 2008, Effective and Structural Connectivity in the Human Auditory Cortex, *Journal of Neuroscience* **28**(13), 3341–3349.
- Varela, F., Lachaux, J., Rodriguez, E. and Martinerie, J.: 2001, The brainweb: phase synchronization and large-scale integration, *Nature Reviews Neuroscience* **2**(4), 229–239.
- Voges, J., Volkmann, J., Allert, N., Lehrke, R., Koulousakis, A., Freund, H. J. and Sturm, V.: 2002, Bilateral high-frequency stimulation in the subthalamic nucleus for the treatment of Parkinson disease: correlation of therapeutic effect with anatomical electrode position, *Journal of Neurosurgery* **96**(2), 269–79.
- Volkmann, J., Joliot, M., Mogilner, A., Ioannides, A. A., Lado, F., Fazzini, E., Ribary, U. and Llinas, R.: 1996, Central motor loop oscillations in parkinsonian resting tremor revealed by magnetoencephalography, *Neurology* **46**(5), 1359–70.

Bibliography

- von Ellenrieder, N., Muravchik, C., Wagner, M. and Nehorai, A.: 2009, Effect of head shape variations among individuals on the EEG/MEG forward and inverse problems, *IEEE Transactions on Biomedical Engineering* **56**(3), 587.
- Walnut, D.: 2004, *An introduction to wavelet analysis*, Birkhauser.
- Wang, S., Chen, Y., Ding, M., Feng, J., Stein, J., Aziz, T. and Liu, X.: 2007, Revealing the dynamic causal interdependence between neural and muscular signals in parkinsonian tremor, *Journal of the Franklin Institute* **344**(3-4), 180–195.
- Wang, X., Chen, Y. and Ding, M.: 2008, Estimating Granger causality after stimulus onset: A cautionary note, *NeuroImage* **41**(3), 767 – 776.
- Weaver, F. M., Follett, K., Stern, M., Hur, K., Harris, C., Marks, W. J., J., Rothlind, J., Sagher, O., Reda, D., Moy, C. S., Pahwa, R., Burchiel, K., Hogarth, P., Lai, E. C., Duda, J. E., Holloway, K., Samii, A., Horn, S., Bronstein, J., Stoner, G., Heemskerk, J. and Huang, G. D.: 2009, Bilateral deep brain stimulation vs best medical therapy for patients with advanced Parkinson disease: a randomized controlled trial, *Journal of the American Medical Association* **301**(1), 63–73.
- Wei, W.: 1982, The effects of systematic sampling and temporal aggregation on causality. a cautionary note, *Journal of the American Statistical Association* **77**(6745), 6316–319.
- Wendling, F., Ansari-Asl, K., Bartolomei, F. and Senhadji, L.: 2009, From EEG signals to brain connectivity: A model-based evaluation of interdependence measures, *Journal of Neuroscience Methods* **183**(1), 9–18.
- Wiener, N.: 1956, The theory of prediction, in E. F. Beckenbach (ed.), *Modern mathematics for the engineer*, McGraw-Hill, New York.

Bibliography

- Wilcoxon, F.: 1945, Individual comparisons by ranking methods, *Biometrics Bulletin* **1**(6), 80–83.
- Wilke, M., Lidzba, K. and Krägeloh-Mann, I.: 2009, Combined functional and causal connectivity analyses of language networks in children: A feasibility study, *Brain and Language* **108**(1), 22 – 29.
- Winterhalder, M., Schelter, B., Hesse, W., Schwab, K., Leistrütz, L., Klan, D., Bauer, R., Timmer, J. and Witte, H.: 2005, Comparison of linear signal processing techniques to infer directed interactions in multivariate neural systems, *Signal Processing* **85**(11), 2137–2160.
- Wooldridge, J. M.: 2009, *Introductory econometrics: a modern approach*, 4th edn, South-Western Cengage Learning, Mason, Ohio.
- Zhong, Y., Wang, H., Lu, G., Zhang, Z., Jiao, Q. and Liu, Y.: 2009, Detecting functional connectivity in fMRI using PCA and regression analysis, *Brain Topography* **22**(2), 134–144.
- Zhou, Z., Chen, Y., Ding, M., Wright, P., Lu, Z. and Liu, Y.: 2008, Analyzing brain networks with PCA and conditional Granger causality, *Human Brain Mapping* **30**, 2197–2206.
- Zhou, Z., Ding, M., Chen, Y., Wright, P., Lu, Z. and Liu, Y.: 2009, Detecting directional influence in fMRI connectivity analysis using PCA based Granger causality, *Brain Research* **1289**, 22–9.
- Zimmerman, J. B. and Thiene, P. and Harding, J. T.: 1970, Design and operation of stable rf-biased superconducting point-contact quantum devices, and a note on the properties of perfectly clean metal contacts, *Journal of Applied Physics* **41**(41), 1572–1580.

Appendix **A**

Results for all Causality Measures

Table A.1: Results of the different filter types for LOOM with Kus-model
 Abbreviations: std - standard deviation; pn - phase neutral filter; npn - non-phase neutral filter; fo - filter order; butter - Butterworth filter; ellip - elliptic filter; lp - low-pass filter; hp - high-pass filter.

	sPDCtrue		sPDCfalse		PDCtrue		PDCfalse		DTFtrue		DTFfalse		dDTFtrue		dDTFfalse		Htrue		Hfalse	
	mean	std	mean	std	mean	std	mean	std	mean	std	mean	std	mean	std	mean	std	mean	std	mean	std
no filter	.01	0.05	0.01	0.02	0.00	0.00	0.07	0.07	0.00	0.00	0.18	0.08	0.74	0.24	0.10	0.03	0.75	0.13	0.10	0.02
butter_npn_1Hz_hp_fo6	0.00	0.00	0.00	0.01	0.00	0.00	0.07	0.04	0.00	0.00	0.21	0.07	0.09	0.11	0.03	0.02	0.45	0.09	0.06	0.01
cheby1_npn_1Hz_hp_fo6	0.00	0.00	0.00	0.01	0.00	0.00	0.07	0.04	0.00	0.00	0.23	0.09	0.01	0.04	0.02	0.02	0.59	0.05	0.08	0.01
cheby2_npn_1Hz_hp_fo6	0.00	0.00	0.00	0.01	0.00	0.00	0.07	0.04	0.00	0.00	0.22	0.08	0.16	0.14	0.04	0.03	0.45	0.09	0.06	0.01
ellip_npn_1Hz_hp_fo6	0.01	0.03	0.01	0.02	0.00	0.00	0.20	0.08	0.00	0.00	0.34	0.10	0.27	0.18	0.07	0.04	0.58	0.14	0.09	0.03
butter_pn_1Hz_hp_fo3	0.07	0.11	0.11	0.05	0.00	0.01	0.36	0.08	0.00	0.00	0.53	0.09	0.85	0.15	0.18	0.03	0.59	0.17	0.15	0.03
cheby1_pn_1Hz_hp_fo3	0.02	0.06	0.15	0.04	0.00	0.01	0.42	0.08	0.00	0.00	0.62	0.09	0.77	0.20	0.15	0.04	0.42	0.15	0.14	0.04
cheby2_pn_1Hz_hp_fo3	0.07	0.11	0.09	0.04	0.00	0.02	0.32	0.06	0.00	0.00	0.47	0.08	0.34	0.14	0.15	0.04	0.42	0.17	0.14	0.02
ellip_pn_1Hz_hp_fo3	0.01	0.03	0.14	0.04	0.00	0.00	0.42	0.07	0.00	0.00	0.61	0.09	0.48	0.23	0.14	0.04	0.40	0.15	0.14	0.03
butter_npn_80Hz_hp_fo8	0.28	0.21	0.12	0.06	0.01	0.03	0.49	0.11	0.00	0.01	0.57	0.09	0.17	0.17	0.08	0.03	0.82	0.19	0.19	0.05
cheby1_npn_80Hz_hp_fo8	0.83	0.19	0.20	0.08	0.33	0.24	0.42	0.16	0.02	0.07	0.54	0.10	0.50	0.22	0.10	0.03	0.89	0.14	0.15	0.03
cheby2_npn_80_hp_fo8	0.54	0.23	0.12	0.05	0.05	0.09	0.36	0.09	0.00	0.01	0.48	0.10	0.40	0.18	0.08	0.03	0.70	0.18	0.13	0.04
ellip_npn_80Hz_lp_fo8	0.09	0.15	0.02	0.03	0.00	0.00	0.20	0.07	0.00	0.00	0.29	0.10	0.22	0.21	0.04	0.03	0.49	0.14	0.09	0.03
butter_pn_80Hz_lp_fo4	0.25	0.22	0.23	0.15	0.03	0.08	0.59	0.13	0.01	0.03	0.61	0.09	0.23	0.20	0.08	0.04	0.82	0.20	0.19	0.05
cheby1_pn_80Hz_lp_fo4	0.50	0.23	0.16	0.08	0.08	0.13	0.44	0.13	0.00	0.03	0.58	0.09	0.39	0.21	0.10	0.03	0.66	0.18	0.14	0.04
cheby2_pn_80Hz_lp_fo4	0.46	0.22	0.35	0.16	0.12	0.15	0.60	0.17	0.02	0.07	0.58	0.12	0.71	0.25	0.11	0.03	0.88	0.18	0.15	0.04
ellip_pn_80Hz_lp_fo4	0.23	0.20	0.09	0.04	0.00	0.01	0.38	0.09	0.00	0.01	0.56	0.10	0.32	0.24	0.08	0.04	0.82	0.16	0.13	0.03
butter_npn_160Hz_lp_fo8	0.00	0.02	0.03	0.03	0.00	0.00	0.29	0.07	0.00	0.00	0.47	0.08	0.01	0.04	0.06	0.03	0.31	0.17	0.13	0.03
cheby1_npn_160Hz_lp_fo8	0.00	0.02	0.07	0.04	0.00	0.00	0.38	0.07	0.00	0.00	0.54	0.09	0.04	0.08	0.08	0.03	0.41	0.19	0.18	0.05
cheby2_npn_160Hz_lp_fo8	0.00	0.00	0.01	0.01	0.00	0.00	0.20	0.06	0.00	0.00	0.28	0.09	0.00	0.02	0.03	0.02	0.25	0.17	0.06	0.03
ellip_npn_160Hz_lp_fo8	0.00	0.00	0.01	0.01	0.00	0.00	0.18	0.06	0.00	0.00	0.32	0.08	0.01	0.06	0.03	0.03	0.32	0.15	0.05	0.02
butter_pn_160Hz_lp_fo4	0.00	0.01	0.03	0.02	0.00	0.00	0.29	0.06	0.00	0.00	0.47	0.08	0.01	0.04	0.06	0.03	0.28	0.17	0.13	0.03
cheby1_pn_160Hz_lp_fo4	0.00	0.00	0.12	0.07	0.00	0.00	0.38	0.07	0.00	0.00	0.57	0.10	0.01	0.04	0.12	0.06	0.24	0.22	0.18	0.09
cheby2_pn_160Hz_lp_fo4	0.02	0.05	0.02	0.02	0.00	0.00	0.27	0.10	0.00	0.00	0.34	0.10	0.10	0.16	0.04	0.03	0.57	0.24	0.13	0.04
ellip_pn_160Hz_lp_fo4	0.00	0.00	0.01	0.02	0.00	0.00	0.18	0.06	0.00	0.00	0.32	0.08	0.01	0.05	0.03	0.03	0.31	0.16	0.05	0.02

Table A.2: Results of the different filter types for random permutation with Kus-model

Abbreviations: std - standard deviation; pn - phase neutral filter; npn - non-phase neutral filter; fo - filter order; butter - Butterworth filter; ellip - elliptic filter; lp - low-pass filter; hp - high-pass filter.

	sPDC ^{true}		sPDC ^{false}		PDC ^{true}		PDC ^{false}		DTF ^{true}		DTF ^{false}		dDTF ^{true}		dDTF ^{false}		H ^{true}		H ^{false}	
	mean	std	mean	std	mean	std	mean	std	mean	std	mean	std	mean	std	mean	std	mean	std	mean	std
no filter	0.00	0.02	0.00	0.00	0.00	0.02	0.00	0.00	0.58	0.07	0.16	0.01	0.57	0.08	0.08	0.01	0.60	0.00	0.16	0.00
butter_npn_1Hz_hp_fo6	0.00	0.00	0.08	0.04	0.00	0.00	0.08	0.04	0.00	0.00	0.21	0.05	0.00	0.01	0.14	0.03	0.00	0.00	0.70	0.11
cheby1_npn_1Hz_hp_fo6	0.00	0.00	0.10	0.03	0.00	0.00	0.10	0.03	0.00	0.00	0.27	0.03	0.00	0.00	0.20	0.04	0.00	0.00	0.84	0.09
cheby2_npn_1Hz_hp_fo6	0.00	0.00	0.04	0.03	0.00	0.00	0.04	0.03	0.00	0.00	0.12	0.03	0.00	0.00	0.09	0.03	0.00	0.00	0.54	0.12
ellip_npn_1Hz_hp_fo6	0.00	0.03	0.10	0.05	0.00	0.03	0.10	0.05	0.00	0.00	0.19	0.05	0.09	0.12	0.22	0.07	0.00	0.00	0.69	0.09
butter_pn_1Hz_hp_fo3	0.43	0.07	0.14	0.04	0.43	0.07	0.14	0.04	0.40	0.00	0.24	0.03	0.52	0.15	0.22	0.05	0.18	0.17	0.61	0.08
cheby1_pn_1Hz_hp_fo3	0.42	0.06	0.18	0.05	0.42	0.06	0.18	0.05	0.40	0.00	0.27	0.04	0.38	0.14	0.28	0.06	0.00	0.00	0.68	0.00
cheby2_pn_1Hz_hp_fo3	0.47	0.09	0.08	0.03	0.47	0.09	0.08	0.03	0.41	0.04	0.11	0.03	0.80	0.15	0.16	0.02	0.40	0.00	0.27	0.04
ellip_pn_1Hz_hp_fo3	0.41	0.05	0.15	0.04	0.41	0.05	0.15	0.04	0.40	0.00	0.25	0.03	0.42	0.14	0.24	0.06	0.00	0.01	0.63	0.07
butter_npn_80Hz_lp_fo8	0.02	0.08	0.16	0.02	0.02	0.08	0.16	0.02	0.00	0.00	0.22	0.05	0.00	0.01	0.17	0.04	0.00	0.00	1.00	0.00
cheby1_npn_80Hz_lp_fo8	0.03	0.08	0.16	0.02	0.03	0.08	0.16	0.02	0.00	0.02	0.27	0.06	0.00	0.00	0.25	0.05	0.00	0.00	1.00	0.00
cheby2_npn_80_lp_fo8	0.01	0.05	0.14	0.03	0.01	0.05	0.14	0.03	0.00	0.00	0.21	0.05	0.00	0.00	0.17	0.04	0.00	0.00	0.99	0.02
ellip_npn_80Hz_lp_fo8	0.00	0.01	0.12	0.03	0.00	0.01	0.12	0.03	0.00	0.00	0.18	0.03	0.00	0.00	0.17	0.04	0.00	0.00	0.99	0.02
butter_pn_80Hz_lp_fo4	0.01	0.05	0.16	0.02	0.01	0.05	0.16	0.02	0.00	0.00	0.23	0.08	0.00	0.00	0.18	0.10	0.00	0.00	0.99	0.00
cheby1_pn_80Hz_lp_fo4	0.00	0.00	0.23	0.04	0.00	0.00	0.23	0.04	0.00	0.00	0.47	0.09	0.00	0.00	0.55	0.09	0.00	0.00	1.00	0.00
cheby2_pn_80Hz_lp_fo4	0.02	0.06	0.19	0.03	0.02	0.06	0.19	0.03	0.00	0.00	0.35	0.08	0.00	0.00	0.36	0.08	0.00	0.00	1.00	0.00
ellip_pn_80Hz_lp_fo4	0.00	0.03	0.28	0.04	0.00	0.03	0.28	0.04	0.00	0.00	0.59	0.08	0.00	0.00	0.57	0.09	0.00	0.00	1.00	0.00
butter_npn_160Hz_lp_fo8	0.00	0.01	0.08	0.04	0.00	0.01	0.08	0.04	0.00	0.00	0.24	0.07	0.00	0.00	0.20	0.04	0.00	0.00	1.00	0.00
cheby1_npn_160Hz_lp_fo8	0.00	0.00	0.11	0.05	0.00	0.00	0.11	0.05	0.00	0.00	0.28	0.06	0.00	0.00	0.26	0.05	0.00	0.00	1.00	0.00
cheby2_npn_160Hz_lp_fo8	0.00	0.00	0.07	0.04	0.00	0.00	0.07	0.04	0.00	0.00	0.15	0.04	0.00	0.00	0.18	0.04	0.00	0.00	0.98	0.04
ellip_npn_160Hz_lp_fo8	0.00	0.00	0.04	0.03	0.00	0.00	0.04	0.03	0.00	0.00	0.13	0.04	0.00	0.00	0.18	0.04	0.00	0.00	0.99	0.03
butter_pn_160Hz_lp_fo4	0.00	0.01	0.09	0.04	0.00	0.01	0.09	0.04	0.00	0.00	0.29	0.06	0.00	0.00	0.27	0.05	0.00	0.00	1.00	0.00
cheby1_pn_160Hz_lp_fo4	0.00	0.00	0.11	0.04	0.00	0.00	0.11	0.04	0.00	0.00	0.33	0.06	0.00	0.00	0.33	0.06	0.00	0.00	1.00	0.00
cheby2_pn_160Hz_lp_fo4	0.00	0.00	0.11	0.04	0.00	0.00	0.11	0.04	0.00	0.00	0.18	0.04	0.00	0.00	0.23	0.04	0.00	0.00	1.00	0.00
ellip_pn_160Hz_lp_fo4	0.00	0.00	0.05	0.04	0.00	0.00	0.05	0.04	0.00	0.00	0.16	0.05	0.00	0.00	0.20	0.04	0.00	0.00	1.00	0.00

Table A.3: Results of the different filter types for LOOM with Schelter-model
 Abbreviations: std - standard deviation; pn - phase neutral filter; npn - non-phase neutral filter; fo - filter order; butter - Butterworth filter; ellip - elliptic filter; lp - low-pass filter; hp - high-pass filter.

	sPDCtrue		sPDCfalse		PDCtrue		PDCfalse		DTFtrue		DTFfalse		DDTftrue		DDTffalse		Htrue		Hfalse	
	mean	std	mean	std	mean	std	mean	std	mean	std	mean	std	mean	std	mean	std	mean	std	mean	std
no filter	0.01	0.03	0.00	0.01	0.00	0.00	0.13	0.10	0.00	0.00	0.69	0.10	0.21	0.14	0.33	0.08	0.18	0.07	0.24	0.09
butter_npn_1Hz_hp_fo6	0.01	0.03	0.00	0.01	0.00	0.00	0.13	0.09	0.00	0.00	0.69	0.11	0.22	0.14	0.32	0.08	0.17	0.06	0.25	0.09
cheby1_npn_1Hz_hp_fo6	0.01	0.04	0.00	0.01	0.00	0.00	0.13	0.10	0.00	0.00	0.68	0.11	0.21	0.14	0.32	0.09	0.19	0.08	0.23	0.10
cheby2_npn_1Hz_hp_fo6	0.01	0.03	0.00	0.01	0.00	0.00	0.13	0.09	0.00	0.00	0.69	0.11	0.22	0.14	0.33	0.09	0.17	0.07	0.25	0.09
ellip_npn_1Hz_hp_fo6	0.01	0.03	0.00	0.01	0.00	0.00	0.14	0.10	0.00	0.00	0.68	0.12	0.21	0.15	0.32	0.08	0.19	0.07	0.24	0.10
butter_pn_1Hz_hp_fo3	0.05	0.08	0.04	0.06	0.00	0.01	0.34	0.16	0.00	0.01	0.75	0.14	0.31	0.16	0.28	0.10	0.37	0.14	0.16	0.09
cheby1_pn_1Hz_hp_fo3	0.04	0.07	0.11	0.10	0.00	0.01	0.48	0.16	0.00	0.00	0.82	0.13	0.29	0.16	0.33	0.12	0.29	0.12	0.23	0.10
cheby2_pn_1Hz_hp_fo3	0.03	0.06	0.00	0.01	0.00	0.01	0.17	0.11	0.00	0.00	0.66	0.12	0.31	0.16	0.27	0.09	0.21	0.09	0.21	0.09
ellip_pn_1Hz_hp_fo3	0.11	0.12	0.02	0.04	0.00	0.01	0.39	0.14	0.00	0.00	0.78	0.13	0.62	0.17	0.11	0.08	0.39	0.16	0.12	0.08
butter_npn_80Hz_lp_fo8	0.04	0.07	0.02	0.04	0.00	0.00	0.39	0.13	0.00	0.00	0.81	0.12	0.41	0.17	0.16	0.09	0.25	0.14	0.22	0.10
cheby1_npn_80_lp_fo8	0.05	0.08	0.02	0.04	0.00	0.01	0.36	0.13	0.00	0.01	0.72	0.13	0.44	0.17	0.16	0.10	0.24	0.14	0.13	0.08
cheby2_npn_80_lp_fo8	0.05	0.08	0.01	0.03	0.00	0.00	0.30	0.13	0.00	0.00	0.69	0.13	0.46	0.17	0.18	0.10	0.19	0.12	0.15	0.08
ellip_npn_80Hz_lp_fo8	0.11	0.11	0.02	0.04	0.00	0.01	0.39	0.14	0.00	0.00	0.78	0.13	0.62	0.17	0.10	0.08	0.41	0.14	0.12	0.08
butter_pn_80Hz_lp_fo4	0.27	0.15	0.03	0.05	0.01	0.03	0.42	0.15	0.00	0.01	0.78	0.13	0.72	0.16	0.08	0.08	0.55	0.19	0.10	0.08
cheby1_pn_80Hz_lp_fo4	0.49	0.18	0.07	0.08	0.05	0.08	0.48	0.16	0.00	0.01	0.67	0.15	0.86	0.13	0.05	0.06	0.79	0.17	0.05	0.06
cheby2_pn_80Hz_lp_fo4	0.20	0.14	0.04	0.05	0.00	0.02	0.43	0.15	0.00	0.01	0.71	0.15	0.63	0.18	0.09	0.08	0.51	0.18	0.11	0.09
ellip_pn_80Hz_lp_fo4	0.07	0.04	0.03	0.01	0.00	0.00	0.12	0.29	0.00	0.00	0.12	0.74	0.15	0.40	0.10	0.20	0.13	0.23	0.10	0.22
butter_npn_160Hz_lp_fo8	0.04	0.07	0.02	0.04	0.00	0.00	0.39	0.14	0.00	0.00	0.80	0.12	0.42	0.17	0.17	0.10	0.24	0.14	0.23	0.10
cheby1_npn_160Hz_lp_fo8	0.03	0.06	0.01	0.02	0.00	0.00	0.22	0.12	0.00	0.00	0.70	0.11	0.35	0.16	0.24	0.10	0.24	0.12	0.23	0.11
cheby2_npn_160Hz_lp_fo8	0.03	0.06	0.01	0.02	0.00	0.00	0.20	0.11	0.00	0.00	0.65	0.13	0.28	0.16	0.22	0.09	0.24	0.10	0.16	0.09
ellip_npn_160Hz_lp_fo8	0.02	0.05	0.00	0.02	0.00	0.00	0.19	0.11	0.00	0.00	0.70	0.10	0.34	0.17	0.27	0.09	0.19	0.12	0.26	0.10
butter_pn_160Hz_lp_fo4	0.33	0.14	0.04	0.06	0.01	0.04	0.43	0.14	0.00	0.02	0.88	0.12	0.63	0.17	0.13	0.09	0.63	0.18	0.09	0.08
cheby1_pn_160Hz_lp_fo4	0.04	0.08	0.01	0.02	0.00	0.00	0.28	0.12	0.00	0.00	0.64	0.13	0.44	0.17	0.14	0.09	0.32	0.13	0.13	0.08
cheby2_pn_160Hz_lp_fo4	0.04	0.07	0.01	0.03	0.00	0.00	0.28	0.13	0.00	0.00	0.71	0.12	0.35	0.17	0.24	0.10	0.28	0.13	0.24	0.09
ellip_pn_160Hz_lp_fo4	0.04	0.07	0.01	0.03	0.00	0.00	0.28	0.13	0.00	0.00	0.71	0.12	0.35	0.17	0.24	0.10	0.28	0.13	0.24	0.09

Table A.4: Results of the different filter types for random permutation with Scheluter-model

Abbreviations: std - standard deviation; pn - phase neutral filter; npn - non-phase neutral filter; fo - filter order; butter - Butterworth filter; ellip - elliptic filter; lp - low-pass filter; hp - high-pass filter.

	sPDC ^{true}		sPDC ^{false}		PDC ^{true}		PDC ^{false}		DTF ^{true}		DTF ^{false}		dDTF ^{true}		dDTF ^{false}		H ^{true}		H ^{false}	
	mean	std	mean	std	mean	std	mean	std	mean	std	mean	std	mean	std	mean	std	mean	std	mean	std
no filter	0.01	0.04	0.01	0.03	0.01	0.04	0.01	0.03	0.01	0.04	0.40	0.07	0.01	0.03	0.41	0.08	0.00	0.01	0.69	0.11
butter_npn_1Hz_hp_fo6	0.01	0.03	0.01	0.02	0.01	0.03	0.01	0.02	0.01	0.04	0.39	0.08	0.01	0.03	0.41	0.08	0.00	0.01	0.68	0.12
cheby1_npn_1Hz_hp_fo6	0.01	0.03	0.01	0.03	0.01	0.03	0.01	0.03	0.01	0.04	0.42	0.08	0.01	0.03	0.42	0.08	0.00	0.00	0.71	0.11
cheby2_npn_1Hz_hp_fo6	0.01	0.04	0.01	0.03	0.01	0.04	0.01	0.03	0.01	0.04	0.39	0.07	0.01	0.03	0.42	0.08	0.00	0.01	0.69	0.11
ellip_npn_1Hz_hp_fo6	0.01	0.03	0.01	0.03	0.01	0.03	0.01	0.03	0.01	0.04	0.41	0.08	0.01	0.03	0.43	0.09	0.00	0.01	0.71	0.11
butter_pn_1Hz_hp_fo3	0.07	0.09	0.26	0.12	0.07	0.09	0.26	0.12	0.05	0.08	0.51	0.14	0.07	0.11	0.37	0.16	0.01	0.04	0.89	0.10
cheby1_pn_1Hz_hp_fo3	0.05	0.08	0.28	0.12	0.05	0.08	0.28	0.12	0.04	0.07	0.54	0.15	0.04	0.07	0.63	0.15	0.01	0.04	0.89	0.11
cheby2_pn_1Hz_hp_fo3	0.03	0.06	0.12	0.10	0.03	0.06	0.12	0.10	0.02	0.05	0.41	0.12	0.02	0.06	0.47	0.13	0.00	0.02	0.77	0.13
ellip_pn_1Hz_hp_fo3	0.05	0.08	0.26	0.13	0.05	0.08	0.26	0.13	0.04	0.07	0.52	0.15	0.05	0.08	0.58	0.16	0.01	0.05	0.86	0.11
butter_npn_80Hz_lp_fo8	0.00	0.00	0.23	0.11	0.00	0.00	0.23	0.11	0.00	0.01	0.67	0.14	0.00	0.01	0.62	0.10	0.00	0.00	1.00	0.00
cheby1_npn_80Hz_lp_fo8	0.00	0.00	0.39	0.11	0.00	0.00	0.39	0.11	0.00	0.00	0.79	0.12	0.00	0.01	0.77	0.12	0.00	0.00	1.00	0.00
cheby2_npn_80_lp_fo8	0.00	0.02	0.14	0.09	0.00	0.02	0.14	0.09	0.00	0.00	0.59	0.13	0.00	0.02	0.55	0.09	0.00	0.00	1.00	0.00
ellip_npn_80Hz_lp_fo8	0.00	0.01	0.09	0.08	0.00	0.01	0.09	0.08	0.00	0.01	0.50	0.13	0.00	0.01	0.54	0.09	0.00	0.00	1.00	0.00
butter_pn_80Hz_lp_fo4	0.00	0.01	0.24	0.10	0.00	0.01	0.24	0.10	0.00	0.00	0.68	0.14	0.00	0.01	0.63	0.10	0.00	0.00	1.00	0.00
cheby1_pn_80Hz_lp_fo4	0.05	0.08	0.28	0.12	0.05	0.08	0.28	0.12	0.04	0.07	0.54	0.15	0.04	0.07	0.63	0.15	0.01	0.04	0.89	0.11
cheby2_pn_80Hz_lp_fo4	0.00	0.01	0.36	0.13	0.00	0.01	0.36	0.13	0.00	0.00	0.75	0.14	0.00	0.01	0.71	0.13	0.00	0.00	1.00	0.00
ellip_pn_80Hz_lp_fo4	0.00	0.01	0.33	0.12	0.00	0.01	0.33	0.12	0.00	0.00	0.75	0.14	0.00	0.01	0.69	0.12	0.00	0.00	1.00	0.00
butter_npn_160Hz_lp_fo8	0.00	0.02	0.09	0.08	0.00	0.02	0.09	0.08	0.00	0.02	0.58	0.11	0.00	0.02	0.54	0.07	0.00	0.00	1.00	0.00
cheby1_npn_160Hz_lp_fo8	0.00	0.00	0.15	0.10	0.00	0.00	0.15	0.10	0.00	0.01	0.66	0.12	0.00	0.01	0.57	0.09	0.00	0.00	1.00	0.00
cheby2_npn_160Hz_lp_fo8	0.01	0.03	0.03	0.05	0.01	0.03	0.03	0.05	0.01	0.04	0.46	0.10	0.02	0.05	0.47	0.08	0.00	0.00	1.00	0.00
ellip_npn_160Hz_lp_fo8	0.02	0.05	0.01	0.03	0.02	0.05	0.01	0.03	0.03	0.05	0.36	0.07	0.01	0.03	0.39	0.09	0.00	0.00	1.00	0.00
butter_pn_160Hz_lp_fo4	0.00	0.02	0.09	0.07	0.00	0.02	0.09	0.07	0.00	0.02	0.57	0.12	0.00	0.01	0.54	0.08	0.00	0.00	1.00	0.00
cheby1_pn_160Hz_lp_fo4	0.00	0.02	0.15	0.10	0.00	0.02	0.15	0.10	0.00	0.01	0.66	0.12	0.00	0.01	0.59	0.09	0.00	0.00	1.00	0.00
cheby2_pn_160Hz_lp_fo4	0.01	0.03	0.06	0.07	0.01	0.03	0.06	0.07	0.00	0.02	0.46	0.11	0.00	0.02	0.49	0.08	0.00	0.00	1.00	0.00
ellip_pn_160Hz_lp_fo4	0.01	0.04	0.06	0.07	0.01	0.04	0.06	0.07	0.01	0.04	0.41	0.08	0.00	0.02	0.47	0.08	0.00	0.00	1.00	0.00

Table A.5: Variation of filter order with LOOM and Kus-model
Abbreviations: std - standard deviation; pn - phase neutral filter; npn - non-phase neutral filter; fo - filter order; butter - Butterworth filter; ellip - elliptic filter; lp - low-pass filter; hp - high-pass filter.

	sPDCtrue		sPDCfalse		PDCtrue		PDCfalse		DTFtrue		DTFfalse		dDTFtrue		dDTFfalse		Htrue		Hfalse	
	mean	std	mean	std	mean	std	mean	std	mean	std	mean	std	mean	std	mean	std	mean	std	mean	std
butter_npn_80Hz_lp_fo2	0.02	0.07	0.01	0.02	0.00	0.00	0.12	0.05	0.00	0.00	0.25	0.08	0.02	0.06	0.02	0.02	0.09	0.13	0.08	0.03
butter_npn_80Hz_lp_fo3	0.04	0.09	0.01	0.02	0.00	0.00	0.16	0.06	0.00	0.00	0.29	0.09	0.06	0.10	0.03	0.02	0.29	0.22	0.07	0.03
butter_npn_80Hz_lp_fo4	0.07	0.12	0.02	0.03	0.00	0.00	0.22	0.07	0.00	0.00	0.36	0.09	0.11	0.13	0.04	0.03	0.48	0.23	0.10	0.03
butter_npn_80Hz_lp_fo5	0.15	0.18	0.04	0.04	0.00	0.00	0.27	0.08	0.00	0.00	0.42	0.09	0.14	0.14	0.05	0.03	0.58	0.22	0.12	0.04
butter_npn_80Hz_lp_fo6	0.24	0.22	0.06	0.04	0.00	0.01	0.31	0.08	0.00	0.00	0.45	0.09	0.12	0.14	0.05	0.03	0.65	0.22	0.14	0.04
butter_npn_80Hz_lp_fo7	0.28	0.23	0.08	0.05	0.00	0.01	0.36	0.11	0.00	0.00	0.52	0.10	0.13	0.17	0.06	0.03	0.78	0.22	0.17	0.04
butter_npn_80Hz_lp_fo8	0.28	0.21	0.12	0.06	0.01	0.03	0.49	0.11	0.00	0.01	0.57	0.09	0.17	0.17	0.08	0.03	0.82	0.19	0.19	0.05
butter_pn_80Hz_lp_fo2	0.02	0.08	0.01	0.02	0.00	0.00	0.12	0.05	0.00	0.00	0.25	0.08	0.02	0.07	0.02	0.02	0.08	0.12	0.08	0.03
butter_pn_80Hz_lp_fo3	0.13	0.16	0.04	0.04	0.00	0.01	0.33	0.08	0.00	0.00	0.46	0.09	0.15	0.14	0.05	0.03	0.64	0.23	0.14	0.04
butter_pn_80Hz_lp_fo4	0.25	0.22	0.23	0.15	0.03	0.08	0.59	0.13	0.01	0.03	0.61	0.09	0.23	0.20	0.08	0.04	0.82	0.20	0.19	0.05
butter_pn_80Hz_lp_fo5	0.43	0.23	0.31	0.16	0.05	0.10	0.61	0.15	0.00	0.03	0.61	0.09	0.36	0.20	0.36	0.04	0.71	0.16	0.18	0.04
butter_pn_80Hz_lp_fo6	0.45	0.23	0.46	0.16	0.08	0.13	0.72	0.14	0.01	0.05	0.65	0.09	0.47	0.21	0.11	0.04	0.81	0.15	0.16	0.04
butter_pn_80Hz_lp_fo7	0.48	0.24	0.49	0.16	0.10	0.15	0.76	0.12	0.02	0.07	0.66	0.10	0.47	0.21	0.10	0.03	0.90	0.15	0.15	0.03
butter_pn_80Hz_lp_fo8	0.48	0.26	0.51	0.17	0.11	0.15	0.77	0.13	0.04	0.10	0.63	0.11	0.51	0.24	0.51	0.04	0.97	0.08	0.14	0.02
ellip_npn_80Hz_lp_fo2	0.00	0.02	0.01	0.01	0.00	0.00	0.12	0.06	0.00	0.00	0.22	0.08	0.04	0.10	0.02	0.02	0.28	0.18	0.04	0.02
ellip_npn_80Hz_lp_fo3	0.24	0.21	0.05	0.04	0.00	0.00	0.19	0.07	0.00	0.00	0.32	0.09	0.19	0.16	0.04	0.03	0.60	0.21	0.09	0.03
ellip_npn_80Hz_lp_fo4	0.07	0.13	0.02	0.02	0.00	0.00	0.17	0.06	0.00	0.00	0.30	0.10	0.16	0.18	0.04	0.03	0.43	0.18	0.08	0.03
ellip_npn_80Hz_lp_fo5	0.34	0.25	0.07	0.05	0.00	0.00	0.28	0.08	0.00	0.00	0.41	0.09	0.17	0.17	0.04	0.03	0.67	0.20	0.10	0.03
ellip_npn_80Hz_lp_fo6	0.08	0.13	0.02	0.03	0.00	0.00	0.20	0.08	0.00	0.00	0.29	0.10	0.23	0.20	0.04	0.03	0.48	0.14	0.09	0.03
ellip_npn_80Hz_lp_fo7	0.32	0.25	0.07	0.05	0.00	0.02	0.30	0.08	0.00	0.00	0.43	0.10	0.18	0.16	0.05	0.03	0.68	0.21	0.10	0.03
ellip_npn_80Hz_lp_fo8	0.09	0.15	0.02	0.03	0.00	0.00	0.20	0.07	0.00	0.00	0.29	0.10	0.22	0.21	0.04	0.03	0.49	0.14	0.09	0.03
ellip_pn_80Hz_lp_fo2	0.00	0.03	0.01	0.01	0.00	0.00	0.18	0.07	0.00	0.00	0.35	0.09	0.09	0.12	0.03	0.02	0.22	0.20	0.09	0.04
ellip_pn_80Hz_lp_fo3	0.39	0.22	0.12	0.06	0.02	0.07	0.44	0.17	0.00	0.01	0.48	0.13	0.25	0.19	0.07	0.03	0.80	0.23	0.16	0.05
ellip_pn_80Hz_lp_fo4	0.23	0.20	0.09	0.04	0.00	0.01	0.38	0.09	0.00	0.01	0.56	0.10	0.32	0.24	0.08	0.04	0.82	0.16	0.13	0.03
ellip_pn_80Hz_lp_fo5	0.46	0.21	0.14	0.05	0.03	0.08	0.50	0.11	0.00	0.02	0.49	0.10	0.33	0.21	0.07	0.03	0.95	0.11	0.17	0.04
ellip_pn_80Hz_lp_fo6	0.22	0.19	0.10	0.05	0.00	0.02	0.41	0.09	0.00	0.00	0.58	0.10	0.27	0.20	0.08	0.04	0.84	0.15	0.13	0.03
ellip_pn_80Hz_lp_fo7	0.48	0.21	0.14	0.06	0.03	0.07	0.50	0.11	0.00	0.01	0.49	0.10	0.35	0.21	0.08	0.03	0.93	0.11	0.17	0.04
ellip_pn_80Hz_lp_fo8	0.23	0.20	0.10	0.05	0.00	0.01	0.40	0.09	0.00	0.00	0.58	0.10	0.27	0.22	0.09	0.04	0.84	0.15	0.14	0.03

Table A.6: Increase in low-pass filters with LOOM and Kus-model:

Abbreviations: std - standard deviation; pn - phase neutral filter; npn - non-phase neutral filter; fo - filter order; butter - Butterworth filter; ellip - elliptic filter; lp - low-pass filter; hp - high-pass filter.

	sPDCtrue		sPDCfalse		PDCtrue		PDCfalse		DTFtrue		DTFfalse		dDTFtrue		dDTFfalse		Htrue		Hfalse	
	mean	std	mean	std	mean	std	mean	std	mean	std	mean	std	mean	std	mean	std	mean	std	mean	std
no filter	0.01	0.05	0.01	0.02	0.00	0.00	0.07	0.07	0.00	0.00	0.18	0.08	0.74	0.24	0.10	0.03	0.75	0.13	0.10	0.02
butter_npn_80Hz_lp_fo8	0.28	0.21	0.12	0.06	0.01	0.03	0.49	0.11	0.00	0.01	0.57	0.09	0.17	0.17	0.08	0.03	0.82	0.19	0.19	0.05
butter_npn_100Hz_lp_fo8	0.12	0.16	0.05	0.04	0.00	0.00	0.34	0.07	0.00	0.00	0.52	0.09	0.06	0.10	0.06	0.03	0.56	0.25	0.15	0.04
butter_npn_120Hz_lp_fo8	0.00	0.01	0.01	0.02	0.00	0.00	0.21	0.06	0.00	0.00	0.33	0.08	0.02	0.06	0.04	0.02	0.08	0.11	0.08	0.03
butter_npn_160Hz_lp_fo8	0.00	0.02	0.03	0.03	0.00	0.00	0.29	0.07	0.00	0.00	0.47	0.08	0.01	0.04	0.06	0.03	0.31	0.17	0.13	0.03
butter_npn_320Hz_lp_fo8	0.00	0.00	0.01	0.02	0.00	0.00	0.20	0.06	0.00	0.00	0.39	0.08	0.00	0.02	0.05	0.03	0.19	0.09	0.07	0.03
butter_npn_480Hz_lp_fo8	0.00	0.00	0.00	0.00	0.00	0.00	0.08	0.04	0.00	0.00	0.22	0.07	0.00	0.01	0.02	0.02	0.02	0.06	0.05	0.03
ellip_npn_80Hz_lp_fo8	0.09	0.15	0.02	0.03	0.00	0.00	0.20	0.07	0.00	0.00	0.29	0.10	0.22	0.21	0.04	0.03	0.49	0.14	0.09	0.03
ellip_npn_100Hz_lp_fo8	0.01	0.04	0.01	0.02	0.00	0.00	0.25	0.07	0.00	0.00	0.35	0.09	0.04	0.09	0.02	0.02	0.32	0.16	0.05	0.03
ellip_npn_120Hz_lp_fo8	0.00	0.01	0.01	0.02	0.00	0.00	0.21	0.06	0.00	0.00	0.33	0.08	0.02	0.06	0.04	0.02	0.08	0.11	0.08	0.03
ellip_npn_160Hz_lp_fo8	0.00	0.00	0.01	0.01	0.00	0.00	0.18	0.06	0.00	0.00	0.32	0.08	0.01	0.06	0.03	0.03	0.32	0.15	0.05	0.02
ellip_npn_320Hz_lp_fo8	0.00	0.00	0.00	0.01	0.00	0.00	0.11	0.05	0.00	0.00	0.22	0.08	0.00	0.01	0.02	0.02	0.05	0.09	0.02	0.02
ellip_npn_480Hz_lp_fo8	0.00	0.00	0.00	0.00	0.00	0.00	0.08	0.05	0.00	0.00	0.22	0.07	0.00	0.01	0.03	0.02	0.02	0.06	0.05	0.02

Table A.7: Results for notch filter, decimating and interpolating the data with LOOM and Kus-model
Abbreviations: std - standard deviation; pn - phase neutral filter; npn - non-phase neutral filter; interp - interpolate.

	sPDCtrue		sPDCfalse		PDCtrue		PDCfalse		DTTtrue		DTTfalse		dDTTtrue		dDTTfalse		Htrue		Hfalse	
	mean	std	mean	std	mean	std	mean	std	mean	std	mean	std	mean	std	mean	std	mean	std	mean	std
no filter	0.011	0.045	0.006	0.016	0.000	0.000	0.074	0.069	0.000	0.000	0.178	0.083	0.736	0.240	0.104	0.033	0.748	0.131	0.102	0.019
50 Hz artefact	0.000	0.000	0.262	0.056	0.000	0.000	0.769	0.055	0.000	0.000	0.999	0.004	0.007	0.036	0.257	0.061	0.000	0.000	0.974	0.033
notch pn	0.000	0.000	0.001	0.006	0.000	0.000	0.086	0.048	0.000	0.000	0.201	0.076	0.004	0.029	0.018	0.021	0.037	0.081	0.032	0.020
notch npn	0.014	0.052	0.003	0.009	0.000	0.000	0.095	0.045	0.000	0.000	0.210	0.076	0.037	0.084	0.020	0.021	0.056	0.108	0.046	0.027
interp linear	0.000	0.000	0.000	0.002	0.000	0.000	0.078	0.048	0.000	0.000	0.202	0.077	0.000	0.000	0.012	0.016	0.010	0.044	0.083	0.007
interp cubic	0.000	0.000	0.000	0.003	0.000	0.000	0.078	0.047	0.000	0.000	0.188	0.073	0.000	0.009	0.014	0.018	0.010	0.044	0.083	0.008
interp ft	0.333	0.196	0.046	0.027	0.004	0.027	0.069	0.050	0.195	0.242	0.101	0.036	1.000	0.000	0.135	0.000	1.000	0.000	0.135	0.000
interp spline	0.000	0.000	0.002	0.007	0.000	0.000	0.150	0.053	0.000	0.000	0.331	0.083	0.001	0.013	0.043	0.022	0.083	0.099	0.093	0.014
decimate 3	0.000	0.000	0.005	0.012	0.000	0.000	0.135	0.054	0.000	0.000	0.233	0.083	0.006	0.035	0.024	0.020	0.032	0.073	0.087	0.012
decimate 4	0.000	0.000	0.002	0.007	0.000	0.000	0.102	0.051	0.000	0.000	0.245	0.089	0.015	0.055	0.020	0.021	0.003	0.030	0.079	0.013
decimate 6	0.001	0.013	0.026	0.023	0.000	0.000	0.202	0.054	0.011	0.046	0.313	0.091	0.103	0.124	0.050	0.026	0.220	0.100	0.112	0.016
decimate 10	0.188	0.134	0.097	0.031	0.004	0.029	0.293	0.067	0.194	0.143	0.382	0.096	0.452	0.237	0.085	0.031	0.394	0.092	0.134	0.019

Table A.8: Regression coefficients for the sPDC, PDC and DTF with MEG data in combination with LOOM

Abbreviations: std - standard deviation; cs - coupling strength; dl - data length; nf - noise factor; moa - model order above the true one; mob - model order below the true one; * - $p \leq 0.05$.

	sPDC			PDC			DTF			
	missed coefficient	std	false positive coefficient std	missed coefficient	std	false positive coefficient std	missed coefficient	std	false positive coefficient std	
constant	3.00E+00	3.43E-01*	-2.41E+00	2.29E-01*	-2.41E+00	2.29E-01*	-2.64E+00	7.40E-01*	1.88E+00	2.44E-01*
cs	-7.90E+00	2.55E-01*	2.27E+00	1.52E-01*	7.33E+00	2.87E-01*	1.01E+01	6.24E-01*	-1.50E+00	1.57E-01*
cs*cs	3.11E+00	8.60E-02*	-8.81E-01	4.53E-02*	-3.01E+00	9.04E-02*	7.08E-01	1.45E-01*	6.80E-01	4.63E-02*
cs*dl	-4.31E-04	4.06E-05*	3.64E-04	2.37E-05*	4.25E-04	4.20E-05*	-3.41E-04	6.12E-05*	-3.41E-04	2.47E-05*
cs*nf	-2.50E-01	4.91E-02*	8.17E-02	2.81E-02*	1.88E-01	5.21E-02*	-5.45E-02	8.23E-02*	-6.01E-02	2.88E-02*
dl	-1.21E-04	1.30E-04	-1.87E-03	7.99E-05*	2.55E-04	1.34E-04	1.47E-03	1.82E-04	1.38E-03	8.59E-05*
dl*dl	-4.35E-08	1.87E-08*	2.04E-07	1.02E-08*	2.56E-08	1.88E-08	-1.56E-07	1.08E-08*	-1.37E-07	1.10E-08*
dl*nf	1.18E-04	3.01E-05*	6.99E-05	1.45E-05*	-1.39E-04	3.05E-05*	-6.87E-05	1.52E-05*	-6.09E-05	1.52E-05*
nf	1.23E+00	1.52E-01*	2.00E-01	8.02E-02*	-9.54E-01	1.68E-01*	-3.46E-02	2.54E-01*	-3.09E-01	8.38E-02*
nf*nf	-1.84E-01	3.41E-02*	-9.60E-02	1.70E-02*	1.76E-01	3.43E-02*	5.39E-02	1.78E-02*	1.02E-01	1.76E-02*
moa	-6.63E-02	1.34E-02*	3.58E-02	8.03E-03*	-1.50E-01	2.12E-02*	4.18E-02	3.37E-02*	4.41E-02	8.41E-03*
moa*moa	1.11E-03	1.88E-04*	-1.65E-04	1.08E-04	2.01E-03	3.24E-04*	-3.42E-04	1.12E-04*	1.64E-03	4.34E-04*
moa*cs	-2.27E-03	4.11E-03	-4.00E-04	2.32E-03	-7.93E-02	7.53E-03*	5.43E-04	2.41E-03	-2.94E-01	2.01E-02*
moa*dl	-1.42E-06	2.17E-06	-5.94E-06	1.14E-06*	-6.36E-06	2.96E-06*	5.38E-06	1.21E-06*	1.22E-05	3.65E-06*
moa*nf	1.48E-02	2.79E-03*	-3.31E-03	1.37E-03*	-1.22E-03	3.96E-03	2.52E-03	1.43E-03	1.32E-02	5.35E-03*
mob	3.43E-01	1.18E-01*	-2.08E-02	5.34E-02	-1.18E+00	1.37E-01*	-2.30E-02	5.63E-02	-3.20E-01	1.84E-01
mob*mob	-8.79E-02	9.74E-03*	-2.77E-03	4.04E-03	1.50E-01	1.16E-02*	1.31E-02	4.26E-03*	9.42E-02	1.31E-02*
mob*cs	3.90E-01	3.95E-02*	2.17E-02	1.47E-02	-3.05E-01	4.13E-02*	-1.11E-02	1.53E-02	-1.65E+00	1.66E-01*
mob*dl	1.04E-04	1.95E-05*	3.31E-05	8.33E-06*	-9.69E-05	1.98E-05*	-3.06E-05	8.68E-06*	-1.76E-04	2.34E-05*
mob*nf	-1.44E-01	2.63E-02*	-1.45E-02	9.07E-03	1.32E-01	2.69E-02*	3.70E-03	9.41E-03	2.11E-01	4.11E-02*

Table A.9: Regression coefficients for the dDTF and H with MEG data in combination with LOOM
 Abbreviations: std - standard deviation; CS - coupling strength; dl - data length; nf - noise factor; moa -
 model order above the true one; mob - model order below the true one; * - $p \leq 0.05$.

	DDTF		H			
	missed coefficient	std	false positive coefficient	std		
constant	-2.34E+00	4.49E-01*	5.75E-01	2.89E-01*		
cs	2.85E+00	3.40E-01*	-1.19E+00	1.88E-01*		
cs*cs	-6.83E-01	1.14E-01*	5.53E-02*	5.38E-01*		
cs*dl	2.97E-04	5.36E-05*	-2.74E-04	3.04E-05*		
cs*nf	-6.43E-01	6.73E-02*	1.76E-01	3.46E-02*		
dl	5.36E-04	1.65E-04*	8.12E-04	1.02E-04*		
dl*dl	-2.91E-08	2.35E-08	-5.45E-08	1.29E-08*		
dl*nf	-1.14E-04	3.66E-05*	-6.39E-05	1.78E-05*		
nf	1.02E+00	1.92E-01*	-9.33E-01	9.77E-02*		
nf*nf	-1.72E-02	4.34E-02	1.43E-01	2.02E-02*		
moa	8.50E-02	1.74E-02*	-3.15E-02	9.60E-03*		
moa*moa	-9.39E-04	2.45E-04*	2.48E-04	1.27E-04		
moa*cs	-2.67E-02	5.57E-03*	1.00E-03	2.81E-03		
moa*dl	4.99E-06	2.71E-06	1.20E-06	1.40E-06		
moa*nf	-2.47E-03	3.51E-03	4.87E-03	1.63E-03*		
mob	-4.27E-01	1.37E-01*	1.94E-01	6.47E-02*		
mob*mob	8.68E-02	1.11E-02*	-1.40E-02	4.84E-03*		
mob*cs	-3.98E-01	4.51E-02*	-4.45E-02	1.89E-02*		
mob*dl	-1.09E-04	2.16E-05*	-2.30E-05	1.00E-05*		
mob*nf	1.82E-01	2.86E-02*	2.09E-02	1.09E-02		
			missed coefficient	std	false positive coefficient	std
constant			5.87E-02	5.59E-01	-2.81E+00	2.78E-01*
cs			2.46E+00	4.38E-01*	2.06E+00	1.93E-01*
cs*cs			-5.91E-01	1.39E-01*	-6.53E-01	5.80E-02*
cs*dl			-2.84E-04	7.90E-05*	-4.73E-04	2.96E-05*
cs*nf			-3.45E-01	8.07E-02*	2.61E-01	3.59E-02*
dl			-8.70E-04	2.19E-04*	2.45E-03	9.57E-05*
dl*dl			2.53E-07	3.14E-08*	-2.88E-07	1.22E-08*
dl*nf			-9.95E-05	4.81E-05*	-7.30E-06	1.72E-05
nf			-1.36E-01	2.29E-01	-5.73E-01	9.66E-02*
nf*nf			8.88E-02	5.09E-02	3.99E-02	2.06E-02
moa			8.68E-02	2.16E-02*	-7.36E-02	9.57E-03*
moa*moa			1.89E-04	2.94E-04	7.54E-06	1.29E-04
moa*cs			-2.53E-02	6.53E-03*	1.53E-02	2.90E-03*
moa*dl			-2.39E-05	3.41E-06*	1.28E-05	1.35E-06*
moa*nf			5.53E-03	4.03E-03	-1.15E-03	1.64E-03
mob			-2.93E-01	1.73E-01	7.18E-02	6.26E-02
mob*mob			6.81E-02	1.44E-02*	-4.59E-03	4.74E-03
mob*cs			-1.11E-01	7.82E-02	-1.17E-02	1.83E-02
mob*dl			-1.47E-04	2.89E-05*	-2.51E-05	9.41E-06*
mob*nf			1.59E-01	4.00E-02*	5.94E-03	1.06E-02

Table A.10: Regression coefficients for the sPDC, PDC and DTF with EEG data in combination with LOOM; Abbreviations

Abbreviations: std - standard deviation; cs - coupling strength; dl - data length; nf - noise factor; moa - model order above the true one; mob - model order below the true one; * - $p \leq 0.05$.

	sPDC			PDC			DTF			
	missed coefficient	std	false positive coefficient	missed coefficient	std	false positive coefficient	missed coefficient	std	false positive coefficient	
constant	1.42E+00	3.60E-01*	-1.51E+00	2.70E-01*	7.14E-01	7.14E-01	2.84E-01*	2.84E-01*	1.35E+00	2.84E-01*
cs	-6.20E+00	2.57E-01*	2.35E+00	1.96E-01*	5.01E-01*	5.01E-01*	2.00E-01*	2.01E-01*	-1.65E+00	2.01E-01*
cs*cs	2.39E+00	7.68E-02*	-9.06E-01	5.85E-02*	1.45E-01*	1.45E-01*	5.97E-02*	5.97E-02*	8.08E-01	5.97E-02*
cs*dl	-7.25E-04	3.43E-05*	4.55E-04	2.64E-05*	7.07E-05*	7.07E-05*	2.74E-05*	2.76E-05*	-4.44E-04	2.76E-05*
cs*nf	-4.90E-01	4.61E-02*	3.59E-02	3.40E-02	8.21E-02	8.21E-02	3.50E-02	3.47E-02	-3.88E-02	3.47E-02
dl	8.05E-04	1.05E-04*	-2.63E-03	8.16E-05*	4.24E-04	2.06E-04*	2.10E-03	8.78E-05*	2.02E-03	8.83E-05*
dl*dl	-1.77E-07	1.45E-08*	3.30E-07	1.15E-08*	-1.78E-09	2.76E-08	1.22E-08*	1.23E-08*	1.79E-08	1.23E-08*
dl*nf	1.43E-04	2.36E-05*	-1.37E-05	1.70E-05	-1.43E-04	3.93E-05*	2.58E-06	1.80E-05	-1.11E-04	1.75E-05
nf	1.38E+00	1.41E-01*	7.58E-01	1.03E-01*	2.68E-01	2.68E-01	1.07E-01*	1.05E-01*	4.79E-01	1.05E-01*
nf*nf	-1.56E-01	3.13E-02*	-1.41E-01	2.23E-02*	6.47E-02	5.54E-02	2.29E-02*	2.26E-02*	-2.45E-01	2.26E-02*
moa	5.09E-04	1.36E-02*	5.71E-02	1.02E-02*	-1.83E-01	2.68E-02*	2.10E-02	1.06E-02*	-1.18E-01	2.60E-02*
moa*moa	2.59E-02	4.05E-03*	-1.90E-03	2.87E-03	-4.93E-02	7.61E-03*	2.17E-03	2.95E-03	9.84E-02	2.96E-03
moa*dl	9.29E-06	1.92E-06*	-7.13E-06	1.42E-06*	-1.53E-05	3.51E-06*	7.95E-06	1.51E-06*	-1.22E-05	3.34E-06*
moa*nf	7.90E-03	2.61E-03*	-1.00E-02	1.79E-03*	3.03E-03	4.52E-03	1.87E-03*	1.84E-03*	-4.34E-03	9.43E-03
mob	2.96E-01	1.17E-01*	-8.57E-03	6.31E-02	-7.18E-01	1.73E-01*	-3.64E-02	6.62E-02	-4.62E-01	1.56E-01*
mob*mob	-5.52E-02	9.25E-03*	7.73E-03	5.43E-03	6.80E-02	1.24E-02*	1.41E-03	5.69E-03	6.90E-02	1.15E-02*
mob*cs	2.48E-01	3.89E-02*	-2.26E-02	1.86E-02	-1.01E-01	5.76E-02*	1.92E-02	1.90E-02	-6.05E-01	6.20E-02*
mob*dl	4.80E-05	1.64E-05*	1.70E-05	8.71E-06	-7.01E-05	2.30E-05*	-1.17E-05	9.17E-06	-1.02E-04	2.04E-05*
mob*nf	-5.41E-02	2.11E-02*	-2.68E-02	1.24E-02*	2.22E-02	3.05E-02	2.44E-02	1.28E-02	3.01E-02	2.78E-02

Table A.11: Regression coefficients for the dDTF and H with EEG data in combination with LOOM
 Abbreviations: std - standard deviation; cs - coupling strength; dl - data length; nf - noise factor; moa -
 model order above the true one; mob - model order below the true one; * - $p \leq 0.05$.

	missed		dDTF		missed		H	
	coefficient	std	coefficient	std	coefficient	std	coefficient	std
constant	-2.65E+00	4.75E-01*	1.94E+00	3.44E-01*	1.28E+00	4.82E-01*	-3.10E+00	3.07E-01*
cs	3.10E+00	3.46E-01*	-1.30E+00	2.49E-01*	6.12E-01	3.45E-01	8.74E-01	2.32E-01*
cs*cs	-9.55E-01	1.08E-01*	9.73E-01	7.44E-02*	-2.72E-01	1.05E-01*	-1.47E-01	7.10E-02*
cs*dl	1.64E-04	4.78E-05*	-2.74E-04	3.58E-05*	3.85E-04	4.80E-05*	-5.67E-04	3.26E-05*
cs*nf	-5.67E-03	6.60E-02	1.70E-01	4.34E-02*	-2.51E-01	6.24E-02*	2.76E-01	4.06E-02*
dl	9.19E-04	1.38E-04*	2.41E-04	1.08E-04*	-2.09E-03	1.45E-04*	3.07E-03	9.27E-05*
dl*dl	-1.34E-07	1.93E-08*	4.68E-09	1.52E-08	3.53E-07	2.08E-08*	-3.80E-07	1.30E-08*
dl*nf	1.28E-04	3.15E-05*	-1.99E-05	2.25E-05	-2.01E-04	3.36E-05*	5.49E-05	1.91E-05*
nf	5.85E-01	1.92E-01*	1.61E+00	1.28E-01*	5.60E-01	1.92E-01*	-7.60E-01	1.14E-01*
nf*nf	-1.92E-01	4.27E-02*	2.67E-01	2.78E-02*	1.12E-02	4.33E-02	1.37E-02	2.45E-02
moa	7.38E-02	1.81E-02*	-3.17E-02	1.25E-02*	1.09E-01	1.88E-02*	-8.00E-02	1.16E-02*
moa*moa	-1.02E-03	2.58E-04*	3.22E-04	1.79E-04	-4.09E-04	2.75E-04	2.57E-05	1.65E-04
moa*cs	-2.30E-02	5.41E-03*	-1.09E-02	3.62E-03*	-1.73E-02	5.59E-03*	1.50E-02	3.52E-03*
moa*dl	7.44E-06	2.50E-06*	2.33E-06	1.88E-06	-1.59E-05	2.69E-06*	1.22E-05	1.67E-06*
moa*nf	-3.96E-03	3.49E-03	1.31E-02	2.18E-03*	-1.01E-03	3.58E-03	4.94E-03	2.03E-03*
mob	-2.20E-01	1.38E-01	1.39E-01	7.96E-02	-2.08E-01	1.54E-01	9.71E-02	7.01E-02
mob*mob	4.68E-02	1.11E-02*	-2.10E-02	6.95E-03*	4.67E-02	1.24E-02*	-1.50E-02	5.98E-03*
mob*cs	-2.13E-01	4.45E-02*	2.30E-02	1.10E-05	-2.20E-01	4.82E-02*	3.33E-02	2.05E-02
mob*dl	-4.94E-05	1.93E-05*	4.30E-06	1.50E-02*	-2.87E-05	2.14E-05	-1.47E-05	9.34E-06
mob*nf	3.43E-02	2.64E-02	5.34E-02	1.50E-02*	4.27E-02	2.62E-02	9.74E-03	1.30E-02

Table A.12: Regression coefficients for the sPDC, PDC and DTF with EMG data in combination with LOOM

Abbreviations: std - standard deviation; cs - coupling strength; dl - data length; nf - noise factor; moa - model order above the true one; mob - model order below the true one; * - $p \leq 0.05$.

	sPDC			PDC			DTF			
	missed coefficient	std	false positive coefficient std	missed coefficient	std	false positive coefficient std	missed coefficient	std	false positive coefficient std	
constant	3.28E+00	2.27E-01*	-3.65E+00	7.97E-02*	2.06E+00	1.05E-01*	-1.07E+00	4.09E-01*	2.93E+00	1.05E-01*
cs	-5.15E+00	1.44E-01*	2.40E+00	8.01E-02*	-1.31E+00	8.96E-02*	1.09E+00	3.06E-01*	-1.36E+00	9.15E-02*
cs*cs	2.05E+00	4.72E-02*	-6.90E-01	2.87E-02*	-1.10E+00	9.22E-02*	-4.58E-01	1.08E-01*	4.07E-01	3.12E-02*
cs*dl	-2.88E-04	2.30E-05*	-8.81E-05	1.30E-05*	4.12E-05*	9.75E-05	-3.70E-05	4.25E-05	6.64E-05	1.52E-05*
cs*nf	-4.33E-01	3.50E-02*	8.63E-02	1.45E-02*	-9.80E-03	6.34E-02	-7.96E-02	1.75E-02*	-8.36E-02	1.65E-02*
dl	2.13E-05	7.34E-05	1.11E-04	2.29E-05*	2.68E-04	1.29E-04*	-3.18E-04	3.22E-05*	4.40E-04	1.44E-04*
dl*dl	-6.41E-08	9.90E-09*	2.17E-08	3.37E-09*	-3.23E-09	1.74E-08	8.94E-09	4.40E-09*	2.01E-08	2.34E-08
dl*nf	3.67E-06	1.82E-05	2.07E-06	4.65E-06	1.69E-05	2.73E-05	-1.01E-05	7.23E-06	-7.16E-06	3.22E-05
nf	4.40E-02	1.07E-01	-1.61E-01	2.67E-02*	-2.88E-01	1.76E-01	3.20E-01	4.11E-02*	-1.07E+00	1.92E-01*
nf*nf	1.35E-01	2.37E-02*	1.72E-02	5.24E-03*	-1.80E-02	3.35E-02	-4.71E-02	8.75E-03*	2.40E-01	4.44E-02*
moa	-3.87E-02	8.24E-03*	-1.88E-03	2.25E-03	-4.87E-02	1.53E-02*	4.91E-02	2.99E-03*	-6.11E-02	1.76E-02*
moa*moa	1.91E-04	1.16E-04	4.99E-05	2.54E-05*	6.34E-04	2.01E-04*	-2.76E-04	3.45E-05*	5.35E-04	2.58E-04*
moa*cs	1.88E-02	2.50E-03*	1.63E-03	9.93E-04	-5.87E-03	5.39E-03	-2.74E-03	1.13E-03*	7.55E-03	4.69E-03
moa*dl	7.65E-06	1.25E-06*	-1.71E-06	3.35E-07*	-4.91E-06	2.03E-06*	1.26E-06	4.49E-07*	-7.00E-06	2.48E-06*
moa*nf	6.38E-03	1.87E-03*	-2.92E-03	3.99E-04*	-7.88E-03	2.78E-03*	1.80E-03	6.25E-04*	-4.76E-03	3.18E-03
mob	3.02E-01	8.24E-02*	1.48E-02	1.39E-02	-3.83E-01	1.19E-01*	-6.20E-02	1.94E-02*	7.24E-01	1.26E-01*
mob*mob	-5.93E-02	6.38E-03*	3.54E-04	8.21E-04	3.29E-02	9.44E-03*	7.57E-03	1.30E-03*	7.71E-02	1.02E-02*
mob*cs	1.18E-02	2.73E-02	2.50E-03	6.04E-03	5.86E-02	4.65E-02	-4.60E-03	7.27E-03	1.50E-01	4.17E-02*
mob*dl	5.16E-05	1.46E-05*	-1.05E-05	1.51E-06*	-2.70E-05	1.88E-05	1.34E-05	2.39E-06*	-6.34E-05	1.67E-05*
mob*nf	1.54E-02	1.77E-02	-3.16E-03	2.00E-03	3.28E-02	2.38E-02	-3.04E-03	3.44E-03	6.01E-02	2.30E-02*

Table A.14: Regression coefficients for the sPDC, PDC and DTF with LFP data in combination with LOOM

Abbreviations: std - standard deviation; cs - coupling strength; dl - data length; nf - noise factor; moa - model order above the true one; mob - model order below the true one; * - $p \leq 0.05$.

	sPDC			PDC			DTF					
	missed coefficient	std	false positive coefficient	missed coefficient	std	false positive coefficient	missed coefficient	std	false positive coefficient			
constant	2.16E+00	2.74E-01*	-4.70E+00	1.47E-01*	1.05E-01*	1.47E-01*	-5.67E-02	5.42E-01	3.26E+00	5.48E-01*	3.50E+00	1.91E-01*
cs	-4.99E+00	1.76E-01*	4.44E+00	1.05E-01*	3.76E-01	3.14E+00	3.38E-01	3.76E-01	-3.14E+00	2.08E-01	-2.09E+00	1.31E-01*
cs*cs	1.53E+00	5.61E-02*	-1.50E+00	3.11E-02*	1.14E-01*	1.03E+00	6.86E-01	1.14E-01*	1.03E+00	-1.15E-01	6.30E-01	3.86E-02*
cs*dl	-6.50E-05	2.55E-05*	-1.52E-05	1.69E-05	6.23E-05*	2.91E-05	-4.07E-04	6.23E-05*	2.91E-05	-3.79E-04	4.33E-05	2.15E-05
cs*nf	-2.73E-01	3.69E-02*	2.75E-01	2.31E-02*	7.63E-02	-2.13E-01	-1.31E-01	7.63E-02	-2.13E-01	2.45E-01	-1.19E-01	2.76E-02*
dl	-8.20E-04	9.29E-05*	-1.71E-04	4.82E-05*	3.24E-04	-3.91E-05	3.24E-04	1.94E-04*	-3.91E-05	1.25E-03	1.42E-04	6.53E-05*
dl*dl	6.92E-08	1.25E-08*	6.52E-08	5.69E-09*	7.23E-08	-1.76E-08	7.23E-08	2.53E-08*	-1.76E-08	-1.53E-07	1.78E-08*	7.99E-09*
dl*nf	-2.15E-05	1.98E-05	4.73E-06	1.13E-05	4.73E-05*	1.57E-05	-1.05E-04	3.43E-05*	1.57E-05	6.99E-06	-2.24E-06	1.44E-05
nf	1.94E+00	1.20E-01*	-1.43E-01	5.95E-02*	2.26E-01*	3.54E-01	-5.85E-01	2.26E-01*	3.54E-01	-8.06E-01	2.25E-01*	7.44E-02*
nf*nf	-2.54E-01	2.63E-02*	-7.99E-02	1.30E-02*	4.98E-02	1.34E-02	8.04E-02	4.98E-02	1.34E-02	1.02E-01	-1.69E-02	1.58E-02
moa	-6.79E-03	1.06E-02	-4.29E-02	4.22E-03*	-1.37E-01	2.07E-02*	-1.37E-01	2.07E-02*	7.70E-02	1.17E-01	1.95E-02	6.30E-03
moa*moa	2.80E-04	1.46E-04	4.44E-04	5.50E-05*	1.96E-03	2.70E-04*	1.96E-03	2.70E-04*	-4.24E-04	8.22E-04	2.46E-04	7.41E-05*
moa*cs	9.36E-03	2.98E-03*	1.25E-02	1.42E-03*	-3.58E-02	6.07E-03*	-3.58E-02	6.07E-03*	-1.41E-02	-6.57E-03	6.49E-03	1.82E-03*
moa*dl	1.44E-06	1.46E-06	-4.83E-06	6.87E-07*	-8.99E-06	2.73E-06*	-8.99E-06	2.73E-06*	1.92E-06	6.57E-06	2.44E-06	9.36E-07*
moa*nf	4.56E-03	2.10E-03*	-1.93E-03	9.76E-04*	1.36E-02	3.78E-03*	1.36E-02	3.78E-03*	-2.81E-04	-7.95E-03	3.58E-03	1.21E-03*
mob	4.43E-01	9.18E-02*	-6.41E-02	2.81E-02*	-7.02E-01	1.47E-01*	-7.02E-01	1.47E-01*	1.02E-01	-5.99E-01	1.22E-01*	4.27E-02
mob*mob	-5.32E-02	7.37E-03*	-7.17E-04	1.77E-03	5.10E-02	1.11E-02*	5.10E-02	1.11E-02*	-2.40E-03	4.38E-03	9.06E-03	2.30E-03
mob*cs	3.99E-02	2.67E-02	1.57E-02	8.71E-03	3.95E-02	4.82E-02	3.95E-02	4.82E-02	-2.91E-02	1.03E-02*	1.93E-03	1.12E-02
mob*dl	4.16E-05	1.40E-05*	-3.80E-07	3.80E-06	-6.90E-05	2.07E-05*	-6.90E-05	2.07E-05*	5.61E-06	-1.53E-05	1.65E-05	4.97E-06
mob*nf	-6.48E-02	2.10E-02*	-4.58E-04	5.61E-03	1.14E-01	3.05E-02*	1.14E-01	3.05E-02*	1.31E-03	7.05E-02	2.55E-02*	6.83E-03

Table A.17: Regression coefficients for the dDTF and H with MEG data in combination with random permutation
 Abbreviations: std - standard deviation; cs - coupling strength; dl - data length; nf - noise factor; moa -
 model order above the true one; mob - model order below the true one; * - $p \leq 0.05$.

	missed		dDTF		missed		H	
	coefficient	std	coefficient	std	coefficient	std	coefficient	std
constant	-8.79E-01	4.04E-01*	1.53E+00	2.68E-01*	1.15E+00	4.82E-01*	3.05E+00	2.31E-01*
cs	3.30E+00	3.14E-01*	-1.25E+00	2.37E-01*	-1.22E+00	4.68E-01*	6.70E-01	2.10E-01*
cs*cs	-1.13E+00	1.07E-01*	-2.68E-01	7.99E-02*	3.99E-02	1.84E-01	-5.87E-01	7.24E-02*
cs*dl	-3.03E-04	4.72E-05*	1.68E-04	3.48E-05*	-8.21E-04	1.13E-04*	2.08E-04	3.04E-05*
cs*nf	1.79E-01	6.66E-02*	7.09E-01	4.78E-02*	-2.40E-01	1.32E-01	3.48E-01	4.41E-02*
dl	1.85E-04	1.33E-04	-5.81E-05	8.60E-05	-6.20E-04	1.85E-04*	-6.53E-04	7.04E-05*
dl*dl	1.92E-08	2.06E-08	-1.43E-09	1.14E-08	2.10E-07	2.89E-08*	9.87E-09*	9.87E-09*
dl*nf	-5.68E-05	3.16E-05	4.69E-05	1.86E-05*	3.91E-06	4.94E-05	-3.66E-05	1.70E-05*
nf	4.73E-01	1.77E-01*	-1.00E+00	1.01E-01*	4.57E-01	2.74E-01	-9.64E-01	9.30E-02*
nf*nf	-1.54E-01	4.22E-02*	-7.42E-02	2.41E-02*	-3.06E-02	6.86E-02	5.36E-02	2.19E-02*
moa	-4.71E-03	1.61E-02	6.45E-03	9.37E-03	-5.01E-02	2.23E-02*	1.09E-01	8.20E-03*
moa*moa	8.67E-05	2.40E-04	-2.76E-04	1.44E-04	2.98E-04	3.37E-04	-6.22E-04	1.25E-04*
moa*cs	1.49E-02	4.64E-03*	-8.56E-03	3.42E-03*	1.85E-02	7.21E-03*	-2.41E-02	3.13E-03*
moa*dl	-4.63E-06	2.24E-06*	-6.04E-07	1.38E-06	2.65E-06	3.03E-06	-6.49E-06	1.22E-06*
moa*nf	1.19E-02	3.17E-03*	-7.93E-04	1.87E-03	-1.14E-02	4.55E-03*	9.81E-03	1.80E-03*
mob	-3.41E-02	1.14E-01	7.30E-02	5.46E-02	-2.03E-01	1.35E-01	3.26E-03	4.85E-02
mob*mob	1.36E-02	9.63E-03	-1.73E-02	3.97E-03*	1.30E-02	1.33E-02	3.51E-03	3.51E-03
mob*cs	-6.14E-02	3.52E-02	5.28E-02	1.65E-02*	-2.21E-02	5.92E-02	1.85E-02	1.43E-02
mob*dl	-2.84E-05	1.58E-05	6.69E-06	6.84E-06	4.55E-05	1.89E-05*	-6.13E-06	5.69E-06
mob*nf	-8.62E-03	2.41E-02	1.16E-02	8.92E-03	6.04E-02	2.94E-02*	2.08E-02	8.40E-03*

Table A.18: Regression coefficients for the sPDC, PDC and DTF with EEG data in combination with random permutation

Abbreviations: std - standard deviation; dl - data length; nf - noise factor; moa - model order above the true one; mob - model order below the true one; * - $p \leq 0.05$.

	sPDC			PDC			DTF					
	missed coefficient	std	false positive coefficient std	missed coefficient	std	false positive coefficient std	missed coefficient	std	false positive coefficient std			
constant	1.32E+00	3.54E-01*	-1.48E+00	3.49E-01*	-1.24E-02	5.00E-01	-1.58E-03	4.94E-01	5.46E-01	5.92E-01	4.71E-02	5.28E-01
cs	2.01E-01	3.21E-01	1.19E-01	3.30E-01	-1.04E-02	4.53E-01	4.83E-03	4.67E-01	8.73E-02	5.30E-01	1.31E-01	4.85E-01
cs*cs	-1.63E-02	1.12E-01	-1.23E-01	1.19E-01	5.64E-03	1.58E-01	-2.02E-03	1.68E-01	-1.21E-01	1.86E-01	-9.09E-02	1.72E-01
cs*dl	2.71E-05	4.04E-05	6.28E-05	3.91E-05	2.44E-07	5.71E-05	-3.08E-07	5.52E-05	-6.84E-05	6.67E-05	-1.55E-05	5.73E-05
cs*nf	-9.38E-02	6.16E-02	-2.23E-02	6.37E-02	7.78E-04	8.71E-02	3.00E-04	9.02E-02	9.96E-02	1.00E-01	3.72E-02	9.38E-02
dl	-1.50E-03	1.13E-04*	7.50E-04	1.10E-04*	6.92E-07	1.59E-04	1.43E-06	1.56E-04	2.27E-04	1.88E-04	1.48E-04	1.65E-04
dl*dl	1.90E-07	1.60E-08*	-1.39E-07	1.63E-08*	9.30E-10	2.26E-08	-8.00E-10	2.31E-08	7.75E-08	2.81E-08*	-3.17E-08	2.41E-08
dl*nf	-4.24E-05	2.39E-05	1.99E-04	2.26E-05*	-1.81E-07	3.38E-05	8.49E-08	3.20E-05	-1.29E-04	3.89E-05*	-7.24E-05	3.37E-05*
nf	2.61E-01	1.55E-01	-2.36E+00	1.56E-01*	-9.81E-03	2.19E-01	6.04E-03	2.21E-01	-6.34E-01	2.52E-01*	2.07E-01	2.33E-01
nf*nf	1.64E-01	4.04E-02*	4.01E-01	4.16E-02*	2.30E-03	5.72E-02	-1.38E-03	5.88E-02	1.10E-01	6.58E-02	-3.55E-02	6.10E-02
moa	7.07E-02	1.52E-02*	-1.28E-02	1.61E-02	1.04E-03	2.15E-02	-1.93E-04	2.27E-02	-8.01E-02	2.59E-02*	3.21E-02	2.37E-02
moa*moa	-2.48E-04	2.30E-04	-9.66E-05	2.45E-04	-5.52E-06	3.25E-04	-2.46E-06	3.46E-04	1.28E-03	3.89E-04*	-7.01E-04	3.57E-04*
moa*cs	-2.27E-03	4.84E-03	-3.36E-03	5.00E-03	-3.47E-05	6.84E-03	-1.55E-05	7.06E-03	7.94E-03	7.91E-03	1.31E-03	7.25E-03
moa*dl	-5.06E-06	1.87E-06	3.00E-06	1.78E-06	-2.22E-07	2.64E-06	1.24E-07	2.52E-06	-1.23E-05	3.06E-06*	3.14E-06	2.62E-06
moa*nf	3.27E-01	9.22E-02*	-3.58E-02	9.03E-02	7.10E-05	3.80E-03	-3.28E-05	3.81E-03	1.16E-02	4.31E-03*	4.21E-03	3.96E-03
mob	-3.07E-02	7.58E-03*	1.82E-03	7.29E-03	6.99E-03	1.30E-01	-1.20E-03	1.28E-01	-4.09E-01	1.61E-01*	1.21E-01	1.34E-01
mob*mob	-2.30E-02	2.92E-02	-3.06E-02	2.74E-02	-4.36E-04	1.07E-02	3.45E-05	1.03E-02	2.72E-02	1.33E-02*	-6.75E-03	1.08E-02
mob*cs	-8.41E-06	1.10E-05	9.81E-06	9.76E-06	-8.33E-07	1.55E-05	3.03E-07	1.38E-05	8.62E-06	1.91E-05	4.71E-06	1.45E-05
mob*dl	-1.54E-02	1.63E-02	1.17E-02	1.54E-02	3.86E-04	2.30E-02	-1.89E-04	2.19E-02	2.77E-02	2.74E-02	-8.56E-03	2.29E-02

Table A.20: Regression coefficients for the sPDC, PDC and DTF with EMG data in combination with random permutation

Abbreviations: std - standard deviation; cs - coupling strength; dl - data length; nf - noise factor; moa - model order above the true one; mob - model order below the true one; * - $p \leq 0.05$.

	sPDC			PDC			DTF				
	missed coefficient	std	false positive coefficient std	missed coefficient	std	false positive coefficient std	missed coefficient	std	false positive coefficient std		
constant	2.97E+00	2.38E-01*	-8.49E+00	1.64E-01*	2.24E-01	9.85E-02*	7.21E-02	-3.47E-01	4.67E-01	3.76E+00	2.61E-01*
cs	-4.91E+00	2.38E-01*	6.11E+00	1.78E-01*	-1.90E-01	3.22E-01	2.25E-01	4.28E-02	4.11E-01	-3.03E+00	2.68E-01*
cs*cs	2.10E+00	9.13E-02*	-1.32E+00	6.89E-02*	4.90E-02	1.32E-01	9.80E-02	-3.86E-02	1.55E-01	7.34E-01	1.01E-01*
cs*dl	1.77E-05	3.47E-05	-1.55E-04	2.54E-05*	2.52E-05	4.90E-05	3.64E-05	-1.77E-06	3.64E-05*	2.02E-04	3.87E-05*
cs*nf	-4.29E-01	5.38E-02*	-9.42E-02	3.77E-02*	-6.69E-03	7.67E-02	5.37E-02	-3.44E-02	9.04E-02	-1.33E-01	5.40E-02*
dl	-1.48E-03	9.56E-05*	9.24E-04	6.00E-05*	-1.32E-04	1.32E-04	8.12E-05	1.57E-05	1.63E-04	-4.02E-04	8.86E-05*
dl*dl	1.81E-07	1.45E-08*	-1.07E-07	9.02E-09*	-5.96E-10	2.09E-08	1.30E-08	7.14E-08	2.46E-08*	5.08E-09	1.30E-08
dl*nf	4.07E-05	2.45E-05	9.48E-05	1.39E-05*	9.07E-07	3.47E-05	6.29E-06	2.00E-05	1.38E-05	-3.89E-05	2.01E-05
nf	1.24E+00	1.49E-01*	-6.25E-01	8.95E-02*	-1.18E-02	2.10E-01	1.26E-01	4.51E-02	2.42E-01	2.61E-01	1.20E-01*
nf*nf	-1.47E-01	3.76E-02*	1.02E-01	2.19E-02*	3.67E-03	5.43E-02	3.15E-02	6.06E-03	6.12E-02	1.64E-02	2.93E-02
moa	4.29E-02	1.29E-02*	-4.55E-02	7.93E-03*	4.22E-03	1.52E-02	1.01E-02	-4.11E-03	2.21E-02	1.29E-02	1.12E-02
moa*moa	2.83E-04	2.12E-04	1.38E-04	1.24E-04	-1.86E-04	2.93E-04	1.76E-04	-7.82E-05	3.42E-04	-2.70E-04	1.68E-04
moa*cs	-9.80E-03	4.27E-03*	1.02E-02	2.86E-03*	4.78E-04	6.05E-03	4.05E-03	1.44E-02	6.93E-03*	2.08E-03	4.19E-03
moa*dl	-9.97E-06	1.86E-06*	6.74E-06	1.09E-06*	2.95E-06	2.64E-06	1.43E-06	-7.67E-07	2.92E-06	2.27E-06	1.58E-06
moa*nf	7.38E-03	3.00E-03*	-4.93E-03	1.63E-03*	3.08E-05	4.25E-03	2.32E-03	-2.91E-04	4.61E-03	4.13E-04	2.18E-03
mob	4.12E-01	8.05E-02*	1.92E-01	4.42E-02*	2.78E-03	9.96E-02	5.92E-02	-2.04E-01	1.40E-01	-5.65E-02	5.85E-02
mob*mob	-4.17E-02	7.06E-03*	4.49E-03	3.32E-03	-1.09E-03	9.73E-03	4.73E-03	2.46E-02	1.18E-02*	-5.07E-03	4.47E-03
mob*cs	-4.28E-02	2.50E-02	-1.28E-01	1.67E-02*	6.63E-04	3.56E-02	2.38E-02	-2.21E-03	4.54E-02	5.86E-02	2.32E-02*
mob*dl	-3.36E-06	1.22E-05	-1.50E-06	5.57E-06	1.42E-05	1.74E-05	8.20E-06	-1.76E-05	2.17E-05	-9.77E-08	8.01E-06
mob*nf	-1.09E-02	1.90E-02	-1.46E-02	8.38E-03	-5.05E-03	2.71E-02	1.19E-02	2.95E-03	2.98E-02	7.64E-03	1.12E-02

Table A.22: Regression coefficients for the sPDC, PDC and DTF with LFP data in combination with random permutation

Abbreviations: std - standard deviation; cs - coupling strength; dl - data length; nf - noise factor; moa - model order above the true one; mob - model order below the true one; * - $p \leq 0.05$.

	sPDC			PDC			DTF				
	missed coefficient	std	false positive coefficient	missed coefficient	std	false positive coefficient	missed coefficient	std	false positive coefficient		
constant	2.22E+00	3.04E-01*	-6.09E+00	2.22E-01*	4.29E-01	3.75E-14	3.13E-01	7.82E-01	4.44E-01	1.84E+00	2.76E-01*
cs	-3.09E+00	2.18E-01*	3.23E+00	1.98E-01*	3.09E-01	-3.14E-14	2.80E-01	-1.23E+00	3.27E-01*	-9.76E-01	2.53E-01*
cs*cs	9.80E-01	8.12E-02*	-5.64E-01	7.31E-02*	1.15E-01	-3.83E-15	1.03E-01	3.63E-01	1.25E-01*	2.14E-01	9.44E-02*
cs*dl	3.09E-05	2.97E-05	-1.56E-04	2.55E-05*	4.21E-05	-4.51E-18	3.60E-05	-5.65E-04	4.85E-05*	3.27E-04	3.47E-05*
cs*nf	-3.01E-01	5.07E-02*	1.84E-01	4.06E-02*	7.17E-02	-2.75E-14	5.74E-02	2.21E-01	7.74E-02*	-2.29E-01	5.34E-02*
dl	-2.08E-03	8.99E-05*	1.10E-03	6.33E-05*	1.27E-04	-8.53E-18	8.95E-05	-1.37E-04	1.37E-04	-1.34E-04	8.27E-05
dl*dl	3.52E-07	1.35E-08*	-1.17E-07	9.37E-09*	1.91E-08	1.95E-21	1.33E-08	9.11E-08	2.13E-08*	-4.13E-08	1.23E-08*
dl*nf	-2.11E-04	2.18E-05*	1.87E-04	1.37E-05*	3.09E-05	-1.11E-17	1.94E-05	1.57E-04	3.48E-05*	-1.28E-04	1.87E-05*
nf	1.96E+00	1.50E-01*	-8.94E-01	9.38E-02*	2.13E-01	6.65E-14	1.33E-01	-6.31E-01	2.24E-01*	8.91E-01	1.15E-01*
nf*nf	-1.76E-01	3.60E-02*	5.95E-02	2.21E-02*	5.09E-02	4.95E-15	3.13E-02	2.31E-02	5.64E-02	-8.60E-02	2.78E-02*
moa	5.43E-02	1.27E-02*	-7.96E-02	9.41E-03*	1.80E-02	-2.05E-15	1.33E-02	-3.99E-02	1.90E-02*	2.96E-02	1.17E-02*
moa*moa	1.82E-04	1.88E-04	6.49E-04	1.53E-04*	2.66E-04	-4.71E-17	2.16E-04	-3.61E-06	2.87E-04	-1.23E-04	1.87E-04
moa*cs	1.19E-02	3.70E-03*	1.71E-02	3.33E-03*	5.24E-03	2.51E-15	4.71E-03	2.48E-02	5.67E-03*	-2.50E-02	4.35E-03*
moa*dl	-1.61E-05	1.60E-06*	4.39E-06	1.15E-06*	2.26E-06	3.64E-19	1.63E-06	5.71E-06	2.57E-06*	-1.20E-06	1.57E-06
moa*nf	1.19E-02	2.57E-03*	-1.73E-02	1.77E-03*	3.64E-03	1.85E-16	2.50E-03	-7.83E-03	3.88E-03*	1.11E-02	2.26E-03*
mob	1.32E-01	8.43E-02	1.28E-01	5.44E-02*	1.19E-01	1.01E-14	7.70E-02	-2.25E-01	1.31E-01	2.41E-02	6.81E-02
mob*mob	-1.48E-02	6.92E-03*	-2.71E-03	4.28E-03	9.78E-03	-1.68E-15	6.05E-03	2.49E-02	1.10E-02*	-4.89E-03	5.45E-03
mob*cs	1.93E-02	2.50E-02	-5.37E-02	1.83E-02*	3.54E-02	5.36E-15	2.59E-02	-9.02E-02	3.90E-02*	-4.65E-03	2.40E-02
mob*dl	1.53E-05	1.21E-05	-1.70E-05	6.13E-06*	1.71E-05	5.21E-19	8.67E-06	-3.17E-05	2.04E-05	4.59E-06	8.49E-06
mob*nf	-3.27E-02	1.68E-02	-2.17E-02	9.08E-03*	2.38E-02	-1.23E-15	1.29E-02	6.20E-02	2.50E-02*	6.90E-03	1.18E-02

Table A.23: Regression coefficients for the dDTF and H with LFP data in combination with random permutation
 Abbreviations: std - standard deviation; cs - coupling strength; dl - data length; nf - noise factor; moa -
 model order above the true one; mob - model order below the true one; * - $p \leq 0.05$.

	dDTF		H	
	missed coefficient	false positive std	missed coefficient	false positive std
constant	5.67E-01	4.17E-01	6.34E-01	6.43E-01
cs	1.03E+00	3.07E-01*	-2.24E+00	2.63E+00
cs*cs	-3.26E-01	1.09E-01*	1.29E+00	2.10E+00
cs*dl	4.84E-05	4.09E-05	1.95E-01*	-1.15E+00
cs*nf	-8.23E-02	7.10E-02	1.06E-04*	1.33E-04
dl	-9.55E-05	1.23E-04	4.42E-01	1.04E-01
dl*dl	-1.02E-07	1.78E-08*	5.37E-04	2.08E-04*
dl*nf	1.40E-04	2.96E-05*	-1.07E-08	2.28E-08
nf	5.94E-01	2.01E-01*	4.49E-05*	-1.47E-04
nf*nf	-1.34E-01	4.70E-02*	-1.73E-01	-4.81E-01
moa	-2.60E-02	1.70E-02	1.28E-01	1.06E-01
moa*moa	-3.48E-04	2.44E-04	1.35E-03	3.75E-04*
moa*cs	-1.94E-04	4.96E-03	-9.57E-03	8.72E-03
moa*dl	1.64E-05	2.11E-06*	1.16E-05	-1.37E-02
moa*nf	-1.29E-02	3.39E-03*	-1.90E-02	4.63E-03*
mob	-1.93E-01	1.13E-01	-2.28E-01	1.47E-01
mob*moa	1.78E-02	9.09E-03	2.42E-02	1.15E-02*
mob*cs	-4.85E-02	3.41E-02	-3.70E-01	5.31E-02*
mob*dl	4.48E-06	1.56E-05	-7.58E-05	1.89E-05*
mob*nf	1.03E-02	2.26E-02	1.04E-01	2.66E-02*
				2.89E-02
				2.80E-01*
				2.55E-01*
				9.53E-02*
				3.55E-05*
				5.31E-02*
				8.62E-05*
				1.28E-08
				1.90E-05*
				1.19E-01*
				2.78E-02*
				1.19E-02*
				1.92E-04*
				4.41E-03*
				1.60E-06*
				-3.96E-06
				1.83E-02
				2.30E-03*
				6.41E-02
				4.99E-03
				2.30E-02*
				1.24E-05
				8.11E-06
				1.12E-02*

Table A.24: Parameter dependencies for the Schelker-model in combination with LOOM (sPDC, PDC, DTF)
 Abbreviations: std - standard deviation; dl - data length; nf - noise factor; moa - model order above
 the true one; mob - model order below the true one; * - $p \leq 0.05$.

	sPDC			PDC			DTF		
	missed coefficient	std	false positive coefficient	missed coefficient	std	false positive coefficient	missed coefficient	std	false positive coefficient
constant	-2.72E-01	2.07E-01	-3.33E-01	6.19E-02*	6.19E-02*	1.30E-01	6.63E-02*		
dl	-2.88E-03	7.03E-05	-6.98E-04	1.81E-05*	1.81E-05*	5.18E-04	1.88E-05*		
dl*dl	5.42E-07	1.06E-08	-3.21E-09	2.28E-09	2.28E-09	1.35E-08	2.37E-09*		
dl*nf	-4.98E-05	1.56E-05*	2.01E-04	4.94E-06	4.94E-06	-2.08E-04	5.01E-06		
nf	3.62E-01	9.51E-02*	3.91E-01	3.43E-02*	3.43E-02*	-3.89E-01	3.50E-02*		
nf*nf	-1.37E-01	1.97E-02*	-8.30E-02	6.76E-03*	6.76E-03*	8.56E-02	6.87E-03*		
moa	9.49E-02	9.51E-03*	-9.36E-03	2.34E-03*	2.34E-03*	1.42E-02	2.61E-03*		
moa*moa	-6.62E-04	1.30E-04*	2.42E-04	2.98E-05*	2.98E-05*	-3.00E-04	3.32E-05*		
moa*dl	-1.89E-05	1.23E-06*	1.70E-06	3.13E-07*	3.13E-07*	4.60E-07	3.28E-07		
moa*nf	4.76E-03	1.71E-03*	-2.38E-03	5.26E-04*	5.26E-04*	2.26E-03	5.45E-04*		
mob	2.20E-01	3.47E-02*	-2.01E-02	8.39E-03*	8.39E-03*	2.15E-02	1.00E-02*		
mob*mob	-7.73E-03	1.62E-03*	4.85E-04	3.56E-04	3.56E-04	-1.96E-04	4.65E-04		
mob*dl	-1.20E-05	4.48E-06*	3.72E-06	1.21E-06*	1.21E-06*	-1.74E-06	1.34E-06		
mob*nf	5.42E-04	6.00E-03	-2.04E-03	1.89E-03	1.89E-03	-3.13E-04	2.08E-03		

Table A.25: Parameter dependencies for the Scheiter-model in combination with LOOM (DDTF, H)
 Abbreviations: std - standard deviation; dl - data length; nf - noise factor; moa - model order above
 the true one; mob - model order below the true one; * - $p \leq 0.05$.

	DDTF				H			
	missed coefficient	std	false positive coefficient	std	missed coefficient	false positive std		
constant	1.02E+00	2.91E-01*	-3.91E-01	7.64E-02*	-7.65E-01	2.68E-01*	7.68E-02	8.92E-02
dl	6.23E-04	1.03E-04*	7.03E-04	2.02E-05*	2.99E-03	8.52E-05*	-9.18E-06	2.65E-05
dl*dl	6.78E-08	1.63E-08*	-2.68E-08	2.55E-09*	-4.51E-07	1.27E-08*	-7.85E-08	3.58E-09*
dl*nf	-4.80E-04	2.30E-05*	-1.39E-04	5.66E-06*	-1.22E-04	1.88E-05*	1.76E-05	6.99E-06*
nf	-1.71E+00	1.43E-01*	1.52E-01	4.40E-02*	-2.03E+00	1.26E-01*	6.20E-02	4.65E-02
nf*nf	5.13E-01	3.14E-02*	-2.71E-02	8.78E-03*	4.93E-01	2.67E-02*	-1.49E-02	9.45E-03
moa	2.79E-02	1.39E-02*	7.69E-03	2.79E-03*	-1.28E-01	1.26E-02*	1.08E-02	3.71E-03*
moa*moa	-7.37E-04	1.98E-04*	-1.60E-04	3.49E-05*	3.51E-04	1.77E-04*	-1.11E-04	5.00E-05*
moa*dl	-5.78E-06	1.82E-06*	-4.80E-07	3.45E-07	1.82E-05	1.52E-06*	4.91E-06	5.12E-07*
moa*nf	3.38E-03	2.56E-03*	-1.96E-04	6.54E-04	8.23E-03	2.34E-03*	-2.44E-03	7.92E-04*
mob	1.06E-01	4.93E-02*	4.62E-03	1.02E-02	-2.25E-01	4.59E-02*	-3.80E-03	1.35E-02
mob*mob	-5.29E-03	2.33E-03*	1.91E-04	4.31E-04	5.21E-03	2.18E-03*	1.33E-03	6.05E-04*
mob*dl	-2.86E-06	6.39E-06*	2.38E-06	1.33E-06	2.45E-05	5.45E-06*	4.14E-06	2.00E-06*
mob*nf	-1.86E-03	8.80E-03*	1.65E-04	2.40E-03	1.13E-02	8.07E-03	-5.96E-03	2.88E-03*

Table A.27: Regression coefficients for the dDTF and H with Schelter-model data in combination with random permutation
 Abbreviations: std - standard deviation; dl - data length; nf - noise factor; moa - model order above the true one; mob - model order below the true one; * - $p \leq 0.05$.

	missed		dDTF		missed		H	
	coefficient	std	coefficient	std	coefficient	std	coefficient	std
constant	3.44E-01	2.70E-01	1.74E-01	2.98E-02*	3.72E+00	2.36E-01*	2.43E-01	1.04E-01*
dl	9.59E-04	8.28E-05*	6.02E-04	1.66E-05*	5.10E-05	7.00E-05	3.02E-04	3.50E-05*
dl*dl	-1.36E-07	1.27E-08*	8.30E-09	1.91E-09*	-2.72E-08	1.01E-08*	1.38E-07	5.10E-09*
dl*nf	1.48E-04	2.18E-05*	-1.43E-04	4.93E-06*	5.94E-06	1.63E-05	-3.63E-04	8.98E-06*
nf	-1.80E+00	1.37E-01*	-1.81E-01	1.69E-02*	-2.28E+00	1.17E-01*	-6.40E-01	5.63E-02*
nf*nf	2.23E-01	3.40E-02*	3.25E-02	3.41E-03*	5.31E-01	2.79E-02*	3.54E-01	1.44E-02*
moa	1.83E-02	1.44E-02	-2.69E-03	1.11E-03*	7.81E-02	1.23E-02*	-4.62E-02	5.30E-03*
moa*moa	-2.33E-04	2.16E-04	-1.83E-05	1.43E-05	-5.52E-04	1.84E-04*	9.87E-04	7.92E-05*
moa*dl	4.90E-06	1.65E-06*	-3.88E-06	2.95E-07*	1.23E-06	1.34E-06	-1.12E-05	6.23E-07*
moa*nf	-3.09E-03	2.75E-03	1.88E-03	2.58E-04	-1.12E-02	2.36E-03*	-5.13E-04	1.07E-03
mob	-9.96E-02	4.97E-02*	1.07E-04	4.45E-03	-1.25E-01	4.17E-02*	-5.78E-02	1.96E-02*
mob*mob	7.64E-03	2.45E-03*	1.29E-06	1.98E-04	1.27E-02	2.01E-03*	1.14E-03	9.83E-04
mob*dl	1.30E-05	5.14E-06*	-2.51E-06	1.14E-06*	4.23E-06	3.98E-06	-8.94E-06	2.31E-06*
mob*nf	-2.27E-02	8.78E-03*	1.00E-03	9.98E-04	-1.69E-02	7.25E-03*	-2.96E-03	3.89E-03

1. **Methoden zur integrierten Analyse metabolischer Netzwerke unter stationären und instationären Bedingungen**
von S. A. Wahl (2008), 245 Seiten
ISBN: 978-3-89336-506-7
2. **Strukturelle Untersuchungen an membranassoziierten Proteinen: NMR-Strukturen des HIV-1 Virus Protein U (39-81) und des humanen CD4 (372-433)**
von M. Wittlich (2008), XVIII, 185 Seiten
ISBN: 978-3-89336-510-4
3. **Identifizierung von physiologischen und artifiziellen Liganden von GABARAP und Charakterisierung der resultierenden Interaktionen**
von J. Mohrlüder (2008), V, 158 Seiten
ISBN: 978-3-89336-511-1
4. **Struktur und Funktion von Transaminasen aus *Corynebacterium glutamicum***
von J. Marienhagen (2008), VI, 154 Seiten
ISBN: 978-3-89336-512-8
5. **Implementierung eines Funk-Protokolls (IEEE 802.15.4) und Entwicklung eines adaptiven Zeitsynchronisationsverfahrens für ein Netzwerk intelligenter und autarker Sensoren**
von M. Schlösser (2008), 77 Seiten
ISBN: 978-3-89336-519-7
6. **Etablierung und Optimierung der sekretorischen Gewinnung thermostabiler Lipasen in Gram-positiven Bakterien**
von H. Brundiek (2008), VIII, 154 Seiten
ISBN: 978-3-89336-520-3
7. **Visuospatial Attention: Neural Correlates and Pharmacological Modulation in Healthy Subjects and Patients with Spatial Neglect**
by S. Vossel (2008), XIV, 176 pages
ISBN: 978-3-89336-526-5
8. **Analyse des Substratspektrums der ClpCP-Protease aus *Corynebacterium glutamicum***
von J.-E. Schweitzer (2008), V, 130 Seiten
ISBN: 978-3-89336-528-9
9. **Adaptive Verfahren zur automatischen Bildverbesserung kernspintomographischer Bilddaten als Vorverarbeitung zur Segmentierung und Klassifikation individueller 3D-Regionen des Gehirns**
von J. Castellanos (2008), VI, 100 Seiten
ISBN: 978-3-89336-539-5

10. **Posttranslationale Regulation der 2-Oxoglutarat-Dehydrogenase in *Corynebacterium glutamicum***
von C. Schultz (2009), VII, 151 Seiten
ISBN: 978-3-89336-560-9
11. **MtrA, ein bifunktionaler Antwortregulator aus *Corynebacterium glutamicum***
von M. Brocker (2009), VI, 125 Seiten
ISBN: 978-3-89336-561-6
12. **Strukturelle Charakterisierung von GABRAP-Ligand-Interaktionen**
von Y. Thielmann (2009), 166 Seiten (getr. pag.)
ISBN: 978-3-89336-563-0
13. **Acceleration on an image reconstruction algorithm for Positron Emission Tomography using a Graphics Processing Unit**
by T. Felder (2009), 97 pages
ISBN: 978-3-89336-566-1
14. **NMR-Lösungsstruktur der Loopregion Tyr⁶⁷ - Leu⁷⁷ des visuellen Arrestins im Komplex mit photoaktiviertem Rhodopsin**
von S. Feuerstein (2009), XVI, 140 Seiten
ISBN: 978-3-89336-571-5
15. **Development of a Process for the Cleavage of a Mucin Fusion Protein by Enterokinase**
by T. Kubitzki (2009), IV, 133 pages
ISBN: 978-3-89336-575-3
16. **Children's health and RF EMF exposure**
project coord. P. Wiedemann (2009), 49 pages
ISBN: 978-3-89336-594-4
17. **Entwicklung einer Signalerfassungselektronik für eine Halbleiter-Photomultiplier (SiPM) Matrix**
von C. Parl (2009), IV, 128 Seiten
ISBN: 978-3-89336-595-1
18. **Medienorientierung biomedizinischer Forscher im internationalen Vergleich**
Die Schnittstelle von Wissenschaft & Journalismus und ihre politische Relevanz
herausg. von H. P. Peters (2009), 364 Seiten
ISBN: 978-3-89336-597-5
URN: urn:nbn:de: 0001-00542
19. **Identifizierung von Interaktionspartnern für HIV-1 Nef und ihre potentielle Relevanz bei der Entwicklung der HIV-assoziierten Demenz**
von J. Mötter (2010), VI, 172 Seiten
ISBN: 978-3-89336-604-0

20. **Biotransformationen mit Cytochrom P450 Monooxygenasen**
von D. Zehentgruber (2010), XI, 147 Seiten
ISBN: 978-3-89336-605-7

21. **Studies on central carbon metabolism and respiration of *Gluconobacter oxydans* 621H**
by T. Hanke (2010), 120 pages
ISBN: 978-3-89336-607-1

22. **Prozessentwicklung zur Produktion von 2-Keto-L-Gulonsäure, einer Vitamin C- Vorstufe**
von B. Osterath (2010), XXI, 213 Seiten
ISBN: 978-3-89336-612-5

23. **Visuell evozierte Antworten der corticalen Areale V1/V2 und V5/MT nach Schachbrettmusterumkehrreizung – Magnetenzephalographische Untersuchungen in Kombination mit cytoarchitektonischen Wahrscheinlichkeitskarten**
von B. U. Barnikol (2010), III, 138 Seiten
ISBN: 978-3-89336-615-6

24. **Biochemische und regulatorische Analyse des TCA-Zyklus und Glyoxylat-Shunts in *Escherichia coli***
von M. Kunze (2010), 191 Seiten
ISBN: 978-3-89336-620-0

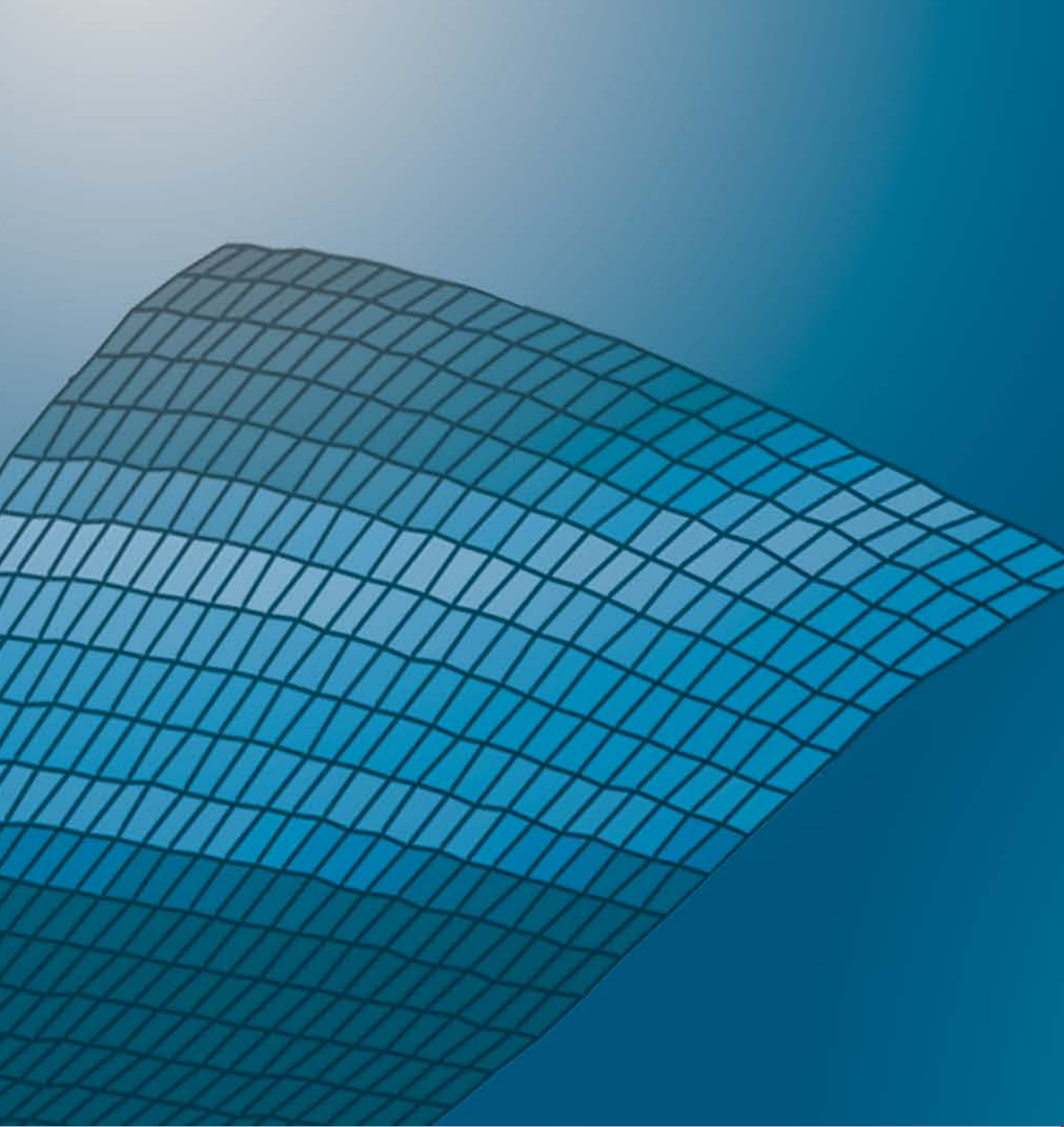
25. **Metabolomanalyse als Grundlage für ¹³C-Stoffflussanalyse und dynamischer Modellierung am Beispiel der Lysinbiosynthese**
von M. G. Wellerdiek (2010), xvi, 182 Seiten
ISBN: 978-3-89336-621-7

26. **Neue Thiamindiphosphat-abhängige Enzyme für die Synthese enantiokomplementärer 2-Hydroxyketone**
von G. Kolter (2010), IX, 168 Seiten
ISBN: 978-3-89336-626-2

27. **Genetische Analyse von Substrat-Translokase-Wechselwirkungen bei der Tat-abhängigen Proteintranslokation in *Escherichia coli***
von F. Lausberg (2010), 174 Seiten
ISBN: 978-3-89336-628-6

28. **Silicium Nanodrähte für die extrazelluläre Ableitung elektrischer Aktivität**
von J. F. Eschermann (2010), xii, 191 Seiten
ISBN: 978-3-89336-639-2

29. **Causality measures between neural signals from invasively and non-invasively obtained local field potentials in humans**
by E. Florin (2010), xxix, 220 pages
ISBN: 978-3-89336-646-0



Gesundheit / Health
Band / Volume 29
ISBN 978-3-89336-646-0

